AIR POLLUTION, NANOTOXICITY AND NEURODEGENERATION; EXPLORING THE RELATIONSHIP BETWEEN ENVIRONMENTAL METALLIC NANOPARTICLES AND HUMAN HEALTH

PhD Thesis

Jessica Hammond

MSci (Hons), MSc (research)

Lancaster University

July 2022

Submitted in part fulfilment of the requirements for the degree of Doctor of Philosophy

Biomedical & Life Sciences | Lancaster University

Abstract

Air pollution and Alzheimer's disease (AD) are two of the largest global health issues faced by society today; air pollution is a recognised risk factor for AD. Particulate matter (PM) is a major component of air pollution and refers to the solid and liquid particulates of varying sizes and compositions that are resuspended in the air. Of these particles, metallic particles in the nanometre range (ultrafine, UFPs; < 0.1 μm) are particularly hazardous due to their pervasiveness, ability to penetrate all major organs in the human body, and ability to generate both inflammatory and oxidative stress responses in humans. Magnetite (Fe_3O_4) nanoparticles (MNPs) and related iron oxides may be of relevance to neurodegeneration. MNPs are found within PM, typically in association with toxic metals, and have been found throughout the human brain, including in association with senile plaques (a key pathological hallmark of AD). MNPs have also been shown to accelerate amyloid beta (Aβ) toxicity and aggregation. MNPs have previously been quantified in a handful of studies to compare AD and control tissue, with mixed results. Improved understanding of the development of AD, the toxic effects of air pollution (especially magnetite and metals), and the relationship between these two phenomena would be highly beneficial to global health.

In order to explore the potential causal link between air pollution and AD, two approaches were taken; metallic and magnetic quantification of post-mortem human brain tissue via superconducting quantum interference device (SQUID) magnetometry and inductively couple plasma mass spectrometry (ICP-MS), and exploration of the cytotoxic effects of ultrafine roadside dust particles (UF-RDPs) on human lung epithelial cells (Calu-3) using different *in vitro* assays.

The concentration of magnetite (measured as magnetic remanence, SIRM) in human brain tissue was not statistically different when comparing AD cases to aged-matched controls. Similarly, there were no differences in metal content between the two groups. Principal component analysis grouped the metals into four components, which are potentially indicators of pollution sources: (1) traffic-related and crustal, (2) fuel oil combustion, (3) biological and tyre/brake wear, and (4) catalytic converters and dental alloys. The distributions of magnetite and metals were heterogenous across different individuals. Significantly lower concentrations of both MNPs and metals were reported in UK samples, compared to previously reported Mexico City samples. Differences were also seen when comparing the *in vitro* response to UF-RDPs from three contrasting cities; Lancaster UF-RDPs increased cell viability, whilst Mexico City UF-RDPs were the most toxic and induced the highest amount of

oxidative stress (ROS production), and Birmingham UF-RDPs were the most pro-inflammatory. These responses are not fully reflected in conventional mass metrics like PM_{10}, as although the greatest cytotoxicity and ROS production was seen with Mexico City UF-RDPs (highest PM_{10} exposure), the strongest pro-inflammatory responses were seen in response to Birmingham UF-RDPs and a potentially tumorigenic or fibrosis related increase in cell viability was seen in response to Lancaster UF-RDPs despite the lower PM_{10} and $PM_{2.5}$ exposures in the UK cities. There is a need for localised air pollution limits which use biologically relevant metrics that address particle size and cover non-exhaust emission sources of PM like road dust to minimize the health risks of air pollution exposure.

Overall, this work demonstrates the presence of exogenous, pollution-derived metals and magnetic nanoparticles within the human brain. Highly reactive and toxic metals and MNPs may exert toxic effects in the brain and have been causally linked to neurodegeneration and AD. The geriatric blood-brain barrier is likely compromised allowing for universal incursion in both AD and age-matched controls, so the use of younger highly exposed individuals such as Mexico City urbanites is critical to identify any changes in metal/magnetic content in the brain decades prior to the presentation of AD. Clear differences were seen across geographical locations when looking at absolute concentrations of MNPs, as well as the composition and induced biological effects of UF-RDPs from different cities. It is thus important to focus on highly localised air pollution regulations to mitigate risk to human health.

Abbreviations

ACh	Acetylcholine
AChE	Acetylcholinesterase
AD	Alzheimer's disease
AJ	Adherens junctions
ALI	Air-liquid interface
ALS	Amyotrophic lateral sclerosis
ANOVA	Analysis of variance
ANS	Autonomic nervous system
APC	Amyloid plaque core, senile plaque core
APOE ε4	Apolipoprotein E ε4
APP	Amyloid precursor protein
Aβ	Amyloid beta
BBB	Blood brain barrier
BC	Black carbon
BDNF	Brain derived neurotropic factor
BSA	Bovine serum albumin
BWP	Brake wear particles
CBF	Cerebral blood flow
CDNPs	Combustion and friction derived nanoparticles
CN	Cognitively normal
CNS	Central nervous system
CSF	Cerebrospinal fluid
CVD	Cardiovascular disease
DBPS	Dulbecco's phosphate buffered saline
DC	Direct current
DEP	Diesel exhaust particles
DU	Unspecified dementia
EELS	Electron energy loss spectroscopy
EGFR	Epidermal growth factor receptor
EMEM	Eagle's minimum essential medium
EPA	Environmental protection agency
FAD	Familial Alzheimer's disease
FBS	Foetal bovine serum
FDA	Food and drug administration
GI	Gastrointestinal
GSH	Glutathione
HPA	Hypothalamus pituitary axis
HR	Hazard ratio
IARC	International agency for research on cancer
ICP-MS	Inductive coupled plasma- mass spectrometry
ICP-OES	Inductive coupled plasma- optical emission spectroscopy
IDE	Insulin degrading enzyme
IL	Interleukin

ILCR	Incremental lifetime cancer risk
IRE	Iron response element
IRM	Isothermal remanence magnetisation
IRP1 (and 2)	Iron regulatory proteins 1 and 2
LAC	Latin America and the Caribbean
LAL	Limulus amoebocyte lysate
LDH	Lactate dehydrogenase
LMIC	Lower- and middle-income countries
MBB	Manchester Brain Bank
MC	Mexico City
MCI	Mild cognitive impairment
MMC	Metropolitan Mexico City
MMSE	Mini mental state examination
MNP-Aβ	Complex of magnetite nanoparticles with amyloid beta
MNPs	Magnetite nanoparticles
MPPD	Multiple pathway particle dosimetry
MRI	Magnetic resonance imaging
MSCs	Human mesenchymal stem cells
NBIA	Neurodegeneration with brain iron accumulation
NDD	Neurodegenerative disease
NDMA	N-methyl-D-aspartate
NEE	Non-exhaust emissions
NFT	Neurofibrillary tangles
NF-κB	Nuclear factor kappa beta
NPs	Nanoparticles, < 0.1 μm, also called UFPs
NRM	Natural remanence magnetisation
OB	Olfactory bulb
OR	Odds ratio
PAH	Polyaromatic hydrocarbons
PCA	Principal component analysis
PD	Parkinson's disease
PET	Positron emission topography
PM	Particulate matter
PM0.2	Particulate matter with aerodynamic diameter < 0.2 μm
PM10	Particulate matter with aerodynamic diameter < 10 μm
PM2.5	Particulate matter with aerodynamic diameter < 2.5 μm
PMD	Post-mortem delay
PNCs	Particle number counts
ppm, ppb	Parts per million, parts per billion
p-tau	Phosphorylated tau
PTFE	Polytetrafluoroethylene
PTSD	Post-traumatic stress disorder
RBD	Rapid eye movement sleep behaviour disorder
RD	Road-deposited or roadside dust
RDPs	Road-deposited or roadside dust particles
ROS	Reactive oxygen species
SAD	Sporadic Alzheimer's disease
SAM	Sympathetic adrenal medullary

SD	Single domain
SD	Standard deviation
SEM	Standard error of the mean
SIRM	Saturation isothermal remanence magnetisation
SOD	Superoxide dismutase
SP	Superparamagnetic
SQUID	Super conducting quantum interference device
T, mT	Tesla, milliTesla
TBHP	Tert-butyl hydroperoxide
TEM	Transmission electron microscopy
TJ	Tight junctions
TRAP	Traffic-related air pollution
UFP	Ultrafine particle < 0.1 µm also called NPs
UFPM	Ultrafine particulate matter
UF-RDPs	Ultrafine road deposited dust particles
UPSIT	The University of Pennsylvania smell identification test
VRM	Viscous remanent magnetization

Table of Contents

List of Figures

List of Tables

Acknowledgements

First and foremost, I would like to express my thanks to Professor David Allsop for believing in me as a PhD student, for the freedom he gave me within my project and for his unwavering positivity. I would also like to thank the Sir John Fisher Foundation for funding this project and supporting the work of the Allsop lab for over 14 years. Thank you to Dr Ed Parkin for recommending me for this project, for the skills and techniques you taught me during my masters and especially for stepping up last minute as a supervisor. Thank you to Professor Barbara Maher for creating a challenging project and your guidance through the journal submission process.

I would like to thank Prof David Mann, Dr Andy Robinson and the staff working at the Manchester Brain Bank for providing me with human brain tissue and especially to those who donated their brains to science. Please consider donating your brain in the future!

I am extremely grateful to Professor Rebecca Killick for a crash course on R and statistics, which saved me many painful hours of screaming at my computer. I would also like to thank Dr Vassil Karloukovski for teaching me all things magnetism, how to master using the 2G, and for always listening and offering a helping hand. Thanks to Dr Tomasz Gonet for his kindness and valuable project discussions. My gratitude goes to Dr Imad Ahmed for collaborating with us on this research, for his dedication to science and for spending all night helping me create synthetic magnetite.

There are many members past and present of Biological and Life Sciences that I would like to thank for their support of the years. A special thanks to my 'lab partners' Dr Norah Ulzheimer, Dr Rachael Smith, Dr Sophie Lau and soon to be a Dr, Rebecca Barker for all your support and for listening to me complain over hot chocolate and to Rachael for proof-reading. Thank you to the technicians for keeping everything up and running despite pandemics and power cuts.

Thank you to my family for putting up with me being hundreds of miles away, for your belief in me, and for always asking me "So when are you going to finish your PhD then?" A special thanks to M.P for always being there for me, and to my writing buddy B.A. Lastly, I would like to thank my partner Anna for listening to me ramble on about my work, her encouragement, reassurance, graphic design skills and constant reminders that I'm a super scientist.

I would like to dedicate this work to my grandad David Dysart; a funny kind man who sadly succumbed to dementia. He was always supportive of my work as in his words "at least some bugger is trying to do something about it"!

Chapter 1 Introduction

1.1 Alzheimer's disease

Alzheimer's disease (AD) is the most common form of dementia, accounting for 60-70% of cases worldwide (WHO, 2021b). In 2015, there were an estimated 46.8 million AD patients worldwide, with this figure expected to increase to 131.5 million by 2050 (Prince et al., 2015). AD has both great personal and financial costs; family and friends experience emotional distress as caregivers and the estimated global cost of AD in 2015 was $818 billion (Prince et al., 2015).

AD is a progressive neurodegenerative disease characterised initially by short term memory loss (a stage known as mild cognitive impairment, MCI), gradually worsening to aphasia (inability to understand and form speech), agnosia (inability to recognise objects and people) and apraxia (inability to carry out voluntary movements) amongst other behavioural and memory issues (Blennow et al., 2006). Up to 15% of people presenting with MCI will go on to develop AD (Petersen, 2004). Clinically, disease stage is determined via psychological tests such as the mini mental state examination (MMSE), during which patients answer a series of questions designed to test their cognitive functions (Folstein et al., 1975).

Life expectancy following an AD diagnosis is 3-10 years, and onset typically occurs after the age of 65 years but can be much earlier in cases with a clear genetic link (Zanetti et al., 2009). Fewer than 5% of AD cases are genetic or 'familial' (FAD) with the remaining 95% being sporadic in nature (SAD). An underlying cause or causes have not been identified for SAD; however, several risk factors have been identified including age, head trauma, vascular conditions (e.g., hypertension) and, more recently, environmental factors.

There is a clear unmet medical need with regards to treatment for AD as current therapeutics only provide symptomatic relief rather than addressing the underlying disease causation. There are two classes of AD therapeutics currently in use - acetylcholinesterase (AChE) inhibitors and glutamate antagonists. Acetylcholinesterase inhibitors, such as rivastigmine and donepezil, target the enzyme acetylcholinesterase, which is responsible for degrading the neurotransmitter acetylcholine (ACh) at the post-synaptic cleft (Everitt and Robbins, 1997). Increased ACh is associated with improved cognitive function (Barnes et al., 2000). Glutamate antagonists target the overstimulation of glutamate, thought to occur in AD (Wang and Reddy, 2017). Memantine (the only current glutamate antagonist used in clinical practice) targets

NDMA (N-methyl-D-aspartate) receptors (Johnson and Kotermanski, 2006, Blanpied et al., 1997). In the unstimulated (resting) state, NDMA receptors are blocked by magnesium ions (Mg^{2+}), however they are voltage-gated cation channels that become active when Mg^{2+} is displaced, which allows for calcium influx and activation (Rogawski and Wenk, 2003). To reduce the overstimulation of NDMA receptors in AD, memantine binds the NDMA receptors with a higher affinity than Mg^{2+}, acting as an uncompetitive antagonist (Johnson and Kotermanski, 2006, Blanpied et al., 1997).Unfortunately, these treatments are only effective in a small subset of patients, with 50% of patients showing no response (Kumar et al., 2015).

In response to the need for effective treatments numerous strategies are being employed to develop therapeutics including immunotherapies (Sevigny et al., 2016), peptide inhibitors of amyloid beta aggregation (Gregori et al., 2017), and repurposing of existing drugs for other conditions such as diabetes (Batista et al., 2018). However, there have been no new therapeutics for AD approved for use in the UK since Memantine in 2011. Controversially, in the US the Food and Drug administration (FDA) recently approved the use of Aducanumab, a monoclonal antibody that targets senile plaques, a key pathological feature of AD (FDA, 2020). It has sparked controversy primarily due to the (re)interpretation of clinical trial data; additional data was collected after phase III trials were stopped due to <20% chance of a positive finding and submitted to the FDA for re-evaluation (FDA, 2020). The FDA approved the treatment despite two identical phase III trials showing opposite results, and without much evidence to show that removal of plaques would slow cognitive decline.

The identification of modifiable risk factors and prevention of disease onset is likely a better approach to minimising disease burden than development of novel drugs. The focus of this study is exploration of a modifiable risk factor which may contribute to the risk of developing dementia – air pollution.

1.1.1 Neuropathology

The two key pathological hallmarks of AD in the brain are senile plaques (extracellular deposits of amyloid beta, Aβ) and neurofibrillary tangles (NFTs) (intracellular aggregates of hyperphosphorylated tau protein (Braak and Braak, 1991). The result of these lesions is a loss of synaptic connections (~45%) and a decrease in the number of neurons in the regions affected (Masliah et al., 1989). In addition to being abundant in AD brains, these structures are also present in the normal ageing brain at significantly lower levels (Knopman et al., 2003). This raises the question as to at what point does plaque/NFT load constitute AD and how is this different to normal ageing? It has even been proposed that AD is a consequence of normal

ageing (Fjell et al., 2014), however there are individuals who live to be very old (>100) with the same pathological changes and no clinical presentation of dementia (Takao et al., 2016), so whilst some of the pathological changes may be part of typical ageing, development of AD itself is unlikely to be a typical ageing process. In addition to plaques and tangles, activated microglia and reactive astrocytes are often observed as well as Hirano bodies (actin-rich inclusions) and cerebral amyloid angiopathy (the accumulation of Aβ concentrating in small arteries and small arteriole walls) (Glenner et al., 1981). Other changes to brain structure are also observed, such as a decrease in brain weight (due to loss of grey matter), decreased cortical thickness (Salat et al., 2004), and increase in ventricle size (due to cerebral spinal fluid build-up) (Nestor et al., 2008).

1.1.2 Braak staging

Neuropathologists Eva and Heiko Braak devised a system for staging the progression of AD based on the histopathological evaluation of human brain tissue, referred to as Braak staging (Braak and Braak, 1991). The Braak staging system follows the topographical pattern of neurofibrillary tau lesions and neuronal loss throughout the brain, which is consistent by area, lamina, and cell type (Braak and Braak, 1985). Stages I-II start in the transentorhinal region, before progressing to the limbic regions (Stages III-IV) and finally the isocortical region (stages V-VI) (Braak and Braak, 1991). Revisions to the initial staging have been suggested; NFTs may appear in the (lower) brainstem prior to the transentorhinal region (Braak et al., 2011).

The distribution of Aβ occurs in 5 phases, Aβ plaques are located in the following regions: phase 1 (at least 1 of basal, temporal, or orbitofrontal neocortex), phase 2 (allocortex, amygdala, higher order areas of the neocortex), phase 3 (secondary neocortical fields, striatum), phase 4 (nearly all of the neocortex, midbrain, inferior colliculi) and phase 5 (lower brainstem and cerebellum) (Thal et al., 2002).

1.1.3 Brain regions affected by AD

One of the first brain regions affected by AD is the medial temporal lobe, which encompasses the entorhinal cortex, hippocampus, and amygdala. The medial temporal lobe is associated with memory, so it is unsurprising that atrophy in this region, coupled with the loss of functional neurons, results in the cognitive decline observed in AD (Squire et al., 2004). The brainstem is also an early site of AD neuropathology, in particular the locus coeruleus and dorsal raphe nucleus (Ji et al., 2021). The limbic system is affected in stages III-IV of Braak staging; this encompasses the medial temporal lobe regions along with the hypothalamus, orbitofrontal cortex, piriform cortex, and olfactory bulbs. The largest decrease in mass is seen

in the cerebral cortex and cortical regions (cortical atrophy) (Perl, 2010), resulting in changes to regions involved in language and reasoning which manifest as difficulties in processing and understanding speech (Wenk, 2003).

1.1.4 Causation hypotheses

Numerous theories exist as to the cause of AD including the cholinergic hypothesis, the amyloid cascade hypothesis, the tau hypothesis, the metal theory, inflammation and oxidative stress-based theories, the mitochondrial hypothesis, or a combination of the aforementioned (Breijyeh and Karaman, 2020). A brief overview of some of the biochemical pathways and key proteins involved in AD are summarised below.

1.1.4.1 The amyloid cascade hypothesis

The amyloid cascade hypothesis (Fig. 1.1.) states that Aβ might accumulate due to genetic predisposition or, in the case of sporadic AD, factors such as ageing and *APOE* allelic composition. If not sufficiently cleared, these Aβ monomers aggregate to form oligomers, which eventually mature into fibrils and deposit into senile plaques. Soluble oligomers increase the production of reactive oxygen species (ROS), leading to oxidative damage and mitochondrial dysfunction which ultimately leads to cell death. Excess Aβ also leads to the hyperphosphorylation of tau, excitotoxicity, and inflammation. The 'stage' or conformation of Aβ is related to its toxicity with the smaller oligomers (e.g., trimers, pentamers) thought to be more toxic than monomers and mature fibrils (Walsh et al., 2002, Sakono and Zako, 2010).

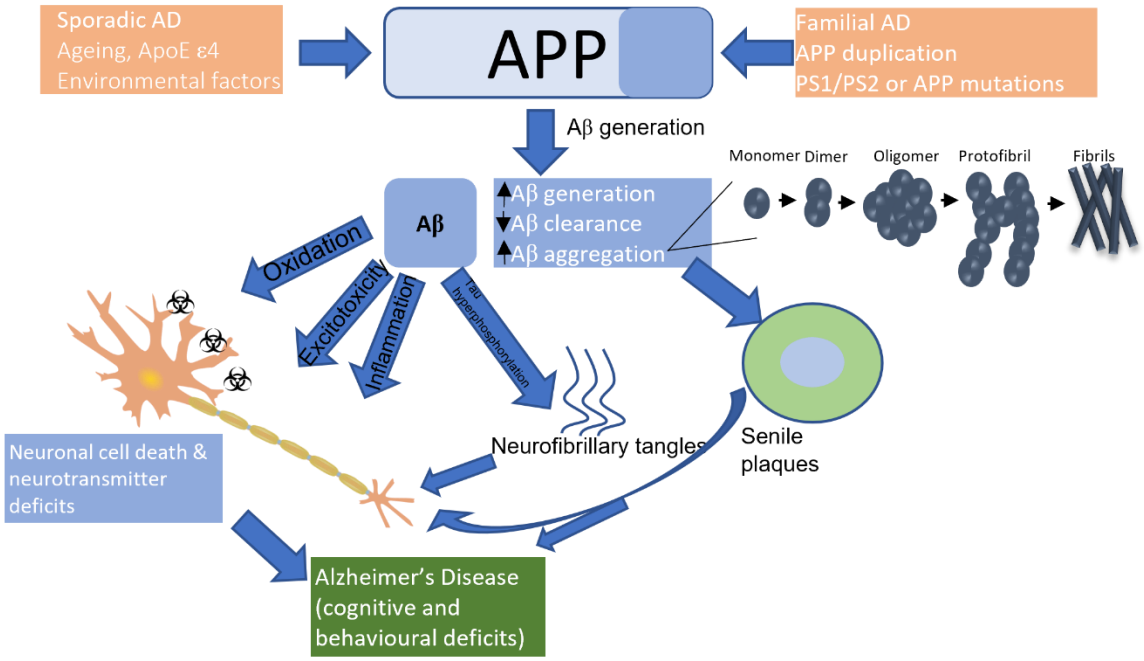

Figure 1.1 The amyloid cascade. Amyloid beta (Aβ) is liberated from the amyloid precursor protein (APP). The generation of Aβ can be influenced by mutations (familial) or other factors such as ageing or environmental factors (sporadic). An increase in Aβ generation, combined with a decrease in its clearance leads to a series of neurotoxic mechanisms such as excitotoxicity and neuroinflammation. In addition to soluble Aβ, aggregates can form which also have neurotoxic effects. These factors as well as the key pathological features of AD (neurofibrillary tangles and senile plaques) lead to neuronal cell death and impairment of neurotransmitter signalling resulting in the cognitive and behavioural defects seen in AD.

Aβ is proteolytically generated from the amyloid precursor protein (APP) (Hardy and Allsop, 1991). Mutations in the *APP* gene are associated with FAD, as well as mutations in genes encoding enzymes involved in APP proteolysis; *PSEN1* and/or *PSEN2* which encode presenilin proteins (Goate et al., 1991, Scheuner et al., 1996). The amyloid cascade hypothesis is further supported by the high incidence of AD in Down's syndrome individuals; the condition is associated with trisomy of chromosome 21 on which the *APP* gene is located (Wiseman et al., 2015).

APP is a type I transmembrane protein which can undergo cleavage via two main pathways: the amyloidogenic and non-amyloidogenic pathways (Fig. 1.2). Approximately 90% of APP is cleaved via the non-amyloidogenic pathway (Octave et al., 2013), liberating extracellular soluble APP alpha (sAPPα), leaving the C83 fragment anchored to the membrane, which precludes Aβ formation. The remaining 10% is cleaved via the amyloidogenic pathway, resulting in the liberation of extracellular soluble APP beta (sAPPβ), leaving the C99 fragment anchored to the membrane which undergoes further cleavage to generate Aβ (Hampel et al.,

2021). The APP proteolytic fragments are involved in different signalling pathways, for example sAPPα is involved in neurite outgrowth (Hasebe et al., 2013).

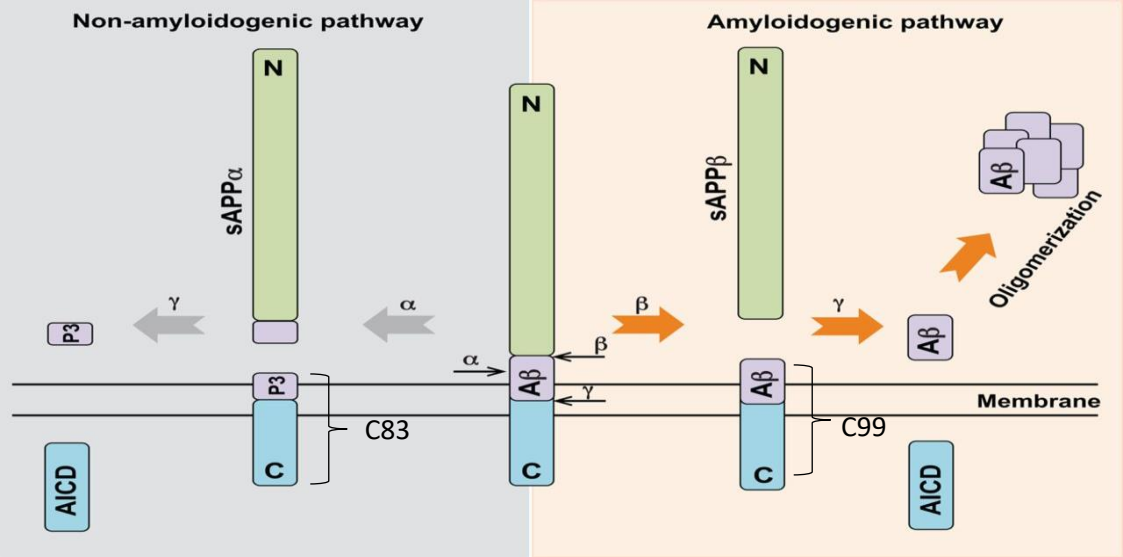

Figure 1.2 APP proteolysis. APP is a transmembrane protein which is cleaved sequentially by secretase enzymes to generate extracellular fragments. In the non-amyloidogenic pathway, soluble APP alpha (sAPPα) is liberated when APP is cleaved by an α-secretase, leaving a C-terminal fragment anchored to the membrane (C83). C83 is then cleaved by γ-secretase to release P3. Alternatively, APP can follow the amyloidogenic pathway; APP is first cleaved by β-secretase (BACE1) to generate soluble APP beta (sAPPβ) and a C-terminal fragment (C99). C99 is then cleaved by γ-secretase to liberate Aβ-peptides. A soluble APP intracellular domain (AICD) fragment is also generated following cleavage of C83 and C99 by γ-secretase. Adapted from (Nicolas and Hassan, 2014).

The enzymes involved in APP proteolysis are collectively referred to as secretases (Zhao et al., 2020). The α-secretase is one of the ADAM (a disintegrin and metalloprotease domain) family of zinc metalloproteinases; primarily ADAM10 but can also be ADAM17 or ADAM9 (Kuhn et al., 2010, Hitschler and Lang, 2022). The β-secretase was identified as BACE1 (beta-site APP cleaving enzyme 1), and it competes with ADAM10 for the APP substrate (Cole and Vassar, 2008). The γ-secretase is a complex of proteins, consisting of presenilin-1 (or presenilin-2), nicastrin, APH-1 (anterior-pharynx defective 1) and PEN-2 (presenilin enhancer 2). Presenilin-1 is the catalytically active subunit, which cleaves APP C-terminal fragments as well as those generated from other transmembrane proteins including Notch, E-Cadherin and Jagged-1 (LaVoie and Selkoe, 2003, Güner and Lichtenthaler, 2020). Amyloid beta is generated when γ-secretase cleaves C99, but this can result in Aβ of varying lengths depending on the site at which C99 was cleaved. Aβ40 is the predominant species in the brain (Zou et al., 2002), but other forms exist between 34 and 50 amino acids in length, including the more toxic Aβ42 (which is predominantly found in senile plaques and promotes aggregation of Aβ monomers) and Aβ38 (which is not related to AD pathology) (Page et al., 2008). Aggregation of the Aβ42

peptide occurs more rapidly than the more common Aβ40 form (Jarrett et al., 1993). Aβ is cleared by enzymatic and non-enzymatic pathways. In the enzymatic pathway, Aβ is cleared by a group of proteolytic enzymes known as Aβ-degrading enzymes such as insulin-degrading enzyme (IDE), endothelin-converting enzyme, plasmin, matrix metalloproteinase-9 (MMP-9), and neprilysin (Baranello et al., 2015). There are several non-enzymatic methods of Aβ clearance from the brain including transcytosis across the BBB, phagocytosis by microglia, and clearance via the glymphatic system. Soluble Aβ is transcytosed across the BBB through brain endothelial cells via the low-density lipoprotein receptor-related protein 1 (LRP-1) and ABC transporter sub-family A and B member 1 (ABCA1 and ABCB1 respectively) (Hampel et al., 2021). Once Aβ has crossed the BBB, it is sequestered by soluble transporters (e.g., soluble LRP1) which prevent it from being transported out of free circulation into the interstitium. Microglia, the resident immune cells of the brain, are activated in response to Aβ, engulfing soluble and fibrillar forms of Aβ and degrading them (Wyss-Coray et al., 2003, Ries and Sastre, 2016). Microglia (astrocytes specifically) are an important part of the glymphatic system, a clearance network which removes macroscopic waste (i.e., proteins and metabolites) from the central nervous system (Jessen et al., 2015) via a system of perivascular channels on astrocytes (aquaporin 4, AQP4) which allow CSF to move into the brain parenchyma, driving interstitial fluid towards perivenous space for drainage (Iliff et al., 2012). Degradation of these clearance mechanisms in conjunction with elevated Aβ levels may lead to a toxic build-up of Aβ, however there is contrasting evidence such as mixed reports of increases or decreases in Aβ clearance mechanisms e.g. IDE activity with disease severity (Zhang et al., 2018, Miners et al., 2009).

1.1.4.2 The tau hypothesis

AD can be considered a tauopathy; a neurodegenerative disease in which the microtubule associated protein, tau, aggregates into neurofibrillary tangles (NFTs). Encoded by the *MAPT* gene, tau is found predominantly in neurons where it plays an important role in the cytoskeleton by binding to and stabilising microtubules (Johnson and Stoothoff, 2004). Unlike *APP*, there are no known mutations of *MAPT* associated with FAD, but mutations in *MAPT* are associated with other dementias like frontotemporal dementia (Shafei et al., 2020).

There are six isoforms of tau which are subject to post translational modification, such as phosphorylation. Phosphorylation of tau can interfere with microtubule dynamics and, in AD, hyperphosphorylation of the protein is observed which is thought to cause aggregation and the formation of insoluble aggregates (Johnson and Stoothoff, 2004). Hyperphosphorylated tau is arranged in paired helical filament and straight filament structures, which aggregate to

form the NFTs deposited intracellularly in neurons and which, ultimately, lead to neuronal death. To initiate aggregation, a tau 'seed' is needed; tau is believed to spread in a prion-like manner between networks of connected cells (DeVos et al., 2018). In addition, tau can propagate Aβ toxicity by increasing cleavage of APP to liberate the peptides (Bright et al., 2015) and/or by trapping them in endosomes (Arnsten et al., 2021).

As the progression of AD is more closely aligned with tau pathology than with Aβ (Braak and Braak, 1991), it may be a more appropriate therapeutic target. Furthermore, decline in cognition and loss in brain weight are more closely related to NFTs than Aβ, again suggesting that the role of tau may be more important than that of Aβ in AD pathogenesis (Giannakopoulos et al., 2003). However, phosphorylated tau (p-tau) is also found in the brains of young children and chimpanzees. Chimpanzees do not develop neurodegenerative AD, so the presence of p-tau may be a marker of ageing rather than AD itself (Finch and Austad, 2012). Conversely, young children with p-tau have been shown to have cognitive deficits at an early stage of life (Calderón-Garcidueñas et al., 2016a) (see section 1.2.3), which could be a consequence of early ageing or very early development of AD.

1.1.4.3 The metal theory of AD

Within the AD brain, alterations to several essential and non-essential metals have been reported including copper, zinc, iron, aluminium, lead, and mercury (Bonda et al., 2011). Of these, the essential transition metals copper, iron and zinc are studied most often, and all three are found in high concentrations in and around senile plaques (James et al., 2017). The distribution of copper, iron, and zinc also varies across senile plaques; the rim has elevated copper, iron and zinc compared to the neuropil, and the plaque core has elevated iron and zinc compared to the neuropil, with the total concentration in senile plaques and AD neuropils higher than control neuropil from aged-matched controls (Lovell et al., 1998). Aside from being found in plaques, copper, iron, and zinc have been implicated in Aβ oligomerization and aggregation, as well as the generation of ROS (in the case of copper and iron) (Mutter et al., 2018, Dorlet et al., 2009). For example, Zinc (300 nM and above) has been shown to induce Aβ aggregation *in vitro* (Bush et al., 1994). There are several high-affinity metal binding sites in the N-terminal region of Aβ e.g. His-rich residues 1-16, which mediate aggregation. Expression of APP, which would impact Aβ levels, is also influenced by copper, zinc and iron with various metal binding sites present on the APP gene (Gerber et al., 2017, Rogers et al., 2008). The focus here will be on iron; however, copper and zinc also play important roles in the AD and non-AD brain.

Zinc is an important cofactor for over 200 enzymes throughout the body (Jan et al., 2002) and plays an essential role in the brain as a neuromodulator, regulating several functions such as cell proliferation (including neurogenesis) and the release of inflammatory cytokines (Choi et al., 2020, Corniola et al., 2008, Jarosz et al., 2017). Along with copper, zinc is vital for the antioxidant enzyme Cu/Zn superoxide dismutase (SOD) and further acts as an antioxidant by upregulating metallothionein expression (Prasad, 2014). Zinc is an important component of ADAM zinc metalloproteinases, which cleave APP in a way that precludes liberation of Aβ (Figure 1.2), as well as IDE, an Aβ clearance enzyme (Gough et al., 2011). Abnormal zinc homeostasis has been linked to AD, so zinc has been explored as a potential therapeutic intervention for AD. For example, PBT2 is a compound that increases the cellular uptake of zinc, thus reducing extracellular zinc with the aim of reducing Aβ aggregation and deposition. PBT2 has been shown to be safe in phase II clinical trials, with initial promising results from small clinical trials (improved cognition and reduction of Aβ levels in serum) (Faux et al., 2010, Lannfelt et al., 2008), however larger clinical trials concluded there was no significant benefit over the placebo (Summers et al., 2022). There is not a clear consensus on whether zinc concentrations are altered in the AD brain (at the regional level), with reports of no change (Plantin et al., 1987, Szabo et al., 2015, Scholefield et al., 2020, Cornett et al., 1998a, Rulon et al., 2000, Stedman and Spyrou, 1997, Srivastava and Jain, 2002, Akatsu et al., 2011), increases (Andrási et al., 2000, Samudralwar et al., 1995, Deibel et al., 1996, Xu et al., 2017, Schrag et al., 2011a, Lovell et al., 1998, Rao et al., 1999, Religa et al., 2006, Danscher et al., 1997) , or decreases in zinc levels compared to age matched controls (Ward and Mason, 1987, Wenstrup et al., 1990, Andrási et al., 2000, Andrási et al., 1995, Xu et al., 2017, Panayi et al., 2002, Corrigan et al., 1993). These studies have been conducted across different decades, using a variety of analytical methods on tissue samples originating from different geographic locations, which could explain the discrepancy in results reported. Plaque counts could also account for some of the variation seen, as accumulation of zinc (as high as 1mM) in senile plaques is a recognised phenomenon (Dong et al., 2003, Miller et al., 2006). High (~mM) concentrations of zinc promote toxicity, whilst low concentrations (<50 μM) have been shown to be neuroprotective (Lovell et al., 1999). The concentration of zinc (as well as other conditions like pH and form of Aβ) also alters the impact it has on Aβ aggregation, with low zinc concentrations preventing Aβ aggregation and promoting aggregation at higher concentrations (Danielsson et al., 2007), which could explain the toxicity seen at high concentrations. Zinc deficiency is linked to cognitive deficits and is a suspected risk factor for developing AD (Sun et al., 2022). Recently, zinc deficiency has been shown to induce

inflammatory responses in microglia of APP/PS1 mice via the NLRP3 (NACHT, LRR, and PYD domains-containing protein 3) inflammasome (Rivers-Auty et al., 2021), which has been implicated in AD pathogenesis through the release of cytokines, Aβ deposition and NFTs (Bai and Zhang, 2021, Ising et al., 2019). Zinc levels must be tightly regulated in the brain to prevent AD-related pathological changes.

Copper is an essential element that is critical for development of the central nervous system as it is necessary for several key processes including formation of myelin, antioxidant defence (e.g. Cu/Zn SOD), adenosine triphosphate (ATP) synthesis (part of cytochrome c oxidase), and synthesis of neurotransmitters (Scheiber et al., 2014). Copper participates in biochemical reactions, often as part of cuproenzymes, by donating and receiving electrons, cycling between Cu^{+} and Cu^{2+}, with a small pool of copper as free or 'labile' copper. Unlike zinc, copper is redox active; labile copper reacts with O_2 to generate damaging ROS via the Fenton reaction (Figure 1.3) (Kanti Das et al., 2015). Oxidative stress is a key feature of AD, and copper dyshomeostasis may contribute to oxidative stress/damage (see 1.1.4.4). Hydrogen peroxide is generated when Ab is complexed to copper ions, and the morphology of the resulting aggregates changes from fibrillar to amorphous depending on the ratio of copper to peptide(Mayes et al., 2014). The dyshomeostasis of copper has been implicated in several neurodegenerative diseases including Huntington's disease (HD), amyotrophic lateral sclerosis (ALS), Parkinson's disease (PD) and AD (Fox et al., 2007, Sheykhansari et al., 2018, Scholefield et al., 2021). As with zinc, there are conflicting reports on the concentration of copper in the AD brain compared to age-matched controls. Some studies have shown elevated copper in the AD brain (Lovell et al., 1998, Rao et al., 1999), no change (Yoshimasu et al., 1980, Ward and Mason, 1987, Szabo et al., 2015, Corrigan et al., 1993, Religa et al., 2006), or widespread copper deficiencies (Plantin et al., 1987, Scholefield et al., 2020, Andrási et al., 1995, Deibel et al., 1996, Xu et al., 2017, Schrag et al., 2011a, Magaki et al., 2007, Akatsu et al., 2011). However, a recent meta-analysis of 56 studies concluded copper levels decreased in AD brain samples and increased in AD serum/plasma samples relative to healthy age matched controls (Squitti et al., 2021). A deficiency in copper could promote the generation of Aβ, by altering APP proteolysis (Gerber et al., 2017, Cater et al., 2008). Despite an apparent decrease in copper levels, high concentrations (mM) of copper have been found in association with AD senile plaques (Miller et al., 2006, Lovell et al., 1998, Rembach et al., 2013). This abnormal distribution of copper likely leaves other brain regions deficient in copper, and therapeutic interventions to restore a normal copper distribution have been explored, for example PBT2 targets copper as well as modulating zinc (Faux et al., 2010). Both APP and Aβ

have copper binding sites, and the binding of copper to either protein can have pathological consequences (Atwood et al., 2000). When copper binds to APP or Aβ, it is catalytically reduced to Cu^{2+}, and Cu^{2+} ions have been shown to enhance Aβ fibril formation and aggregation under physiological conditions (Faller et al., 2013, Barritt and Viles, 2015). The reduction of copper generates ROS, which could contribute to Aβ oligomer toxicity and neuronal damage (Ejaz et al., 2020). Removal of Cu^{2+} from Aβ prevents the aggregation of Aβ *in vitro*, promotes the degradation of Aβ and precludes the formation of H_2O_2 (Wu et al., 2008). Thus chelation of copper is a potential therapeutic intervention, but a targeted approach focusing on copper in senile plaques would be advantageous in order to not further deplete the already low copper levels in the AD brain.

Iron is the most abundant transition metal in the brain and is involved in important processes throughout the body, most notably as a key component of haemoglobin necessary for oxygen transport in red blood cells (Abbaspour et al., 2014) and as a cofactor for enzymes involved in ATP generation, but also has crucial functions in the brain including the synthesis of neurotransmitters (dopamine and serotonin) (Kuhn et al., 1980, Kaladhar and Narasinga Rao, 1982) and production of myelin (Connor and Menzies, 1996). Iron exists in two states; Fe^{3+} (ferric) iron and Fe^{2+} (ferrous) iron and the ability to transition between the two states makes it an incredibly versatile element. Ferric iron can be reduced to the more toxic ferrous iron which then takes part in Fenton chemistry to generate hydroxyl radicals (Winterbourn, 1995) (Fig.1.3). This is only possible in the case of unbound iron, which is part of the labile iron pool thus levels of free iron must be tightly regulated to prevent toxicity induced by the resulting ROS generation. Excess ROS generation leads to oxidative stress, which if not sufficiently dealt with via antioxidant defences leads to oxidative damage to lipids, nucleic acids, and proteins, eventually leading to a specialised form of cell death known as ferroptosis (Dixon et al., 2012). To prevent this, iron is typically stored in ferritin, haemosiderin, or transferrin iron storage proteins as well as utilised in haemoglobin and neuromelanin (Chiancone et al., 2004). Most iron in the brain is non-heme iron; metalloproteins, low molecular weight complexes, storage proteins, ionic iron, and iron oxides (Haacke et al., 2005). Iron oxide exists in the brain in different forms; ferrihydrite, goethite, hematite, magnetite, maghemite, and wüstite (Collingwood and Telling, 2016). The dyshomeostasis of iron has been implicated in neurodegenerative disease, and iron is a key element in the pathogenesis of AD.

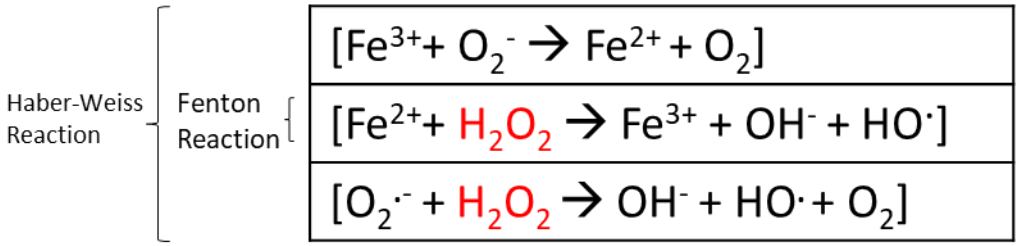

Figure 1.3 Fenton reaction. Ferrous iron reacts with hydrogen peroxide in Fenton's reaction to form a hydroxyl radical (a reactive oxygen species). The Haber-Weiss reaction is catalysed by iron and Fenton's reaction is the intermediate step of the reaction. Both are a source of oxidative stress in cells.

Free iron cannot diffuse across the hydrophobic blood brain barrier (BBB) and, instead, enters the brain via endocytosis into brain capillary endothelial cells using the glycoprotein transferrin (Fishman et al., 1987). Once in the brain, homeostasis of iron is tightly controlled to prevent toxic accumulation of free iron (Fig. 1.4). Ferritin, the primary iron storage protein, is a globular protein composed of 24 subunits (either heavy, H-ferritin or light, L-ferritin) arranged to form an inner core of approximately 8 nm in dimeter (Collingwood and Dobson, 2006). One molecule of ferritin can store 4500 iron atoms, and 90% of non-heme iron is stored as ferritin (Morris et al., 1992). The ferroxidase activity (conversion from Fe^{2+} to Fe^{3+}) of ferritin is conducted via the H-ferritin subunits. The expression of ferritin is controlled by iron regulatory proteins 1 and 2 (IRP1 and IRP2), which are sensitive to cellular iron levels (Zhou and Tan, 2017). IRPs control the expression of ferritin, ferroportin and transferrin receptor mRNA by binding to iron-response elements (IREs) in the untranslated regions of mRNA transcripts, either supressing or enhancing translation in response to iron levels (Rogers et al., 2008). The amyloid precursor protein also possesses an iron response element (IRE), so levels of APP and Aβ are also influenced by iron levels (Rogers et al., 2002). Accumulation of iron may arise as a result of alterations to key proteins involved in iron homeostasis, such as decreased expression of ferritin (Faucheux et al., 2002), dysfunction of ferritin (Cozzi et al., 2010) and/or reduced iron capacity of transferrin (Hare et al., 2015b).

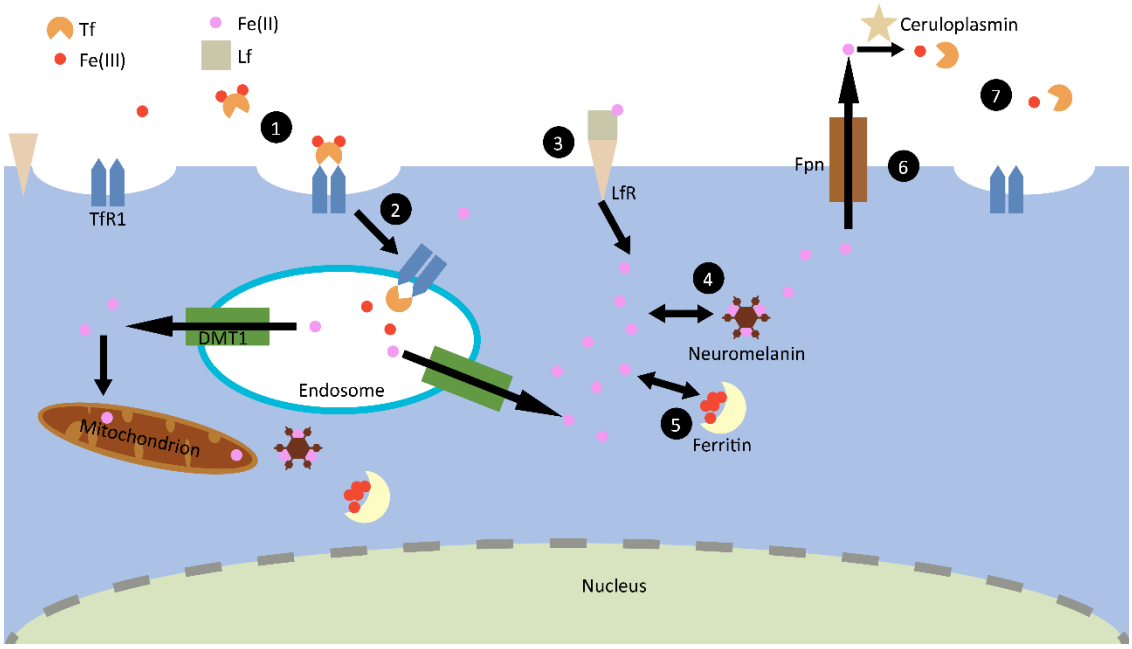

Figure 1.4. Iron homeostasis in the brain. Iron (Fe (III)) and transferrin (Tf) form a complex (1) which then enters the brain via endocytosis, through transferrin receptors (TfR). The Fe-TfR complex passes across the endosomal membrane (2), where iron is released from the complex due to progressive acidification. Fe (III) is reduced to Fe (II) via the ferrireductase six-transmembrane epithelial antigen of the prostate 3 (STEAP3) (Ohgami et al., 2005). Fe (II) passes across the endosomal membrane through DMT1 (divalent metal transporter 1). Fe (II) also enters cells in the form of lactoferrin, which enters via lactoferrin receptors (3). Fe (II) once inside associates with neuromelanin (4) and binds to ferritin (5). Within the ferritin core, Fe (II) is reduced to the less toxic Fe (III) (5). Fe (II) is exported from the neuron via ferroportin (Fpn) (6) where ceruloplasmin oxidises it to Fe (III) (Batista-Nascimento et al., 2012). This Fe (III) is then ready to re-enter the cell associated with Tf (7).

Disrupted iron homeostasis is associated with a number of diseases; iron deficiency (particularly in early age) has been associated with cognitive and developmental delays (Hare et al., 2015a), and anaemia, whilst iron overload has been suggested to play a role in several neurodegenerative diseases (NDDs) including AD and PD (Ashraf et al., 2020, Myhre et al., 2013, Salazar et al., 2006) and is the primary pathological cause of a rare group of inherited neurological disorders known as neurodegeneration with brain iron accumulation (NBIA) (Iankova et al., 2021). Iron levels increase with age, usually plateauing between 40 and 60, but may continue to accumulate in the case of NDD (Hallgren and Sourander, 1958, Bartzokis et al., 1997).

There is a lack of consensus on whether iron levels are altered in the AD brain, with studies reporting increases (Andrási et al., 2000, Andrási et al., 1995, Szabo et al., 2015, Samudralwar et al., 1995, Deibel et al., 1996, Hare et al., 2016, Xu et al., 2017, Schrag et al., 2011a, Lovell et al., 1998, Srivastava and Jain, 2002, Rao et al., 1999), decreases (Ward and Mason, 1987, Andrási et al., 1995, Andrási et al., 2000, Corrigan et al., 1993, Magaki et al., 2007), or no change (Plantin et al., 1987, Wenstrup et al., 1990, Scholefield et al., 2020, Cornett et al., 1998a, Stedman and Spyrou, 1997, Griffiths and Crossman, 1993, Religa et al., 2006, Akatsu

et al., 2011) across different populations using a range of brain regions and methods of analysis. A 2010 meta-analysis of studies comparing iron in AD and control brains noted that the putamen was the only region where iron levels were consistently elevated and that there was a citation bias favouring studies reporting increases in iron in AD (Schrag et al., 2011b). A further meta-analysis in 2014 incorporated additional studies and found iron was elevated in 8 brain regions in AD without any publication bias: frontal lobe, parietal lobe, temporal lobe, amygdala, putamen, globus pallidus, cingulate cortex, and caudate nucleus (Tao et al., 2014).

Dysregulation of metal ions in AD may arise due to a failure of metal transport, leading to increased levels of redox-active metals which induce oxidative stress, a key feature of AD. The failure of metal transport may be due to mutations or functional problems with the APP pathway; presenilins import ~50% of copper and zinc into cells (Bush, 2013) and APP facilitates the export of iron from cells (Duce et al., 2010) so changes in APP cell biology could result in metal imbalances. The brains of AD patients are deficient in copper enzymes (Maynard et al., 2005), and the metal promotes the neuroprotective non-amyloidogenic pathway (Cater et al., 2008), so its deficiency may lead to reciprocally increased Aβ generation.

Metal ions also facilitate the generation of reactive oxygen species *in vivo* (Stohs and Bagchi, 1995) and influence Aβ aggregation. Aβ40 and Aβ42 aggregation is accelerated by aluminium, iron, and zinc but not copper, magnesium, or calcium (Mantyh et al., 1993). Aβ42 is more toxic than Aβ40 due to its greater tendency to aggregate, this is because Aβ42 has a stronger reducing potential, and Aβ toxicity is mediated by the reduction of Cu^{2+} and Fe^{3+} (Bonda et al., 2011). Aβ, α-synuclein and prion protein have also been found to generate hydrogen peroxide when bound to redox-active metal ions, leading to oxidative stress (Allsop et al., 2008, Mayes et al., 2014, Cheignon et al., 2017, Cheignon et al., 2018). The dysregulation of metal homeostasis may be influenced by the incursion of metals from the environment, such as from metal-rich particulate matter (see section 1.2) (Cory-Slechta et al., 2020).

1.1.4.4 Inflammation and oxidative stress in AD

Oxidative stress is the result of an imbalance between the generation of ROS, free radicals, and reactive nitrogen species, and the effectiveness of the cellular antioxidant defence mechanisms. It is a common feature of NDDs and is also increased in association with normal ageing (Harman, 1992). Reactive oxygen species are produced as part of normal metabolism as a by-product of oxygen and are chemically reactive species containing oxygen such as the hydroxyl radical (OH.). As the name suggests, they are highly reactive and cause damage to different cellular components by oxidising them such that electrons are taken from the target

molecule to form a more stable oxygen species. Oxidation of macromolecules disrupts their function and can activate antioxidant response mechanisms. Molecular markers of oxidative damage include 4-hydroxynonenal (lipid peroxidation), carbonyl adducts (protein oxidation), 8 hydroxyguanine (DNA oxidation) and mitochondrial dysfunction (Berlett and Stadtman, 1997, Mylonas and Kouretas, 1999, Markesbery and Lovell, 2006). Oxidative stress in AD arises due to metal dyshomeostasis, Aβ generation and aggregation, and neuroinflammation (microglia generate ROS and reactive nitrogen species) (Mhatre et al., 2004). It is this stress that causes damage to neurons and other cells ultimately resulting in cell death and the cognitive/behavioural symptoms of AD.

1.1.5 AD risk factors

The greatest risk factor for the development of AD is ageing (Kawas et al., 2000). Other risk factors include genetic factors, cardiovascular conditions such as type 2 diabetes, stroke and hypertension, head injury (e.g., from boxing), *APOE* (apolipoprotein E allelic composition), and environmental factors (Plassman et al., 2000, Mayeux et al., 1995, Kivipelto et al., 2001, Bekris et al., 2010, Chen et al., 2017b). Women are approximately 2-3 times more likely than males to develop AD (Niu et al., 2017). The extent to which risk factors influence the development of AD differs depending on age; some factors like education are important from early life, whilst other factors such as hypertension can be more important in middle age (Anstey et al., 2021, Lennon et al., 2019), or from development to old age such air pollution. Air pollution exposure may begin *in utero*(Finch and Morgan, 2020), oocytes are formed in the grandmaternal uterus which can be exposed to ultrafine particles (UFP) (Finch and Morgan, 2020) across the placenta (Liu et al., 2021, Bongaerts et al., 2022) . It is possible that this exposure at a vital time of development could predispose individuals to the development of AD, however this needs to be explored further. Conversely, air pollution exposure in later life has also been attributed to 2% of dementia cases (Livingston et al., 2020).

Fully penetrative gene mutations are associated with FAD and occur in three genes involved in the generation of Aβ: *APP*, *PS1* and *PS2*. A series of such mutations were identified in families with FAD, such as the Swedish double mutation in *APP* in which the lysine and methionine immediately upstream of the β-secretase cleavage site are substituted with asparagine and leucine resulting in enhanced generation of Aβ (40 and 42) (Haass et al., 1995).

Genetic risk factors are also associated with SAD, with a heritability estimate of 58-70% for both males and females (Gatz et al., 2006). The apolipoprotein E ε4 allele is a well-characterised risk factor. The ε4 form aids Aβ deposition as it promotes fibrilization and plaque

formation (Corder et al., 1993, Kim et al., 2009) whereas the normal function of apolipoprotein is to transport lipids between cells and tissues (Mahley and Rall, 2000). The risk of developing AD increases 3-fold in *APOE* ε4 heterozygotes and 15-fold in homozygotes (Farrer et al., 1997). The search for other risk genes associated with SAD has identified other candidates from genome wide associated studies (GWAS), such as triggering receptor expressed on myeloid cells (*TREM2*) (Liu and Yu, 2019). *TREM2* in the central nervous system (CNS) is primarily expressed by microglia and plays a role in immunological signalling cascades to stimulate proliferation, phagocytosis, pro-inflammatory responses, and rearrangement of the cytoskeleton amongst other functions. Mutations in *TREM2* such as the rare R47H variant have been associated with a loss of protein function and a 3-fold increased risk of developing AD (Jonsson et al., 2013).

AD rarely occurs without another co-morbidity, the majority of which are vascular related such as stroke. The brain is highly vascularised with cerebral blood flow (CBF) tightly regulated to meet a high oxygen demand. A decrease in CBF is associated with AD and many other neurodegenerative diseases, along with disruption to the BBB (Korte et al., 2020). In AD, these vascular changes may arise as a consequence of neuronal death but may also contribute to cognitive decline and disease progression as they promote Aβ aggregation (Rius-Pérez et al., 2018).

AD has also been described as 'Type 3 diabetes' due to the dysregulation of glucose metabolism and insulin signalling seen in the afflicted brain (de la Monte and Wands, 2008). Obesity and Type 2 diabetes are both risk factors for AD, probably due to the role that altered insulin signalling may play in Aβ aggregation and toxicity, coupled with insulin-resistance in the brain leading to disruption of glucose metabolism and energy provision (Nguyen et al., 2020).

Social and environmental factors are also thought to contribute to the risk of developing AD. A lack of education, depression and social isolation have all been suggested as risk factors, stemming from a reduction in cognitive challenges which increases the risk of cognitive decline (Dotson et al., 2010, Sharp and Gatz, 2011). Various environmental factors such as exposure to air pollution, exposure to environmental toxins (e.g., pesticides), or smoking have also been linked to an increased risk of developing AD (Livingston et al., 2020). Environmental toxins such as air pollution that accelerate the ageing processes have been termed gerogens (Finch and Morgan, 2020). Exposure to hazardous chemicals/compounds may increase oxidative stress in the brain, or act via other toxic mechanisms to accelerate ageing and/or

cause neuronal damage as seen in AD (Chin-Chan et al., 2015). For example, magnetite (an iron oxide which is released from diesel exhaust engines, amongst other sources) has been found in the brains of individuals with AD (Maher et al., 2016), inside senile plaques (Everett et al., 2018), and can accelerate the aggregation of Aβ (Mir et al., 2012). The interplay of genetics and the environment (G X E) influence a person's risk of developing AD (Finch and Morgan, 2020). For example, epidemiological studies have demonstrated that *APOE* ε4 carriers/homozygotes are more susceptible to air pollution-associated AD risk enhancements (Cacciottolo et al., 2017, Kulick et al., 2020).

The *Lancet* commission recently reported three new modifiable risk factors for dementia (Livingston et al., 2020); excessive alcohol consumption (1%), traumatic brain injury (3%) and air pollution (2%), in addition to the 9 previous factors they reported in 2017; lower education attainment (7%), hypertension (2%), hearing impairment (8%), smoking (5%), obesity (1%), depression (4%), physical inactivity (2%), diabetes (1%) and low social contact (4%) (percentages shown refer to the reduction in dementia prevalence if the risk factor was eliminated) (Livingston et al., 2017). Collectively, these modifiable risk factors account for 40% of dementia worldwide (Livingston et al., 2020)

1.2 Air pollution and AD

Air pollution is a complex mixture of pollutants of varying size in both the gaseous and particulate states. Components of air pollution include but are not limited to; particulate matter (PM), black/elemental carbon (BC) carbon monoxide (CO), ozone (O_3), sulphur dioxide (SO_2) and nitrogen dioxide (NO_2). Both indoor air and outdoor (ambient) air can be polluted, though typically from different sources. Indoor air pollution is often associated with cooking and heating, such as the use of indoor fires whilst ambient air pollution is primarily a representation of anthropogenic activities in the wider world such as transport and industry. Chronic and acute exposure to both indoor and ambient air pollution is linked to negative cardiovascular, neurological, and pulmonary outcomes, but the focus in the current study will be on ambient air pollution and PM.

Over 99% of the world's population are exposed to ambient air pollution levels above the World Health Organisation's (WHO) recommended annual limits, with an estimated 4.6 million premature deaths attributed to such exposure in 2016 (WHO, 2021a). The impact of air pollution on health is not limited to mortality; a wealth of pre-existing conditions such as asthma and allergies are exacerbated by exposure to such high levels of air pollution.

Epidemiological studies have suggested a link between exposure to air pollution (particularly traffic-related pollution) and the incidence of neurodegenerative diseases including AD (see 1.2.2). Furthermore, air pollution is known to exacerbate many of the risk factors associated with AD such as cardiovascular disease, so may act to increase risk of AD both directly and indirectly (Livingston et al., 2020). This is particularly relevant in relation to our changing climate; the incidence of AD in Europe attributed to air pollution could rise from 4.8% at present, to 9.7% by 2050 (Guzmán et al., 2022). Air pollution is estimated to cost NHS England £5.56 billion between 2017 and 2035, with an estimated annual cost of over £7000 per case of dementia across health and social care (Pimpin et al., 2018). Reduction of air pollution could reduce this financial and social care burden; it has been estimated that a reduction in air pollution exposure by 1 $\mu g/m^3$ in Sweden could reduce the financial burden of dementia in the country by 13-15% as a result of a 12% decrease in dementia cases attributed to the phenomenon (Kriit et al., 2021).

1.2.1 Particulate matter (PM)

The solid and liquid droplets suspended in air pollution are collectively termed particulate matter (PM). PM can be divided by the aerodynamic particle diameter; coarse particles with a diameter 2.5 – 10 µm (PM_{10}), fine particles with a diameter 0.1 - 2.5 µm ($PM_{2.5}$), and ultrafine particles with a diameter <0.1 µm ($PM_{0.1}$). PM is a consequence of the natural and anthropogenic activities in the surrounding environment. Natural contributors include soil, windblown dust, pollen, endotoxins (bacteria), viruses, volcanic eruptions, sea water spray, and forest fires. Anthropogenic sources of ambient PM include burning of fossil fuels, vehicle exhaust fumes, aviation, smoking, brake wear, tyre/road surface debris, resuspension of road dust, and industrial/manufacturing processes. In terms of chemical composition, metals are major components of PM, e.g., Fe, Cr, Cu, Mn, Ni, Pb, Al, Zn, and V have been reported in PM from different sources (Gonet et al., 2021a, Wiseman et al., 2021, Osornio-Vargas et al., 2003). The presence of Ca, Na, Al, Fe, and/or K is often attributed to soil/natural sources (Yatkin and Bayram, 2007). Elements like Fe are present in the natural environment and produced from anthropogenic sources, so it is challenging to specify the origin or source apportionment of each element within the complex PM mixture. Volatile organic compounds such as polyaromatic hydrocarbons (PAHs) are also often present in PM, adsorbed to particles. The composition of PM varies by location on a local, national, and international scale due to differences in geography (affecting natural components of PM) and differences in human activity. PM composition is also influenced by season and climate. Collectively, these factors alter PM composition, which in turn alters the resultant toxic effects (see 1.5) (Osornio-Vargas

et al., 2003, Gustafsson et al., 2019, Gualtieri et al., 2009, Johansson et al., 2007, He et al., 2020).

Safe levels of PM (quantified in terms of μg/m^3 air) are conventionally regulated according to the PM mass concerned. The current WHO recommended annual mean limits are 5 μg/m^3 for $PM_{2.5}$ and 15 μg/m^3 for PM_{10} (WHO, 2021a). These recommendations are routinely exceeded on a global scale and are rarely enshrined in law. In the UK, the Air Quality Standards Regulations 2010 set the legal limits to 25 μg/m^3 for $PM_{2.5}$ and 40 μg/m^3 for PM_{10} (Environmental Protection Agency, 2010). However, mass-based regulations do not take in to account the number of particles to which a person is exposed. In this respect, UFPs represent the vast majority of particles within PM (estimated 90-99.9% of total particles (Meng et al., 2013, Johansson et al., 2007)). However, due to their small density, they contribute the least in terms of mass; a PM mass of 10 μg m^3 could correspond to 2.4 x10^6 20 nm particles or just a single 2.5 μm particle/m^3 (Oberdorster et al., 1995). UFPs can also penetrate further into tissue (see 1.3) and have been reported to have higher toxicity than their larger counterparts, due to their high surface area reactivity (Oberdörster et al., 1994).

When referring to UFPs, particle number counts (PNCs) are typically reported instead of mass-based exposures. However, there is a poor relationship between $PM_{2.5}$ and PNC; reducing one does not necessarily reduce the other (de Jesus et al., 2019). Using PM_{10} and $PM_{2.5}$ to monitor pollution levels and estimate health risks is, therefore, an outdated set of metrics and newer metrics are needed to account for UFP exposure and to account for other pollution sources such as non-exhaust emissions (NEE) and road-deposited dust. Furthermore, as PM is heterogenous, blanket regulations for a country are also inappropriate given that PM composition can vary dramatically, so a more regional approach would also be beneficial.

PM (particularly UFP) can cause damage to virtually any part of the cell resulting in DNA damage, oxidative stress, compromised membrane integrity, and altered mitochondrial metabolism (Figure 1.5).

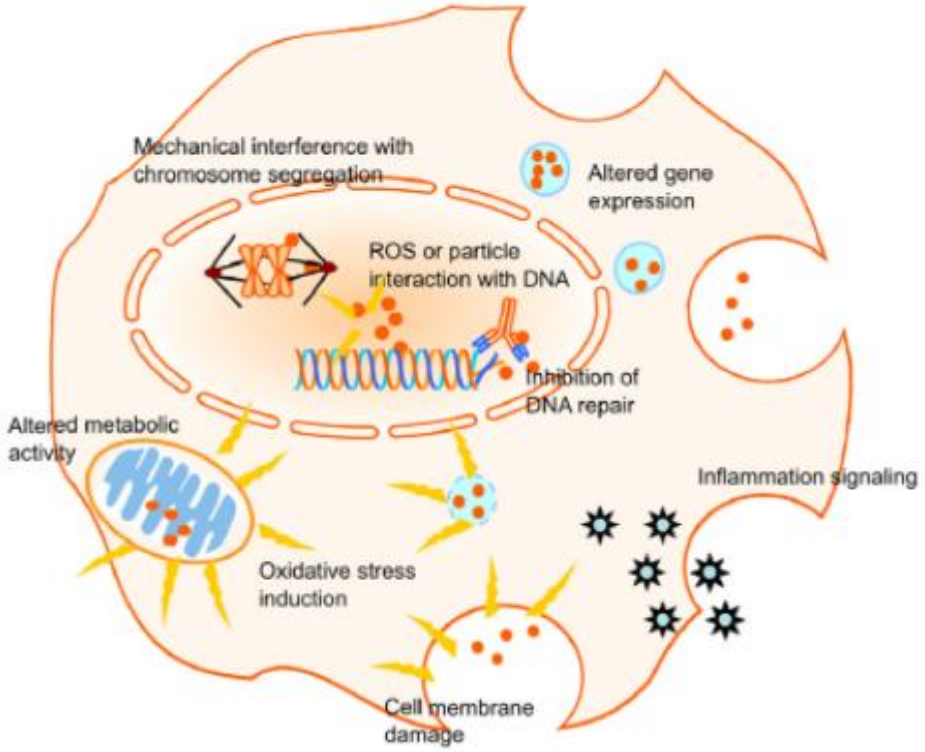

Figure 1.5 Cellular mechanisms of nanoparticle-induced damage. Ultrafine particles (UFPs) or nanoparticles enter cells via endocytic mechanisms and/or interact with cell surface receptors. Once taken up by the cell, UFPs can cause oxidative damage to lipids, proteins, and DNA either through direct interaction or by generation of reactive oxygen species (ROS). Damaged proteins and lipids alter the integrity of the cell membrane and damage organelles such as the mitochondria. When in a state of oxidative stress, the cell can release cytokines as part of a pro-inflammatory response. At high and/or persistent exposure levels, UFPs can change tissue function, cause damage, and potentially lead to cell death. Figure taken from (Colognato et al., 2012)

1.2.2 Epidemiological studies

The effect of air pollution exposure on the risk of dementia and AD has been examined in numerous epidemiological studies across the world, including the UK (Carey et al., 2018, Pimpin et al., 2018, Dimakakou et al., 2020, Tonne et al., 2014), US (Shi et al., 2021, Shi et al., 2020, Wang et al., 2021, Chen et al., 2015, Iaccarino et al., 2021, Shaffer et al., 2021, Kulick et al., 2020, Wilker et al., 2015, Younan et al., 2019, Cacciottolo et al., 2017, Rhew et al., 2021), Germany (Ranft et al., 2009), Taiwan (Chang et al., 2014, Jung et al., 2015), Canada (Chen et al., 2017a, Yuchi et al., 2020), Mexico (Salinas-Rodríguez et al., 2018), Hong Kong (Ran et al., 2021), Sweden (Grande et al., 2020, Oudin et al., 2016, Åström et al., 2021, Oudin et al., 2017, Oudin et al., 2019), Spain (Sunyer et al., 2015), and France (Mortamais et al., 2021), with the majority of studies reporting increased risk of dementia with increasing exposure to air

pollution. However, a meta-analysis of 66 articles published up until 31st December 2020 concluded that there was substantial heterogeneity in the findings of air pollution and dementia studies, with several methodological limitations across the studies, including poor spatial resolution of air pollution exposure, single measurements at one moment in time rather than longitudinal studies over time, limited residential data or not accounting for migration, relying on medical records rather than clinically validated dementia diagnoses, and potential selection bias (Weuve et al., 2021). The authors concluded that on balance there was some suggestion of a connection between dementia risk and air pollution with the strongest evidence pertaining to $PM_{2.5}$ and cognitive decline (Weuve et al., 2021). The findings of some of these studies, which focus on AD/dementia risk and $PM_{2.5}$ or NO_2, are summarised in Table 1.1.

Table 1.1 Air pollution and associated hazard ratio (HR) of developing Alzheimer's disease (AD) or unspecified dementia (DU).

Country	N	Dementia	HR	Pollutant	Mean conc.	Reference
US	12,456,447	AD	1.08	$PM_{2.5}$	9.3 μg/m^3	(Shi et al., 2021)
US	12,456,447	AD	1.03	NO_2	17.1 ppb	(Shi et al., 2021)
US	4,166	AD	1.11	$PM_{2.5}$	10.1 μg/m^3	(Shaffer et al., 2021)
US	4,166	DU	1.16	$PM_{2.5}$	10.1 μg/m^3	(Shaffer et al., 2021)
Hong Kong	57,775	DU	1.20	$PM_{2.5}$	35 μg/m^3	(Ran et al., 2021)
UK	130,978	AD	1.10	$PM_{2.5}$	15.7 μg/m^3	(Carey et al., 2018)
UK	130,978	AD	1.23	NO_2	37.1 ppb	(Carey et al., 2018)
France	7,066	AD	1.20	$PM_{2.5}$	15-36 μg/m^3	(Mortamais et al., 2021)
Sweden	2,927	DU	1.54	$PM_{2.5}$	8.4 μg/m^3	(Grande et al., 2020)
Sweden	2,927	DU	1.14	NO_x	25.9 μg/m^3	(Grande et al., 2020)
Sweden	1,806	AD	1.38	NO_x	26 μg/m^3	(Oudin et al., 2016)
Sweden	1,567	AD	1.53	NO_x	26 μg/m^3	(Oudin et al., 2019)

Aside from dementia risk, other metrics have been used to explore the relationship between air pollution and AD, such as measures of cognition, brain volume and Aβ plaque counts/locations. A US study reported that for each increase in 3.27 μg/m^3 exposure to $PM_{2.5}$, there was a 0.11 year faster decline in episodic memory in individuals who typically have a slow decline in episodic memory (Wang et al., 2021). Similarly, another US study reported that each increase of 2.81 μg/m^3 $PM_{2.5}$ was associated with an acceleration of 19.3% in the annual decline rate for trials 1-3, and 14.8% for list B (types of memory tests) (Younan et al., 2019),

whilst a UK study reported that a 1.1 μg/m^3 increase in $PM_{2.5}$ was associated with a decline of 0.03 over 5 years in standardised memory scores (Tonne et al., 2014).

The apparent changes in memory and cognition associated with air pollution may be due to structural changes in the brain. Schikowski (2015) found that air pollution measurements were cross-sectionally associated with lower cognitive scores in semantic memory and visual processing tests, suggesting that visuospatial regions of the brain are affected by traffic-related air pollution. Furthermore, a decrease in white matter volume in the total brain, and association areas (average 6.23 and 4.47 cm^3 respectively) was reported with each cumulative exposure to 3.49 μg/m^3 $PM_{2.5}$ in a study of 1403 US residents, roughly equivalent to 1-2 years of brain ageing (Chen et al., 2015). In addition to gross pathological changes, amyloid positron emission topography (PET) scans for Aβ plaques have been used to explore the relationship between AD and air pollution; the odds ratio (OR) for a positive scan with each increase of 4 μg/m^3 increase in $PM_{2.5}$ was 1.10 (1.05-1.15) for the 2002-2003 period and 1.15 (1.05-1.26) for the period 2015-2016 (Iaccarino et al., 2021).

Although many studies look at air pollution or $PM_{2.5}$ in general, there has also been a focus on traffic-related air pollution (TRAP) and AD, particularly through examining the risk of living in close proximity to major roads. A large population-based study of over 2 million Ontario residents found a 7-11% increased risk of developing dementia for those living near (<50m) major roads (Chen et al., 2017b). Another Canadian study reported a 3-15% increase in dementia risk depending on road type, with a 9% increase in non-Alzheimer's dementia for every additional 1.5 μg/m^3 $PM_{2.5}$ exposure (Yuchi et al., 2020). Taken together, these studies suggest a potential increase in risk of dementia with increasing exposure to air pollution (in particular $PM_{2.5}$) which can manifest as structural changes in the brain and be observed with brain imaging and cognitive tests.

An individual's risk of developing AD is likely to be mitigated by the interaction between their environment (e.g., traffic exposure) and other genetic risk factors. *APOE* has been suggested to play a role in gene-environment interactions for dementia (Finch and Morgan, 2020), particularly in regions with high levels of pollution such as Mexico City (Calderón-Garcidueñas and de la Monte, 2017). The mechanism by which these interactions result in the neuropathological changes seen in dementia is unknown but has been suggested to involve a shared inflammatory mechanism between air pollution exposure and *APOE* ε4 (Kulick et al., 2020). Female carriers of *APOE* ε4 alleles have been reported to be more susceptible to the air pollution related risk of developing dementia, and cognitive decline (Schikowski et al.,

2015, Cacciottolo et al., 2017, Kulick et al., 2020). Schikowski *et al.* (2015) demonstrated that the detrimental effects of traffic load and $PM_{2.5}$ on cognitive function were only observed in women with at least one *APOE* ε4 allele, suggesting *APOE* genotype may regulate vulnerability to environmental exposures. Associations between cognitive decline, *APOE* ε4 alleles, and air pollution exposure were also reported in a US study of 3647 women (Cacciottolo et al., 2017). A 21% acceleration in cognitive decline and dementia was attributed to high residential $PM_{2.5}$ exposure (above 12 μg/m^3 US EPA, environmental protection agency, standard), and the incidence of both dementia and global cognitive decline varied significantly by *APOE* genotype; *APOE* ε4 homozygotes (4/4) > *APOE* ε4 heterozygotes (3/4) > non-carrier of *APOE* ε4 (3/3). Similarly, a study of 4821 Manhattan residents found a faster rate of cognitive decline in residents with at least one *APOE* ε4 allele, with increasing exposure to air pollution (median $PM_{2.5}$ exposure 15 μg/m^3) (Kulick et al., 2020). There were no differences when stratifying by sex, but race-ethnicity did have a significant impact with no effect of *APOE* ε4 on cognitive decline in non-Hispanic Black residents. In contrast to these three studies, Oudin *et al.* (2019) found no effect of the *APOE* ε4 allele on dementia risk in a Swedish cohort of 1567 participants. Like the Manhattan study, both male and female participants were included, and when stratifying by sex there was no difference in the outcome. The authors suggest their results may be specific to their studied cohort, as the distribution of *APOE* ε4 varies across populations (Oudin et al., 2019). Furthermore, Kulick et al reported difference in air-pollution related *APOE* ε4 risk of cognitive decline varied with race-ethnicity (Kulick et al., 2020), so the Swedish population may be less susceptible to the risks. Ambient air pollution levels varied significantly across the studies, with the Swedish cohort being exposed to the lowest level of pollution (<8 μg/m^3) (Oudin et al., 2019), the US studies mid-range (>12 μg/m^3) (Cacciottolo et al., 2017, Kulick et al., 2020), and the German cohort being exposed to the highest levels of pollution (33.3 μg/m^3 1995 baseline, 17.4 μg/m^3 2007 follow-up) (Schikowski et al., 2015). It is therefore possible that the modifying effect of *APOE* ε4 on air pollution-related dementia risk and/or cognitive decline is only present with high exposure scenarios, as seen in Ruhr (Schikowski et al., 2015) and Mexico City (Calderón-Garcidueñas and de la Monte, 2017). Caution must be taken when comparing these works, as different statistical approaches were used, different modelling and spatial resolution of pollutant exposures, different measures of impact (i.e., dementia risk or cognitive decline), different cognitive testing approaches, and they were conducted in different locations so may be subject to different sociocultural backgrounds. However, there is some emerging evidence suggesting a link between *APOE*

genotype and risk of dementia/ cognitive decline in areas of high air pollution exposure, which warrant further investigation.

The majority of epidemiological studies focus on mainly white populations, and higher income countries, ignoring lower- and middle-income countries (LMIC) which are home to approximately two thirds of people living with dementia globally (Patterson, 2018). The higher prevalence of dementia in LMICs may be due to genetic and race-ethnicity susceptibility factors but is also likely due to the higher prevalence of modifiable risk factors in these countries, such as lack of secondary education and exposure to the highest levels of air pollution globally. For example, a 2021 study found that in 2015, 55% of Latin American sub-cities had a mean $PM_{2.5}$ exposure above the WHO limit (10 μg/m^3 at the time of study) and, in Mexico in particular, 65% of those aged <5, 70% >65 and 67% of the population of any age were exposed to $PM_{2.5}$ above the WHO limit (10 μg/m^3 at the time, now 5 μg/m^3) (Gouveia et al., 2021). A cross-sectional study of elderly residents in Mexico found that those in areas of high $PM_{2.5}$ exposure had decreased cognitive functioning and, for every 10 μg/m^3 increase in $PM_{2.5}$, the likelihood of a lower score on the three-word memory test significantly increased (Salinas-Rodríguez et al., 2018).

Although air pollution regulations in Latin America and the Caribbean (LAC) are generally lax, with little data acquired from ground site monitoring, it has been estimated that the improvement of air quality in the region together with the elimination of other risk factors like obesity and hypertension could eliminate up to 56% of dementia cases (Dos Santos et al., 2021).

1.2.3 Exposure to Mexico City air pollution and AD

Mexico City is a so-called megacity with a dense urban population of over 9 million (within the Mexico City Metropolitan area of over 20 million residents) (INEGI, 2020), which has served as a site of interest in AD and air pollution studies due to the historically high levels of air pollution in the city. In 1992, Mexico City was declared the most polluted city in the world by the United Nations and WHO (World Health and Global Environment Monitoring, 1992) but since then levels of air pollution have slowly declined in response to significant mitigation measures (Molina et al., 2019, Molina, 2021). However, Mexico City remains one of the most polluted cities in the world and, in fact, levels of lead in Mexico City street dust have not declined in the past decade, despite the introduction of unleaded petrol over 30 years ago (Morales et al., 2020). Although petrol in Mexico City no longer contains lead, the number of vehicles in use had increased by 159% in 2015. In addition, another source of vehicle-derived

lead, brake pads, could be responsible for the high levels of the metal, particularly in road dust, and its increased environmental persistence (Morales et al., 2020). Average annual $PM_{2.5}$ and PM_{10} levels for Mexico City in 2018 were 22 and 47 $\mu g/m^3$ respectively, over twice the WHO guidelines at that time (10 and 20 $\mu g/m^3$ respectively) (SEDEMA, 2021).

Magnetite nanoparticles (MNPs) are one component of PM which have been identified as potentially hazardous and associated with NDD (see section 1.4). MNPs which bear a striking similarity to environmental combustion and friction derived NPs (CDNPs), have been reported in frontal lobe tissue from Mexico City residents (ages 3-85) and elderly Manchester (UK) residents (ages 62-92) (Maher et al., 2016) (Figure 1.6). The study showed that younger Mexico City residents (<40 years) had high concentrations of MNPs, often comparable to or even exceeding those observed in the elderly Manchester cohort. The authors also reported that the rounded particles originated from the environment and, potentially, entered the brain via the olfactory bulb (Maher et al., 2016) (see 1.3.1). CDNPs have also been found in heart tissue, primarily the left ventricle, from children, dogs, and young adult Mexico City residents exposed to high levels of PM (Calderón-Garcidueñas et al., 2019b). Higher concentrations (up to 22 billion NPs/g ventricular tissue) were reported in Mexico City samples (~2-10x) than control tissue samples. Structural abnormalities were observed in the mitochondria, associated with 10-30 nm MNPs, along with up-regulation of left ventricle cellular prion protein (PrP^C) levels, a marker of oxidative stress (Calderón-Garcidueñas et al., 2019b). As such, exposure to high levels of MNPs could contribute to the pathogenesis of cardiovascular disease, as well as AD.

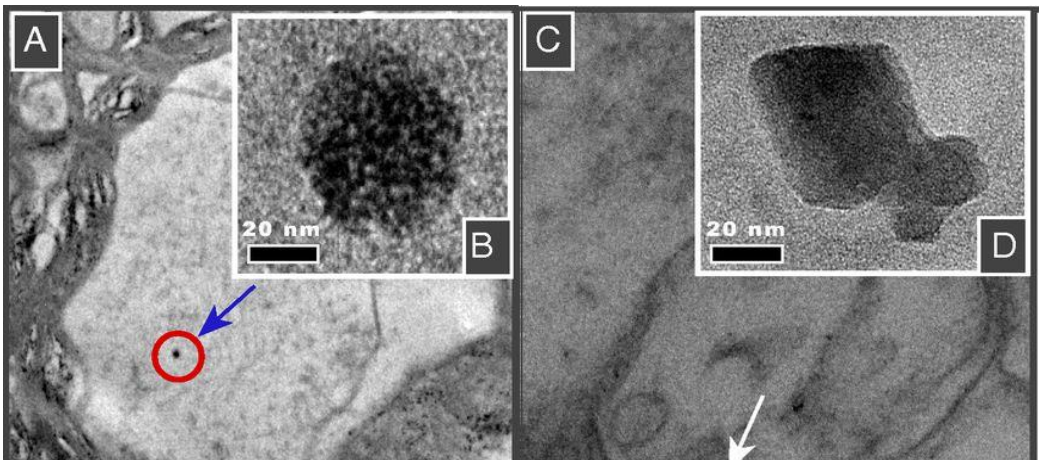

Figure 1.6 Magnetite nanoparticle morphologies in human brain tissue. Magnetite nanoparticles (MNPs) are strongly magnetic mixed Fe^{2+}/Fe^{3+} iron oxide particles with diameters ≤100 nm. Transmission electron micrographs of thin sections of frontal tissue from Manchester, UK and Mexico City, Mexico residents highlight two different morphologies of particles; rounded particles (A, higher magnification B) thought to have originated from combustion and friction processes under high temperature, and angular or euhedral particles (C, higher magnification D) thought to form in situ. The identification of magnetite as the iron oxide species was confirmed by EELS spectra. Adapted from (Maher et al., 2016).

Key pathological hallmarks of AD and PD have been found in lifelong residents of Mexico City, as young as 11 months of age (Calderón-Garcidueñas et al., 2018a, Calderón-Garcidueñas et al., 2018b). Hyperphosphorylated tau was observed in the brainstem of an 11-month-old baby estimated to have been exposed to 20 $\mu g/m^3$ cumulative $PM_{2.5}$ (Calderón-Garcidueñas et al., 2018a). The estimate of cumulative PM includes intrauterine life, as air pollution nanoparticles have been identified in macrophage-enriched placental cells isolated from human placenta (Liu et al., 2021), and in cord blood (Bongaerts et al., 2022), indicating exposure to PM begins *in utero*(Liu et al., 2021). However, the 11-month-old child is a single case i.e., n=1, so it is important to examine further cases at this early stage of life to see if the presence of AD hallmarks (following high PM exposure) is a population-wide phenomenon. Aβ 17-24 and p-tau were present in 202 of 203 forensic autopsies of young Mexico City residents (age 25.36 ± 9.23 y), as were inflammatory markers (e.g., IL1, NF-κB, TNFα, IFN, and TLRs) and α-synuclein (Calderón-Garcidueñas et al., 2018a, Calderón-Garcidueñas et al., 2018b, Calderón-Garcidueas et al., 2012). Decreased levels of $A\beta_{1-42}$ and brain derived neurotropic factor (BDNF) in cerebrospinal fluid (CSF) of Mexico City residents (Calderón-Garcidueñas et al., 2016a) mirrors a study by Forlenza *et al.* (2015) where lower levels of BDNF were reported in CSF from AD patients compared to healthy controls, and disease progression was associated with lower CSF BDNF levels, lower CSF $A\beta_{1-42}$ levels, and with lower MMSE scores (Forlenza et al., 2015).

Epigenetic gene regulation is one proposed mechanism linking air pollution to AD; lower levels of H3K9me2/me3 (repressive post-translational modifications observed in AD patients (Mansuroglu et al., 2016)) were found in the brains of Mexico City residents compared to low-exposure control brains, along with the presence of hyperphosphorylated tau, Aβ plaques, and CDNPs (Calderón-Garcidueñas et al., 2020b). Neither Aβ nor p-tau were observed in control samples.

Cognitive, behavioural, and pathological hallmarks of AD have been recorded in young Mexico City urbanites exposed to high levels of air pollution (Calderón-Garcidueñas et al., 2020d). The authors demonstrated that approximately 75% of otherwise clinically healthy lifelong residents (age 21.03 ± 5.76 y) of Mexico City, Villahermosa or Reynosa exhibited gait and balance dysfunction as measured by Berg and Tinetti tests (Calderón-Garcidueñas et al., 2020d). Gait and balance are functions co-ordinated by the brainstem, and are also altered in NDD (Wennberg et al., 2017). The brainstem is a site of AD/PD pathology (Grinberg et al., 2011), and markers of NDD pathology (e.g., p-Tau, Aβ, α-synuclein) have been extensively reported in the brainstems of Mexico City residents (Calderón-Garcidueas et al., 2012,

Calderón-Garcidueñas et al., 2016a, Calderón-Garcidueñas et al., 2011, Calderón-Garcidueñas et al., 2021a). Impaired cognition has also been reported in Mexico City urbanites (age 21.6 ± 5.88 y) with 55% of participants exhibiting Montreal Cognitive assessment scores indicative of MCI or dementia (Calderón-Garcidueñas, 2019 #1180}.

Post-traumatic stress disorder (PTSD) is thought to increase the risk of developing dementia, whilst rapid eye movement sleep behaviour disorder (RBD) has been documented in dementia patients (Nilaweera et al., 2020). Mexico City residents with PTSD have been shown to be at an increased risk of RBD (Calderón-Garcidueñas et al., 2021a). The olfactory bulb is a proposed route of entry to the brain for environmental NPs, and olfaction is altered in AD patients (Attems et al., 2014) (see 1.3.1.). Reduced olfactory function was reported in Mexico City residents; 12% of controls had olfaction deficits in comparison to 35.5% of Mexico City residents who scored significantly lower on a smell test (University of Pennsylvania Smell Identification Test, UPSIT) (Calderón-Garcidueñas et al., 2010).

Whilst there is a growing body of evidence suggesting a connection between air pollution exposure in Mexico City residents, and development of NDD, many of the pathological studies have relatively small case numbers, suffer from a lack of suitable 'controls,' and would benefit from comparisons with studies of young urban and rural residents from other cities around the world. It is virtually impossible to have a control for these types of exposure studies owing to the number of potentially confounding genetic and environmental differences between subjects, so a compromise is reached by using subjects from areas with lower PM exposures.

1.3 Entry of environmental nanoparticles into the brain

The brain is protected by the BBB, a protective cellular barrier that isolates the brain from the rest of the body and regulates the passage of substances in and out of the brain (Zhou et al., 2018). The BBB is a highly impermeable barrier, composed primarily of specialised endothelial cells that form blood vessels in the brain, so transport of NPs directly across the BBB is perhaps not the most likely route of entry into the brain, although this has been shown to be possible for particles <200 nm (Smith et al., 2016). UFPs administered intravenously failed to cross the BBB of rats (Gulyaev et al., 1999), and the modification of NPs to facilitate crossing of the BBB is one of the major technical challenges within nanomedicine (Zhou et al., 2018). However, it is worth noting that, with age and disease, the integrity of the BBB is compromised (Montagne et al., 2015, Erdő et al., 2017, Sweeney et al., 2018) and air pollution NPs may increase permeability (Oppenheim et al., 2013, Calderón-Garcidueñas et al., 2008) facilitating their transit across the BBB (Oberdörster et al., 2004). Alternatively, NPs may avoid the BBB by

directly penetrating the olfactory bulb following inhalation (1.3.1). Other pathways linking NP exposure to their presence in the brain include the lung-brain axis (section 1.3.2) and gut-brain axis. In addition to physical translocation of NPs to the brain, the release of biological factors (such as cytokines) and interaction with the autonomic nervous system (ANS) in response to pollutants also play key roles in mediating the resulting neurological effects (Snow et al., 2018, Liao et al., 2020, Chen et al., 2018).

1.3.1 Nose to brain transport

The nasal mucosa is the first cellular barrier to NP incursion following inhalation and is composed of respiratory epithelium and olfactory epithelium which is directly linked to the olfactory bulb in the brain through the trigeminal and occipital nerves (Figure 1.7). In addition to the physical barrier, mucociliary clearance mechanisms are in place to clear inhaled NPs from the respiratory tract e.g., cilia, mucus, and sneeze/coughing reflexes (Kirch et al., 2012), as well as innate and adaptive immune responses which can be induced by the release of signalling molecules from the nasal epithelium such as cytokines and growth factors (Parker and Prince, 2011). A decline in the function of these protective mechanisms as seen with age, disease and/or air pollution exposure (Chason et al., 2018, Calderón-Garcidueñas et al., 2001, Steelant et al., 2016), can result in greater penetration of particles into tissue, and fewer clearance or antioxidant mechanisms can result in large numbers of (toxic) particles in sustained contact with cells of the respiratory tract.

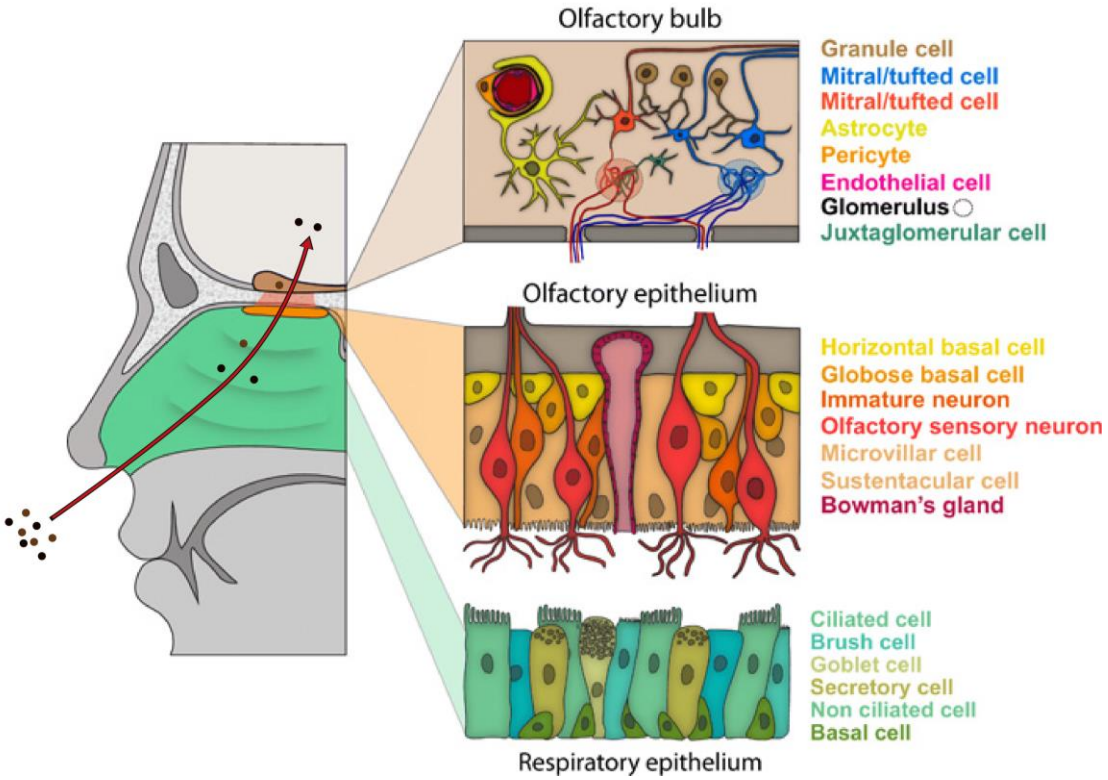

Figure 1.7 Structure of the olfactory pathway. Sagittal view of the human nasal cavity which is composed of respiratory epithelium (green) and olfactory epithelium (orange), which connect to the olfactory bulb (brown). Major cell types in the epithelial tissue are shown. The sustentacular cells play a key role in detoxification of inhaled toxicants and may act in a phagocytic capacity to remove cell debris (Doty, 2015). The olfactory bulb is connected to the nasal cavity environment via olfactory sensory neurons. Adapted from (Brann et al., 2020).

The olfactory bulb (OB) is in contact with the external environment, providing a direct entry route to the brain for environmental particles including viruses, bacteria and UFPs. Smaller particles (<1-2 nm) deposit more efficiently in the olfactory region than larger particles (≥3 nm) (Garcia et al., 2015). Transport pathways from the nose to the brain include axonal transport via olfactory neurons (Oberdörster et al., 2004, De Lorenzo, 1970), axonal transport via the trigeminal nerve (Lewis et al., 2005), paracellular or transcellular transport via olfactory sustentacular epithelial cells (Calderón-Garcidueñas et al., 2003, Gartziandia et al., 2016) and travelling in systemic circulation and penetrating the BBB (Wallenborn et al., 2007). For example, 50 nm gold particles (De Lorenzo, 1970), 36 nm carbon NPs (Oberdörster et al., 2004), and 15 nm CdSe/ZnS quantum dots have been detected in the OB or olfactory nerves, thought to have occurred as a result of axonal transport (Hopkins et al., 2014). Particles up to 200 nm in size can undergo transcellular transport following nasal inhalation (Madane and Mahajan, 2016). The method of transport is likely highly dependent on the physicochemical composition of the particles; graphene oxide (GO) nanosheets (large, 1-35 um; small, 29 nm – 1.9 um; ultrasmall, 10 – 550 nm) translocated from the nose to the brain in mice, in a size-dependent manner, with translocation of ultrasmall GO detected in all regions measured (cortex, hippocampus, striatum, OB, cerebellum, pons, medulla), with a gradient of particle

concentration from the OB to distal sites (Newman et al., 2020). Translocation happened within 3h, which the authors suggest may have occurred via transcellular or paracellular transport via the sustentacular olfactory cells (Newman et al., 2020).

The OB has been proposed as a portal of entry into the brain for environmental NPs (MNPs and CDNPs) (Maher, 2019, Maher et al., 2016, Calderón-Garcidueñas et al., 2010, Calderón-Garcidueñas et al., 2019a). NPs in the brain, particularly metal NPs, may exert toxic effects via inducing protein misfolding, activating pro-inflammatory responses and/or causing oxidative stress/damage to cells. UFPs have been found in the OB of children and young adults (< 25 y) in Mexico City, accompanied by the presence of α-synuclein in OB neurons and up-regulation of antioxidant and pro-inflammatory markers (COX2, IL-1β and CD14) (Calderón-Garcidueñas et al., 2008). Aβ42 was detected in the OB or olfactory nerve neurons in 83% of Mexico City residents and was not detected in any control OBs taken from residents of less polluted cities (Calderón-Garcidueñas et al., 2010). The authors proposed the OB as a portal of entry, with PM accumulating in areas of the respiratory tract (nasal epithelium, olfactory epithelium, bowman glands and OB neurons). Assuming a typical breathing rate of 7.5 L/min and a deposition rate of 0.1% for ~20 nm particles Garcia *et al*. (2015) estimated that an individual could be exposed to an estimated 150,000 MNPs per hour (Maher, 2019). MNPs with a morphology that bears a striking resemblance to environmental particles formed under high temperature (Figure 1.6) have been found in human brain tissue from the UK and Mexico City, and similar particles have also been identified in the OB of Mexico City residents (Maher et al., 2016, Calderón-Garcidueñas et al., 2008, Calderón-Garcidueñas et al., 2010). In contrast, Gilder *et al.* (2018) argued that, if the OB were the portal of entry for MNPs, one would expect a decreasing gradient of magnetic material centred around the OB region. The authors demonstrated that, in formalin-fixed brain, whilst the OB was an order of magnitude more magnetic than the cerebral cortex, so too were the pineal gland and choroid plexus which are distal to the OB, with the highest concentrations of MNPs in the brainstem (Gilder et al., 2018). The authors subsequently posited that the MNPs were biogenic in origin.

Olfaction refers to the detection, identification, discrimination, and memory of different odours (smells). Olfactory dysfunction is a consequence of normal ageing (Dan et al., 2021), but is even more prevalent in NDD (90-100% of AD cases) (Attems et al., 2014), and has also been reported in response to occupational exposure to various chemicals (Gobba, 2006), including air pollution (Ranft et al., 2009, Ajmani et al., 2016, Calderón-Garcidueñas et al., 2010).The *APOE* ε4 allele modifies the risk of developing AD, but is also thought to increase the susceptibility to olfactory dysfunction; *APOE* ε4 carriers with olfactory deficits have a

higher risk of cognitive decline (Calhoun-Haney and Murphy, 2005, Josefsson et al., 2017). The extent of pathological changes in the OB has also been linked to olfactory dysfunction and the exacerbation of AD symptoms (Wilson et al., 2009). Olfactory dysfunction seen in response to air pollution exposure could, therefore, increase the risk of developing NDD, particularly for *APOE* ε4 carriers. Exposure to air pollution also appears to influence protein mis-folding in the OB and has been proposed to initiate a prion-like propagation of NDD (Rey et al., 2018). The authors proposed that air pollutants could gain access to the brain via the olfactory epithelium/OB where the integrity of cellular and immunological responses has weakened (e.g., with age or in response to chronic pollutant exposure), as well as induce local misfolding of proteins (e.g., Aβ) within the olfactory epithelium/OB which go on to propagate protein misfolding elsewhere in the brain via the olfactory pathway.

1.3.2 Lung-brain axis

The extent to which inhaled NPs penetrate the respiratory tract is dependent on their physicochemical properties; particles with a diameter greater than 10 µm become trapped in the nose and throat and do not penetrate to the lung, whilst particles in the range 2-10 µm enter the upper respiratory tract (tracheobronchial tree) and are subject to mucociliary clearance (Leikauf et al., 2020, Lee et al., 2021). Particles in the nanometre range penetrate furthest into the lungs, reaching the alveoli, but are also capable of depositing in several regions; ~30% of 10-100 nm particles deposit in the alveolar region (Oberdörster, 1989) but for particles around 30 nm and below, a shift is seen towards tracheobronchial deposition. Particles can then translocate to extrapulmonary organs via the circulatory system (Kreyling et al., 2002, Oberdörster et al., 2004, Oberdörster et al., 2002, Wallenborn et al., 2007, Geiser, 2010, Lu et al., 2020). Additionally, the lung can influence the brain via the release of inflammatory mediators into circulation, changes in metabolism, interaction via the hypothalamus pituitary adrenal axis (HPA) and stimulation of nervous impulses (Figure 1.8)(Bajinka et al., 2021). These mechanisms are common to PM, bacteria, and viruses, and collectively form the bidirectional pathways between the lung and the brain, known as the lung-brain axis.

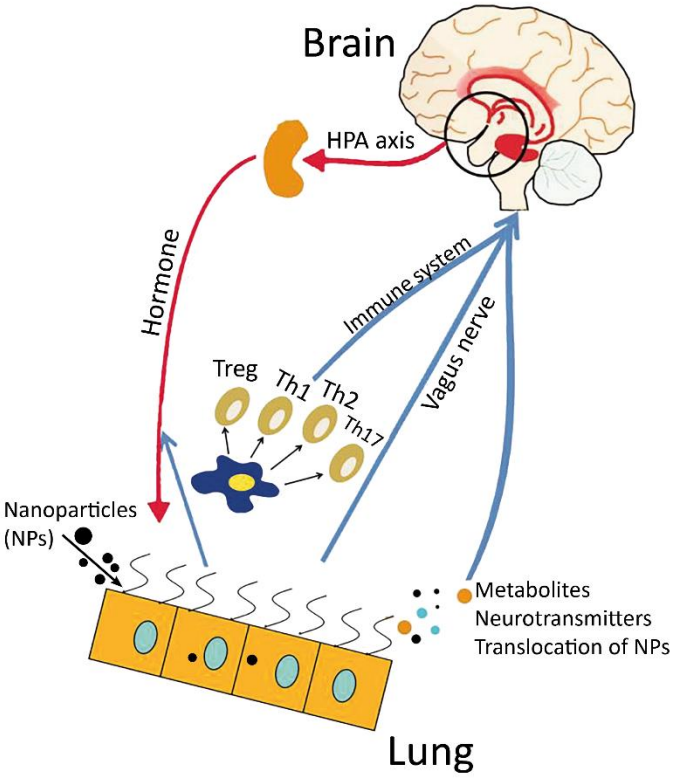

Figure 1.8 Pathways involved in lung-brain axis. Several pathways are co-ordinated to form the lung-brain axis, which can trigger responses in the brain to particulate matter (PM) exposure in the lung. The same pathways are also utilised in response to pathogens. Particulate matter can translocate to the brain via systemic circulation. Metabolites, neurotransmitters, and immune modulators such as cytokines and chemokines can also travel via the systemic circulation and travel across the blood brain barrier. Nervous impulses such as stimulation of the vagus nerve are also involved in the lung's response to PM. Hormonal responses to PM are regulated by the hypothalamus-pituitary-adrenal axis (HPA), causing metabolic and immunological responses. Adapted from (Bajinka et al., 2021).

The lung epithelium forms an important barrier between the external environment and deeper tissue layers. This barrier is maintained by specialised cellular connections known as tight junctions (TJ) and adherens junctions (AJs) junctions which anchor cells together (Anderson et al., 2004). TJs form a semi-permeable barrier which facilitates the (regulated) paracellular transport of ions, small molecules, and water (Xian et al., 2020). TJs and AJs are involved in a host of signalling pathways, regulating cell proliferation and differentiation (González-Mariscal et al., 2020) as well as stimulating the production of chemoattractants, cytokines, and chemokines to recruit an immune response to pathogens and foreign particles like PM (Iwasaki et al., 2017). The integrity of the pulmonary epithelium is known to become damaged with pulmonary disease and/or with exposure to respiratory irritants like PM (Calderón-Garcidueñas et al., 2007). This damage allows for greater incursion and retention of PM, production of ROS and pro-inflammatory responses which affect the lung and extrapulmonary organs, as well as pathogenic changes in the lung such as pulmonary fibrosis

(Conti et al., 2018, Manke et al., 2013), smooth muscle cell hyperplasia, peribronchiolar fibrosis, and the presence of hyperplastic epithelium (Calderón-Garcidueñas et al., 2007)

Lung burden with UFPs is typically quite low but can be overwhelmed if particles are not cleared (Oberdörster et al., 2002). Phagocytic cells in the lungs (e.g., neutrophils, macrophages) engulf PM and travel up the mucociliary escalator where they are swallowed and enter the gastrointestinal (GI) tract for clearance (Leikauf et al., 2020). Larger particles or agglomerates (>1 μm) are more readily phagocytosed than smaller particles (Oberdörster et al., 2005), and the clearance of nanoparticles is less efficient, resulting in longer contact times between nanoparticles and epithelial cells and more opportunity to translocate through the lung epithelial barrier (Braakhuis et al., 2014, Geiser et al., 2005). Cells that have phagocytosed PM can evade the mucociliary clearance mechanisms if such mechanisms are impaired/overwhelmed and can travel in circulation to the brain or re-enter the interstitium and travel to lymph nodes (Geiser, 2010). The proportion of nanoparticles translocated to extrapulmonary organs in *in vivo* studies is typically low; <1% iridium particles in rats (Kreyling et al., 2002) and ~0.2% gold particles in healthy human volunteers (Miller et al., 2017). In contrast, Oberdörster *et al.* (2002) found a significant increase in ^{13}C particle number in the livers of male Fischer 344 rats. The authors propose rapid clearance occurs in the lungs, with particles moving to the GI tract via mucociliary clearance, and from circulation after moving from interstitial sites via the lymphatic system or endothelium exposure (Oberdörster et al., 2002). The physicochemical composition of PM is likely critical in determining the fate of particles in the body.

Particles do not need to physically translocate to the brain to induce pathogenic changes which can also arise in response to cytokine release, metabolic changes, and nervous signals (Fig 1.8). Inhalation of air pollutants triggers a stress response in autonomic sensory nerves relayed to the hypothalamus via the brainstem, which in turn activates by the hypothalamus pituitary adrenal (HPA) and sympathetic adrenal medullary (SAM) axes (Hodge et al., 2021). The HPA and SMA axes are important mediators of the neuroendocrine stress response to air pollutants, resulting in metabolic and innate immune responses, coupled with oxidative and physiological stress which, if prolonged, may contribute to allostatic overload and pathogenic changes observed in AD (Thomson, 2019). Thus, chronic inflammation in the lung can affect the inflammatory state of the brain.

1.4 Magnetite

Magnetite (Fe_3O_4) is a ferromagnetic complex of oxide (O_{2-}), Fe^{2+}, and Fe^{3+} ions which is found as natural mineral deposits but is also present in the environment as a consequence of anthropogenic activities such as fuel combustion, aviation, and frictional brake wear (Maher, 2019). Other sources of magnetite include synthesised products such as ink toner (Ataeefard et al., 2014) and cosmetics (Khan and Cohen, 2019), and in the future magnetite could be released in to the environment following medical uses of (bio)engineered products such as magnetic resonance imaging (MRI) contrast agents (Avasthi et al., 2020) and anti-neoplastic agents (Mandriota et al., 2019). Magnetite nanoparticles (<100 nm) are abundant in particulate matter (Gonet et al., 2021a), brake wear (Gonet et al., 2021b), tyre wear (Thorpe and Harrison, 2008), and the underground (Moreno et al., 2015, Loxham et al., 2015, Loxham et al., 2020), and typically have partial surface oxidation to another iron oxide, maghemite (Collingwood and Telling, 2016).

In humans, MNPs have been detected in all major organs of the body (Liu et al., 2021, Sant'Ovaia et al., 2015, Calderón-Garcidueñas et al., 2019b, Murros et al., 2019, Maher et al., 2016) and, within the brain, have been reported in the brainstem (Gilder et al., 2018, Sant'Ovaia et al., 2015), frontal lobe (Maher et al., 2016, Calderón-Garcidueñas et al., 2019b, Sant'Ovaia et al., 2015), temporal lobe (Sant'Ovaia et al., 2015, Brem et al., 2005a, Bulk et al., 2018), temporal gyrus (van der Weerd et al., 2020, Hautot et al., 2003, Pankhurst et al., 2008), hippocampus (Dobson, 2002, Dobson and Grassi, 1996, Dunn et al., 1995, Quintana et al., 2006, Hirt et al., 2006, Sant'Ovaia et al., 2015, Khan and Cohen, 2019, Brem et al., 2006), cerebellum (Gilder et al., 2018, Kirschvink et al., 1992a, Sant'Ovaia et al., 2015) , globus pallidus (Sant'Ovaia et al., 2015, Svobodová et al., 2019) and olfactory bulb (Gilder et al., 2018, Sant'Ovaia et al., 2015). Biogenic MNPs in the human brain have been suggested to have a similar function to MNPs in birds (Heyers et al., 2010) i.e., magnetoreception/navigation (Wang et al., 2019a) and/or are thought to be involved in formation and long-term storage of memory (Banaclocha et al., 2010, Alfsen et al., 2018).

MNPs can be grouped in to three categories: biogenic, exogenous, and plaque associated. Biogenic MNPs may form within ferritin via *in* situ crystallisation, as a result of incomplete oxidation or overloading of the 8 nm ferritin core and may explain some of the iron elevation seen with age/AD (Quintana et al., 2004). Biogenic magnetite has an angular or euhedral structure (see Fig 1.6) and closely resembles MNPs found in magnetotactic bacteria (formed through biomineralization of magnetite within magnetosomes) (Baumgartner et al., 2013, Mann, 1993, Mann et al., 1984, Gorobets et al., 2017). In contrast, exogenous MNPs formed

under high temperatures (~300 °C) generally have a more rounded/spherical structure (Kukutschová et al., 2011, Maher et al., 2016). Plaque-associated MNPs with a dominantly rounded morphology have been found co-localised to Aβ fibres, within senile plaque cores (Everett et al., 2018, Plascencia-Villa et al., 2016). Plascencia-Villa *et al.* (2016) propose biogenic formation of plaque associated MNPs is a two-step process; smaller MNPs (2-7 nm) form as a result of ferritin core overload, whilst larger MNPs (~80 nm but also up to 200-600 nm (Everett et al., 2018) are a consequence of aggregation.

Particles bearing a striking similarity to combustion and friction derived exogenous MNPs have been found in the human brain and are thought to enter the organ via the OB (Maher et al., 2016) (see 1.3.1.). Exogenous pollution derived MNPs have been implicated in the development NDD; elevated levels of magnetite have been reported in the AD-afflicted brain (Hautot et al., 2003, Pankhurst et al., 2008), the Fe^{2+} ions in these particles can participate in Fenton chemistry (Fig 1.3), MNPs have been found within senile plaques (Plascencia-Villa et al., 2016) and can accelerate Aβ aggregation (Mir et al., 2012) (Mirsadeghi et al., 2016) (Mahmoudi et al., 2013), enhance Aβ toxicity and reduce spontaneous activity in *in vitro* neural network models (Teller et al., 2015). Furthermore, epidemiological, magnetic, *in vitro*, and *in vivo* studies collectively suggest that the entry of environmental MNPs to the brain may result in ROS generation, neuroinflammation and alterations to Aβ and tau levels and conformations (Maher et al., 2016, Dadras et al., 2013, Mir et al., 2012, Calderón-Garcidueñas and de la Monte, 2017, Coccini et al., 2017, Fahmy et al., 2020, Kim et al., 2006, Veranth et al., 2007, Yarjanli et al., 2017, Chen et al., 2017b). Thus, exposure to MNPs (and iron-rich NPs in general) may be an important environmental risk factor in the development of AD and other NDDs, though further work is needed to establish any causal link.

1.4.1 Measuring magnetite in the brain

Identification and quantification of iron (in its various forms) within the brain utilises a variety of spectroscopic, microscopic, histological, magnetic, and analytical techniques. The two primary analytical techniques used in the current study are inductively couple plasma mass spectrometry (ICP-MS) and superconducting quantum interference device (SQUID) magnetometry. These techniques are utilised for the study of post-mortem tissue which has the disadvantage of representing a fixed moment in time, i.e., a snapshot of the iron levels after death.

1.4.1.1 SQUID magnetometry

The ferromagnetic properties of iron can be exploited to quantify the iron oxide nanoparticle content of a material such as brain tissue. Magnetic methods are also gaining traction as a form of quantifying and examining PM (Gonet et al., 2021a). Quantification is reliant on measuring the remanence of the material; remanence is the magnetisation remaining in a ferromagnetic material once the external magnetic field is removed. Magnetic fields cause changes in electrical current which are detected by the SQUIDs and translated to a numerical/computer output. There are several types of remanences including natural, isothermal, saturated and anhysteretic remanences. Natural remanence magnetisation (NRM) is the baseline remanence of a material which is present without any external experimental field applied; it exists due to exposure to the earth's magnetic field. All materials have an NRM but not all have a measurable NRM.

Isothermal remanence (IRM) simply refers to the measurement of remanence at a constant temperature. Saturation isothermal remanence magnetisation (SIRM) is the IRM measured when the material is fully saturated and can be used to approximate the magnetite concentration of the tissue. Saturation occurs when a maximal field (~1T in this case) is applied and no further magnetisation occurs. Estimations of magnetite/maghemite concentrations are made by comparing experimental SIRM values with empirically determined SIRM values for pure magnetite/maghemite samples of known sizes (Maher, 1988). IRM acquisition is the measurement of IRM using incrementally larger applied fields until saturation, with remanence measured following removal of each new field. This acquisition shows the coercivity of the material; a measure of how magnetically 'hard' or 'soft' a material is. Materials have their own coercivity of remanence values; for magnetite, the coercivity value is around 300 mT, making it a relatively soft magnetic material.

IRM measurements are typically conducted at either room temperature (300 K) or at very low temperatures (5 K). The choice of temperature depends on the predicted mineral composition of the sample, or the mineral of interest, as magnetic properties of materials can change at different temperatures. For example, 8 nm oleic acid coated magnetite nanoparticles have a blocking temperature of 130 K (Chesnel et al., 2014), this is the temperature below which all the particles are superparamagnetic. Blocking temperature is a narrow range of temperature change which causes a change from the superparamagnetic state to a stable state (Neel, 1949). When a material is superparamagnetic, the electrons give fields in opposite directions and cancel each other out, so when trying to measure the remanence of such a material, the overall signal is zero. Whether a material is superparamagnetic or not can be altered by

changing the temperature as this increases the energy available to electrons changing their configuration such that the opposing moments no longer cancel each other out. The blocking temperature is specific to minerals e.g., 8 K for ferrihydrite (Dubiel et al., 1999) compared to 130 K for magnetite (Chesnel et al., 2014), but also specific for the particle or grain size e.g., 130 K for 8 nm magnetite vs 150K for 19.4 nm magnetite (Cullity and Graham, 2008). Particles of magnetite smaller than ~20-30 nm are superparamagnetic at room temperature (~293 K) and so do not have detectable remanence magnetisation but, when the temperature is lowered, they are no longer superparamagnetic and, therefore, measurable (Dunlop and Özdemir, 1997). Typically, a mixed approach to magnetic measurements is taken, by either using different temperatures (van der Weerd et al., 2020), or using different measurement techniques that will capture the profile of (primarily) one material at a time.

The importance of utilising different magnetic and spectroscopic analyses is clear when comparing magnetite and maghemite (the oxidised from of magnetite). Both compounds are similar in their magnetic properties and chemical composition such that it is often not possible to distinguish between the two. For instance, maghemite usually saturates at 300 mT and so does magnetite and the experimentally derived values for single domain non interacting particles of magnetite and maghemite are very close (46 Am^2Kg^{-1} and 41 Am^2Kg^{-1}, respectively) (Moskowitz et al., 1993). Therefore, it is best practice to use a variety of techniques (magnetic, spectroscopic, and microscopic) to definitively identify the species of magnetic material present in tissue.

1.4.1.2 ICP-MS

ICP-MS identifies elemental composition; the sample is ionised via inductively couple plasma and then mass spectrometry is used to detect the ions. Ions can be detected as low as 1 part per billion ($1x10^9$) (Grochowski et al., 2019). Trace metals in the brain are present in the parts per million (ppm) range whilst ultra-trace elements are present in the parts per billion (ppb) range (Brown and Milton, 2005). The most frequently used techniques in recent years for trace/ultra-trace analysis of human tissue are ICP based; ICP-MS and ICP-OES (inductively coupled plasma optical emission spectroscopy). ICP-MS, used in the current study, is a spectrometry method which relies on ionisation of the sample to give single-positive ions via the medium of inductively coupled plasma. Once generated, the ions pass through ionic cones and travel to quadrupoles (mass spectrometer) where they are separated by their mass/charge ratios before passing to the detector (photomultiplier). The elements measured are compared to elemental standards and, ideally, to a suitable (certified, or standard) reference sample. However, in the case of human tissue no such standards are available and

so alternative standards such as bovine liver SRM 1577b may be used. An obvious advantage of ICP-MS is low detection limits (nmol/L) which is crucial for trace and ultra-trace element analysis. However, ICP-MS analysis is not without its challenges; samples must be liquid and, as such, the processing of samples is prone to the induction of artefacts. Use of laser ablation (LA-ICP-MS) to study materials in their solid state, and without destruction of the tissue is an advantageous alternative (Hare et al., 2017). In addition to measuring the elemental composition of human brain tissue, ICP-MS has been used extensively to profile the composition of PM samples including roadside dust (Wiseman et al., 2021, He et al., 2018, Miguel et al., 1997, Dytłow and Górka-Kostrubiec, 2021).

1.4.2 Magnetite in brain tissue

Magnetite (as well as maghemite) was first detected in human brain tissue in 1992 using SQUID magnetometry (Kirschvink et al., 1992a). The particles were thought to form *in situ*, and resemble biogenic particles formed in magnetotactic bacteria due to their similar morphology and crystallographic properties (Kirschvink et al., 1992a, Dunn et al., 1995, Mann et al., 1984, Moskowitz et al., 1993). Subsequent magnetometry, spectroscopic and microscopy studies have confirmed the presence of MNPs in brain tissue (Collingwood et al., 2008, Maher et al., 2016, Sant'Ovaia et al., 2015, van der Weerd et al., 2020, Bulk et al., 2018, Dobson, 2002, Schultheiss-Grassi et al., 1999).

The concentration of MNPs in human hippocampus has been shown to increase with age in males but not females (Dobson, 2002). Similarly, the mass of magnetite/maghemite particles (primarily 30 - 300 nm diameter) increased in the brains of male subjects (aged 19- 89 years) as measured *in vivo* by magnetoencephalogram (Khan and Cohen, 2019). A study of fixed whole brains, however, showed no difference in MNP concentration with age, possibly due to the joint analysis of female and male data and small number of subjects but also to the fact that the SIRM signals were several magnitudes lower than other studies and may not have accurately reflect MNP concentrations (Gilder et al., 2018).

Biogenic MNPs could explain the elevated levels of iron seen in AD as these increased levels do not correlate to an increase in ferritin or transferrin (Fischer et al., 1997), and transferrin is decreased in several AD brain regions. A limited number of studies have compared the levels of magnetite in AD brain tissue to controls, finding either an elevation of MNPs in AD tissue, or no significant differences (though often these studies employ small sample sizes due to the difficulty of obtaining human brain tissue). Elevated magnetite concentrations were reported in the superior temporal gyrus of female AD cases (n=3) compared to controls (n=3) (Hautot

et al., 2003). An expansion of this study combined this data with an additional 16 samples and confirmed the original findings (Pankhurst et al., 2008). In contrast, when comparing 22 AD temporal cortex samples to 14 age and sex-matched controls, no difference in magnetite concentration was found, but larger particles were present in AD tissue (Bulk et al., 2018). This is similar to a study of medial temporal gyrus tissue where, again, no difference was found in magnetite concentration (n=9 for each group) but two populations of particles were present, one of which dominated in the AD group (van der Weerd et al., 2020). Comparison of four normal brains (cerebellum and cerebral cortex) to two AD brains also failed to demonstrate a difference in magnetite concentration (Kirschvink et al., 1992a). Another study measured MNP concentrations in cervical (neck) skin from 10 PD patients to 10 healthy controls and found no difference in MNP concentrations between the groups (Murros et al., 2019).

Biogenic MNPs are thought to be the products of biological processes, produced within ferritin via *in situ* crystallisation (Quintana et al., 2004) (Quintana and Gutiérrez, 2010). Excess iron in AD may be found as increased iron atoms in the 8 nm ferritin core but, if there is an overload of the core or loss of function, then magnetite may form as a result (Dobson, 2001), accounting for the excess iron levels observed in AD. However, the presence of particles greater than 8 nm in diameter suggests other mechanisms must be involved in MNP presence in the brain (see 1.4.3). Additionally, Murros *et al.* (2019) reported the presence of non-biogenic MNPs (neither spherical nor euhedral in shape) in the cervical (neck) skin of PD patients and controls thought to originate from the GI tract possible from ingestion of MNPs within food, bacteria and/or drinking water.

Environmentally derived MNPs are another potential origin of the excess iron observed in the AD-afflicted brain, and a possible explanation for the presence of particles greater than 8 nm in diameter (Figure 1.9). The presence of biogenic and exogenous MNPs in the brain may be reflected in the two different populations of particles observed in the temporal gyrus (van der Weerd et al., 2020). Examination of human frontal lobe tissue from Mexico City residents and Manchester Brain Bank samples via SQUID magnetometry, electron energy loss spectra (EELS) and transmission electron microscopy (TEM) found magnetite and maghemite NPs ranging from 10-150 nm (median diameter 18 nm) (Maher et al., 2016). The morphology of some of the MNPs (uniform spherical particles with a resemblance to pollution derived particles formed under high temperature and pressure) (Chen et al., 2006, Liati et al., 2015) (Fig 1.6) was in stark contrast to the euhedral biogenic particles reported previously (Kirschvink et al., 1992a, Schultheiss-Grassi et al., 1999). The authors suggest the olfactory bulb as the route of entry into the brain (see 1.3). Other studies of Mexico City brain tissue found particles

resembling combustion and friction derived nanoparticles (CFDNPs) in the olfactory nerve (Calderón-Garcidueñas et al., 2018b), and in frontal lobe tissue (Calderón-Garcidueñas et al., 2019b). Such cases display AD pathology ('AD continuum') from 11 months to 40 years of age (Calderón-Garcidueñas et al., 2018a). Thus, inhalation of environmental MNPs likely contribute to MNP levels in the brain, alongside biogenic MNPs.

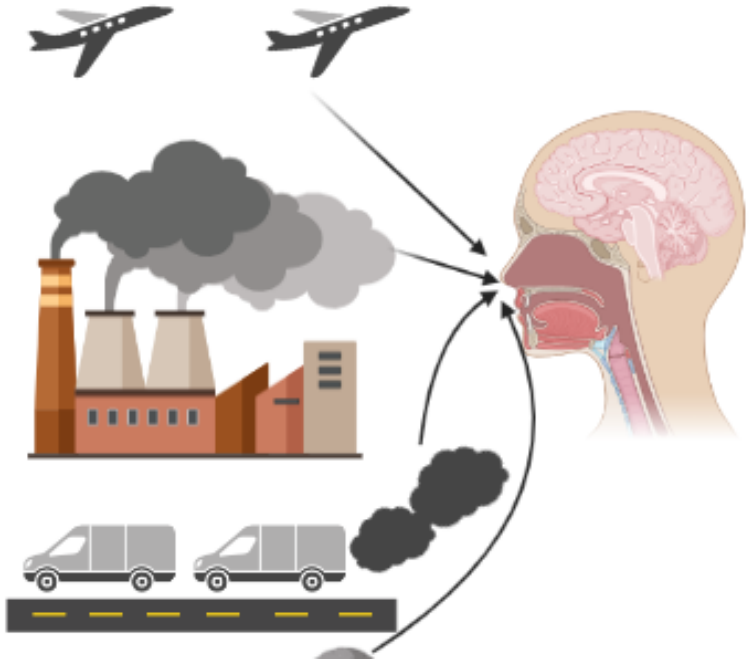

Figure 1.9 Environmental magnetite nanoparticles in the human brain. Magnetite nanoparticles (MNPs) are produced from diesel engines in cars and planes and from industrial sources. The MNPs are released into the air and are inhaled from the environment. The olfactory bulb, a nerve that bridges the connection between the nasal passage and the brain, is a proposed route for environmental MNPs to reach the brain following inhalation.

In contrast, Gilder *et al.* (2018) proposed that the distribution of MNPs is genetically determined, as evidenced by the uniform distribution of MNPs across seven whole brains (divided into cerebellum, cerebellar cortex, and brainstem) stored in formalin for several decades. The highest concentrations of MNPs were found in the brainstem, followed by the cerebellum and cerebellar cortex, suggesting that the inhalation of MNPs and incursion via the OB is unlikely as a gradient of magnetic material would be expected from the OB decreasing towards distal sites which was not observed in the tissue samples (Gilder et al., 2018). The argument that a gradient of magnetic material would be expected from the point of incursion assumes that the material moves through the tissue via diffusion and does not consider brain fluid dynamics. Magnetic material may travel through brain tissue via other mechanisms of movement such as bulk flow (e.g., of interstitial fluid) (Hladky and Barrand, 2014, Ray et al., 2019) which could partially explain the distribution patterns observed.

The dissolution and re-precipitation of MNPs inside human mesenchymal stem cells (MSCs) following exposure to engineered MNPs has been observed (Van de Walle et al., 2019); deposition and accumulation of MNPs is likely a dynamic process so analysis of post-mortem tissue may only reflect the most recent exposure(s) prior to dissolution. Similarly, exposing the same MSCs to magnetosomes from bacteria (composed of a magnetite core surrounded by a phospholipid bilayer) resulted in the same phenomenon; re-precipitation as ~8 nm MNPs (Curcio et al., 2020). Clearance of iron oxide nanoparticles is also seen in MSCs, with 50% of cell-associated iron lost after 3 days and ~90% lost after 27 days (Mazuel et al., 2016).

In vivo clearance of iron oxide nanoparticles and biodegradation of a magnetite-based ferrofluid in rat brain has also been reported (Wang et al., 2011, Polikarpov et al., 2014, Gabbasov et al., 2016), with degradation likely taking place in the endosomal system (Soenen et al., 2010). Therefore, it is possible that the concentration and distribution of exogenous magnetite in the brain may reflect only the most recent exposure(s) (Maher, 2019).

1.4.3 Magnetite, AD pathology and toxicity

The presence of exogenous MNPs in the brain and apparently elevated magnetite levels in AD tissue are not sufficient to prove a causal link with the disease. However, there is a growing body of evidence to suggest a role for MNPs in AD progression. Iron is known to accumulate in senile plaques, with elevations seen in the rim and core of the structures compared to surrounding neuropils (Lovell et al., 1998). Characterisation of plaque-associated iron has revealed the presence of several iron oxides including magnetite/maghemite, ferrihydrite and wüstite, as well as free iron ions (Fe^{2+}, Fe^{3+}) and, more recently, zero valence iron (Fe^{0}) (Everett et al., 2018, Collingwood et al., 2008, Everett et al., 2021b, Plascencia-Villa et al., 2016). Isolated amyloid plaque cores (APCs) have been shown to contain predominantly 2-7 nm MNPs, with a smaller number of 8 – 40 nm particles observed (Collingwood et al., 2008). The authors posited that the smaller particles likely formed within the ferritin core, following incomplete oxidation, whilst the larger particles likely represented aggregates of the smaller ferritin-core sized MNPs or breakdown of the ferritin protein core allowing for larger particles (Collingwood et al., 2008). A further study also looking at APCs isolated from AD brains demonstrated the presence of ~8 to 50 nm particles with spectral and crystallographic properties consistent with magnetite (Plascencia-Villa et al., 2016). These MNPs were associated with the plaques but not bound to fibrils and their size (greater than the ferritin core) was attributed to the formation of aggregates (Plascencia-Villa et al., 2016). Alternatively, incursion of environmentally derived MNPs e.g., via the OB, could explain the presence of particles larger than 8 nm in diameter (Maher et al., 2016). The dominant cubic

iron oxide in AD ferritin cores is thought to be magnetite/maghemite, in contrast to physiological ferritin which predominantly consists of ferrihydrite (Quintana et al., 2004). Formation of ~8 nm iron particles is thought to be a preventative measure to avoid iron cytotoxicity, as evidenced by the precipitation of ~8.4 nm biosynthesised NPs within human stem cells exposed to maghemite nanoparticles (Van de Walle et al., 2019).

The binding of free iron to Aβ represents an additional/alternative pathway for the generation of MNPs. At pH 7.4, Fe^{3+} ions were reduced to Fe^{2+} in the presence of aggregating Aβ42 *in vitro* (Khan et al., 2006). The formation of redox-active Fe^{2+} and MNPs following Aβ aggregation in the presence of different forms of Fe^{3+} further supports the hypothesis that Aβ mediates reduction of Fe^{3+} (from e.g., ferrihydrite) to the more toxic Fe^{2+}, generating ROS in the process (Everett et al., 2014a, Everett et al., 2014b). A similar phenomenon is thought to take place *in vivo* within APCs of APP/PS1 transgenic mice; iron bearing fibrillar aggregates with similarity to human AD APC fibrils were identified, with an increase in Fe^{2+} phases in AD mice compared to wild-type mice (Telling et al., 2017). Iron is stored as Fe^{3+} phases and, as such, there are many available sources of Fe^{3+} available to be reduced to Fe^{2+} such as labile iron, hemosiderin at microbleeds, external pollution derived MNPs, and ferrihydrite (within ferritin), providing a rich and constant source of ROS to induce oxidative damage in neurons (Everett et al., 2018). Redox cycling of iron may explain the presence of ferritin-core sized magnetite within APC; Aβ can cycle iron from ferrihydrite to magnetite and to wüstite (the oxidation product of magnetite) (Everett et al., 2014a, Everett et al., 2018).

The formation of the MNP-Aβ complex could precede the formation of free MNPs as the attraction between iron and iron binding sites on Aβ is usually weak, and crystallisation of MNPs may stabilise the interaction between iron and Aβ (Mir et al., 2012). Mir *et al.* (2012) suggested that Fe^{2+} and Fe^{3+} bind Aβ42, bringing the ions together to facilitate the formation of MNPs which in turn entrap Aβ in a fibrillar structure resulting in stabilisation. Pre-formed MNPs incubated with Aβ42 had a very minimal attraction, possibly due to the neutral surface charge of the particles (Mir et al., 2012). Further studies from the same group support this hypothesis; iron bound to oligomeric Aβ42 structures which self-assembled into fibrils initiating MNP precipitation and concentration of iron hydroxides within a 'woolly ball' structure of fibrils (Tahirbegi et al., 2016). In both experiments (Mir et al., 2012, Tahirbegi et al., 2016), the resulting MNPs were consistent with MNPs isolated from amyloid plaque cores taken from AD brains (Collingwood et al., 2008), so precipitation of MNPs from iron ions via an amyloid intermediate is another suggested mechanism for the generation of MNPs seen within AD tissue.

The MNP-Aβ complex is thought to have toxic consequences and may play a role in AD progression. Exposing PC12 cells to a complex of SiO_2-coated MNPs and Aβ40 for 48 h decreased cell viability by ~20% whereas no significant decrease was observed for either MNPs or Aβ40 alone (Jia et al., 2017). A complex of MNP-Aβ42 caused deterioration of an *in vitro* rat neuronal network model of AD, affecting the connections between cells (functional organisation) and diminishing the activity of individual neurons leading to neuronal apoptosis; effects that were not seen with MNP or Aβ42 only under the same conditions (Teller et al., 2015).

Ultrafine particulate matter (UFPM) can enhance the fibrillation of proteins (i.e., Aβ42,α-synuclein), which accumulate in the OB along with neuroinflammation, similar to the prion hypothesis (Rey et al., 2018). MNPs in particular have been shown to enhance the fibrillation and aggregation of Aβ *in vitro*; incubation of 20 nm superparamagnetic iron oxide nanoparticles (SPIONs) (a term which encompasses magnetite) accelerated Aβ42 fibrillation at high concentrations (and positive charge) whilst inhibiting fibrillation at low concentrations (Mirsadeghi et al., 2016). Fibrillation was enhanced further when the SPIONs were subjected to a magnetic field (Mirsadeghi et al., 2016). Similarly, dextran coated SPIONs with a 5 nm iron oxide core (~15 nm diameter with coating) also inhibited Aβ42 fibrillation at a low concentration but accelerated fibrillation at higher concentrations (and positive surface charge) (Mahmoudi et al., 2013). Incubation of 15 – 45 nm SiO_2-coated MNPs with Aβ40 accelerated Aβ40 aggregation, possibly due to the fact that MNPs tend to aggregate due to ferrimagnetic attractions (Jia et al., 2017). A shift towards larger aggregates was also observed i.e., high molecular weight oligomers rather than dimers (Jia et al., 2017).

Conversely, MNPs might also prevent amyloid aggregation; 26 nm MNPs inhibited lysozyme aggregation at high concentrations (Bellova et al., 2010) and, interestingly, 4.5 nm MNPs incubated for 24h with CSF from 19 AD patients and 9 age-matched controls eliminated amyloid (Aβ42, tau) pre-aggregated *in vivo*, with AD proteins more resistant to the anti-aggregation effects (Gažová et al., 2010). MNPs had no effect on the aggregation of insulin fibrils (Chen et al., 2016b), whilst high concentrations of 50 – 100 nm MNPs interfered with microtubule dynamics (tau and tubulin binding) and altered the structure of tubulin (Dadras et al., 2013). Protein-capped iron oxide (Fe_3O_4) nanoparticles reduced tau aggregation by 49% *in vitro* (Sonawane et al., 2019).

MNPs have been shown to possess a peroxidase-like activity catalysing the oxidation of peroxidase substrates including H_2O_2 (Gao et al., 2007, He et al., 2015). In contrast,

Gumpelmayer *et al.* (2018) stated that MNPs possess no intrinsic peroxidase activity but, notably, the authors used the Aβ1-16 fragment which is non-toxic, lacks the ability to aggregate and is not typically redox-active (Gumpelmayer et al., 2018, Maher, 2019). Ferrous iron can decompose H_2O_2 to free radicals (Fig.1.3) rather than to water and oxygen. It is possible that MNPs may exert a toxic effect on cells by generating ROS through the oxidation of H_2O_2, causing oxidative damage (Maher, 2019). Toxicity from MNPs and MNP-Aβ complexes may arise as a consequence of the magnetic fields generated by MNPs; magnetite/maghemite crystals can produce free radicals via triplet state stabilisation (Scaiano et al., 2008) and alter biochemical reaction rates (Timmel et al., 1998) due to the presence of strong magnetic fields (Collingwood et al., 2008).

The MNP-Aβ complex is a proposed therapeutic target in AD. Proton irradiation of an MNP-Aβ42 complex increased the proportion of redox-inactive Fe^{3+}, included fibrinolysis and β-amyloidosis *in silico* and in the presence of rat cortical neurons (Choi and Kim, 2018). A similar effect has been observed *in vivo*; in APP/PS1 and 5xFAD mice, Fe^{3+} was the predominant iron form in proton stimulation-treated brains and was accompanied by the degradation of MNP-Aβ fibrils (Seo et al., 2021). Proton stimulation is thought to induce a conformational change in MNPs by transfer of electrons, causing them to dissociate from the Aβ fibrils and subsequently be engulfed and degraded by microglia (Seo et al., 2021). The treatment does not appear to damage neuronal cells, however, as magnetite is thought to have a biological function in the formation of long-term memory (Alfsen et al., 2018, Banaclocha et al., 2010), manipulation of MNP and MNP complexes would need to be carefully considered to avoid potentially detrimental effects

1.5 Environmental air pollution toxicity

Modelling of chronic and acute exposures to PM *in vitro* and *in vivo* is not without challenges. The typical paradigm for cell culture is a liquid-based culture in which cells are either suspended in nutrient medium or adhered to a support and bathed in medium. Exposure to airborne PM does not occur in a liquid environment, so modelling exposure to PM in this way may not accurately reflect the fluid dynamics of an environmental exposure. Alternative approaches include the use of cultures at the air-liquid interface (ALI), and the utilisation of aerosol dosing systems (He et al., 2020, Cooney and Hickey, 2011), which may be more representative of the inhalation of PM (Lacroix et al., 2018). One advantage of choosing a liquid culture is a greater bank of established studies and characterisation of cell lines grown in this manner, making the comparison of different studies easier. However, the comparison of PM studies is highly challenging; different doses, timepoints, endpoints, assays, culture

methods, cell types and sensitivities, different PM compositions/sources, and sampling of PM at various times of the year all render the comparison of studies difficult.

Particle size is critical to toxicity; particles with a smaller diameter (i.e., nano, ultrafine) can penetrate further into tissue and have a larger surface area to volume ratio, allowing for a greater number of chemical interactions than larger particles of the same mass (see 1.2.1). The focus in the current study will be on the *in vitro* toxicity of airborne PM, particularly the effects of (ultrafine) PM and roadside dust on lung epithelial cells. Lung epithelial cells are the first contact point for inhaled particles, so have been widely used to characterise the *in vitro* response to inhaled pollutants (Puisney et al., 2018, He et al., 2020, Alfaro-Moreno et al., 2009, Cooney and Hickey, 2011, Gualtieri et al., 2009, Wang et al., 2020a, Sun et al., 2021, Yang et al., 2016a). The immortalised cell lines used for these experiments include the tumour-derived human bronchial epithelial cell line, Calu-3, the non-tumour derived human bronchial epithelial cell line, BEAS-2B, and the tumour-derived human alveolar basal epithelial cell line, A549.

1.5.1 Roadside PM

Cytotoxicity studies of PM are commonly used to explore the spatial, temporal, and physicochemical nature of PM in relation to toxic effects in human cell models. Different biological responses have been reported when comparing airborne pollution particles from different cities (Tung et al., 2021, Sun et al., 2021, Yang et al., 2016a) and when comparing regions or zones from the same city (Chen et al., 2019, De Vizcaya-Ruiz et al., 2006, Osornio-Vargas et al., 2003). These differences likely arise from differing composition of the pollutants in each area, reflecting the surrounding sampling environment, such as transport activities (He et al., 2020, Loxham et al., 2015, Loxham et al., 2020, Chen et al., 2019, Moreno et al., 2015, Pant et al., 2015, Zhang et al., 2019). The roadside environment is particularly rich in metals, including iron-rich particles like magnetite, from vehicle emissions and other traffic-derived sources including road-deposited dust, brake wear, tyre wear, road paint, road wear/abrasion (Wang et al., 2017, Gonet et al., 2021a, Gonet et al., 2021b). Heavily-trafficked roads are a key feature of highly-polluted megacities, such as Mexico City, and TRAP (traffic related air pollution) is a significant source of (ultrafine) pollution to which residents in those cities are exposed; TRAP forms 66% of $PM_{0.2}$ (Habre et al., 2021). Pollution at the roadside is not limited to the immediate vicinity; a recent estimation of the zone of influence roads have on the surrounding land covers at least 70% of Great Britain (Phillips et al., 2021), so the effects of road pollution (consisting of light, noise, NO_2, heavy metals, $PM_{2.5}$ and PM_{10}) and roadside dust may extend further than currently anticipated. One method of minimising the impact of PM

is the use of trees at the roadside; trees capture particles and have reduced indoor air PM_{10} by >50% in Lancaster (Maher et al., 2013), and reduced cadmium and lead exposure by >50% in Istanbul (Ozdemir, 2019).

PM collected at the roadside has been associated with cardio, pulmonary and NDD (see 1.2.2). *In vitro* and *in vivo* toxicology models often look at the effects of exposure on cell survival (viability), oxidative stress/damage, and inflammatory responses. Generation of ROS, e.g., in response to PAHs or redox active transition metals present in PM, are key to determining the fate of exposed cells. Excess ROS can induce oxidative stress in the cell if antioxidant defences like glutathione (GSH) are unable to restore oxidative balance (see 1.2.1). Direct oxidation of macromolecules can also occur e.g., lipid peroxidation. If this oxidative damage/stress is persistent, and overcomes antioxidant defences, the cell can activate signalling cascades ending in the ROS-sensitive transcription factors or activator protein 1 (AP-1), to recruit the immune system (Baeza-Squiban et al., 1999, Dagher et al., 2007). If the immune and antioxidant defences are overwhelmed, the cell instead may start the process of cell death via apoptosis or necrosis (Figure 1.10). PM is also known to induce proliferation in cells (Bayram et al., 2006), which may be a compensatory mechanism in response to the damage (Abbas et al., 2010), or be a pathogenic process i.e., fibrosis (Churg et al., 2003) or tumorigenesis.

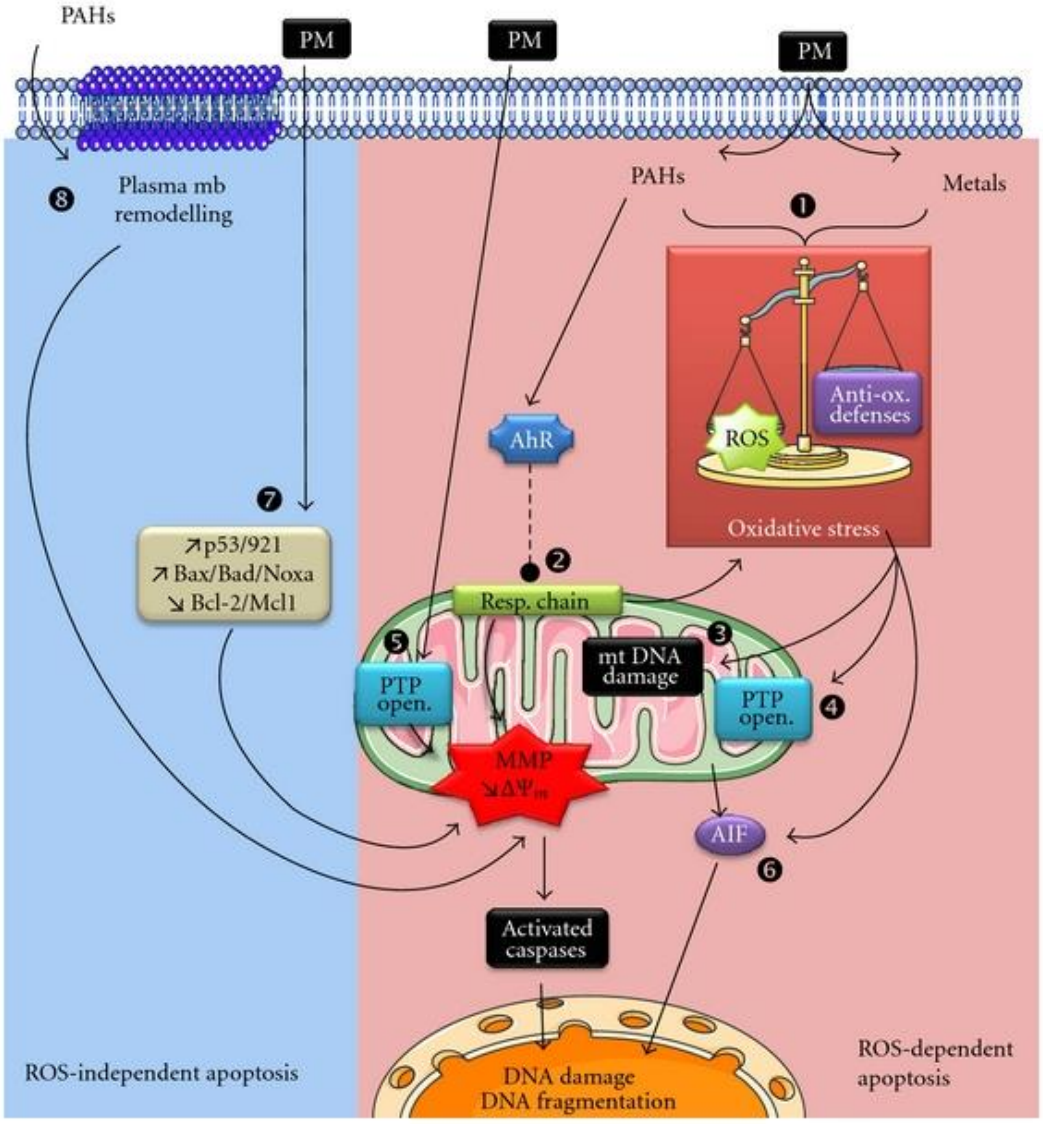

Figure 1.10 Pathways involved in particulate matter cytotoxicity. Particulate matter (PM) can trigger cell death via apoptosis in a reactive oxygen species (ROS)-dependent pathway (pink area) or ROS-independent pathway (blue area). Polyaromatic hydrocarbons (PAHs) and metals are key components of PM that are strong inducers of ROS. Generation of ROS stimulates antioxidant defences in the cell, however, if the balance between ROS and antioxidant defences is tipped towards ROS, the cell is in a state of oxidative stress (1). PAHs can activate the aryl hydrocarbon receptor (AhR), which in turn has been suggested to induce H2O2 and O2.- production in mitochondria (2). ROS damage mitochondrial DNA (3), cause lipid peroxidation in the mitochondrial membrane, and cause the permeability transition pore (PTP) complex to open (4). Diesel particles can directly permeate the mitochondrial membrane and open the PTP complex (5). The apoptogenic activity of apoptosis inducing factor (AIF) can be enhanced in response to xenobiotics, air pollutants or ROS induced by air pollutants (6). Alternatively, independent of ROS, apoptosis may be triggered following a decrease in survival proteins of the BCl-2 family of proteins following PM exposure (7). The remodelling of lipid rafts in the plasma membrane by PAHs has also been shown to trigger apoptosis (8). Figure taken from (Andreau et al., 2012).

Rather than looking at PM samples in their entirety, some toxicity studies focus on individual components, such as specific elements or organic compounds, to identify the most toxic components of PM. However, this neglects any synergistic effects that may be present with

total PM and is a rather time-consuming and impractical process to isolate and test hundreds to thousands of individual components (Park et al., 2018). A more efficient approach is to look at components by their source of origin. This is typical when looking at the composition of PM via source apportionment analysis (Gonet et al., 2021a, Gustafsson et al., 2008, Harrison et al., 2003, Men et al., 2018).

The combination of source apportionment studies and cytotoxicity studies could give an indication as to which sources of PM are most toxic, e.g., diesel exhaust particles (DEP), brake wear particles (BWP), tyre wear particles (Sun et al., 2021, Xu et al., 2020a). Exposing Calu-3 cells to BWPs (nano- and micro-scale) caused increased (~2 x) ROS generation, decreased cell viability (35% decrease for nano- and 81% decrease for micro-particles at 300 µg/ml) and a dose-dependent increase (for micro- but not for nanoparticles) in release of the pro-inflammatory cytokine, interleukin 6 (IL-6) (Puisney et al., 2018). Similarly, exposure of Calu-3 cells to diesel exhaust particles (DEP) caused a dose-dependent increase in ROS generation (up to ~30%) and interleukin 8 (IL-8) release (up to 115%), albeit with no change in cell viability. Exposing A549 cells to the same DEPs decreased IL-8 release (non-significantly), did not alter ROS production, and decreased cell viability (up to ~20%) for media suspension treatments (Cooney and Hickey, 2011). Road-deposited dust is another 'source' of PM, which both derives from and contributes to airborne PM.

1.5.2 Road-deposited dust

Road-deposited dust or roadside dust (RD) is the deposition of airborne PM on or near road surfaces. RD can be aerosolised following disturbances by the wind or passing vehicles and contribute to PM. However, RD also acts as a sink for pollutants and can accumulate additional particles or compounds *in situ*, including heavy metals (Duong and Lee, 2011), various non-exhaust emission (NEE) sources like tyre and road wear (Gonet et al., 2021a), volatile organic compounds (i.e., PAHs) (Mon et al., 2020), and phthalic esters (Li et al., 2020a). Although natural and anthropogenic sources contribute to RD composition, anthropogenic sources are thought to be the most significant contributors (Morales et al., 2020). Due to the pervasive nature of RD, the toxic composition, frequency of exposure (growing urbanisation), ability to penetrate the lungs and reach all major organs (in the case of UFPs), it is potentially a major hazard to human health. Unlike PM, there are no regulations on the exposure to RD at present.

Despite the potential hazard, there are limited studies of the toxicity of RD, with the majority of researchers taking a statistical approach (i.e., hazard modelling), following physicochemical

investigation of samples. A study of RD in 10 megacities in China identified positive correlations between vehicle emissions and coal combustion with ROS production and lactate dehydrogenase (LDH) release in A549 cells (Sun et al., 2021). Metal content in RD was heterogenous; northern cities contained higher concentrations of heavy metals (Cr, Mn, Cu, Zn, Ni, Pb) and PAHs than southern cities, with the ROS production and cytotoxicity more pronounced in cells exposed to northern city RD. In general, the northern Chinese cities are more industrial and consume more energy (coal combustion) (Sun et al., 2021). Positive matrix factorisation (PMF) (similar to principal component analysis) of the chemical composition indicated four contributing components: industrial emissions (PAHs and heavy metals), crustal/natural sources (Al, Si, Ca, Ti, Fe), coal combustion (Ti, Fe, Zn, Pb) and vehicle emissions (Pb, Zn, subset of specific PAHs) (Sun et al., 2021). Thus, the observed differences in cytotoxicity and oxidative stress between the cities are thought to be reflective of the anthropogenic activities surrounding them, primarily due to differences in vehicle, industrial and coal emissions (Sun et al., 2021). A similar study focused on the effects of 50 μg/ml RD on tight junctions in human pharyngeal epithelial cells (FaDu) (Tung et al., 2021). Similar to the previous study, LDH release increased, in general, with oxidative stress induced by ROS a possible mechanism of this cytotoxicity. Proinflammatory responses (increase in IL-6) were reported in response to Wuhan, Shanghai and Beijing RD. Key proteins involved in the maintenance of epithelial barriers, occludin and E-cadherin, were reduced following exposure to RD, with an up-regulation in expression and activation of epidermal growth factor receptor (EGFR) (Tung et al., 2021). When active, EGFR is phosphorylated, and can activate signalling pathways (e.g., MAPK) that trigger NF-κB activation and a decrease in expression of proteins needed for tight junctions (Jeong et al., 2017). A similar phenomenon was reported in human nasal epithelial cells in response to $PM_{2.5}$ (Xian et al., 2020), and disrupted epithelial barriers are key features of Mexico City residents exposed to high levels of pollution (see 1.2.3). Total metal concentrations in RD were correlated with cell viability, occludin and E-cadherin levels, suggesting the metal components of RD (which likely derive from traffic sources) are critical to the observed cytotoxic response and changes to barrier integrity (Tung et al., 2021). The changes to adhesion proteins may arise in response to ROS; ROS can cause internalisation of occludin in endosomes and can also reduce E-cadherin levels by hypermethylation of the E-cadherin promoter (Wu et al., 2012, Caraballo et al., 2011). As such, metals, particularly redox active transition metals, appear to be key components of RD with respect to pathological changes such as weakening of epithelial barriers.

A decrease in viability was also seen in response to RD from South Korea in human adherent lung fibroblasts (WI-38) and human foreskin fibroblasts (BJ) (Kim and Koh, 2020, Koh and Kim, 2019). In an initial study of 100 µm RD particles from 7 sites in South Korea, 1 mg/ml exposure for 72 h decreased viability by 50% for 3 of the sites, and by less than 25% from the remaining sites in both cell lines (Koh and Kim, 2019). The summed metal contents, and specifically Ni, Cr and Zn content correlated with the cytotoxic response. Metal content of the samples had a close relationship with the organic carbon content from industrial or traffic emissions, and to a lesser extent the organic content also correlated to cytotoxicity (Koh and Kim, 2019). The authors then expanded their work to look at 28 different city sampling sites in South Korea (Kim and Koh, 2020). Cytotoxic responses were observed using the same cell lines and methods (aside from the choice of viability assay); 15 out of 28 samples induced less than a 20% decrease in viability at the highest dose (2 mg/ml), whilst 3 samples induced over 50% decrease in viability at the highest dose. As with the previous study, metal content and organic (hydrocarbon) content (from industrial and traffic sources) was correlated to cytotoxicity (Kim and Koh, 2020). The difference in magnitude of cytotoxic response across the two studies could be a consequence of using different viability assays; there are numerous challenges to conducting *in vitro* studies of particles due to their optical and physical properties (particularly UFPs) causing interference with traditional biological assays (Ong et al., 2014). Such differences can also result from differing composition of RD at each sample site, typically heterogenous responses are observed in multi-site studies of RD and PM due to the heterogenous composition of the samples studied (Tung et al., 2021, Sun et al., 2021, Yang et al., 2016a).

Exposing multiple cell types to a range of PM from different sources (exhaust, biomass burning, coal combustion, road dust, ammonium sulphate and ammonium nitrate, and secondary organic aerosols), Park *et al*. (2018) suggested that traffic is a key factor in determining the toxic effects of $PM_{2.5}$, with combustion sources overall being more toxic than non-combustion derived sources. The oxidative potential of the RD sample was in the mid-range of the samples tested, and ROS generation in A549 cells increased by ~50% in response to 60 µg/ml RD for 24 h (Park et al., 2018).

Human corneal epithelial cells (2.040 pRSV-T), human liver (HepG2), and human skin cell lines (KERTr) have also been used for RD toxicity testing to model other routes of RD entry into the body - ocular (eye), dermal (skin) and ingestion (liver) (Yoon et al., 2018, Huang et al., 2015). Exposing 2.030 pRSV-T cells to RD (Seoul, Korea) which had been re-aerosolised to $PM_{2.5}$ and PM_{10}, Yoon and colleagues found that the soluble fraction affected cell membrane integrity

and had a higher metal and ion content, whilst the insoluble fraction altered mitochondrial activity (Yoon et al., 2018). A typical exposure would encompass both soluble and insoluble fractions of RD and PM, but the soluble fraction is perhaps of greater concern due to transport in biological fluids. The viability of HepG2 and KERTr cells decreased by up to 52.9% and 71.4% respectively, following a 72h exposure to the water-soluble fraction of RD from Guangzhou, China (Huang et al., 2015). The metal(loid) content of the RD was identified as critical to cytotoxicity, but experiments using specific metals in isolation did not fully explain the cytotoxic effects seen, suggesting a synergistic effect of the metal(loids) present and/or other components of RD such as the organic content may also be responsible for cytotoxicity.

Whilst the cytotoxicity of fine (0.1 - 2.5 μm) RD has been explored in a limited number of studies, the effects of the ultrafine (<0.1 μm) fraction of RD, which is most abundant (by particle number) and potentially most toxic (due to high surface area reactivity and capacity to penetrate deeper into tissues), are poorly understood.

1.6. Project Aims

The aim of the current research was to explore the relationship between environmental air pollution nanoparticles, particularly magnetite, in relation to Alzheimer's disease and human health. Further understanding of any causal link between air pollution and AD is essential to mitigate negative health effects through strict and accurate legislative limits on air pollution. This was explored through magnetic investigations and metallic profiling of post-mortem human brain tissue and investigation of the cytotoxic, biological effects of ultrafine roadside dust particles from different cities on human lung epithelial cells. Detailed aims are as follows:

- Develop a method for the magnetic characterisation of human brain tissue, accounting for potential sources of contamination (Chapter 2)
- Quantify the magnetic nanoparticle content of human brain tissue (Manchester, UK) from different regions of the brain (Cerebellum, Entorhinal Cortex, Frontal lobe, Occipital lobe, and Temporal lobe) to look at the distribution of magnetic nanoparticles throughout the brain (Chapter 2)
- Compare the magnetic nanoparticle content of human brain tissue (Manchester, UK) of Alzheimer's disease cases compared to non-demented elderly controls (Chapter 2)
- Examine the concentrations of metals in human brain tissue (Manchester, UK), looking at regional distributions and relationships between metals as possible indicators of specific air pollution sources and/or portals of entry into the brain (Chapter 3)

- Quantify the magnetic nanoparticle content of human brainstem tissue from forensic cases from Mexico City, Mexico to look at nanoparticle portal of entry into the brain (Appendix D)
- Extract ultrafine (nano) particles from roadside dust from Lancaster, UK, Birmingham, UK, and Mexico City, Mexico, and examine the cytotoxic, oxidative stress and pro-inflammatory responses in Calu3 (human lung epithelial cells) (Chapter 4)
- Compare the responses of human lung epithelial cells to ultrafine roadside dust particles from different cities and suggest which component(s) of the samples are responsible for the observed biological effects (Chapter 4)

Each data chapter (Chapters 2-4) of this thesis was written as a publication. Details of the publication status and journal destination are presented at the beginning of each chapter, alongside an explanation of the author's contribution to the work.

Chapter 2 (Paper 1) Variation in the concentration and regional distribution of magnetic nanoparticles in human brains (Alzheimer's disease and controls), from the UK

2.1 Abstract

The presence of magnetite nanoparticles (MNPs) in the human brain was attributed until recently to endogenous formation; associated with a putative navigational sense, or with pathological mishandling of brain iron within senile plaques. Conversely, an exogenous, high-temperature source of brain MNPs has been newly identified, based on their variable sizes/concentrations, rounded shapes/surface crystallites, and co-association with non-physiological metals (e.g., platinum, cobalt). Here, we examined the concentration and regional distribution of brain magnetite/maghemite, by magnetic remanence measurements of 146 samples of fresh/frozen tissues, from Alzheimer's disease (AD) and pathologically unremarkable brains (80-98 years at death) from the Manchester Brain Bank (MBB), UK. The magnetite concentrations varied between individuals, and across different brain regions, with no significant difference between AD and non-AD samples. Similarly, all the elderly MBB brains contain varying concentrations of non-physiological metals (e.g., lead, cerium), indicating universal incursion of environmentally sourced particles, likely across the geriatric blood-brain barrier (BBB). Cerebellar Manchester samples contained significantly lower (~9 x) ferrimagnetic content compared with those from a young (29 yrs ave.), neurologically damaged Mexico City cohort. Investigation of younger cohorts, prior to loss of BBB integrity, seems essential to understand early brain impacts of exposure to exogenous magnetite/maghemite and other metal-rich pollution particles.

Published: **Hammond, J.,** Maher, B.A., Ahmed, I.A.M. and Allsop, D. Variation in the concentration and regional distribution of magnetic nanoparticles in human brains, with and without Alzheimer's disease, from the UK. *Sci Rep* **11,** 9363 (2021).

Author contributions statement

JH prepared brain samples, performed magnetic analyses, assisted with experimental design, analysed the data, and wrote the paper. BAM conceived the study, assisted with brain sample preparation, and contributed to writing, reviewing, and editing the paper. IAA carried out ICP-MS on Manchester Brain Bank samples and commented on the paper. DA advised on experimental design and commented on the paper.

2.2 Introduction

Iron is an essential and versatile element present in various forms throughout the brain, and its most abundant transition metal. Its ubiquity reflects its ease in changing solubility via valence state; gaining an electron to convert from insoluble ferric (Fe^{3+}) to soluble ferrous state (Fe^{2+}) and vice versa. Iron not only participates in biochemical reactions, such as the generation of ATP in mitochondria and transport of oxygen via haemoglobin, but is also a crucial part of brain-specific functions such as axon myelination (Connor and Menzies, 1996) and synthesis of various neurotransmitters, like dopamine (Youdim and Green, 1978). This versatility comes at a price; the ease of valence change can have detrimental effects if, for example, free (unbound) iron becomes available to react with oxygen and produce damaging free radicals. To protect the body from the 'darker' side of iron reactivity, iron levels and compounds are tightly regulated. Excess labile (free) iron is sequestered and stored, and ferrous iron oxidised to less reactive ferric forms.

Regional accumulation of iron and of magnetite in the brain during normal ageing has been reported (Zecca et al., 2004, Xu et al., 2008, Khan and Cohen, 2019) but is also evident in several neurodegenerative diseases (NDD) including Alzheimer's disease (AD)(Ward et al., 2014), Parkinson's disease (PD) (Jellinger et al., 1990) and amyotrophic lateral sclerosis (ALS)(Kwan et al., 2012). Meta-analysis of published data (up to 2014) indicates elevated iron in several regions of AD brains: the caudate nucleus; globus pallidus; cingulate cortex; putamen; amygdala; temporal lobe; parietal lobe; and frontal lobe (Tao et al., 2014). A common theme amongst NDD is evidence of oxidative damage and dyshomeostasis of metals including iron, copper, and zinc (Myhre et al., 2013, Sheykhansari et al., 2018, Trist et al., 2018). Iron (particularly Fe^{2+}) can cause oxidative damage (stress) by generating reactive oxygen species (ROS) via the Fenton reaction (Allsop et al., 2008). ROS, including superoxide anion (O_2^-), peroxide (O_2^{2-}) and hydroxyl radicals ($HO^\bullet$), are highly reactive, interacting indiscriminately with different cellular components including DNA, lipids, and proteins leading to altered enzyme activity, mutations, and membrane permeability. These interactions may ultimately lead to cell death via apoptosis, autophagy, necrosis or ferroptosis (Dixon et al., 2012).

To protect the brain from ROS-induced damage, iron is tightly regulated by two key proteins: the iron transporter protein, transferrin; and the iron storage protein, ferritin. Ferritin comprises a protein cage, approximately 12 nm in diameter, with an 8 nm hollow core. The protein cage contains 3-fold and 4-fold ion transporter channels that facilitate iron transport into the core, which can hold up to 4500 atoms of iron (Rouault and Cooperman, 2006). Fe^{2+}

is oxidised within this core to the less toxic Fe^{3+} and stored as ferrihydrite ($Fe_2O_3.0.5(H_2O)$). Interruptions to this process may be pathological; reduced iron capacity of transferrin (Hare et al., 2015b), impaired functioning of ferritin (Cozzi et al., 2010) or decreased expression of ferritin (Faucheux et al., 2002) are all proposed mechanisms for the iron accumulation observed in NDD (Friedman et al., 2011).

Another suspected cause of reportedly increased iron in the ageing brain is the presence of discrete particles of iron oxides, including magnetite (Kirschvink et al., 1992a, Maher et al., 2016, Brem et al., 2006), maghemite (Kirschvink et al., 1992a, Maher et al., 2016, Brem et al., 2006), ferrihydrite (Quintana and Gutiérrez, 2010), goethite (Quintana and Gutiérrez, 2010), haematite (Brem et al., 2006, Quintana et al., 2004) and wüstite (Quintana and Gutiérrez, 2010). Of these iron oxides, magnetite may be of particular importance due to its Fe^{2+} content (Fe^{2+} can participate in Fenton chemistry), and its reported direct associations with amyloid plaques (Teller et al., 2015, Plascencia-Villa et al., 2016) and NDD (Dobson, 2001). Magnetite (Fe_3O_4) is a strongly magnetic material, comprising a close-packed array of oxide (O^{2-}) ions; Fe^{3+} ions occupy tetrahedral holes and both Fe^{3+} and Fe^{2+} occupy octahedral holes. Magnetite nanoparticles often display some degree of surface oxidation towards their oxic counterpart, maghemite (Maher et al., 2016).

Three different forms of magnetite/maghemite nanoparticles (MNPs) have been reported to occur in the human brain: biogenic MNPs (with a suggested role in magnetic field sensing); plaque-associated MNPs (reportedly arising from iron mishandling); and exogenous MNPs (displaying high-temperature morphologies and co-associated with other metals, including non-physiological species). Those biogenic MNPs which have been linked with sensing of the Earth's magnetic field are well-formed, euhedral particles (i.e., with sharp, well-defined crystal faces), and mostly around 10-70 nm (Kirschvink et al., 1992a). Such well-formed MNPs strongly resemble MNPs formed in other organisms, such as magnetotactic bacteria; their 'bio-engineered' size optimises the torque sensed from the geomagnetic field (Kirschvink et al., 1992a). In magnetotactic bacteria, formation of such well-formed magnetite crystals, with optimised particle sizes, occurs through biomineralization of magnetite, possibly via a ferrihydrite precursor, within membrane-bound organelles ('magnetosomes')(Mann et al., 1984).

More recently, in contrast to these euhedral endogenous MNPs, dominantly-rounded MNPs have been observed directly associated with senile plaques, key pathological hallmarks of AD (Plascencia-Villa et al., 2016, Everett et al., 2018). These plaque-associated MNPs were 8 - ~80

nm in diameter, co-localised with β-amyloid (Aβ) fibres and comprised a mixture of magnetite and maghemite (the oxidised form of magnetite), with Fe^{2+} and zero-valent iron also present within the plaque cores (Plascencia-Villa et al., 2016, Everett et al., 2018). MNPs in the 2-7 nm range were also reported, consistent with formation inside the ferritin core (Plascencia-Villa et al., 2016). Conversely, those plaque-associated MNPs of several 10s of nm (Plascencia-Villa et al., 2016) greatly exceed ferritin core dimensions. Plascencia-Villa et al. thus suggest a two-stage formation process; smaller MNPs formed via *in situ* transformation of ferrihydrite within ferritin cores, which then somehow agglomerate to form the much larger, often rounded magnetite particles observed, up to ~ 80 nm diameter (Plascencia-Villa et al., 2016) and sometimes up to 200-600 nm (Everett et al., 2018). A role for Aβ in the biosynthesis of MNPs has also been proposed. Isolated amyloid plaque cores from AD patients were found to contain iron in a range of oxidation states; and Aβ suggested to cycle iron from ferrihydrite to magnetite to wüstite, resulting in generation of a constant stream of ROS-producing iron species (Everett et al., 2018). Hence, these plaque-associated magnetite and co-occurring iron oxide particles are suggested to be endogenous, resulting from iron dyshomeostasis related to NDD (Everett et al., 2018).The proposed precipitation of pathological MNPs in human brain ferritin (Quintana and Gutiérrez, 2010, Quintana et al., 2004) might reflect failure to complete Fe^{2+} oxidation, or an overload of ferritin, possibly accounting for the elevated iron levels observed in AD (Dobson, 2001).

Additionally, or alternatively, inhalation of exogenous, airborne magnetite and maghemite pollution particles can constitute another source of rounded brain MNPs, larger than those formed within ferritin cores (Maher et al., 2016, Maher, 2019). The characteristic morphology (e.g. often rounded shapes and interlocking surface crystallites), and size distribution (<10 to > 100 nm) of MNPs found in the frontal cortex, and their association with other metals (particularly metals not normally present in the body, such as platinum) mirror those of the MNPs which occur in abundance in airborne particulate matter (PM) pollution (Maher et al., 2016) - at heavily-trafficked roadsides, for example. Similarly distinctive MNPs and co-associated metals have been found in the human brainstem (Calderón-Garcidueñas et al., 2020a), heart (Calderón-Garcidueñas et al., 2019b, Maher et al., 2020), blood and pleural effusions (Lu et al., 2020) and placenta (Liu et al., 2021). Magnetite and other iron-rich NPs are formed readily at high temperatures (i.e. > 100 °C) as by-products of combustion and friction (Gonet and Maher, 2019, Maher et al., 2013), occurring at particle number concentrations of ~ $10^8/m^3$ air at the roadside, for example (Maher et al., 2016). Other prolific

sources of airborne MNPs include coal-burning power plants, industrial sources, and indoor emissions, e.g., from open fires (Maher et al., 2021) and office printers (Gminski et al., 2011).

The discovery of intact air pollution nanoparticles inside the frontal cortex indicates inhalation as their portal of entry, followed by translocation via the olfactory bulb (Maher et al., 2016, Oberdörster et al., 2004). In animal studies with male Fischer-344 rats exposed to high doses of titanium dioxide, nanoparticles <200 nm in diameter accessed the olfactory bulb (OB) directly (Oberdörster et al., 2004), evading the BBB. The presence of distinctive, acicular titanium-rich nanoparticles in the brainstem and the neuroenteric system indicates ingestion/swallowing of environmental particles as an additional nanoparticle portal of entry (Calderón-Garcidueñas et al., 2020a).

MNPs have been the subject of numerous toxicity studies, with mixed results e.g., (Fahmy et al., 2020, Ankamwar et al., 2010). Given the association of MNPs with senile plaques (Teller et al., 2015, Plascencia-Villa et al., 2016, Everett et al., 2018), peroxidase-like activity (Borelli et al., 2012), enhancement of Aβ aggregation (Mir et al., 2012) and reported ability to disrupt microtubule dynamics (perhaps by binding to the microtubule protein tau) (Dadras et al., 2013), exposure to airborne MNPs has been identified as a potential environmental risk factor for NDD (Maher, 2019, Maher et al., 2016). Exposure to airborne particulate matter (PM) is significantly associated with increased incidence of NDD. In the U.S., the risk of dementia in older women almost doubled in places where exposure to $PM_{2.5}$ (aerodynamic diameter < 2.5 µm) was greater than the Environmental Protection Agency's standard. A large-population (2.2 million) study in Ontario, Canada found that residents living within 50 m of major roads had up to 14% increased prevalence of dementia (Chen et al., 2017b). Although it is not yet clear which specific component/s of PM are causally related to this increased risk, it seems improbable that repeated inhalation of exogenous Fe^{2+} -bearing and other iron-rich nanoparticles, and their uptake (and possible dissolution) within the brain, constitutes a harmless exposure (Maher, 2019).

In counter-argument, a recent study of seven whole brains, divided into cerebral cortex, cerebellum and brainstem (not from AD cases), reported a uniform distribution of magnetite in each brain; highest concentrations localised in the brainstem, followed by the cerebellum and the cerebral cortex (Gilder et al., 2018). These authors suggest that their observed uniformity of magnetite distribution indicates a genetic, rather than environmental, control; and that the OB pathway can be discounted as a potential entry portal for MNPs found within the distal brainstem. However, the brain samples in this study had been stored for several

decades in formalin; some evidence exists for magnetite dissolution in tissues exposed to formalin (Dobson and Grassi, 1996).

Given that brain iron appears to be locally elevated in various NDDs, knowledge of the distribution and forms of iron found in disease and non-disease states is important for understanding whether iron perturbation is causally linked to NDD. The first identification of magnetite/maghemite in human brains was made using superconducting quantum interference device (SQUID) magnetometry (Kirschvink et al., 1992a), a powerful tool for identifying the location and concentrations of magnetically-ordered iron in the brain. Few studies so far have compared the concentration of MNPs in AD and control brains. Kirschvink et al. (1992) found no difference between 4 normal and 2 AD brains (samples comprising cerebral cortex & cerebellum) (Kirschvink et al., 1992a); Bulk et al. (2018) saw no difference between 22 AD and 14 control samples (temporal cortex) (Bulk et al., 2018). A recent study reported no difference in magnetite concentration (but higher ferrihydrite concentrations) in the medial temporal gyrus of 9 AD patients compared to 9 controls (van der Weerd et al., 2020). In contrast, when looking at females specifically, higher magnetite concentrations were reported in the superior temporal gyrus of AD patients compared to controls (n=3 AD and 3 controls, with a subsequent study combining those samples with 16 new samples) (Pankhurst et al., 2008).

Here, we used SQUID magnetometry to examine the concentration of magnetite/maghemite in AD cases and age-matched controls (19 AD cases, 11 controls, aged 80-98 years from the Manchester Brain Bank, UK), across five brain regions: the frontal, temporal, and occipital lobes; the cerebellum; and the entorhinal cortex. This is the first investigation, to our knowledge, of regional magnetite/maghemite variations in AD cases. Additionally, we examined the concentration of some non-physiological, exogenous (i.e., pollution-derived) metals - specifically, lead, cerium, platinum, and aluminium - in each brain region, in both AD and non-AD samples.

Our new data identify marked variations in the concentration and distribution of magnetite/maghemite throughout the different brain regions. Significantly higher ferrimagnetic concentrations were found in the frontal lobe compared to the entorhinal cortex. The highest magnetite/maghemite concentration of all Manchester samples analysed was found in the frontal cortex of a 93-year-old female AD case. However, no significant difference in ferrimagnetic concentration was found between our elderly AD cases compared to controls. The Manchester brain magnetite/maghemite concentrations were on average 11

× higher than those reported for formalin-stored brains. Cerebellar magnetic concentrations for the Manchester samples were ~9 × lower than those measured by us for samples from a much younger, neurologically damaged cohort, from the more highly polluted Mexico City area (Calderón-Garcidueñas et al., 2020a). Unequivocally exogenous metal species (lead, cerium, platinum, aluminium) were found in similar concentrations in both AD and control Manchester samples.

2.3 Methods

2.3.1 Brain samples

Institutional ethics approval was granted by the Faculty of Health and Medicine Research and Ethics Committee (Lancaster University, FHMREC18101 and FHMREC18102). All samples were obtained, processed, and stored in accordance with the Human Tissue Act and institutional ethical guidelines.

2.3.1.1 Manchester Brain Bank samples

Tissue samples were supplied by the Manchester Brain Bank (MBB), U.K. (part of the Brains for Dementia Research programme, jointly funded by Alzheimer's Research UK and the Alzheimer's Society) with ethical review and approval by the MBB Management Committee and the Newcastle and North Tyneside I Regional Ethics Committee. Individuals (or their relatives) elect (with informed consent) to donate to the MBB, producing a self-selecting, elderly study group. Group characteristics are summarized in Table 2.1.

A large (~30 g) sample of fresh/frozen tissue was obtained from the cerebellum, and frontal, occipital, and temporal lobes, from 30 individuals (Supplementary Table A2). Of the 30 individuals, 17 were female (14 AD, 3 controls) and 13 male (5 AD, 8 controls), age range 80 to 98 years. For 27 of these individuals, the entorhinal cortex was sampled as a separate entity (~0.5 g), whereas the 'temporal lobe' samples may or may not encompass entorhinal cortex tissue. The entorhinal cortex was chosen as a region of interest as it is a site of early AD pathology (Van Hoesen et al., 1991). All samples originated from the right hemisphere; accompanying data including Braak staging, plaque, and tangle counts were from the corresponding left hemisphere sample (provided by the MBB). Individuals were selected to give broadly a group of individuals that were cognitively normal (controls, n=11) and a group with AD/dementia pathology (n=19) ranging from Braak stage III to VI (Braak and Braak, 1991). Individuals were classified as either control or AD based on their pathology (Supplementary Table A2).

Table 2.1 Summary of sample group characteristics, for Alzheimer's disease (AD) and controls. Significant p values are indicated in bold and are the result of Mann Whitney-U tests (aside from sex which was determined via chi-squared test).

Variable	Controls (n=11)	AD (n=19)	P value
Age (years)	90 ± 3	88 ± 5	0.112
Males (Females)	8 (3)	5 (14)	**0.013**
Post-mortem delay (PMD, hours)	80 ± 56	67 ± 32	0.701
Whole brain weight (g)	1197 ± 173	1125± 112	0.291

2.3.1.2 Mexico City Brain samples

Mexico City brain samples were provided by Dr Lilian Calderón-Garcidueñas, with ethical approval from the University of Montana. Ethical approval for working with these samples was also granted by the Faculty of Health and Medicine Research and Ethics Committee, Lancaster University (FHMREC18102). Upon arrival at Lancaster University, the samples were treated in the same manner as the MBB samples in terms of the preparation, measurement, and analysis. These samples have been described previously (Calderón-Garcidueñas et al., 2020a) and were magnetically measured at the Centre for Environmental Magnetism and Palaeomagnetism, Lancaster University.(Van Hoesen et al., 1991, Braak and Braak, 1991)

2.3.2 Subsampling and control for airborne contamination

The MBB samples were obtained and frozen between 6- and 156-hours post-mortem. Care was taken to ensure minimum exposure of samples to potential sources of magnetic contamination, and any such source was quantified (Supplementary Table A1). Sample external surfaces were trimmed with a ceramic knife to remove any contamination incurred during autopsy (e.g., metal fragments from surgical instruments or the saw used to open the skull). Each trimmed sample was divided into 3 approximately equal sub-samples, with an additional small subsample (0.2 g) taken for metals analysis by ICP-MS. All sub-sampling and processing of samples took place in a class II biological safety cabinet inside a class III biological laboratory. Surfaces and the ceramic knife were treated with 70 % ethanol (with unmeasurable magnetic content). The magnetic content of the safety cabinet air throughflow was quantified, by saturation isothermal remanence magnetisation (SIRM) measurements of pumped air samples, on magnetically- 'clean' polytetrafluoroethylene (PTFE) filters.

The tissue samples were freeze-dried for 48 hours using a Christ Alpha 2-4 LD plus freeze drier. Freeze-dried masses range from 0.125 to 3.054 g (average 0.781 g), except for the much smaller entorhinal cortex samples (average 0.080 g). To preclude operator bias, samples were

prepared, measured, and analysed blind. All magnetic values were mass-normalized for freeze-dried brain weight (kg).

2.3.3 Magnetic Analyses

The SIRM can be used to approximate ferrimagnetic concentrations (Maher et al., 2016) . All measurements were carried out at room temperature (293 K ±0.5 K) using SQUID magnetometry, with a RAPID 2G DC magnetometer (2G Enterprises, California USA; mean background noise level ~1 x 10^{-12} Am^2), at the Centre for Environmental Magnetism and Palaeomagnetism, Lancaster University. The natural remanent magnetisation (NRM, i.e., the sample magnetisation prior to artificial magnetisation in the lab) and/or SIRM of each individual styrene sample pot (and clingfilm) was measured and subtracted, in order to isolate the NRM and/or SIRM of the tissue sample. Sample NRMs were measured for the majority of Manchester samples (83 of 146 samples) (Supplementary Figure A1). No *a priori* assumptions were made with regards to sample NRM values; measurable NRMs might result from viscous remanent magnetisation (VRM) acquired from prior, *in situ* magnetisation of tissue (e.g., via environmental magnetic fields). Based on typical 'background' readings (holder, pot, clingfilm), we determined an experimental cut-off value of 2 x 10^{-11} Am^2; any values below this were deemed unmeasurable. Similarly, van der Weerd et al report their noise floor as of the order of 10^{-11} Am^2 (van der Weerd et al., 2020). On the basis of our cut-off value, 5 Manchester samples were unmeasurable (for SIRM).

SIRMs were generated in a direct (DC) field of 1 Tesla (T), using a Newport 4" Electromagnet Type A; demagnetisation steps of 5, 10, 15, 20, 25, 30, 40, 50, 75 and 100 milliTesla (mT) utilised the 2G's integrated AF demagnetiser. IRM acquisition curves were obtained for a sub-set of samples, using stepwise DC fields of 10, 20, 50, 100, 200, 300 and 1000 mT using the 2G IRM unit. Samples were measured immediately following acquisition of SIRM. Concentrations of magnetite and of maghemite were calculated from the measured SIRM values, using experimentally-derived values of 13.8 Am^2 kg^{-1} for ~31 nm interacting, mixed, single domain and superparamagnetic magnetite (Maher, 1988) and 12.0 Am^2 kg^{-1} for ~31 nm interacting, mixed, single domain and superparamagnetic maghemite (Maher, unpublished data).

2.3.4 Metals Analysis

A small (0.2 g) fresh frozen subsample was taken from each sample (not from the entorhinal cortex due to the limited mass available). Samples were accurately weighed (wet-weight) in acid-cleaned PTFE containers and digested at 60 °C for 6 hours in a digestion solution buffered

at pH 7.0. The digestion solution comprised 20 units/ml purified papain (Sigma Aldrich), 0.5 mM EDTA and 0.5 mM cysteine. All solutions and reagents were prepared from MillliQ water (≥18.2 MΩ) in a metal-free laboratory. The digestion solution was then filtered using (< 0.1 µm PTFE Omnipore membrane filter) to preclude any particulate contamination from the papain. At the end of this enzymatic digestion, solutions were transferred to 50 ml acid-washed Teflon centrifuge tubes and centrifuged at 4500 rpm for 45 min. The clear supernatant was then filtered (<0.1 µm PTFE membrane filter) and acidified using 2% ultrapure HNO_3 (Optima, Fisher Scientific) for bioavailable trace metals analysis using a Perkin Elmer NexION 350D inductively coupled plasma mass spectrometer (ICP-MS) with a reaction/collision cell. Helium was used as a collision gas and ammonia used in the dynamic reaction cell to eliminate polyatomic interferences. The instrument was calibrated with 31 elements of a working standard and verified by SLRS-6 water Certified Reference Material.

2.3.5 Statistical Analysis

All statistical analysis was conducted using SPSS 24 software (IBM). Normality tests were performed using the Shapiro-Wilk test. Data were log-transformed to reduce skewness. Specific tests were either a one-way ANOVA (with Tukey's post-hoc), Kruskal-Wallis test, independent samples t test or independent samples Mann-Whitney U test, depending on the degree of normality of the data. Significance level (α) was set to 0.05.

2.4 Results

Measurable amounts of ferrimagnetic material (as determined by SIRM) were detected in most of the Manchester samples (141 measurable; 5 unmeasurable). As for previous brain samples from Manchester, and Mexico City (Maher et al., 2016), the majority of magnetic remanence is acquired by 100 mT (Figure 2.1), and close to saturation at 300 mT. Such behaviour is typical of the presence of a magnetically-'soft', magnetite-like component, and consistent with other studies of magnetite in human brain tissue (Kirschvink et al., 1992a, Maher et al., 2016).

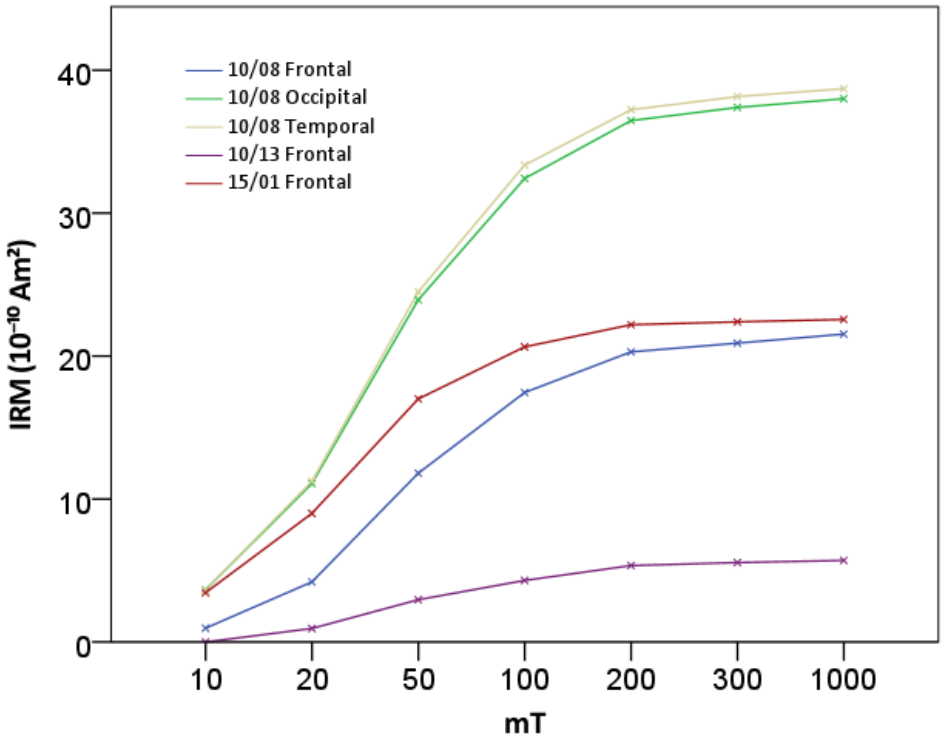

Figure 2.1 Room-temperature IRM acquisition of human brain tissue, Manchester Brain Bank samples.

Mass-normalized SIRMs of the Manchester brain samples ranged from 0.06 to 13.69 x 10^{-6} $Am^2 kg^{-1}$ (median 0.49 x 10^{-6} $Am^2 kg^{-1}$), equating to between ~4 and 992 ng of magnetite g^{-1} tissue (median 36 ng magnetite g^{-1}) and median of 0.44 x 10^9 MNPs g^{-1} or equating to between ~5 and 1140 ng of maghemite g^{-1} tissue (median 41 ng maghemite g^{-1}) and median of 0.83 x 10^9 MNPs g^{-1} (Tables 1-2, Figure 2.2). These SIRM values are on average ~11 × higher than those reported for formaldehyde-stored brains (at 293 K) (Gilder et al., 2018). They are similar in magnitude (Supplementary Figure A4) to those obtained (at 5 K and 100 K) for fresh/frozen brain samples, from the medial temporal gyrus (van der Weerd et al., 2020) (SIRMs measured at temperatures below 293 K e.g. 77 K,100 K, are often higher, as they capture the additional remanence of magnetic particles so small (<~30 nm) as to be magnetically unstable at room temperature).

Table 2.2 Magnetite concentration and particle number of human brain samples from AD and control brains from Manchester Brain Bank, UK. Magnetite concentrations were calculated using an empirically-derived value for SIRM SP/SD magnetite of 13.8 Am^2 kg-1, for interacting, mixed single domain (SD) and superparamagnetic (SP) magnetite, of mean particle size 31 nm (Maher, 1988), rather than the 'conventional' SIRM magnetite value of 46 Am^2 kg^{-1}, which is applicable only to pure, non-interacting, single domain (50 nm) magnetite particles. The number of magnetite particles/g dry tissue can then be estimated by dividing the mass of magnetite (per 1g dry tissue wt.), by the mass of 1 magnetite particle (8.07224^{-11} µg).

	AD	Control
Min SIRM (10^{-6} Am^2 kg^{-1})	0.08	0.06
Max SIRM (10^{-6} Am^2 kg^{-1})	13.69	5.33
Median SIRM (10^{-6} Am^2 kg^{-1})	0.45	0.56
Min magnetite ng g^{-1}	5.79	4.35
Max magnetite ng g^{-1}	992.03	386.23
Median magnetite ng g^{-1}	32.68	40.58
Min particles 10^9 g^{-1}	0.07	0.05
Max particles 10^9 g^{-1}	12.29	4.78
Median particles 10^9 g^{-1}	0.40	0.50

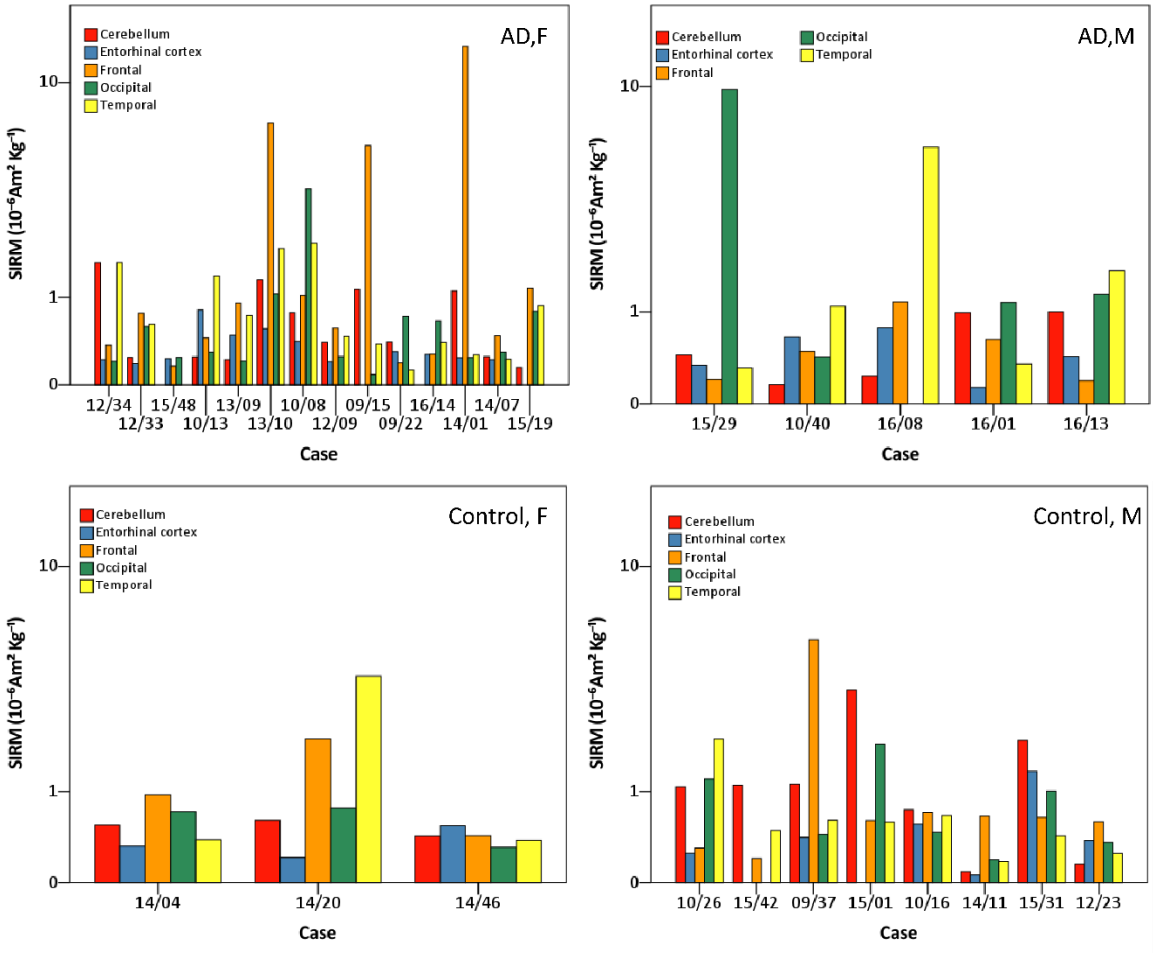

Figure 2.2 Regional distribution of mass normalised SIRM values for human Alzheimer's disease (AD) and control brains from Manchester Brain Bank, UK. Individuals are arranged in each panel by ascending age (80-98 years) and split by sex (F = female, M= male).

Critically, for the 5 brain regions (cerebellum, entorhinal cortex, frontal, occipital, and temporal lobes) from the Manchester individuals (n=30), there is no evidence of homogeneity of magnetite/maghemite distribution; the regional content of brain magnetite/maghemite varies from one individual to another (Figure 2.2). Nor is there any evidence for increasing brain ferrimagnetic content or iron content with age for persons aged 80 - 98 years.

Comparison of AD regions with their control region counterparts showed no significant difference in magnetite concentration (Independent Mann Whitney-U test) (Figure 2.3, Table 2.2, Supplementary Table A3). Examination of all Manchester individuals showed higher concentrations of magnetite/maghemite in the frontal lobe compared to the entorhinal cortex (one-way ANOVA on log-transformed data with Tukey's post hoc, p=0.021) (Figure 2.3, Supplementary Figure A2). Higher magnetic concentrations were seen in the frontal lobe of female AD cases compared to female controls; however, no statistical difference was seen when comparing any region between AD and controls (as a whole or stratified by sex) (Kruskal-Wallis test on untransformed data) (Supplementary Table A3). Analysis of the data excluding the occipital sample from case 15/29, which has an unusually high NRM, shows higher ferrimagnetic concentrations in both the frontal and temporal lobes compared to the entorhinal cortex (one-way ANOVA on log-transformed data with Tukey's post hoc, p=0.015 and p=0.049 respectively). Given the observed variability in magnetic content, a larger number of AD and controls (approximately 93 in each group) is needed for robust statistical analysis.

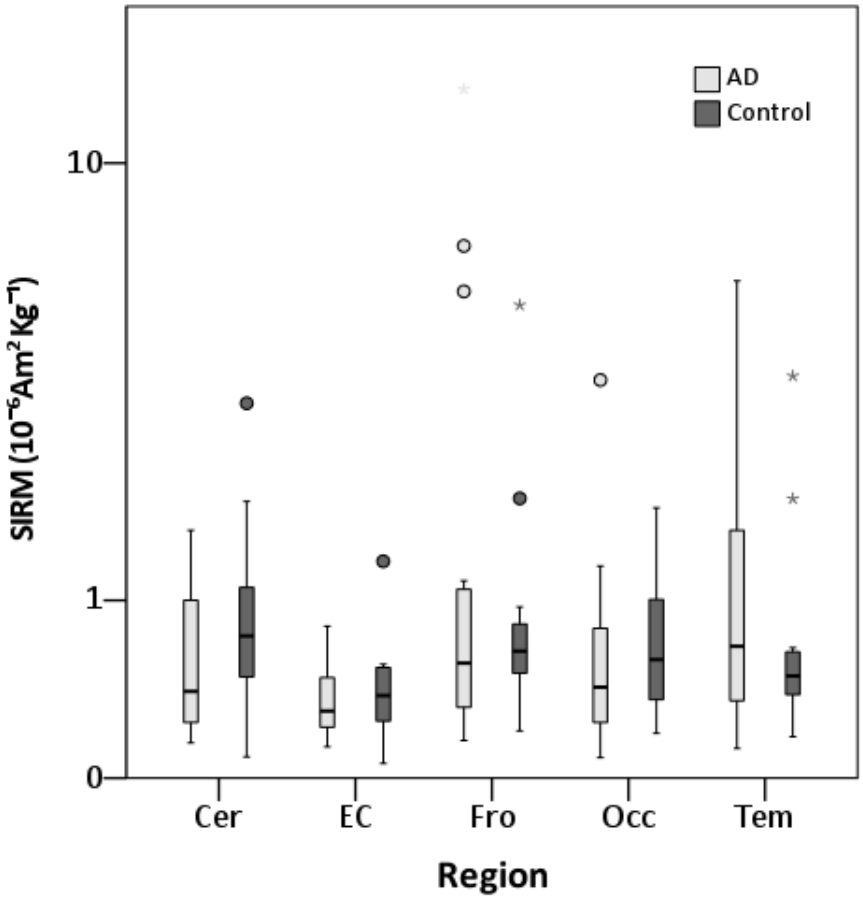

Figure 2.3 Mass-normalised SIRM values of human brain regions from AD and control brains from Manchester, UK. Box plot represents room temperature (293K) measurements of freeze-dried human tissue from AD or control brains from the cerebellum (n=17 AD, 11 Control), entorhinal cortex (n=17 AD, 11 control), frontal lobe (n=19 AD, 11 control), occipital lobe (n=19 AD, 10 control), and temporal lobe (n=18 AD, 11 control). Outliers (○) are more than 1.5x the interquartile range, extremes (*) are more than 3x the interquartile range.

As with the magnetite/maghemite concentrations, no significant differences were seen when comparing regional concentrations of exogenous metals in AD cases compared to controls (Figures 2.4-2.5, Supplementary Tables A4-A7).

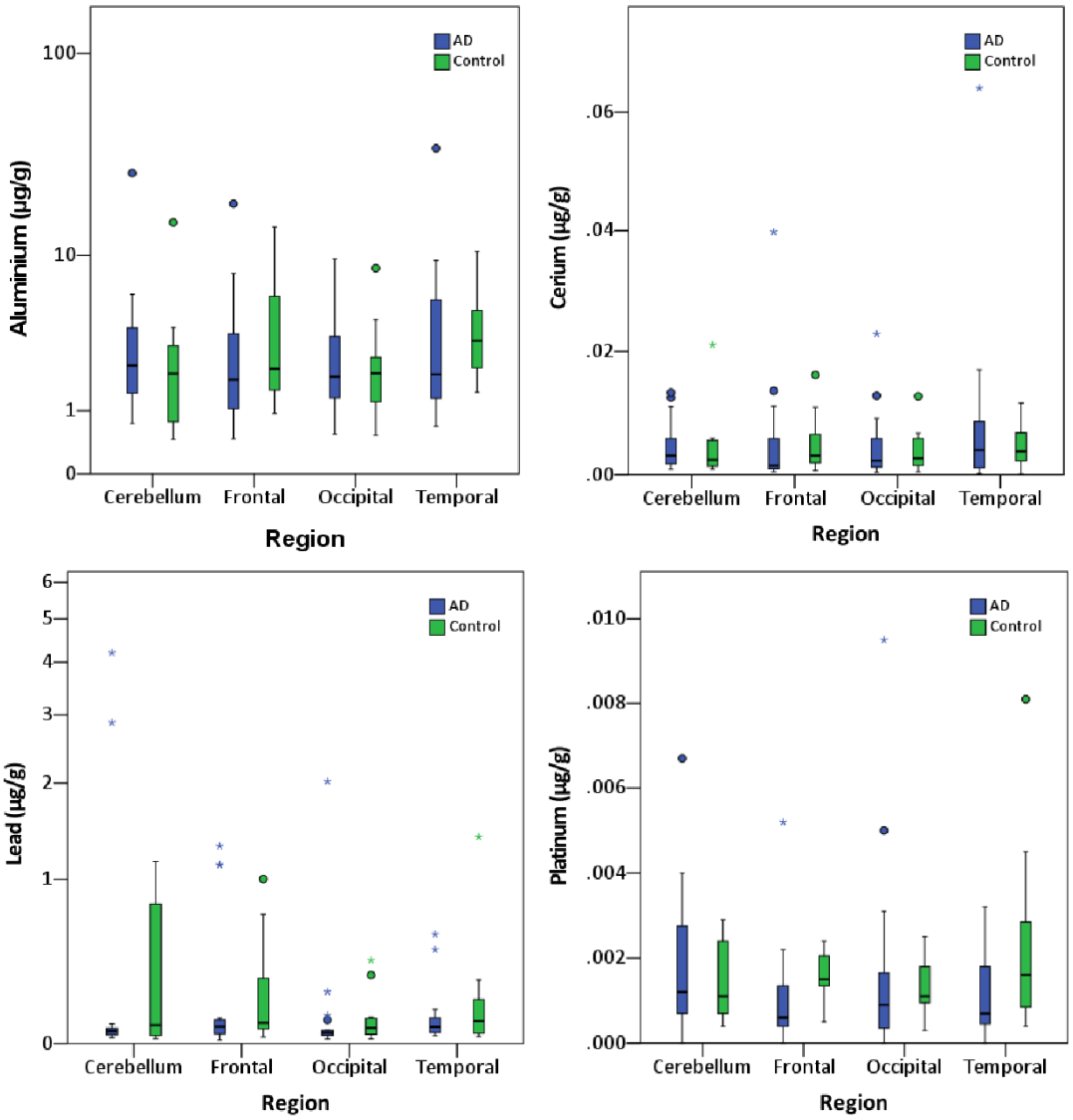

Figure 2.4 Mass-normalised concentrations of exogenous metals in human brain regions from AD and control brains from Manchester Brain Bank, UK. Box plots represent ICP-MS measurements of aluminium, cerium, lead and platinum in freeze-dried human tissue from AD (n=19) or control (n=11) brains from the cerebellum, frontal lobe, occipital lobe, and temporal lobe. Outliers (○) are more than 1.5x the interquartile range, extremes (*) are more than 3x the interquartile range.

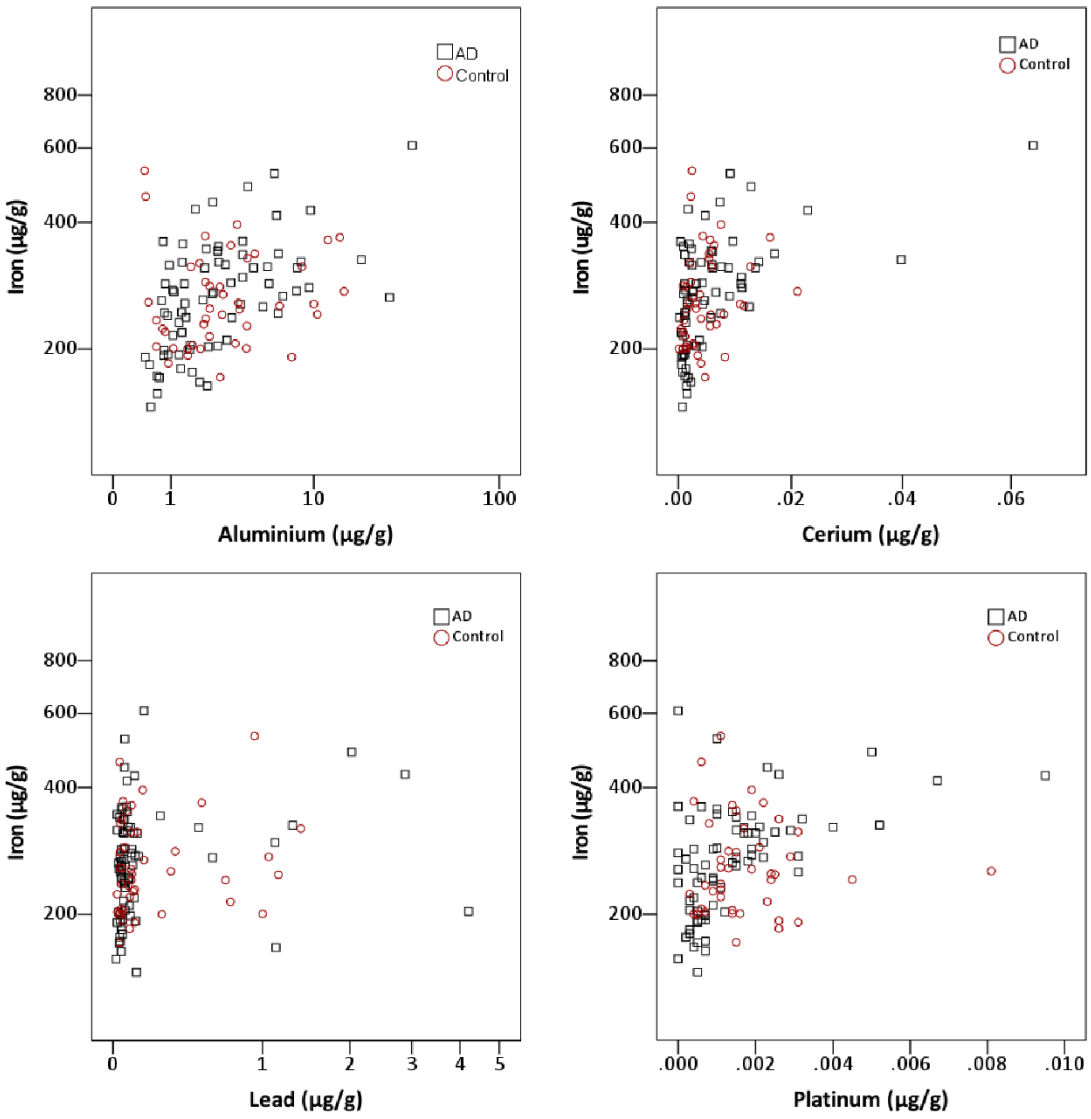

Figure 2.5 Mass-normalised concentrations of exogenous metals in human brain regions from AD and control brains from Manchester Brain Bank, UK. Scatter plots represent ICP-MS measurements of aluminium, cerium, iron, lead and platinum in freeze-dried human tissue from AD (n=19) or control (n=11) brains from the cerebellum, frontal lobe, occipital lobe, and temporal lobe.

We can usefully compare the concentration of cerebellar magnetite/maghemite in our elderly Manchester cohort with previously reported data for a separate, much younger population, with lifelong residence in Metropolitan Mexico City (MMC)(Calderón-Garcidueñas et al., 2020a). The MMC samples were freeze-dried and measured, in Lancaster's Centre for Environmental Magnetism & Palaeomagnetism, in the same way as the Manchester samples (Calderón-Garcidueñas et al., 2020a). Mass-normalized SIRMs of MMC cerebellum samples ranged from 0.20 to 36.23 x 10^{-6} Am^2 kg^{-1} with a median of 2.25 x 10^{-6} Am^2 kg^{-1}, equating to ~14 to 2625 ng of magnetite g^{-1} tissue with a median of 163 ng of magnetite g^{-1} tissue (Calderón-Garcidueñas et al., 2020a). This is equivalent to a range of 0.18 to 32.52 x 10^{9}

particles g^{-1} with a median of 2.02 x 10^9 particles g^{-1}. Comparison of all cases from Mexico City showed significant difference between the 3 regions measured (Kruskal-Wallis test p=0.0114), specifically between the SN and cerebellum (Kruskal-Wallis, pairwise comparison with Bonferroni correction p=0.008). The highest concentration of magnetite/maghemite was found in the cerebellum, followed by the tectum/tegmentum and the substantia nigra.

In contrast to the Manchester samples, samples from Mexico City (Calderón-Garcidueñas et al., 2020a) were from forensic cases (sudden deaths, no brain injury), are a much younger population (aged 12 - 85 years, mean age 29 years; compared to Manchester: aged 80 - 98 years, mean age 89 years), are primarily male, and display neurological damage, previously linked with exposure to high levels of particulate air pollution (Calderón-Garcidueñas et al., 2019a). Both Manchester and Mexico City samples were prepared, measured, and analysed in the same manner, using the same magnetometer. Significantly higher magnetite/maghemite concentrations were found in the Mexico City samples compared to the Manchester samples (Independent samples Mann- Whitney U test on untransformed data, $p<0.001$). The ferrimagnetic concentrations in the Mexico City samples (all regions) are on average ~5 × higher than those of their Manchester counterparts (Figure 2.6).

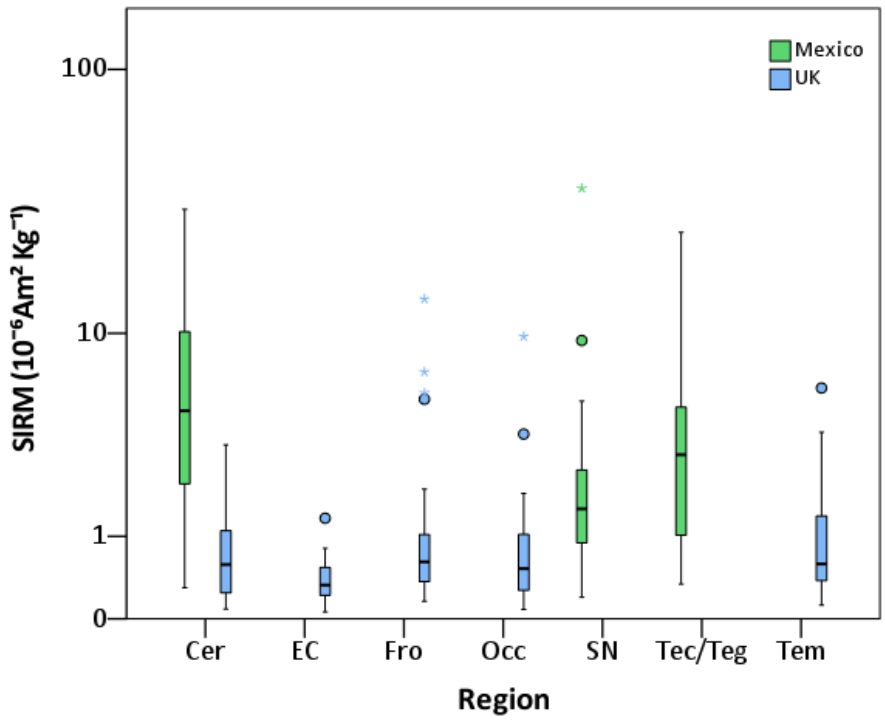

Figure 2.6 Box plot of mass normalised SIRM values of human brain regions from Manchester, UK and Mexico City, Mexico. Box plots depict the mass-normalised (freeze-dried weights) saturation isothermal remanence magnetisations (SIRMs) of human brain tissue samples measured at 293 K from the cerebellum, entorhinal cortex , frontal lobe, occipital lobe and temporal lobe of individuals from Manchester, UK, (blue) along with the cerebellum, substantia nigra (SN), and tectum/tegmentum from Mexico City, Mexico (green)(Calderón-Garcidueñas et al., 2020a). Outliers (○) are more than 1.5x the interquartile range, extremes (*) are more than 3x the interquartile range.

2.5 Discussion

Discrete nanoparticles of the mixed Fe^{2+}/Fe^{3+}iron oxide, magnetite, and maghemite have been found in senile plaques e.g. (Plascencia-Villa et al., 2016) and within the frontal cortex (Maher et al., 2016), globus pallidus (Svobodová et al., 2019), temporal lobe (Bulk et al., 2018), superior temporal gyrus (Pankhurst et al., 2008), brainstem (Gilder et al., 2018, Calderón-Garcidueñas et al., 2020a), cerebellum (Calderón-Garcidueñas et al., 2020a), and hippocampus (Schultheiss-Grassi et al., 1999) of the human brain, but any relationship between these ferrimagnets and NDD is as yet poorly understood. Using SQUID magnetometry on fresh-frozen human tissue samples, we find a heterogenous distribution of magnetite/maghemite across the brain regions sampled from AD and controls from northern England. Magnetite concentrations are significantly higher in the frontal and temporal lobes (particularly affected in AD) compared to the entorhinal cortex. Conversely, no significant difference either in brain magnetite/maghemite or in exogenous metal (Pb, Pt, Ce, Al) concentrations was found between AD and controls in this elderly northern England cohort.

Notable is that significantly higher ferrimagnetic concentrations are present in the cerebellum of younger forensic cases from Mexico City (Calderón-Garcidueñas et al., 2020a) compared to the much older northern England brains.

Given the variability in regional distribution of magnetic particles, across elderly AD and control groups from northern England (Figure 2.2), we find no evidence for genetic control of the magnetite/maghemite distribution in the human brain. In contrast, a recent study of seven whole brains found an identical distribution pattern of magnetic particles across seven studied brains, thence attributed to endogenous, genetically controlled formation of magnetite (Gilder et al., 2018). Their SIRMs are systematically much lower than those reported here (our MBB samples are on average ~9 × more magnetic, and the Mexico City cerebellar samples are on average ~61 × more magnetic (Calderón-Garcidueñas et al., 2020a)) (Supplementary Figure A3). Gilder et al. (Gilder et al., 2018) further suggest that the maximum values they observe, for the brainstem and cerebellum – i.e., distal from the OB - cannot be accounted for by intake of exogenous ferrimagnetic particles via the nasal route. However, not only are nanoparticles likely to be transported through the brain (Newman et al., 2020), but the brainstem may have an additional entry portal via the gut wall and neuroenteric system (Calderón-Garcidueñas et al., 2020a).

One explanation for Gilder et al.'s (2018) low SIRM values is their use of formalin-fixed tissue; 10% formaldehyde was replenished over a storage interval of several decades. Evidence exists for magnetite dissolution by formalin in human tissue; e.g. ~50% reduction in SIRM after 1 week in formalin (Dobson and Grassi, 1996). The storage duration may be important. No changes in magnetite concentration were reported for paired frozen and fixed tissue samples after 5 months in formalin (van der Weerd et al., 2020). Storage for several years in formalin caused transformation from ferritin-like iron to non-ferritin iron as observed by Mössbauer spectroscopy (Gałązka-Friedman et al., 1996), whereas storage for 1 week did not change the magnetic particle size, as measured by SQUID magnetometry (Dobson and Grassi, 1996). Gilder et al.'s (2018) SIRM values - of the order of 10^{-8} - 10^{-7} Am^2 kg^{-1} - may represent only the remaining fraction of magnetite/maghemite resisting dissolution or transformation during the decades-long period of brain storage in formalin (Gilder et al., 2018). In contrast, the tissue samples here have been subjected only to freeze-drying; their measured, room-temperature SIRMs (of the order of 10^{-5} - 10^{-8} Am^2 kg^{-1}) are equal to or less than other published SIRM data

on human brain tissue (Supplementary Figure A4) (Kirschvink et al., 1992a, Maher et al., 2016, Brem et al., 2005b, van der Weerd et al., 2020, Pankhurst et al., 2008).

A previous magnetic study reported higher magnetite concentrations in the temporal lobe of female AD patients compared to controls (Pankhurst et al., 2008); similarly, a meta-analysis found higher iron content in the temporal lobe of AD patients compared to controls (Tao et al., 2014). Here, higher magnetite/maghemite concentrations were evident in the frontal and temporal lobes. However, we found no significant difference in magnetite concentration between the AD and control samples from northern England, U.K. Based on the variability in ferrimagnetic content observed here, power analysis suggests that larger numbers of samples (~100 per group) would be required for robust statistical analysis.

For the MBB cohort (i.e., AD + controls), higher magnetite/maghemite concentrations were found in the frontal and temporal lobes compared to the entorhinal cortex (Figure 2.3, Supplementary Figure A2), and highest magnetite concentrations in the frontal lobes of two female AD cases. Magnetite content may be elevated in the frontal lobe due to its proximity to the OB, a proposed entry route (Oberdörster et al., 2004, Maher et al., 2016, Kanninen et al., 2020) of environmental/airborne magnetite(Kirschvink et al., 1992a). MNP concentrations are also high in the temporal lobe, the cortical region which first shows AD pathology - enriched in both senile plaques and neurofibrillary tangles, the two key pathological markers of AD. Plaques also occur in normal ageing, and MNPs appear to associate with senile plaques (Plascencia-Villa et al., 2016, Everett et al., 2018).

The entorhinal cortex is one of the first brain regions to show AD pathology (Braak and Braak, 1991), and receives input from the OB, also an early-affected region. Olfactory dysfunction is a possible biomarker for AD development, with correlation to tau biomarkers and significant olfactory dysfunction seen in population studies, e.g. (Murphy, 2019). Pollution NPs have been reported in the OB (e.g.(Calderón-Garcidueñas et al., 2010)), and nasal mucosa, with the OB a proposed entry route to the brain (Maher et al., 2016). Here, the higher magnetite concentrations seen in temporal and frontal lobes, compared to the entorhinal cortex, may reflect “nose to brain” transport pathways. Translocation of 10-550 nm graphene oxide (GO) nanosheets from the OB to distal sites (including cerebellum, hippocampus, striatum, midbrain, pons, and medulla) has recently been shown in mice, attributed to a combination of transcellular and paracellular movement of particles through and/or between olfactory epithelial cells (Newman et al., 2020). GO nanosheets were found in the OB 3 hrs. after

administration, and in more distal structures (including cortex, hippocampus, cerebellum) within 24 hrs.

It is notable that, in addition to variable ferrimagnet concentrations, brain samples from both our AD and controls contain varying concentrations of metal species of unequivocally exogenous origin (Pb, Al, Ce, Pt). As with the magnetite/maghemite concentrations, there is no significant difference between the exogenous metal (Al, Pt, Pb, Ce) contents of our N. England AD and control brain regions (Figures 2.4-2.5, Supplementary Tables A4-A7). Similarly non-physiological metal species, including vanadium, nickel, manganese, chromium, and lead, were reported in frontal lobe samples from Mexico City, with significantly higher manganese, nickel and chromium in Mexico City brains compared to less-polluted controls (from Veracruz, Mexico (Calderón-Garcidueñas et al., 2013b)).

The brain should be protected from incursion of such metals via the tight junctions of the blood-brain barrier (BBB). That both the AD and non-AD brains here contain readily measurable concentrations of exogenous metals (including traffic-derived Pt and Ce) indicates both variable levels of pollution exposure, and, critically, suggests the likely loss of BBB integrity across both of these elderly groups (aged 80 to 98 years at death). The timing of BBB breakdown in the investigated individuals is unknown but may have occurred at a relatively late life stage. BBB permeability is greater in older (aged 55 - 91yr) cognitively normal (CN) individuals compared to young (aged 23 - 47 yr.) CN individuals, and even greater in the mildly cognitively impaired (aged 55 - 85 yr.) compared to older CN individuals (Montagne et al., 2015). Interestingly, the metal element, Ce, which is present in all our Manchester cohort, only appeared in the urban particulate pollution 'mix' from 1998 onwards (i.e. when our investigated individuals were ~ 60 yrs. or older), when it was introduced as an anti-knock fuel additive (Maher, 2019). Lead was removed from vehicle fuel in the UK in 1999, but remains a common component of airborne particulate pollution because it is widely used in vehicle ignition systems, fuel tanks, spark plugs etc. (Maher et al., 2008). Critically, the loss of BBB integrity suggested across all of our elderly Manchester cohort, i.e., both AD and 'controls', would obscure any possible relationships between metal pollution exposures in earlier life and subsequent development of neurological damage.

Ferrimagnetic concentrations are significantly lower (~9 × lower) in the cerebellar samples from the MBB cohort compared with much younger Mexico City forensic cases (Calderón-Garcidueñas et al., 2020a). Given the possibility of particle dissolution and clearance by the brain (Maher, 2019), the location/environment to which a young person is chronically exposed

may be reflected - as a 'snapshot', at postmortem - by the composition and concentration of exogenous metals present (Kirschvink et al., 1992a), such as platinum, cerium, and co-associated MNPs. Mexico City is highly polluted ($PM_{2.5}$ 32 μg/m^3 on average for 2009) compared to e.g., Manchester, U.K. ($PM_{2.5}$ 12 μg/m^3 on average for 2009). Studies have shown co-association between the abundant, intra-cellular presence of metal-rich nanoparticles and neurodegeneration, including brain inflammation and markers of AD pathology, even in children as young as 11 months e.g., (Calderón-Garcidueñas et al., 2020a, Calderón-Garcidueñas et al., 2019a). As noted above, the integrity of the BBB is known to deteriorate with age and NDD. Yet the Mexico City forensic cases, which comprise a much younger cohort (mean age 29 years) than the Manchester cohort (mean age 89 years), have significantly higher concentrations of brain magnetite/maghemite. In the absence of environmental insult, the BBB integrity of young individuals should be relatively intact, or minimally altered (Calderón-Garcidueñas et al., 2008). The high concentrations of magnetite/maghemite and metals seen in the young Mexico City brains thus most likely reflect their high lifelong and/or recent exposure to air pollution via inhalation and/or ingestion (Calderón-Garcidueñas et al., 2020a). Age-matched controls from a less-polluted city (Veracruz, Mexico) show no such neuropathology and much lower brain nanoparticle content.

Levels of exposure to airborne, iron-rich, and co-associated metal-rich pollution nanoparticles will be spatially and temporally variable not only across different urban areas but also between different cities worldwide, dependent on emission sources (traffic, domestic and industrial) and population proximity to those sources. Annual mean concentrations of airborne magnetite nanoparticles in Beijing, for example, have recently been reported as 75.5 ± 33.2 ng m^{-3} (~0.1% of $PM_{2.5}$ mass), with strong seasonal variations (Zhang et al., 2020a). Magnetite concentrations up to 0.8% of $PM_{2.5}$ mass have been reported in Thessaloniki, the second largest city in Greece (Kermenidou et al., 2021). Given such reported variations, both epidemiological and forensic analyses would be valuable in identifying any specific dose-response associations between exposures to airborne magnetic nanoparticles and both neurodegenerative and cardiovascular deficits (Maher, 2019, Maher et al., 2020).

In summary, given the high probability of BBB degradation in the very elderly, and the possibility of at least some dissolution and clearance from the brain, it is improbable that exogenous pollution particles merely accumulate with time/age. Hence, there may be little correlation in the very elderly between brain magnetite/maghemite and metal content either with age or AD status. Conversely, investigation of young, highly exposed individuals, with relatively intact BBB, may provide the information key for understanding the sub-cellular

impacts of air pollution particles on the brain in early life, and the neurological damage manifested often decades later in the life course.

2.6 Conclusions

1. We find a heterogenous distribution of magnetite/maghemite across AD and cognitively normal brains from northern England, as determined by SQUID magnetometry. The observed heterogeneity negates a previous suggestion of universal, genetic control on the distribution of magnetite/maghemite within the brain. Conversely, such variations are consistent with different levels of exposure to and/or clearance of exogenous magnetic nanoparticles, which occur in abundance at the roadside, for example, but are also emitted by industry, residential fires, some occupational sources etc.
2. In the northern England cohort, highest magnetite concentrations were found in the frontal lobe in both AD and controls.
3. There were no significant differences in either the ferrimagnetic content or the concentrations of other metal pollutants (Al, Pb and unequivocally vehicle-derived metals, e.g., Pt and Ce) between the AD and the controls from northern England. These data suggest loss of BBB integrity in both elderly groups, with potentially enhanced incursion of exogenous, metal-bearing particulates from a late life stage (i.e., > ~ 60 yrs.).
4. Compared to the elderly northern England cohort, magnetite/maghemite concentrations were significantly higher in the much younger Mexico City forensic cases, where BBB integrity would be expected. Common to the young Mexico City cohort is their lifelong exposure to much higher levels of particulate air pollution compared to their elderly northern England counterparts.
5. Investigation of any causal role of magnetite/maghemite and other metal-bearing air pollution nanoparticles should focus on young, apparently healthy cohorts, in order to identify any associations between early neuropathology and air pollution exposures, especially regarding particulate composition, size distribution, portals of entry (e.g., inhalation vs ingestion), and specific, sub-cellular biological targets. Such information is essential in order to understand the initiation and early development of neuropathology in the decades prior to clinical manifestation of NDD in later life.

Acknowledgements

JH receives a funded studentship from the Sir John Fisher Foundation. We acknowledge the support of the Manchester Brain Bank by Alzheimer's Research UK and Alzheimer's Society through their funding of Brains for Dementia Research (BDR) initiative, and service support costs from Medical Research Council.

Additional information

Competing interest: The authors declare no competing interests.

Chapter 3 (Paper 2) Trace and ultratrace metal concentrations in human brain tissue from Alzheimer's disease and controls

3.1 Abstract

Investigation of the metal content of various brain regions from Alzheimer's disease patients has shown perturbation in elements such as Fe, Cu, and Zn, relative to controls. Iron oxide nanoparticles (magnetite) of both biogenic and anthropogenic origin have also been reported in the brain and are often associated with other exogenous metals. We examined the concentration and distribution of 22 metals and 3 metalloids in the cerebellum, frontal, temporal, and occipital lobes of Alzheimer's disease cases (n=19) and controls (n=11) using inductively coupled plasma mass spectrometry. The metal concentrations varied between individuals, with no difference in concentration between Alzheimer's disease and controls. The distribution of Cu, Mn, and Se varied significantly with region, with elevated concentrations of these elements in the cerebellum compared to the frontal, temporal and occipital lobes. Principal component analysis revealed 4 elemental groupings (and inferred/likely environmental sources): component 1, Ce, Hg, Ti, Sb, Al, Co, W (traffic-related and crustal); component 2, Mo, V, Ni, Ag, Sr, Cr, Sn (fuel oil combustion); component 3; Cu, Mn, Fe, Se, Zn, Cd (biological and brake/tyre wear); and component 4, Ta, Pd, Pt (catalytic converters and dental alloys). These results indicate universal incursion of exogenous particles, likely traversing the compromised geriatric blood brain barrier. Monitoring of metals using post-mortem bio-bank samples from different age groups and geographical locations seems key to understanding the impacts of metals exposure on neurodegenerative disease pathogenesis, which may start several decades prior to clinical manifestation.

Hammond, J., Ahmed, I.A.M. & Maher, B.A. Trace and ultratrace metal concentrations in human brain tissue from Alzheimer's disease and controls. In preparation for submission to *Metallomics*

Author contributions statement

JH: validation, formal analysis, data curation, writing – original draft, writing – review & editing, visualization **IAA**: conceptualization, methodology, validation, investigation, resources, writing- review & editing **BAM**: conceptualization, writing – review & editing, supervision.

3.2 Introduction

Many of the ~20 elements that are essential to human biology are metals (e.g., Cu, Co, Fe, Mn, Mo, Zn) or metalloids (i.e., elements with properties intermediate to metals and nonmetals, e.g., As, Sb, Se), typically present in bulk or trace amounts (ppm, 1-1000 μg/g) (Zoroddu et al., 2019). Other metals such as Hg, Pb, Al and the metalloid, As, are not known to have any physiological function in humans and typically occur in ultratrace (ppb, < 1μg/g) amounts within tissue (Zoroddu et al., 2019). Humans are exposed to metals and metalloids in the environment from a variety of natural and anthropogenic sources through water, air, food, cosmetics, and medicines (Supplementary Table B1).

In the human brain, Fe, Cu and Zn are the most abundant metals; Fe is crucial in myelination and neurotransmitter synthesis, Cu is needed for the antioxidant enzyme Cu/Zn superoxide dismutase (SOD) and the vital respiratory chain enzyme cytochrome c, and Zn is a cofactor for over 200 enzymes and a neuromodulator involved in neurotransmitter release (Ward et al., 2014, Magaki et al., 2007, Jan et al., 2002). Although they play vital roles, levels of metals must be tightly regulated to prevent deficiencies and/or to prevent neurotoxicity. Redox active metal ions such as Fe(II/III) and Cu(I/II) can mediate the generation of harmful reactive oxygen species (ROS) such as superoxide ($O_2^{\bullet}$) via the Fenton reaction. If cells are not able to deal with excess ROS, cellular components (e.g., DNA, lipids, proteins) are oxidised, placing the cell in a state of oxidative stress which if not resolved can lead to apoptosis (Kanti Das et al., 2015, Winterbourn, 1995). As a highly oxidative organ, the brain is particularly susceptible to oxidative damage, and has lower levels of cellular antioxidant defences (e.g., catalase, glutathione) compared to other tissues (Halliwell, 2006, Cobley et al., 2018). Labile or 'free' metals are often highly reactive, so complexing these metals within metalloproteins (e.g., iron storage in ferritin, copper in ceruloplasmin) reduces the amount of reactive labile metal available to generate oxidative damage (Friedman et al., 2011). The brain is protected from circulating metals by the blood brain barrier (BBB) and blood-cerebrospinal fluid barrier, both of which are cellular barriers held together by tight junctions, with metal transporter proteins to facilitate controlled passage of numerous metals into the brain (Skjørringe et al., 2015). However, nanoparticles are capable of penetrating the BBB, and so may interfere with metal homeostasis in the brain by causing inactivation or breakdown of metalloenzymes responsible for detoxifying ROS (Sokolova et al., 2020). The integrity of these protective barriers is weakened with age, and with neurodegenerative disease, allowing for uncontrolled influx of metals (Erdő et al., 2017, Sweeney et al., 2018).

Dyshomeostasis of metals in the human brain has been associated with various neurological and neurodegenerative diseases, including Alzheimer's disease (AD), Parkinson's disease, multiple sclerosis, and schizophrenia (Cilliers, 2021, Cory-Slechta et al., 2020, Mealer et al., 2020). AD is the most common form of dementia, characterised by two key pathological hallmarks composed of aberrantly folded protein; extracellular deposits of amyloid beta (Aβ) in senile plaques, and intracellular inclusions of hyperphosphorylated tau in neurofibrillary tangles (NFTs)(Braak and Braak, 1991). There is currently no definitive known cause of sporadic cases of AD; it is thought to arise due to a complex interplay between genetic and environmental factors in the decades prior to clinical manifestation. Oxidative stress, metal dyshomeostasis and air pollution have been suggested to play a role in AD pathogenesis (Bush, 2013, Kanti Das et al., 2015, Calderón-Garcidueñas et al., 2020c, Dos Santos et al., 2021, Maher, 2019, Everett et al., 2021a). The essential metals, Fe, Cu, and Zn, have been implicated in AD progression, promoting Aβ synthesis, depositing in senile plaques, enhancing aggregation of Aβ and tau (both metal-binding proteins), and reducing their clearance (Lovell et al., 1998, Bolognin et al., 2011, Kim and Lee, 2021, Sastre et al., 2015, Plascencia-Villa et al., 2016). Toxic metals such as Pb, Cd, Al, As, and Hg have also been implicated in AD pathogenesis due to their effects on cognition, ability to cross the BBB, ability to induce oxidative stress, and pro-pathogenic effect on Aβ and tau (Rahman et al., 2021, Bakulski et al., 2020, Cory-Slechta et al., 2020, Cornett et al., 1998b). Arsenic, for example, is an infamous poison; long term exposure to this highly toxic metalloid resulted in cognitive deficits in an elderly Texan population and has been shown to increase phosphorylation of tau, increase Aβ levels and induce inflammation *in vitro* (O'Bryant et al., 2011, Zarazúa et al., 2011).

Ex vivo studies have been conducted since the 1950s on post-mortem human brain tissue samples to establish baseline concentrations of different elements in the normal human brain for comparison with those measured in different disease states, e.g. (Harrison et al., 1968, Wenstrup et al., 1990, Stedman and Spyrou, 1995, Cornett et al., 1998a, Rahil-Khazen et al., 2002, Ramos et al., 2014b) (Supplementary Table B2). Advances in analytical techniques have enabled greater sensitivity and spatial resolution than previous studies; inductively coupled plasma (ICP) mass spectrometry (-MS) and optical emission spectrometry (-OES) are two of the most common methods for measuring trace element concentrations in the human brain (Grochowski et al., 2019, Scholefield et al., 2020, Szabo et al., 2015, García et al., 2020, Ramos et al., 2014a, Krebs et al., 2014, Hare et al., 2016, Xu et al., 2017, Cilliers and Muller, 2021). However, consensus is poor regarding changes in metal and metalloid concentrations in AD brain tissue, likely due to differences in analytical methods used, usage of fresh vs fixed tissue

(some evidence of elemental leaching with long term storage in formalin), examination of different regions, use of different hemispheres, inherent biological variation (limited further by small sample sizes), comparison of dry weights to wet weights, geographical differences, occupational differences and age differences between cases and 'controls' (Schrag et al., 2010). Despite these challenges, a meta-analysis of studies published up to 2010 looking at Fe, Cu and Zn in human brains reported that Cu is decreased in AD, Zn is either elevated (in the parietal lobe) or unchanged, and that the putamen was the only region where Fe levels were consistently reported to be elevated in AD cases (Schrag et al., 2011b). The authors noted a citation bias favouring studies reporting increased Fe in AD (Schrag et al., 2011b). . Conversely, a 2014 meta-analysis reported elevated Fe in eight brain regions within the AD brain (Tao et al., 2014). Studies since 2014 have reported elevated Fe in the frontal cortex, hippocampus, entorhinal cortex, and middle temporal gyrus of AD brains, widespread decreases in Cu, and elevations of Zn in regions starkly affected by AD (entorhinal cortex and middle temporal gyrus) and decreases in the cerebellum which is relatively spared from AD pathology (Szabo et al., 2015, Hare et al., 2016, Xu et al., 2017).

Air pollution, in particular ultrafine particulate matter (UFPM, <100 nm aerodynamic diameter), is a rich source of metals in the environment. Humans are exposed to air pollution on a global scale; 99% of the global population is exposed to particulate matter in excess of the (WHO) mean annual limits of 15 $\mu g/m^3$ and 5 $\mu g/m^3$ for PM_{10} and $PM_{2.5}$ (particulate matter with a diameter of 10/2.5 μm or less) respectively (WHO, 2021a). Exposure to high levels of air pollution and living within close proximity to major roads have been identified as risk factors for developing neurodegenerative disease (Maher, 2019, Chen et al., 2017b, Mortamais et al., 2021). However, the specific component(s) of air pollution and mechanisms by which they contribute to pathogenesis are imperfectly understood. UFPM exhibits high penetration to major organs of the body including the brain; the olfactory bulb is a direct portal of entry to the brain, but UFPs may also translocate in circulation following inhalation, and/or travel to the brain via the neuroenteric system following ingestion (Maher et al., 2016, Oberdörster et al., 2004, Calderón-Garcidueñas et al., 2019b, Liu et al., 2021, Calderón-Garcidueñas et al., 2020a, Hammond et al., 2021). Magnetitic nanoparticles (magnetite (Fe_3O_4)/ maghemite (Fe_2O_3)) thought to be of exogenous origin have been reported in the frontal cortex of AD cases in association with non-physiological metals such as platinum (Maher et al., 2016). (Calderón-Garcidueñas et al., 2013b) Magnetite/maghemite nanoparticles (MNPs) have also been reported in the brains of Mexico City residents, along with AD pathology and AD-like cognitive deficits, even in the very young (Calderón-

Garcidueñas et al., 2018a, Calderón-Garcidueñas et al., 2020a, Calderón-Garcidueñas et al., 2020d). MNPs have been implicated in AD; MNPs have been found associated with Aβ plaques, are known to enhance aggregation of Aβ and tau, and have been reported to be toxic to neurons (Plascencia-Villa et al., 2016, Mir et al., 2012, Dadras et al., 2013, Coccini et al., 2017). It is not yet known if exogenous magnetite and other metal-bearing particles undergo dissolution/re-formation and/or clearance in the brain rather than accumulate with age (Van de Walle et al., 2019, Maher, 2019). In our previous study, for an elderly sample group, we found variable brain MNP concentrations, and no significant difference between those in AD brains and age-matched controls. The observed MNP variability identifies the need for larger sample sizes, while the presence of non-physiological metals in both AD and controls indicates universal geriatric loss of BBB integrity (Hammond et al., 2021).

To explore the relationship between essential and environmental metal(loid)s with AD, we used ICP-MS to determine the concentration of 22 metals (Al, Cd, Ce, Cr, Co, Cu, Fe, Pb, Mn, Hg, Mo, Ni, Pd, Pt, Ag, Sr, Ta, Sn, Ti, W, V, & Zn) and 3 metalloids (As, Sb, Se) in the cerebellum, frontal, temporal and occipital lobes of AD cases and age-matched controls (19 AD cases, 11 controls) from the Manchester Brain Bank, UK. A three-way ANOVA was conducted to examine the interaction between metal species, disease state, and brain region, on the measured metal concentrations. As the elements do not exist in isolation, we explored the relationship between metal(loid) species in the brain, and their magnetic content, via linear modelling and principal component analysis (PCA). To our knowledge, we provide the first reported concentrations of palladium (Pd), tantalum (Ta) and tungsten (W) in the human brain, and the first reported concentrations of cerium (Ce) and platinum (Pt) in the AD brain. These data complement and expand on our previous magnetic and metal (Pb, Ce, Pt, Al) characterisation of these samples (Hammond et al., 2021).

3.3 Methods

3.3.1 Brain samples

Tissue samples were supplied by the Manchester Brain Bank (MBB), U.K. (part of the Brains for Dementia Research programme, jointly funded by Alzheimer's Research UK and the Alzheimer's Society) with ethical review and approval by the MBB Management Committee and the Newcastle and North Tyneside I Regional Ethics Committee. The Faculty of Health and Medicine Research and Ethics Committee (Lancaster University) granted institutional ethics approval. All samples were obtained, processed, and stored in accordance with the Human

Tissue Act and institutional ethical guidelines. The samples used have been described previously (Hammond et al., 2021). In summary, fresh frozen brain tissue samples encompassing grey and white matter (right hemisphere) were obtained from the cerebellum, and frontal, occipital, and temporal lobes, from 30 individuals (17 F, 13 M) (Table 3.1). Samples were obtained and frozen between 6- and 156-hours post-mortem and were classified as AD or control based on their pathology, as assessed by a neuropathologist (19 AD, 11 controls). Individuals ranged from 80 to 98 years of age. Case information, including occupational data is available in Supplementary Table B3, and have been reported previously (Hammond et al., 2021).

Table 3.1 Summary of sample group characteristics, for Alzheimer's disease (AD) and controls. Significant p values are indicated in bold and are the result of Mann Whitney-U tests (aside from sex which was determined via chi-squared test). Dry/wet ratios are averages of all samples, ratios on a regional basis are available in Supplementary Table B4.

Variable	Controls (n=11)	AD (n=19)	P value
Age (years)	90 ± 3	88 ± 5	0.112
Males (Females)	8 (3)	5 (14)	**0.013**
Post-mortem delay (PMD, hours)	80 ± 56	67 ± 32	0.701
Whole brain weight (g)	1197 ± 173	1125± 112	0.291
Dry/wet ratio	0.189 ± 0.03	0.187± 0.03	0.653

3.3.2 Subsampling and control for airborne contamination

All sub-sampling and processing of samples took place in a class II biological safety cabinet inside a class III biological laboratory, as described previously (Hammond et al., 2021). A small (~0.2g) subsample was removed from ~30 g samples of fresh frozen tissue, each of which had been surface trimmed with a ceramic knife to remove any contamination incurred during autopsy (e.g., metal fragments from surgical instruments or the saw used to open the skull).

3.3.3 ICP-MS

Each fresh frozen subsample was analysed for 25 elements via ICP-MS as described previously (Hammond et al., 2021). Samples were divided in two, accurately weighed (wet-weight) in acid-cleaned PTFE containers and digested at 60 °C for 6 hours in a digestion solution (20 units/ml purified papain (Sigma Aldrich), 0.5 mM EDTA and 0.5 mM cysteine, pH 7.0). All solutions and reagents were prepared from MillliQ water (≥18.2 MΩ) in a metal-free laboratory. To preclude particulate contamination from the papain, the digestion solution was filtered using < 0.1 µm PTFE Omnipore membrane filter. When enzymatic digestion had

concluded, solutions were transferred to 50 ml acid-washed Teflon centrifuge tubes and centrifuged at 4500 rpm for 45 min. The resulting supernatant (clear) was filtered (<0.1 µm PTFE membrane filter) and acidified using 2% ultrapure HNO_3 (Optima, Fisher Scientific) for bioavailable trace metals analysis using a Perkin Elmer NexION 350D inductively coupled plasma mass spectrometer with a reaction/collision cell. Helium was used as a collision gas and ammonia used in the dynamic reaction cell to eliminate polyatomic interferences. The instrument was calibrated with 25 elements of a working standard and verified by SLRS-6 water Certified Reference Material. Samples were measured in duplicate and are reported as averages (dry weight µg/g). The metal and metalloid species measured are as follows: Al, Cd, Ce, Cr, Co, Cu, Fe, Pb, Mn, Hg, Mo, Ni, Pd, Pt, Ag, Sr, Ta, Sn, Ti, W, V, Zn, and Sb, As and Se.

3.3.4 Statistical Analysis

Each ICP-MS measurement was normalised by dry weight of the sample. Data are presented as mean ± standard deviation (SD) of two replicate measurements. The metal(loid) concentrations were scaled from 0 −1 by dividing the mean concentration by the highest mean concentration measured for that element. Statistical analyses were conducted using scaled data. For Ni, Sr and Pt, the highest mean concentration was omitted from data analysis; these data points were several orders of magnitude larger than other samples, as well as larger than the vast majority of data previously reported in human tissues (Cilliers and Muller, 2021, Stojsavljević et al., 2020, Rahil-Khazen et al., 2002, Corrigan et al., 1993, Ward and Mason, 1987, Szabo et al., 2015). Magnetic data (saturation isothermal remanence magnetism, SIRM), as previously described, were scaled using the same approach (Hammond et al., 2021). ANOVA analysis, Mann-Whitney U tests, chi-squared tests, and PCA was conducted using SPSS 28 software (IBM) (see B.1.1-B.1.1.2). Significance level (α) was set to 0.05 unless otherwise stated. Statistical significance levels used are: ^, $p \leq 0.05$, ^^, $p \leq 0.01$, ^^^, $p \leq 0.001$ ^^^^, $p \leq 0.0001$. R studio 4.1.1 was utilized for linear modelling and the generation of heatmaps.

3.4 Results and Discussion

Measurable amounts of each metal and metalloid species (for brevity, referred to hereafter as 'metals') were detected in the vast majority of samples. Ta was unmeasurable in four samples, Pt unmeasurable in five samples, As unmeasurable in seven samples, and Se (volatile, possibly lost during sample drying) was unmeasurable in 64 samples, i.e., a total of 80 out of 3000 measurements (2.7%) (Bush et al., 1995). The abundance of metals in the samples is as follows; Fe> Zn> Cu> Al> Hg> Mn> Ti> Pd> Sr> Pb> Cd> Mo> Ag> Cr> Ni> W> Se> As> V> Sb> Sn> Co> Ce> Ta> Pt. The cerebellum, frontal, occipital, and temporal lobes (previously characterized magnetically) were selected as they experience AD pathology to different degrees (Hammond et al., 2021). The temporal and frontal lobes are severely affected in AD, with the temporal lobe being one of the first regions affected; the occipital lobe is affected in the latter stages of disease; the cerebellum is relatively spared by AD pathology (Braak and Braak, 1991).

The absolute concentrations are in general agreement with previously published studies; however, comparison is difficult due to differences in sample populations (e.g., age, environment, male vs female) and analytical techniques. For example, our Pb levels are ~10 × those reported by Szabo et al 2015 (Szabo et al., 2015), a study which also utilised ICP-MS to measure Pb in the frontal cortex (fresh-frozen from the right hemisphere) of AD and controls, but the tissue originated from USA residents, the average age of AD cases was 10 years younger than our MBB cases, and the concentrations were reported as wet weight concentrations whilst we report dry-weight values. (Szabo et al., 2015, Panayi et al., 2002, Plantin et al., 1987, Ward and Mason, 1987, Wenstrup et al., 1990, Cornett et al., 1998a, Samudralwar et al., 1995). Zn concentrations measured here were the highest of studies comparing Zn levels in AD and control tissue, which range from 7.9 to 102 µg/g, and use a variety of different analytical methods and sample populations e.g. (Andrási et al., 2000, Andrási et al., 1995, Szabo et al., 2015, Scholefield et al., 2020, Ramos et al., 2014a, Samudralwar et al., 1995, Plantin et al., 1987, Panayi et al., 2002, Ward and Mason, 1987, Wenstrup et al., 1990, Cornett et al., 1998a). There is considerable variation in the absolute concentrations reported in human brain tissue, which is likely due, at least in part, to the environment to which individuals are exposed. For example, the levels of metals in brains from young residents (average age 33.06 y) of the highly polluted Mexico City are several orders of magnitude higher than other reported concentrations of metals in human brain tissue e.g. 67.28 µg/g Pb (ICP-MS, dry weight, frontal lobe) compared to 0.26 µg/g Pb (dry weight) in the frontal lobes of our elderly controls (Calderón-Garcidueñas et al., 2013b). Such high

concentrations could reflect the highly polluted environment, although lead was removed from vehicle fuel in the 1999 (in the UK), it still contributes to air pollution due to its usage in vehicle ignition systems (Hammond et al., 2021). However, a biomonitoring study spanning 20 years following residents living near a hazardous waste incinerator in Tarragona, Spain, also a polluted environment, found no increases in brain metal concentrations over time, and the absolute concentrations were several magnitudes lower than the Mexico City values, e.g., 0.12 µg/g Pb (ICP-MS, wet weight)(García et al., 2020). It is possible the extremely high concentrations seen in the Mexico City samples reflect a failure to clear metals from the brain and/or are an artefact of the measurements. Alternatively, these stark differences in absolute concentrations may be due to a major disadvantage of post-mortem studies; they provide a single measurement or 'snapshot' after death, which does not reflect the dynamic changes to metals and magnetite/maghemite throughout life. Many reports of metal concentrations in brain tissue are from several decades ago, use variable methodology, and lack appropriate controls. Regular studies (e.g., using bio-bank samples) using well-characterised methodologies are needed to accurately reflect changes in the diet and environment of populations over time.

In the current study, we followed strict analytical procedures eliminating trace metal contamination during sample preparation and rigorous ICP-MS routines with external/internal controls and standards solutions, giving high confidence in our measurements.

3.4.1 Comparison of AD and controls

Differences in metal concentrations between AD and control tissue might shed light on potential therapeutic targets and explain the increased risks for AD with exposure to air pollution exposure, a rich source of metals (Maher, 2019, Chen et al., 2017b, Mortamais et al., 2021). However, in this elderly group (average age at death 89 yrs.), there was no significant interaction between disease state and brain region, or disease state and metal species (regional data; Table 3.2, Supplementary Figures B1-B4, all samples; Supplementary Table B5) and previously no significant difference in magnetite/maghemite concentrations observed in the same individuals (Hammond et al., 2021). Marked variation was seen between individuals of both groups, as reflected by the error bars/standard deviation. Dietary exposure could be partially responsible for such variation, however dietary and dental records were unavailable for the cohort studied Previous studies have demonstrated no difference in the concentration of metals measured here between AD and control brains (note that some metals have not yet been reported in AD brains) (Supplementary Table B2). However, significant changes in metal concentrations have also been reported; elevations in Al, Cd, Cr, Cu, Fe, Mn, Hg, and Zn, and

decreases in As, Cd, Cu, Fe, Mn, Se, V and Zn in various brain regions (Supplementary Table B2). As stated previously, comparisons between different post-mortem studies are often difficult due to differences in analytical techniques, experimental design, and fundamental nature of biological diverse samples. Universal (and possibly late stage, i.e., > 60 yrs.) incursion of metals due to likely diminished BBB integrity with AD and advanced age could explain why no differences were seen between the metal concentrations here (Hammond et al., 2021).

Samples were broadly selected to give a range of disease and control tissues which were not intended to be age-, sex- or PMD-matched. There were no significant differences in age, post-mortem delay (PMD), dry/wet ratio or brain weight between the two groups (Table 3.1). PMD here (average 67h AD, 80h control) is longer than many other studies (e.g., 10 hr PMD Szabo et al 2015), and there is some evidence of a decline in As, Mn and Zn concentrations with increasing PMD (Szabo et al., 2015). However, there is no circulating blood at post-mortem and a halting of metabolism, so metals would not be transported away from the brain tissue in the blood, and no significant impact of PMD (measured up to 72h) has been observed, suggesting a minimal impact of PMD on metal concentrations (Varikasuvu et al., 2019, Scholefield et al., 2020, Xu et al., 2017). There was a significant difference in the number of male and female participants across the two groups; however, previous studies have reported no effect of sex when comparing metals in AD and control brains (Stedman and Spyrou, 1997, Panayi et al., 2002). There were no significant differences in metal concentrations when comparing male and female tissue samples (adjusted for the number of comparisons) (Supplementary Tables B6-B7).

Table 3.2 Regional distribution of metal elements in human brain tissue from Alzheimer's disease (n=19) and controls (n=11). Concentrations are reported as µg/g dry tissue.

		Cerebellum		Frontal		Occipital		Temporal	
		AD	Control	AD	Control	AD	Control	AD	Control
Al	Mean	3.92	3.06	3.39	4.76	2.87	2.55	4.92	4.18
	St. dev.	5.67	4.09	4.26	4.83	2.51	2.29	7.71	2.82
Sb	Mean	0.028	0.039	0.042	0.043	0.030	0.030	0.064	0.046
	St. dev.	0.020	0.043	0.056	0.039	0.023	0.040	0.108	0.057
As	Mean	0.084	0.043	0.063	0.106	0.053	0.061	0.084	0.063
	St. dev.	0.118	0.053	0.039	0.198	0.038	0.066	0.079	0.090
Cd	Mean	0.274	0.269	0.188	0.241	0.194	0.214	0.221	0.195
	St. dev.	0.195	0.130	0.089	0.131	0.115	0.123	0.104	0.099
Ce	Mean	0.005	0.005	0.005	0.005	0.005	0.004	0.008	0.005

	St. dev.	0.004	0.006	0.009	0.005	0.006	0.004	0.014	0.004
Cr	Mean	0.071	0.047	0.042	0.210	0.042	0.115	0.081	0.053
	St. dev.	0.109	0.043	0.041	0.355	0.045	0.187	0.116	0.032
Co	Mean	0.025	0.016	0.018	0.017	0.018	0.017	0.025	0.016
	St. dev.	0.014	0.006	0.013	0.008	0.011	0.009	0.018	0.011
Cu	Mean	46.84	44.38	23.75	27.78	27.11	28.94	25.90	24.87
	St. dev.	14.34	9.17	9.24	11.71	8.40	11.23	9.80	6.40
Fe	Mean	279.88	315.60	237.08	263.05	296.17	274.47	316.03	224.86
	St. dev.	82.35	102.61	59.97	76.60	100.23	44.70	108.80	43.23
Pb	Mean	0.419	0.379	0.241	0.260	0.164	0.119	0.125	0.233
	St. dev.	1.122	0.472	0.422	0.333	0.454	0.133	0.150	0.395
Mn	Mean	3.62	3.35	1.87	2.00	1.99	2.06	2.38	1.82
	St. dev.	0.85	0.71	0.66	0.33	0.50	0.41	0.95	0.34
Hg	Mean	3.25	3.06	3.44	3.33	3.05	2.46	4.70	3.32
	St. dev.	2.00	3.74	4.08	2.00	2.78	1.72	6.41	1.94
Mo	Mean	0.113	0.128	0.145	0.225	0.138	0.173	0.179	0.185
	St. dev.	0.034	0.106	0.045	0.164	0.042	0.079	0.107	0.133
Ni	Mean	0.074	0.079	0.072	0.089	0.049	0.073	0.096	0.075
	St. dev.	0.075	0.148	0.062	0.082	0.040	0.075	0.089	0.070
Pd	Mean	0.773	0.709	0.515	1.000	0.294	0.661	0.529	0.590
	St. dev.	1.536	0.607	0.444	0.854	0.275	0.544	0.600	0.493
Pt	Mean	0.002	0.001	0.001	0.002	0.002	0.001	0.001	0.002
	St. dev.	0.002	0.001	0.001	0.001	0.002	0.001	0.001	0.002
Se	Mean	0.172	0.239	0.009	0.035	0.053	0.042	0.036	0.017
	St. dev.	0.269	0.242	0.017	0.045	0.091	0.062	0.051	0.030
Ag	Mean	0.122	0.145	0.107	0.116	0.101	0.108	0.150	0.121
	St. dev.	0.062	0.226	0.090	0.074	0.082	0.075	0.147	0.049
Sr	Mean	0.210	0.311	0.258	0.318	0.205	0.228	0.342	0.214
	St. dev.	0.144	0.400	0.136	0.193	0.154	0.146	0.323	0.088
Ta	Mean	0.003	0.001	0.002	0.003	0.001	0.002	0.002	0.003
	St. dev.	0.003	0.001	0.002	0.002	0.002	0.001	0.001	0.004
Sn	Mean	0.026	0.026	0.028	0.037	0.025	0.030	0.031	0.029
	St. dev.	0.018	0.016	0.021	0.030	0.020	0.019	0.023	0.016
Ti	Mean	0.899	0.866	1.656	1.066	0.829	0.711	1.346	0.907
	St. dev.	0.345	0.750	3.300	0.711	0.485	0.396	1.347	0.469
W	Mean	0.064	0.072	0.059	0.061	0.068	0.056	0.133	0.064
	St. dev.	0.028	0.086	0.048	0.037	0.094	0.038	0.222	0.029

V	Mean	0.037	0.047	0.036	0.062	0.036	0.029	0.042	0.044
	St. dev.	0.022	0.075	0.027	0.076	0.033	0.015	0.035	0.022
Zn	Mean	126.25	116.49	109.43	115.18	100.91	93.45	138.83	108.86
	St. dev.	28.85	22.71	30.38	24.57	23.95	13.10	35.92	24.11

Metallomic analysis of human brain tissue is often limited by tissue availability, making it challenging to match controls and to have sufficient sample size for robust statistical analysis, further complicated by the inherent nature of biological variability across samples and populations. To our knowledge, there are no other published studies of Ta and Pd in human brain tissue, and only two studies looking at Pt in 'control' brains..

3.4.2 Regional distribution

Heterogenous distributions of Fe, Zn, and Cu have been reported in the human brain thought to reflect the structure function relationships of different brain regions (Popescu and Nichol, 2011). The distribution of exogenous metals within the brain could reflect the portal of entry to the brain; for example, Ti-rich nanoparticles have been found in the brainstem of Mexico City residents, thought to have entered the brain via the neuroenteric system (Calderón-Garcidueñas et al., 2020a). Distribution patterns of physiological metals have also been reported, such as the distribution of Fe along the olfactory pathway in AD cases (Samudralwar et al., 1995). Here, we explored the regional distribution of metals; a three-way mixed ANOVA was run to understand the effects of disease state, brain region and metal species on metal concentration (Figure 3.1). There was a statistically significant interaction between metal species and brain region, $p < 0.001$ (see B.1.1). All other two-way interactions were not statistically significant ($p > 0.05$), meaning disease state does not influence metal concentration. Data in Figure 3.1 represent all individuals combined (AD and controls). Mean copper, manganese, and selenium levels were higher in the cerebellum compared to the frontal, occipital, and temporal lobes, $p = <0.001$.

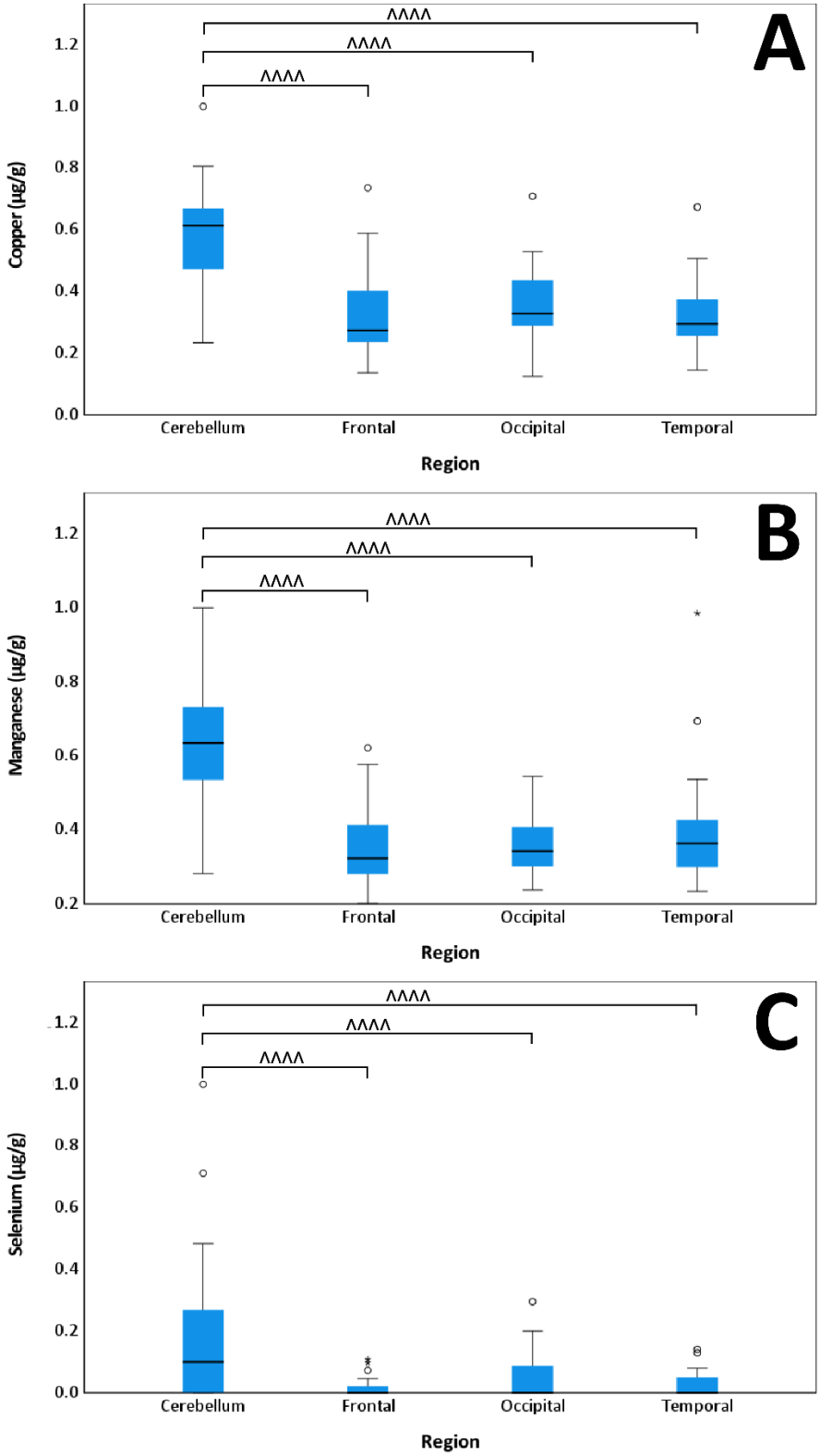

Figure 3.1 Regional distribution of copper, manganese, and selenium in human brain tissue. Box plots depict the concentration of copper (A), manganese (B) and selenium (C) determined via ICP-MS in tissue samples from the cerebellum, frontal, occipital, and temporal lobes from human brain tissue (n=30 per region). Statistical analysis was conducted via a three-way mixed ANOVA with Sidak correction post-hoc comparing the different regions measured (^). Outliers (○) are more than 1.5 × the interquartile range, extremes (*) are more than three times the interquartile range.

These regional distributions are consistent with other studies of post-mortem brains. Rajan et al 1997 found the highest concentration of Cu in the cerebellum of normal brains, and Xu et al 2017 found the highest concentrations of Mn in the cerebellum of controls, the highest Cu in the cerebellum of AD cases and controls, and the highest Se in the cerebellum of AD cases and controls (Xu et al., 2017, Rajan et al., 1997). Xu et al 2017 reported the highest concentration of Mn in the entorhinal cortex of AD cases, followed closely by the cerebellum (2.09 and 2.04 μg/g respectively)(Xu et al., 2017). Several studies also report preferential regional distribution of Fe in both AD and control brains; however, we found no significant between-region Fe differences here (Ramos et al., 2014b). The high concentrations of Mn, Cu, and Se in the cerebellum may be related to the high mitochondrial density (Xu et al., 2017). Future studies would usefully measure precisely neurologically mapped samples from each region to account for intra-sample and intra-regional variations in metal concentrations and look at samples from different disease stages.

3.4.3 Metal relationships

As there were no differences in metal content between AD and control cases, (nor, as reported previously, in SIRM) or between females and males, the 2 sample groups were pooled together to increase the statistical power (Hammond et al., 2021). Heatmaps of effect sizes were generated to identify relationships between the different metals in the brain, with SIRM and region as additional factors (Figure 3.2, Supplementary Figure B5). The SIRM did not influence any of the metal concentrations measured, suggesting no direct relationship between magnetite/maghemite concentrations and the metals measured here. Brain region affected the concentrations of Ce (frontal, $p=0.021$; occipital, $p=0.029$), Cd (frontal, p 0.046), Cu (cerebellum, $p=0.042$), Mn (cerebellum, $p>0.0001$) and Zn (frontal, $p>0.0001$; occipital, $p>0.0001$; temporal, $p>0.0001$), however the regions studied represent relatively large areas of the brain (entire lobes), so it is possible that such relationships exist for other metals in more discrete regions, and/or at the cellular level as seen previously with Hg, Se, and Zn in microsomes from AD temporal gyrus compared to age-matched controls (Wenstrup et al., 1990). SIRM and region were omitted from the heatmap for simplicity (Figure 3.2) but can be seen in Supplementary Figure B5.

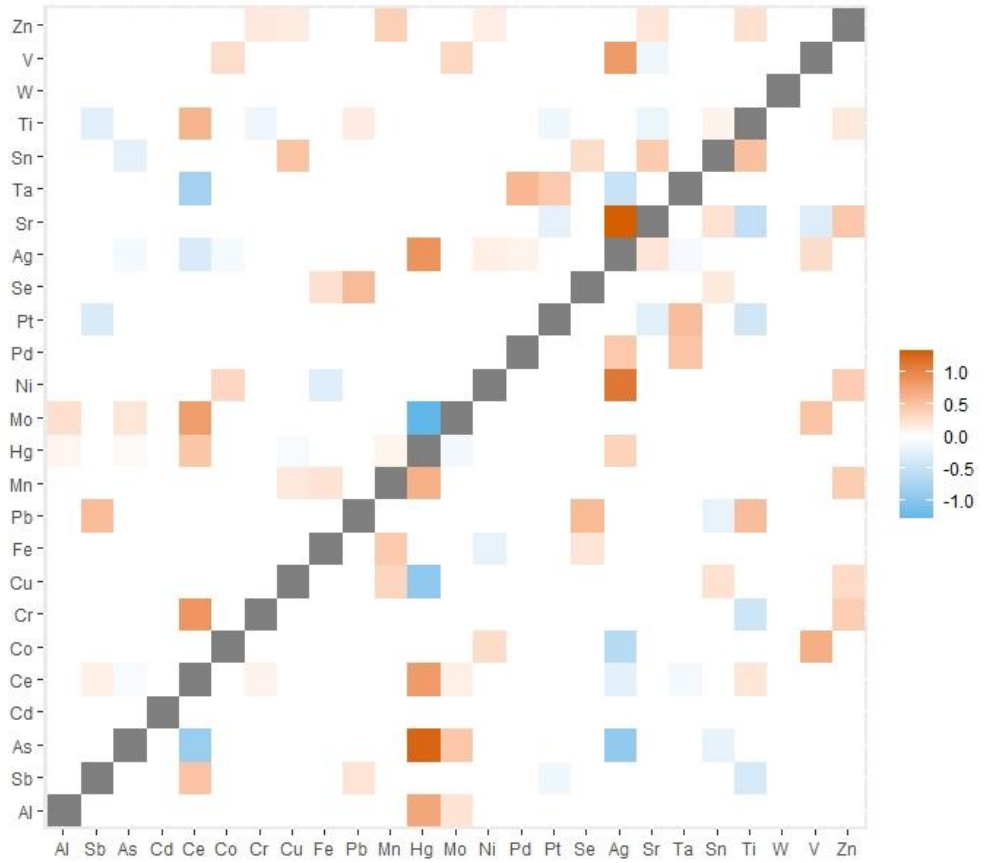

Figure 3.2 Relationship between metal elements in human brain tissue. The concentration of 25 metals was measured in 120 human brain tissue samples via ICP-MS. The heatmap depicts a matrix of effect sizes. Only significant effects are shown ($p>0.05$). Orange represents a positive effect (increase), whilst blue represents a negative effect (decrease).

Linear modelling revealed numerous relationships between different metals (Figure 3.2). Many metals have similar chemical properties and so can substitute for one another in metalloproteins and biochemical reactions. Such substitutions are often antagonistic; toxic metals compete with essential metals for binding sites but do not reproduce the desired biological effects. This can lead to depletion of one metal in favour of another. The positive association seen here between Zn and Mn could reflect the role of Mn in glutamate metabolism and the fact that Zn co-localises with glutamate in the brain (Ramos et al., 2014a). Se was positively associated with Fe, Pb, and Sn, which could indicate the presence of protective mechanisms against toxic metals as Se is a key component of selenoproteins and glutathione peroxidase (antioxidant defences) and is typically depleted in AD (Varikasuvu et al., 2019). Sb was positively associated with Pb, potentially reflecting a common source of origin as both exogenous metals are commonly alloyed together in antimonial lead, which is used in lead-acid storage batteries (Supplementary Table B1). The negative correlation seen between Mo and Hg could reflect the Hg detoxification properties of Mo, stimulating

clearance of Hg from the brain and depleting Mo concurrently (Yamane and Koizumi, 1982). The metals with the most relationships (Ag, Ce, and Ti) could be of particular interest when investigating metals in AD and/or when looking at metals in air pollution as changes to the levels of one of these exogenous metals could affect at least 8 other metals in the brain which could cause a cascade of changes to different metal-involved biochemical pathways. Conversely, W and Cd did not impact on the levels of any other metal, nor were they affected by any other metal, which could indicate a unique source of origin or unique biochemical fate in the brain, or may interact with other elements such as Ca, and Na which have not been measured here.

3.4.4 Principal component analysis

To simplify the matrix of effect sizes, principal component analysis (PCA) was used to reduce the 25 by 25 comparisons into 4 principal components (groups) of metals (Figure 3.3). PCA has been used previously to identify possible sources of toxic element pollution in road dust and was applied here to assess potential sources of metals (especially non-physiological species) in the brain (Wiseman et al., 2021). Use of four components explained 64.4% of the total variance (see B.1.2). The SIRM, As, and Pb, were excluded from analysis for failing to meet inclusion criteria.

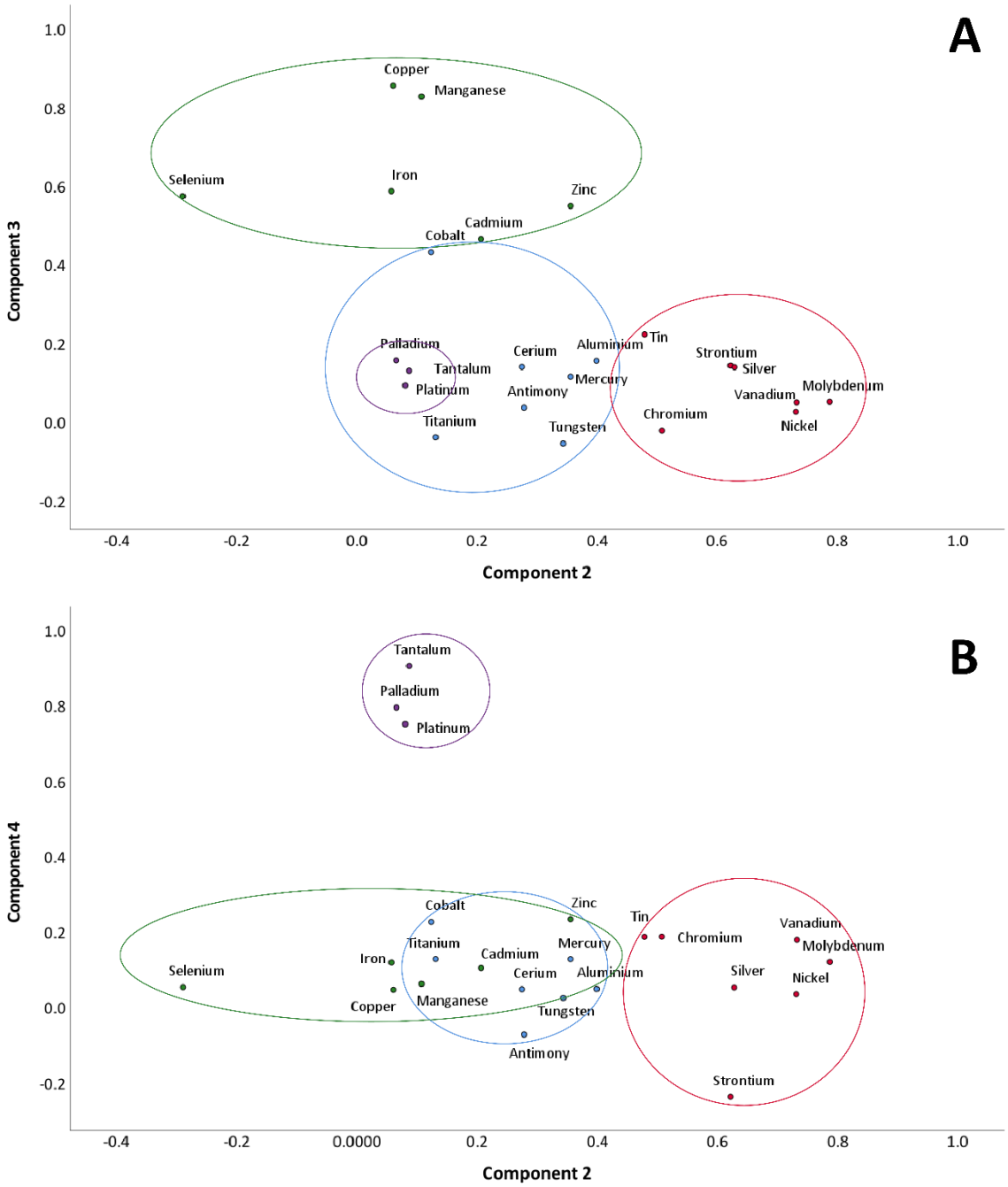

Figure 3.3 Principal component analysis of metal elements in human brain tissue. Plots depict 2 components of a 4-component analysis. A = component 2 and 3, B = component 2 and 4. Colours indicate each component; component 1 (blue), component 2 (red), component 3 (green) and component 4 (purple).

Component 1 (Ce, Hg, Ti, Sb, Al, Co and W) was dominated by unequivocally exogenous metals, Ce, Hg, Ti, and Sb, which likely represent traffic-related sources, as well as crustal materials e.g., Al, Ti (Ashbaugh et al., 2003, Landis et al., 2017). Component 2 (Mo, V, Ni, Ag, Sr, Cr and Sn) could represent metals from combustion; Mo, V and Ni which dominate this component are tracers of fuel oil combustion (Saffari et al., 2014). Component 3 (Cu, Mn, Fe, Se, Zn and Cd) is dominated by Cu, Mn, Fe and Zn which are arguably four of the most important metals in

the brain but are also all released from brake and tyre wear (Gonet et al., 2021b, Gustafsson et al., 2008). Component 4 contained three rare elements, Ta, Pd, and Pt which could represent exposure to emissions from catalytic converters and/or dental alloys (Zhang et al., 2016, Munker et al., 2016). The PCA groupings are indicative of different exogenous pollution sources but could also represent common biological pathways/fates of these metals in the brain. Knowledge of which metals group together, their source, and any biological effects of their presence in brain tissue would be invaluable in the effort to reduce the risk of neurodegenerative disease following exposure to high levels of air pollution. Of note, several elements could belong to more than one component, Co (1 and 3), V (1 and 2), Ag (1 and 2), Sn (1 and 2), Fe (1 and 3), and Zn (1 and 3) (Supplementary Table B8). Crossover between multiple components may arise due to some metals having a known or suspected physiological function but also being present in pollution, as is the case for Co, Fe, and Zn. The duality of elements being both physiological and exogenous complicates the analysis; it is not possible to distinguish between exogenous and physiological metals by measuring total metal concentrations in the tissue. Complementary analysis, such as high-resolution transmission electron microscopy, and electron energy loss spectroscopy (EELS) may allow for a partial separation of exogenous and physiological species, as has been shown previously for magnetite, which often has a spherical shape when formed under high temperatures, and an angular/euhedral shape when formed biogenically (Maher et al., 2016).

3.5 Conclusion

Around 99% of the world's population are exposed to levels of $PM_{2.5}$, a rich source of metals, in excess of 'safe' WHO limits (WHO, 2021a). The brain is a highly oxidative organ with direct ports of entry from the environment (olfactory bulb), as well as circulatory, pulmonary and neuroenteric routes for exogenous metals to enter and induce oxidative stress. Disruption of metal homeostasis has been proposed as a pathogenic mechanism for various neurodegenerative diseases including AD, and exposure to high level of $PM_{2.5}$ has been identified as risk factor for AD. Here, we found no significant difference in metal concentrations between AD and controls possibly due to the BBB being compromised with advanced age, and neurodegenerative disease. Monitoring of metal concentrations at earlier ages may be critical to the understanding of the impact of environmental exposure to metals on AD pathogenesis, particularly as the disease is thought to develop decades prior to clinical manifestation. Although no significant differences in absolute concentrations were found, significant differences between the regional distributions of Cu, Mn and Se were found, with

the cerebellum containing the highest concentrations of metals, potentially due to high mitochondrial density. Linear modelling revealed several significant relationships between metals, with Ag, Ce, and Ti potentially of key importance due to the large number of relationships between these and other metals. The four components from PCA suggest four potential sources of metals: crustal/traffic, fuel oil combustion, biological and brake/tyre wear, and catalytic converters/dental alloys. We present regional metal concentrations to add to existing data on AD and controls, and an exploration of the potential impacts of environmental metals on these concentrations within the brain. Identification of toxic metals key in AD pathogenesis, and their source origin would be invaluable in preventing the onset of a progressive neurodegenerative disease which affects millions globally with no disease modifying treatments currently available.

Acknowledgements

JH receives a funded studentship from the Sir John Fisher Foundation. We acknowledge the support of the Manchester Brain Bank by Alzheimer's Research UK and Alzheimer's Society through their funding of Brains for Dementia Research (BDR) initiative, and service support costs from Medical Research Council. We would like to thank Professor Rebecca Killick for assistance with analysis in R and Professor David Allsop for early discussions of the data.

Chapter 4 (Paper 3) Oxidative stress, cytotoxic, and inflammatory effects of urban ultrafine road-deposited dust from the UK and Mexico in human epithelial lung (Calu-3) cells

4.1 Abstract

Road-deposited dust (RD) is a pervasive form of particulate pollution identified (typically via epidemiological or mathematical modelling) as hazardous to human health. Finer RD particle sizes, the most abundant (by number, not mass), may pose greater risk as they can access all major organs. Here, the first in vitro exposure of human lung epithelial (Calu-3) cells to 0 – 300 µg/ml of the ultrafine (<220 nm) fraction of road dust (UF-RDPs) from three contrasting cities (Lancaster and Birmingham, UK, and Mexico City, Mexico) resulted in differential oxidative, cytotoxic, and inflammatory responses. Except for Cd, Na and Pb, analysed metals were most abundant in Mexico City UF-RDPs, which were most cytotoxic. Birmingham UF-RDPs provoked greatest ROS release (only at 300 µg/ml) and greatest increase in proinflammatory cytokine re-lease; Lancaster UF-RDPs increased cell viability. All three UF-RDPs stimulated ROS production and proinflammatory cytokine release. Given these differing biological impacts, exposure to a mass- or even number-based PM limit in one city may produce worse health consequences than exposure to the same limit in a different city. A combination of new, biologically relevant metrics and localised regulations appears critical to mitigating the global pandemic of health impacts of particulate air pollution and road-deposited dust.

Published: **Hammond, J.,** Maher, B.A., Gonet, T., Bautista, F., and Allsop, D. Oxidative stress, cytotoxicity, and inflammatory effects of urban ultrafine road-deposited dust from the UK and Mexico in human epithelial lung (Calu-3) cells. *Antioxidants* **2022**, 11, 1814.

Author contributions statement

JH: conceptualization, methodology, validation, formal analysis, investigation, writing-original draft, writing – review & editing, visualization, BAM: conceptualization, writing – review & editing, supervision, TG: methodology, investigation, writing – review & editing, FB: resources, writing – review & editing, DA: Supervision

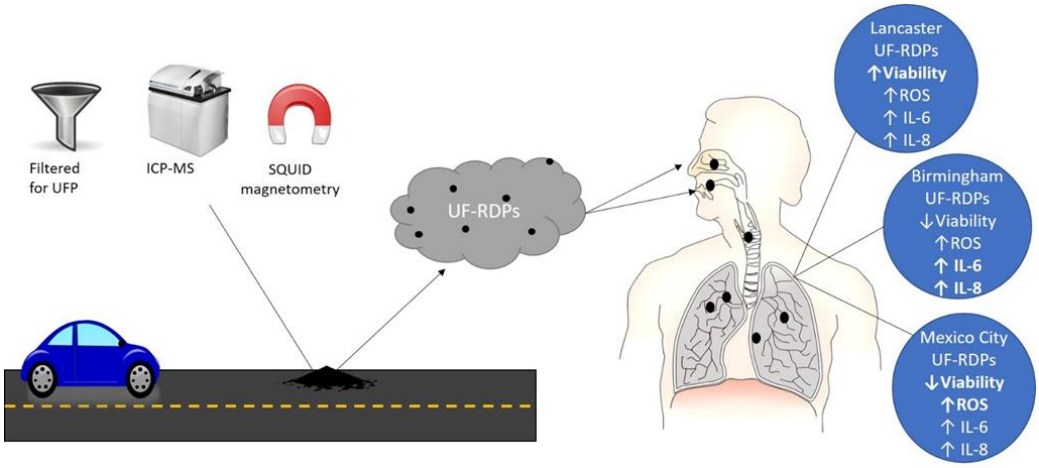

Graphical abstract

4.2 Introduction

Human exposure to outdoor, fine-grained airborne particulate matter ($PM_{2.5}$, with an aerodynamic diameter <2.5 µm) was estimated to be responsible for 8.9 million deaths in 2015 (Burnett et al., 2018); 99% of the world's population is exposed to high particulate pollution levels, i.e., above the World Health Organisation annual mean limits of 15 µg/m^3 for PM_{10} (PM with an aerodynamic diameter <10 µm), and 5 µg/m^3 for $PM_{2.5}$ (WHO, 2021a). Epidemiological studies demonstrate significant associations between PM exposure and adverse health impacts, including pulmonary diseases (Mar et al., 2004, Zhang et al., 2020c), cardiovascular diseases (CVD) (Feigin et al., 2016, Kim et al., 2020), brain tumours (Weichenthal et al., 2020), and neurodegenerative diseases (Chen et al., 2017b, Mortamais et al., 2021). Road-deposited dust (RD) occurs when airborne PM, a mixture of organic and inorganic molecules from anthropogenic and natural sources, settles on/near road surfaces. RD can pose a substantial potential hazard to human health since it comprises an accumulating reservoir of deposited particulates, which can be re-suspended multiple times (e.g., through traffic-induced turbulence), providing multiple opportunities for inhalation/ingestion by all road-users and those living and/or working within close proximity to major roads. RD can further accumulate pollutants in situ, including carbonaceous compounds (Heal and Hammonds, 2014), heavy metals (Duong and Lee, 2011) and polyaromatic hydrocarbons (PAHs) (Mon et al., 2020).

The composition of PM, and thus of RD, is likely to vary significantly on local, national, and international scales. The cellular targets, toxic effects, and mechanisms of specific particle size fractions of PM and RD, and of PM and RD arising from different locations/sources, are currently imperfectly understood. Improved understanding of the specific, causal impacts of PM and RD, and of their differing components, would provide an evidenced rationale for

legislative mitigation to reduce PM emissions; and may also be key in developing new therapeutic approaches to treat those already suffering adverse, PM- and RD-induced health outcomes.

Anthropogenic contributors to RD include not only diesel/petrol exhaust but also non-exhaust emissions (NEE), such as brake wear, tyre and road/asphalt wear, and industrial sources, e.g., combustion-derived emissions from factories, and space heating. Natural contributors include soil, endotoxins (bacteria), pollen, and aeolian dust (Gonet et al., 2021a, Yang et al., 2016b, Pant et al., 2015, Hong et al., 2020). As RD is often derived from diverse sources, its chemical and biological composition also varies, typically by location (Pant et al., 2015), but also with season and climate (Gualtieri et al., 2009). RD often contains a wide range of metal-bearing particulates, some attributable to specific sources; e.g., Ba is an additive in most brake pads (Harrison et al., 2012), TiO_2 in road paint (Al-Kattan et al., 2013) and Pt and Pd are released from catalytic converters (Prichard and Fisher, 2012). The presence in RD of redox-active transition metals and carcinogenic compounds (e.g. PAHs) is detrimental to human health (Kim and Koh, 2020); exposure to PAHs in RD was associated with an incremental lifetime cancer risk (ILCR) of 9.9×10−4 in Taiwanese adults (Mon et al., 2020) (ICLR > 10−4 indicates high carcinogenic risk (Liao and Chiang, 2006)). Several studies report a significant amount of strongly magnetic, iron-rich particles, such as magnetite (Fe_3O_4), in RD (Gonet et al., 2021a, Wiseman et al., 2021). Magnetite nanoparticles (MNPs) are often associated with other metal elements such as Co, Cr, Cu, Mn, Ni, Pb, Zn, (Yang et al., 2016b) and PAHs (Halsall et al., 2008), and magnetic methods are increasingly used for monitoring of airborne PM. MNPs are potential mediators of neurodegeneration; MNPs with a striking similarity to roadside MNPs have been found in human brain tissue (Maher et al., 2016), directly associated with key pathological markers of Alzheimer's disease (senile plaques and neurofibrillary tangles) (Dadras et al., 2013, Plascencia-Villa et al., 2016), and may induce oxidative stress (Maher, 2019), leading eventually to cell death (Ramesh et al., 2012).

RD is estimated to comprise 25.7% of PM_{10} in Brazil (Pereira et al., 2017), 55% of PM_{10} in India (Sahu et al., 2011) and 24.6% of $PM_{2.5}$ in Lanzhou, China (Chen et al., 2019). Conventionally, air quality is monitored by measuring PM mass concentrations (typically reported as the mass (μg) of PM_{10} and/or $PM_{2.5}$ per m^3 air). Such mass-based metrics are usually dominated by coarser PM. Conversely, in terms of particle number concentrations, ultrafine particles (UFPs, <1 μm) are both by far the dominant fraction, and currently unaccounted for when setting PM limits/guidelines (Chen et al., 2016a). UFPs frequently represent the majority of the particles to which humans are exposed (Maher, 2019). Neither RD nor NEE are restricted currently in

terms of exposure limits or emission reductions, despite their abundance (NEEs reportedly form 60% of $PM_{2.5}$ by mass in the U.K. (DEFRA, 2019)), potential risk to human health, and contribution to PM when aerosolized.

Compared with larger PM size fractions, UFPs can disperse more widely in the environment (Chen et al., 2016a) and their toxicity reported to be greater (Weichenthal et al., 2020, Oberdörster et al., 1994), likely due to their high surface reactivity (Wang et al., 2013).

UFPs can penetrate further into the body, e.g., a multiple path particle dosimetry model suggests highest deposition of particles 10-100 nm in size range in the alveolar region, regardless of their density. Alveolar deposition of larger particles (100 nm - 1 μm) requires higher particle density (10 g/cm^3). There is also a high deposition of nanoparticles in the tracheobronchial tract, whilst large particles (<10 μm) deposit primarily in the extra-thoracic and tracheobronchial regions (Braakhuis et al., 2014).

UFPs may enter the body via inhalation into the lungs (Donaldson et al., 2001) and olfactory nerve (Oberdörster et al., 1994), ingestion (Calderón-Garcidueñas et al., 2020a), and/or dermal penetration (Jin et al., 2018). If invading microbes, and foreign bodies like UFPs, evade the thick protective mucus layer in the lungs, epithelial cells are the first cellular line of defence (Figure 4.1). The epithelial cells of the human respiratory system defend against incursion of inhaled particulates, primarily via physical barriers formed by cell adhesion proteins (e.g., E-cadherin) and tight junctions (e.g., occludin). Additional defence arises through the release of chemokines, cytokines, and growth factors, and production of reactive oxygen species (ROS) and nitrogen species and antimicrobial proteins (Hiemstra et al., 2015). Various antioxidants (e.g., glutathione) also have a protective effect, but decrease in abundance deeper into the respiratory tract (i.e., into the regions penetrated by UFPs) (Saffari et al., 2014).

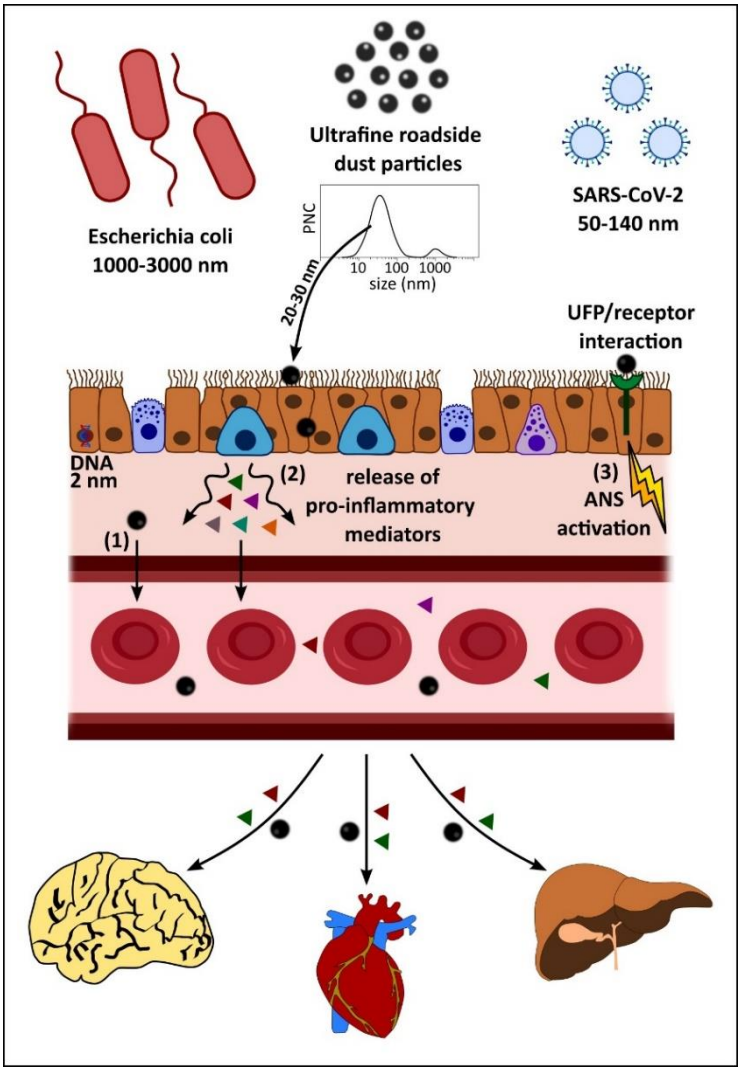

Figure 4.1 Fate of inhaled ultrafine road-deposited dust particles (UF-RDPs) in the human body. Inhalation of UF-RDPs may occur when settled road-deposited dust (RD) particles become aerosolized due to wind conditions and/or traffic movement. RD contains a range of particle sizes as shown by the particle number concentration (PNC) graph (adapted from (Yang et al., 2016b)). UFPs can become trapped in mucus or by cilia lining the airway epithelium but very small particles (~20 - 30 nm) may penetrate between and/or through cells (Yang et al., 2016b). Such incursion is usually impeded by tight junctions between neighbouring cells, but these junctions can become damaged, and/or UFPs may increase paracellular permeability temporarily, allowing for transient opening of tight junctions and passage of particles (Yu et al., 2013). UFPs may also pass transcellularly, travelling through epithelial cells lining the lungs, and can interact/damage cellular components during this passage (Geiser, 2010). The impact of UFP inhalation is not limited to the lungs but extends systemically via 3 possible mechanisms (Snow et al., 2018): 1. incursion into the circulatory system, with subsequent travel to and deposition in extra-pulmonary organs, e.g., (Oberdörster et al., 2004, Calderón-Garcidueñas et al., 2019b, Maher et al., 2020); 2. stimulation of the release of pro-inflammatory mediators from the lungs, which enter the circulation and affect tissues beyond the lungs, e.g., (Chen et al., 2018); and/or 3. interaction of pollutant UFPs with the nerves/receptors in the lung, which activates the autonomic nervous system (ANS) to affect a systemic change or response in the body (Liao et al., 2020). Particles < 200 nm can be transported to the brain directly (Maher et al., 2016, Calderón-Garcidueñas et al., 2020a, Hammond et al., 2021) via the olfactory bulb (Oberdörster et al., 2004), and may also be transported to the central nervous system (CNS) via other nerve pathways (trigeminal, vagus, neuroenteric).

UFP cytotoxicity is likely to arise via different pathways, including oxidative stress, damage to the cell membrane, altered gene expression, mitochondrial dysfunction and/or DNA damage,

including the inability to repair this damage (Braakhuis et al., 2014). Excess oxidative stress can cause a hierarchical oxidative response in cells: exposure to PM/RD generates the production of free radicals and/or ROS (e.g., via the Fenton reaction); altering the oxidant/antioxidant balance within the cell and stimulating expression of cytoprotective proteins. If the stress is prolonged and/or chronic, secretion of cytokines (e.g., IL-6, IL-8) is triggered, inducing an inflammatory response (Tsai et al., 2012, Strieter, 2002). If the oxidative stress does not subside, the cell can undergo death via apoptosis or necrosis (Andreau et al., 2012).

Since they are the first cells to encounter inhaled particulates, human lung epithelial cells have been used to model in vitro toxicity of air pollution, including RD particles, brake wear particles, tyre wear debris and exhaust emissions, e.g., (Gualtieri et al., 2009, Puisney et al., 2018, Abbas et al., 2010, Bayram et al., 2006, Alfaro-Moreno et al., 2009, Huang et al., 2015, Sun et al., 2021). Cytotoxicity studies investigating RD using human cell lines are sparse (Kim and Koh, 2020, Koh and Kim, 2019, Park et al., 2018, Huang et al., 2015, Tung et al., 2021, Sun et al., 2021, Yoon et al., 2018) (Supplementary Table C1); with the majority of studies examining the effects of particles $\leq$ 2.5 µm. Exposing liver (HepG2) and skin (KERTr) cell lines to 66.7µg/100µl RD from Guangzhou, China decreased cell viability after 72h; by 53.9% and 71.4%, respectively (Huang et al., 2015). The decrease in viability was correlated to the sum of total metal (loids) present in the sample, with Zn, Mn, Cu and Ni identified as major components (Huang et al., 2015). The cytotoxicity of UF, traffic-related pollution particles has also been investigated in rat cell models (Morgan et al., 2011, Woodward et al., 2017). Little is known about the biological effects in human cells of the UF fractions of RD, which are potentially hazardous owing to their small size, varied, often metal-rich composition, and abundance in the environment.

To our knowledge, we report here the first investigations of the effects of the ultrafine fraction of RDPs in vitro.

The aims of this study were to: 1) extract and characterize the ultrafine fraction (< 220 nm) of road-deposited dust particles (RDPs) collected at heavily-trafficked sites (Birmingham City Council, 2019, Lancaster City Council, 2020, SEDEMA, 2021) in three contrasting cities; 2) examine the oxidative, cytotoxic, and pro-inflammatory responses of human bronchial epithelial (Calu-3) cells treated with UF-RDPs from these different locations; and 3) compare the cellular effects induced by UF-RDPs from these 3 cities; namely, a small UK city (Lancaster) and larger UK city (Birmingham), compared with the more highly polluted Mexico City.

4.3 Materials and Methods

4.3.1 Sampling sites

The UK RD samples were collected within <0.5 m of heavily-trafficked roads; the A6 at Cable Street (Lancaster, UK) (Gonet et al., 2021a) and A38, close to the Bristol Road Observation Site (Birmingham, UK). The Lancaster site is located near a taxi rank and opposite a bus station, where traffic queues are frequent. The Birmingham site is located close to two busy, traffic-lighted junctions, near the University of Birmingham entrance. Mexico City dust was collected from an area of 1 m^2 of the Constitución de la República Avenue. Sample site information is summarised in Table 4.1.

Table 4.1 Road-deposited dust sample collection sites. *The Cable Street monitoring station in Lancaster started measuring $PM_{2.5}$ from October 2020. An approximate average for Lancaster $PM_{2.5}$ is 8 µg/m^3 based on data available at http://www.ukairquality.net/. PM data obtained from (Birmingham City Council, 2019, Lancaster City Council, 2020, SEDEMA, 2021), population data from (ONS, 2019, Birmingham City Council, 2018, Romero, 2021).

City	Population size (2018)	Site	Traffic	Date collected	Avg. annual PM_{10} (µg/m^3) 2018	Avg. annual $PM_{2.5}$ (µg/m^3) 2018
Lancaster	144,426	(A6) Cable Street		18/10/18	22	No data*
Birmingham	1,141,400	(A38) Bristol Road Observation Site		20/09/19	18	12
Mexico City	8,781,300	Constitución de la República Avenue		06/03/17	47	22

4.3.2 Ultrafine particle extraction from road-deposited dust

The bulk dust samples were dispersed (via sonication) in triple-filtered 100% ethanol and filtered through multiple (at least 3) 0.22 µm polyether sulphone (PES) filters based on a protocol as per (Puisney et al., 2018). A filter pore size of 0.22 µm was used in order to provide sufficient material for repeat cellular analyses. After ethanol evaporation, the concentrated particles (<220 nm, hereafter 'UF-RDPs') were weighed. To form stock solutions, the UF-RDPs were sonicated and re-suspended in 0.5% triple filtered bovine serum albumin (BSA) in dH_2O (Tantra et al., 2010). Each filtered sample originated from a single bulk RD sample.

4.3.3 Inductively couple plasma (ICP) mass spectrometry (-MS) and optical emission spectroscopy (-OES)

The metal content of the UF-RDP samples was quantified by ICP analyses, after acid digestion, at the University of Edinburgh (see SI, supplementary methods).

4.3.4 Superconducting quantum interference device (SQUID) magnetometry

Magnetic methods are non-destructive analyses that have been used to identify combustion- and friction-derived magnetic nanoparticles in human brain (Calderón-Garcidueñas et al., 2020a) and heart tissue (Calderón-Garcidueñas et al., 2019b), as well as to characterize RD and brake wear particles (Gonet et al., 2021a). The magnetic content of the bulk (unfiltered) RDPs was measured with a 2G RAPID cryogenic magnetometer (at the Centre for Environmental Magnetism & Palaeomagnetism, Lancaster University, UK). To identify the presence of ultrafine (~20 – 30 nm) magnetic particles, low-temperature magnetic measurements were made on the extracted UF-RDPs, using an MPMS3 SQUID magnetometer (Quantum Design, USA) at the Department of Physics, University of Cambridge (see SI, supplementary methods).

4.3.5 Endotoxin quantification

Endotoxin concentrations of stock solutions were determined via a quantitative kinetic limulus amoebocyte lysate (LAL) assay kit using the manufacturer's protocol (Thermo Scientific™, Loughborough, UK).

4.3.6 Cell culture

Human lung epithelial cells (Calu-3, ATCC HTB-55™) were selected due to their previous characterization and study as targets of airborne particulate matter (Puisney et al., 2018, Alfaro-Moreno et al., 2009, Gorr et al., 2015, He et al., 2020, Cooney and Hickey, 2011). Calu-3 cells were maintained (until passage 20) in Eagle's minimum essential medium (EMEM) supplemented with 10% (v/v) filter sterilized foetal bovine serum (FBS) (Gibco™, Thermofisher), 1% (v/v) non-essential amino acids, penicillin (50 units/ml), and streptomycin (50 µg/ml) at 37^{o}C, 5% CO_2.

4.3.7 MTS assay

Calu-3 cells were seeded at 40,000 cells/well in a 96 well plate and left overnight to adhere. UF-RDPs at concentrations of 0-300 µg/ml (equivalent to 0.94 - 94 µg/cm^2) were prepared via sonication in UltraMem supplemented with penicillin (50 units/ml), and streptomycin (50 µg/ml). Dose and exposure times were based on a previous study with Calu-3 cells and brake wear particles (Puisney et al., 2018). BSA, used here as a stabilising agent (Tantra et al., 2010), was present at equal concentrations across each set of test conditions; the observed biological responses are values normalised to BSA-exposed controls (see SI, supplementary methods). Following a 24 h exposure, cells were rinsed with Dulbecco's phosphate buffered saline (DPBS) and subjected to an MTS (3-(4,5-dimethylthiazol-2-yl)-5-(3-carboxymethoxyphenyl)-2-(4-

sulfophenyl)-2H-tetrazolium) assay, protocol based on a WST-1 assay as per (Vietti et al., 2013).

4.3.8 Reactive oxygen species (ROS) assay

Calu-3 cells, seeded as above, were incubated with 25 µM of the fluorescent cellular probe CMDCFH2DA (chloromethyl derivative of 2',7'-dichlorodihydrofluorescein diacetate) (Invitrogen™, Massachusetts, USA) in DPBS for 45 mins, prior to particle exposure, at 37^{o}C, 5 % CO_2 (Puisney et al., 2018). 100 µM tert-butyl hydroperoxide (TBHP) was used as a positive control. Fluorescence (excitation 495 nm, emission 529 nm) was measured at 0.5, 1, 2, 3 & 4 hours (see SI, supplementary methods).

4.3.9 Cytokine ELISAs

Following 24 h exposure to UF-RDPs (as above), the media samples were collected, centrifuged (15000 RCF, 15 minutes, 4^{o}C), and analysed for IL-6 and IL-8 concentrations via ELISAs conducted according to the manufacturer's protocol (IL-6 BioLegend, London, UK, IL-8 Invitrogen™ Massachusetts, USA). Cytokine concentrations were calculated from standards fitted using a four-parameter logistic curve-fit with program MyAssays (http://www.myassays.com/) (see SI, supplementary methods).

4.3.10 Statistical Analysis

All experimental results represent 3-4 individual experiments. Data are presented as mean ± standard error of the mean (SEM). Statistical analysis was conducted using SPSS 24 (IBM). Normality tests were performed using the Shapiro-Wilk test. A one-way analysis of variance (ANOVA) (with Dunnett's post-hoc) was performed to compare particle treatments with unexposed control. Comparison of location and concentration was assessed by a two-way ANOVA (with Bonferroni correction post hoc). Statistical significance levels used are: *, $p \leq 0.05$, **, $p \leq 0.01$, ***, $p \leq 0.001$ ****, $p \leq 0.0001$.

4.4 Results and Discussion

In terms of metal compositions of the 3 sets of UF-RDPs, it is notable that nearly all metals analysed are most abundant in the Mexico City UF-RDPs (18 out of 24), compared to the UK dust samples (Figure 4.2; Supplementary Table C2). For example, mass concentrations of Cu and Fe are 67.2 ppm and 77.1 ppm for Mexico City, followed by 29.1 ppm and 55.9 ppm for Lancaster and 19.7 ppm and 14.7 ppm for Birmingham. Conversely, Na is most abundant in the Lancaster UF-RDPs (105,489 ppm), followed by Mexico City (42,163 ppm) and Birmingham (1,003 ppm). Pb concentrations are 8.0 ppm for Lancaster, 1.2 ppm for Mexico City, and 0.7 ppm for Birmingham. Cd was the only analysed element occurring in the greatest concentrations in the Birmingham UF-RDPs (6.1 ppm), followed by Lancaster (1.1 ppm) and Mexico City (below detection limit).

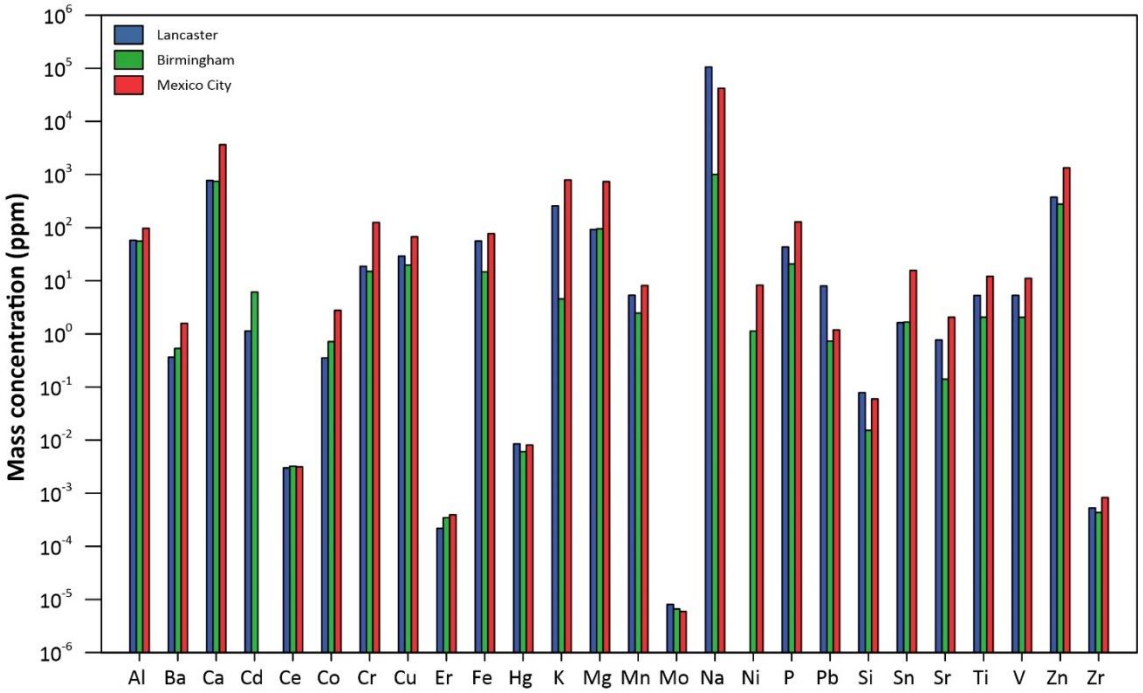

Figure 4.2 Elemental composition of the UF-RDPs from Lancaster, Birmingham, and Mexico City.

In terms of their magnetic content, the measured mass concentration of magnetite in the Mexico City UF-RDPs was between ~0.24 – 0.79 wt.%. The presence of a broad Verwey transition identifies the presence specifically of magnetite, with ultrafine (~20-30 nm) magnetite particles evident from the large (~43%) increase in remanence at low temperature (10 K) compared to that at 300 K (Supplementary Figures C1-C2). Due to the small sample mass extracted, the magnetic content of the Lancaster and Birmingham UF-RDPs was unmeasurable; however, IRM data for the bulk samples can be seen in Supplementary Figure C1.

Calu-3 cells were exposed to UF-RDP doses of between 0 and 300 µg/ml (0.94-94 µg/cm^2). Noteworthy is that significant cellular responses were elicited even at low and intermediate UF-RDP doses, especially for the Mexico City UF-RDPs.

Following 24 h exposure to UF-RDPs (0-300 µg/ml), Calu-3 cell viability varied significantly by sample location. For the Lancaster UF-RDPs, cell viability increased, by 25-35% (Figure 4.3), in a dose-dependent manner (15 µg/ml upwards), similar to our previous studies with synthetic magnetite nanoparticles (unpublished data). Treatment with the Birmingham UF-RDPs caused a significant decrease in cell viability but only at the highest exposure dose (300 µg/ml, 65% decrease). In contrast, Calu-3 cells were most sensitive to the Mexico City UF-RDPs where a dose-dependent decrease in viability was seen - even at the lowest dose (3 µg/ml, 12% decline), up to 30% decline at 300 µg/ml.

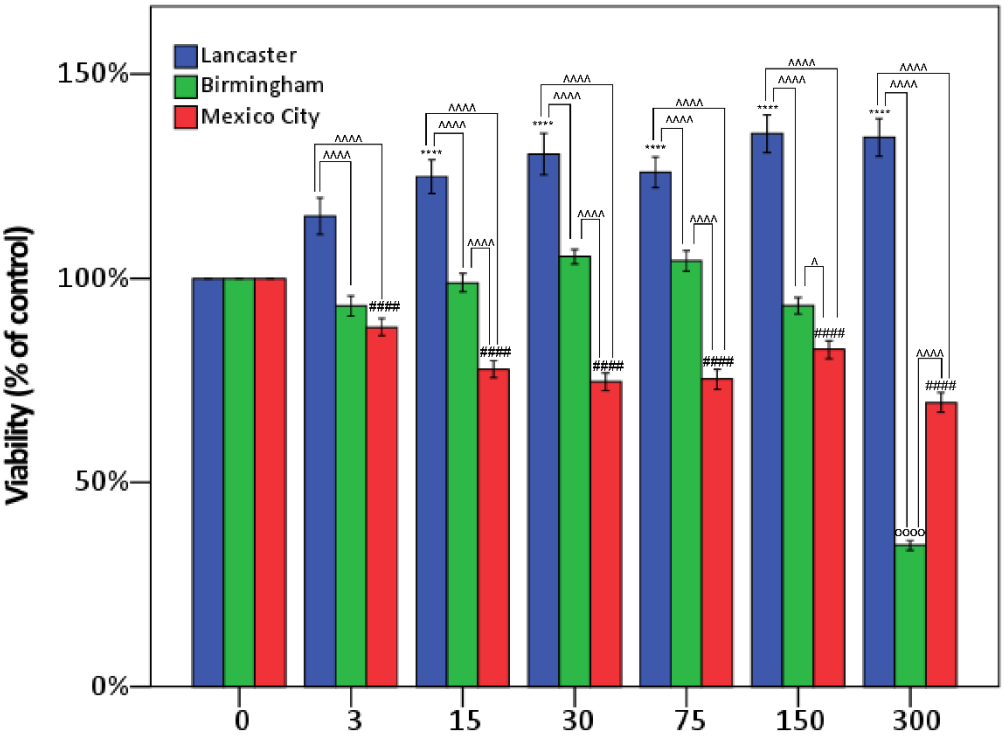

Figure 4.3 Cytotoxicity of <220 nm-sized road-deposited dust particles (UF-RDPs) on Calu-3 cells. Calu-3 cells were exposed to UF-RDPs (0-300 µg/ml) from Lancaster and Birmingham (UK) and Mexico City (Mexico) for 24 h and subjected to an MTS assay, which reflects cell viability. A one-way ANOVA with Dunett's post-hoc was conducted, comparing treated cells to the untreated control (* Lancaster, o Birmingham, # Mexico City) and two-way ANOVA with Bonferroni correction to compare the impacts of the UF-RDPs from the three different locations (^).

The increased viability resulting from the Lancaster UF-RDPs may represent an increase in cell number (proliferation) or metabolic activity. The Pb content of the Lancaster UF-RDPs – sampled close to the city bus station - is notably high, ~8 x higher in the compared with those from Birmingham and Mexico City. Cell proliferation might thus reflect the tumorigenic effect of Pb (Rousseau et al., 2005). Pb was reportedly 4 x higher in settled bus dust relative to background soil (Botsou et al., 2020). Proliferation might also reflect replenishment of damaged epithelial cells, and/or airway remodelling (Abbas et al., 2010); i.e., changes in the composition, structure, or thickness of (structural) elements of the airway. In response to high PM exposure, lungs from female life-long residents of Mexico City displayed extensive airway remodelling including formation of fibrous tissue (pulmonary fibrosis) (Churg et al., 2003).

In contrast, the Mexico City UF-RDPs induced a dose-dependent decrease in cell viability, reflecting reduced metabolic activity or reduced proliferation, and/or cell death. This decreased viability likely reflects the abundance of metals in these UFPs, including Fe, Zn, Mn, Pb, Cu, Cr and Ni (Yang et al., 2016b, Pant et al., 2015). Transition metals can catalyse ROS production in situ via the Fenton reaction leading to oxidative damage to lipids, DNA, and proteins, and eventually cell death (Mazuryk et al., 2020). The majority of the analysed metals occur in greatest concentrations in the Mexico City UF-RDPs (Figure 4.2; Supplementary Table C2). Of these metals, Ba, Co, and Ni may have the strongest influence on the observed cytotoxic response. This is because the other metals (Cr, Cu, V and Zn) which are most abundant in the Mexico City UF-RDPs are present at higher concentrations in Lancaster UF-RDPs than Birmingham UF-RDPs, yet there was no decline in cell viability in response to Lancaster UF-RDPs compared to Birmingham (Figures 2-3; Supplementary Table C2). Ni may be of particular importance, as it is present in the Birmingham and Mexico City UF-RDPs but not in the Lancaster particles (Figure 4.2; Supplementary Table C2); Ni in RD from South Korea was correlated with cytotoxicity (Koh and Kim, 2019). Birmingham UF-RDPs only decreased Calu-3 viability at the highest dose (300 μg/ml), when antioxidant defences likely were overwhelmed.

Elevated ROS was observed from the 30-minute time point for all three cities (Supplementary Figures C3, C4A). At the 4h timepoint, Mexico City UF-RDPs were the most potent, stimulating increased ROS from 75 μg/ml. Birmingham UF-RDPs induced little increase in ROS generation except at the maximum dose (300 μg/ml, 120%), when cell viability also showed maximum decline (Figure 4.4). Lancaster UF-RDPs were least potent in terms of ROS generation. Together, these data suggest that the lower ROS levels induced by Lancaster UF-RDPs could stimulate proliferation (increased cell viability), whereas the higher ROS levels induced by

Mexico City (and Birmingham) UF-RDPs result in cell death via oxidative damage. Some similar responses have been reported for RD samples ≤ 2.5 µm and ≤ 10µm. Up to 180% increase ROS production was observed in human corneal epithelial cells after 24 h exposure to RD from residential areas of the city of Gangdong-Gu, Korea (Yoon et al., 2018). Re-aerosolised $RD_{2.5}$ from 10 Chinese cities displayed correlation between cellular ROS production and heavy metal concentrations (Cr, Mn, Zn, Ni, Pb) (Sun et al., 2021).

In our UF-RDPs, ultrafine magnetite particles (~ 20 – 30 nm) were abundant in the Mexican sample, and we have previously detected magnetite/maghemite in bulk RD at the same sampling sites in Lancaster and Birmingham (Gonet et al., 2021a). Given the catalytic role of Fe (especially Fe^{2+}) in the Fenton reaction, ultrafine magnetite may play a particular role in the dose-dependent increases in ROS generation seen here (Maher, 2019).

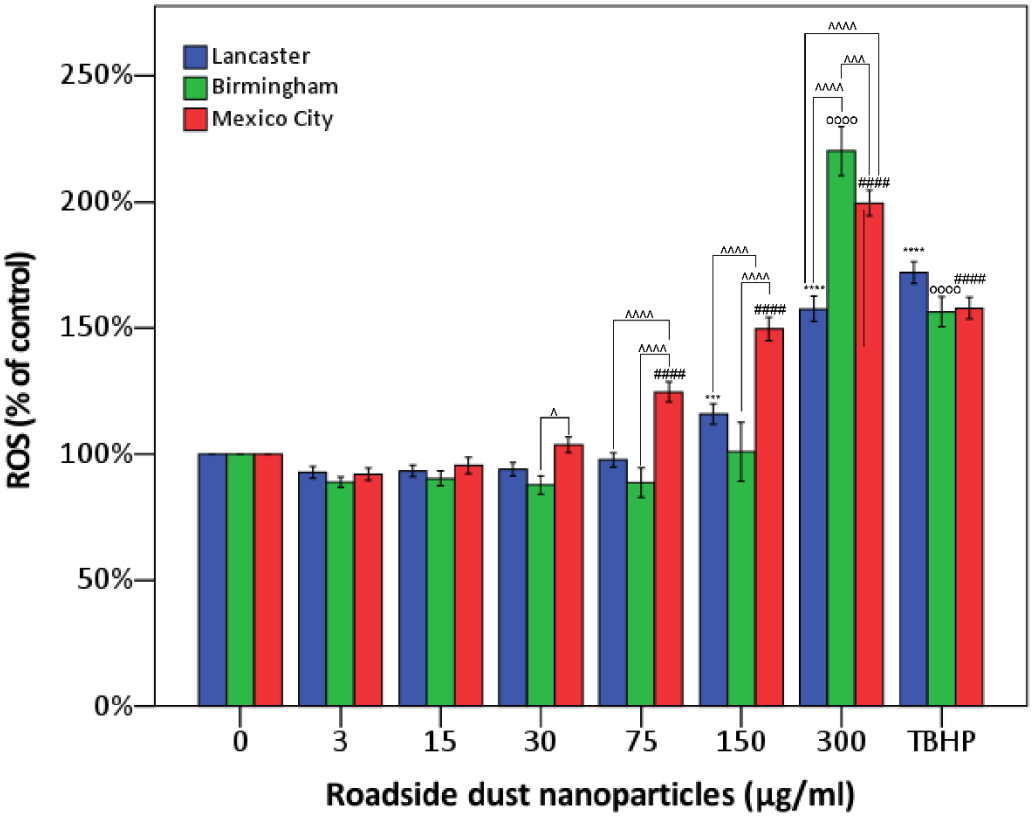

Figure 4.4 Oxidative stress in Calu-3 cells induced by <220 nm-sized road-deposited dust particles (UF-RDPs). Calu-3 cells were loaded with the ROS probe CM DCFH-DA and exposed to UF-RDPs (0-300 µg/ml) from Lancaster and Birmingham (UK) and Mexico City (Mexico). Generation of ROS was measured after 4 h exposure. Tert-butyl hydroperoxide (TBHP) was used at 100 µM as a positive control. A one-way ANOVA with Dunnett's post-hoc was conducted, comparing treated cells to the untreated control. (* Lancaster, o Birmingham, # Mexico City) and two-way ANOVA with Bonferroni correction to compare the impacts of the UF-RDPs from the three different locations (^).

The release of IL-6 and IL-8 cytokines following 24 h exposure to UF-RDPs was quantified by ELISA (Figure 4.5). To account for potential changes in cell number, the ELISA results (Figure 4.5) were adjusted using the MTS data (Figure 4.3). Unadjusted data are given in the SI (Supplementary Figure C5) and generally show similar trends to unadjusted data at non-lethal doses. Following exposure to the extracted UF-RDPs, a dose-dependent increase in IL-6 release was observed in response to doses of 75 μg/ml or above from all three cities, with the greatest increase in release (1648%) in response to 300 μg/ml Birmingham UF-RDPs (Figure 4.5A). An overall dose-dependent increase in IL-8 was observed for Mexico City and Birmingham UF-RDPs, and to a lesser extent for Lancaster UF-RDPs (Figure 4.5B). For Mexico City UF-RDPs, IL-8 release peaked at 75 μg/ml and then declined at the higher doses, possibly due to high cytotoxicity at these doses. The largest increase in both IL-6 and IL-8 was stimulated by the Birmingham UF-RDPs (adjusted data, 1648% and 408%, respectively). Compared with IL-6, IL-8 release displayed significantly greater variation with city source.

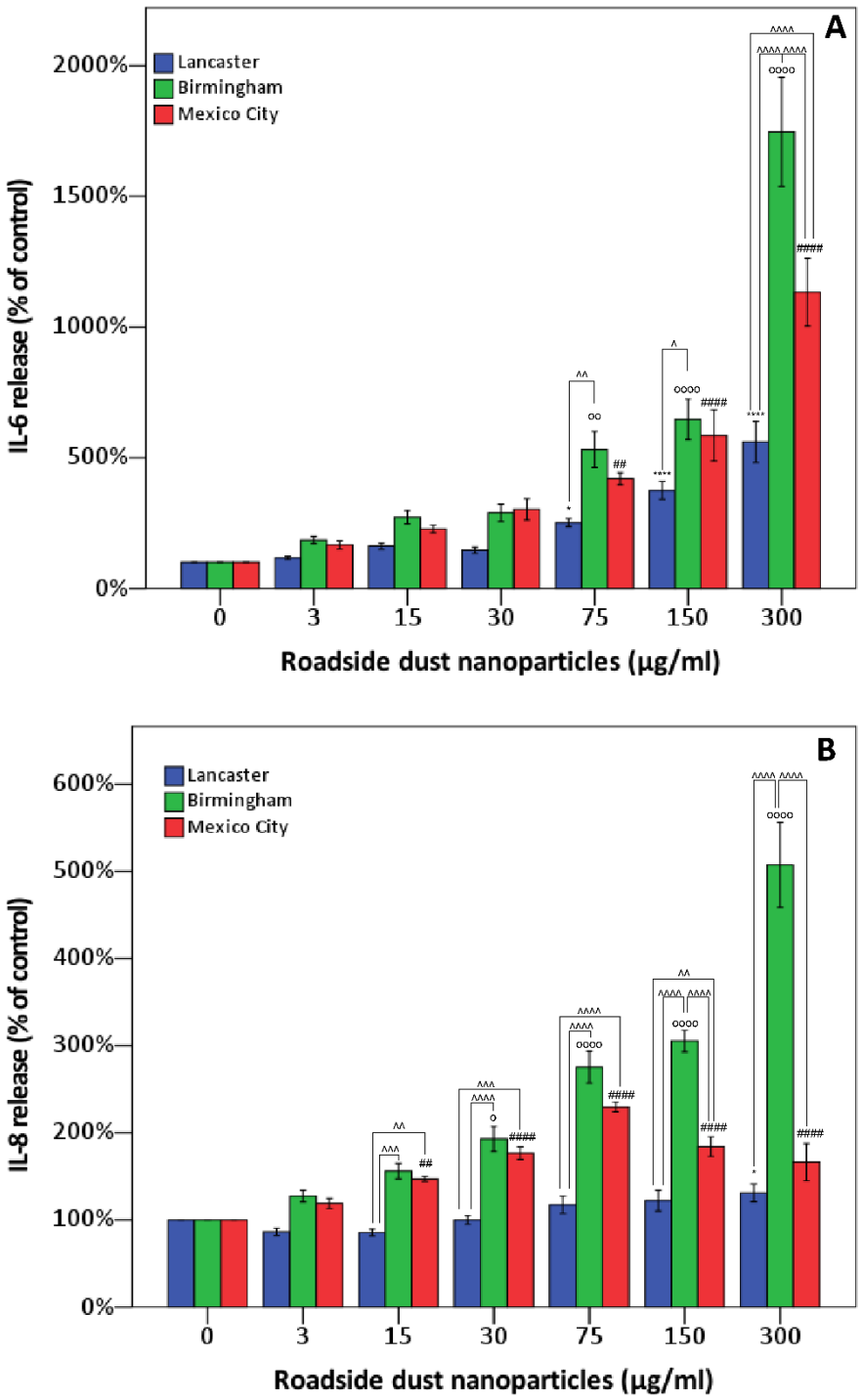

Figure 4.5 Release of pro-inflammatory cytokines in Calu-3 cells treated with <220 nm-sized road-deposited dust particles (UF-RDPs). Calu-3 cells were exposed (0-300 µg/ml) to UF-RDPs from Lancaster and Birmingham (UK) and Mexico City (Mexico) for 24 h. IL-6 (A) and IL-8 (B) concentrations in the media were quantified via ELISA. Data were adjusted using MTS (cell viability) data from Calu-3 cells treated in the same manner. A one-way ANOVA with Dunnett's post-hoc was conducted, comparing treated cells to the untreated control. (* Lancaster, o Birmingham, # Mexico City) and two-way ANOVA with Bonferroni correction to compare the impacts of the UF-RDPs from the three different locations (^).

Toxic concentrations of UF-RDPs may result in cell death, which has been associated with an increase in IL-6 secretion (Vanden Berghe et al., 2006), so examination of sub-lethal concentrations (i.e., viability < 80% (Tung et al., 2021)) is important. Using this criterion, none of the Lancaster UF-RDP doses were lethal, whereas for Mexico City UF-RDPs, 15, 30, 75, and 300 µg/ml doses (corresponding to viability of 78, 75, 75 and 70%, respectively) were lethal. For the Birmingham UF-RDPs, only the maximum dose (300 µg/ml) was lethal. Excluding these data and focusing on sub-lethal doses, elevated IL-6 and IL-8 release was observed in response to UF-RDPs from all three cities from a relatively low dose for IL-8 (15 µg/ml). The largest increases in cytokine release were in response to the Birmingham UF-RDPs (Figure 4.5). Interestingly, Puisney et al. (using the same cell line and methods) report no change in IL-8 secretion in response to 0-300 µg/ml doses of UF brake wear particles (Puisney et al., 2018) but an increase (up to ~350%) in IL-6 secretion. These differences in observed biological response may thus reflect differences in the PM samples tested – UF, dynamometer-derived brake wear (Puisney et al., 2018) compared to our UF-RDPs. The elements most abundant in the dynamometer-derived brake wear particles were Fe and Cu, followed by Si, Al, and Zn, whereas our UF-RDPs are dominated by Na and Ca, followed by Zn, K and Mg. Roadside PM contains not only traffic- and industry-derived compounds, but also naturally-derived elements/metals, including Al, Ca, Fe, K, Mg or Na (de Caritat and Reimann, 2012). Some of the naturally (soil)-derived compounds might also be involved in the Calu-3 biological responses. Alternatively, it is possible that transition metals increase ROS/oxidative damage, decreasing cell viability, and also trigger an inflammatory response in the form of increased IL-6 and IL-8 secretion (Figure 4.6) (Wang et al., 2020a, Shukla et al., 2000).

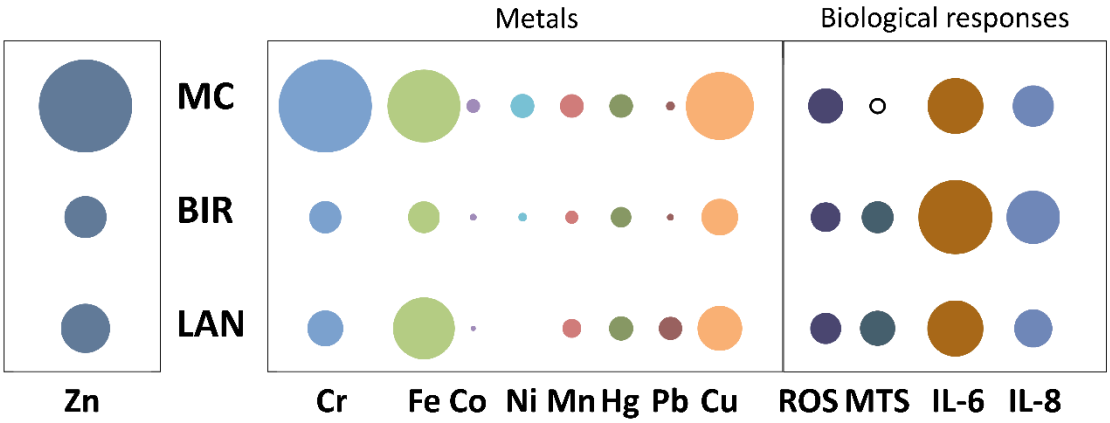

Figure 4.6 Summary of biological responses and heavy metal concentrations of UF-RDPs from Lancaster, Birmingham, and Mexico City in Calu-3 cells. The bubble plot depicts the relative abundance of selected metals (ppm) in UF-RDPs from Mexico City (MC), Birmingham (BIR) and Lancaster (LAN). The concentration of Zn is ~10 fold greater than the other metals so has been scaled separately. The biological responses to 75 µg/ml UF-RDPs are represented as percentages of the untreated control, measured at 24 h (MTS, IL-6, and IL-8) or 4 h (ROS). Solid black outline indicates a decrease, whilst filled circles indicate increases.

RD is, of course, a heterogenous mixture, and other components (not measured here) such as the organic fraction (e.g., carbonaceous compounds, PAHs) are also known to be cytotoxic (Khan and Dipple, 2000), induce ROS generation (Sun et al., 2021, Kumagai et al., 1997), and alter inflammatory responses (Veranth et al., 2006). It is improbable, however, that (semi-) volatile compounds are responsible for the cellular responses observed here since most of these would have been lost in the particle extraction procedure (filtration in ethanol and evaporation). Endotoxins are also present in RD. Endotoxins – pyrogenic molecules shed from gram negative bacteria which are ubiquitous in the environment (Matthias-Maser et al., 2000) – are known to induce ROS production, stimulate inflammatory responses in humans, and are toxic at high levels (Thorn, 2001). Endotoxins were present albeit at low levels (8.75-9.80 EU/mg) in all 3 UF-RDP samples (Supplementary Table C3). Exposing Calu-3 cells to 10 µg/ml LPS (5000 EU/ml) for 4 hours showed no change in ROS generation (data not shown), suggesting that the presence of environmental endotoxins at the concentrations measured did not contribute to the ROS generation observed.

The different biological responses seen here in response to UF-RDPs from the three cities likely derive from differences in UF-RDP physicochemical compositions, and which reflect the biogenic and anthropogenic activities in the surrounding area (Pant et al., 2015), as well as current air pollution regulations. ROS generation is generally higher in PM in the developing world, e.g. Ni and V (tracers of fuel oil combustion), were enriched 5-6 x in $PM_{0.25}$ from Beirut (more permissive regulations) compared to Los Angeles (strict regulations) (Saffari et al., 2014). Here, we see ~8 × higher Ni and 2-5 × higher V in Mexico City compared to the two UK cities. All three samples were collected from heavily trafficked road sites (Table 4.1), where many metals are emitted from traffic-related sources. Ba, Cu and Fe (most abundant in Mexico City UF-RDPs) appear co-associated, and likely originate from the same source, i.e. from brake wear (e.g. (Gonet et al., 2021b)). Zn, also most abundant in Mexico City, has often been reported in tyre wear PM emissions (Gustafsson et al., 2008, Hong et al., 2020). A recent study in Toronto, Canada, observed similar co-associations between traffic-derived metals in RD, including Zn, Mo, Cr, Sn, Pb and Ba (Wiseman et al., 2021). All these metals (along with the remaining transition metals) likely contributed to the strong oxidative response observed in the lung cells exposed to UF-RDPs from the three cities studied here (Figures 6).

One limitation of this study is the difference in sampling collection time (year and season) (Table 4.1). Variable biological responses may reflect the season of sampling, associated with varying ambient PM sources (Gualtieri et al., 2009). Finally, because of the low mass of extractable UFPs, particle number concentrations were not analysed for the 3 samples; nor

was the magnetic content of the UFPs measurable for the UK samples. To enhance further our understanding of the impacts of RD from different locations, with different physicochemical properties, future work would usefully identify the particle size distribution, morphology and any particle changes within the biological media used.

Due to its abundance, reactivity, and pervasiveness at/near roadsides, growing attention is focused on the health impacts of ultrafine PM and RD. The differential oxidative stress, cytotoxic, and inflammatory responses to UF-RDPs we have observed in human lung epithelial cells represent processes which may be pathogenic if exposures to UF-RDPs are prolonged and/or chronic. We have examined lung cells but the effects of exposure to UF-RDPs extend well beyond the lung (Figure 4.1). For example, ultrafine magnetite nanoparticles, like those present in our Mexico City UF-RDPs, have been found in the human brain (Maher et al., 2016). Although a direct inhalation route via the olfactory bulb is possible and likely, our measured brain and road-deposited magnetite concentrations (Gonet et al., 2021a, Hammond et al., 2021), coupled with modelled olfactory deposition rates, indicate that inhalation and circulatory transport must dominate CNS translocation of such particles. Similarly, exogenous metal-rich nanoparticles have been found in the heart (Calderón-Garcidueñas et al., 2019b, Maher, 2019) and the placenta (Liu et al., 2021). Thus, any consequences of exposure to UF-RDPs (including iron-rich, magnetic nanoparticles) are most likely to be systemic.

4.5 Conclusions

The first in vitro exposure of human lung epithelial (Calu-3) cells to the ultrafine fraction of road dust from three contrasting cities (Lancaster and Birmingham UK, and Mexico City, Mexico) resulted in differential oxidative, cytotoxic, and inflammatory responses. Even at low and intermediate UF-RDP doses, significant cellular responses were elicited, especially by the Mexico City UF-RDPs. Given that any (semi-) volatile components are likely to have been lost during the particle extraction process, variations in the solid, metal content of the three sets of UF-RDPs are likely to be linked with the different observed cell responses.

Airborne PM is subject to regulations which rely on mass-based metrics like PM_{10} and $PM_{2.5}$, rather than particle number/composition, while RD is not currently limited/regulated by any legislation. Such mass-based metrics cannot capture the differential biological impacts induced by roadside particles as observed here. We observed a stronger cytotoxic response from Mexico City UF-RDPs compared to the UK cities, and a stronger inflammatory response from Birmingham UF-RDPs. It is therefore illogical to apply the same PM limits across different cities, where exposure to a mass- or even number-based PM limit in one city may have far

worse consequences for health than exposure to the same limit in a different city. A combination of new, biologically relevant metrics, identification of specific components (e.g., metals) of RD that cause toxic effects, and localised regulations each appear critical to mitigating the global pandemic of the health impacts of particulate air pollution and road-deposited dust. A metric that provides an intermediate measurement, such as the lung-deposited surface area (LDSA) which utilises particle size distribution to estimate the surface area concentration of particles that deposit in the lung alveolar region, might be more appropriate (Salo et al., 2021). Not only particle number but also physicochemical composition, and/or specific elemental components (e.g., transition metals) likely require regulation in order to achieve substantive mitigation of the human health impacts of exposure to RD and airborne PM.

Funding: JH receives a funded studentship from the Sir John Fisher Foundation, and TG receives a funded studentship from Jaguar Land Rover. We would like to thank Defying Dementia (Lancaster University) for funding part of this work. FB received financial support from the DGAPA UNAM project IN208621

Data Availability Statement: Data available on request from the authors

Acknowledgments: We would like to thank Dr. Laetitia Pichevin, Edinburgh University for performing the sample digestions and ICP-MS and OES analyses, and Hassan A. Sheikh, University of Cambridge for performing MPMS analyses. FB appreciates the technical support of Rubén Cejudo.

Conflicts of Interest: The authors declare no conflict of interest. The funders had no role in the design of the study; in the collection, analyses, or interpretation of data; in the writing of the manuscript; or in the decision to publish the results.

Chapter 5 Discussion

5.1 Introduction

Air pollution and Alzheimer's disease are two of the largest global issues facing the world at present. Both issues are multifaceted and require a range of methodological and experimental approaches to investigate; this research utilised *in vitro* toxicity testing, magnetic characterisation, and chemical analyses. The focus here is the integration and synthesis of the key findings from each publication chapter (Chapters 2-4) in the context of current literature, and their impact on the fields of AD and air pollution. The main integrated discussion points are the distribution of metals in the human brain, and the variation in responses to environmental particles on an international/regional basis.

5.2 Summary and purpose of the thesis

The research outlined here explores the connections between environmental air pollution nanoparticles, particularly the metal content and magnetite, and human health, with a focus on Alzheimer's disease. The first paper (Chapter 2) quantified the magnetite/maghemite content of human brain tissue from AD cases (n=19) and age-matched non-demented controls (n=11) by superconducting quantum interference device (SQUID) magnetometry, to look at the relationship between magnetic content of brain tissue and AD. The distribution of magnetic particles was also examined, by measuring samples from five different brain regions: the cerebellum, frontal lobe, entorhinal cortex, occipital, and temporal lobes. The distribution of magnetite/maghemite varied between individuals, and no significant difference was found when comparing AD cases to controls. The concentration of four demonstrably exogenous metals (Al, Ce, Pb and Pt) were also measured by inductively coupled plasma mass spectrometry (ICP-MS) and did not vary significantly between AD and controls.

The second paper (Chapter 3) further explored the metal profile of the human brain; ICP-MS was used to measure the concentration of 23 metals and 3 metalloids in human brain tissue samples (taken from the same cohort previously magnetically characterised in paper 1). Four different brain regions (cerebellum, frontal, occipital, and temporal lobes) were measured to look for indications of a portal of entry into the brain. The highest concentration of magnetite was found in the frontal lobe, which encompasses the olfactory bulb (OB) suggesting the OB as a portal of entry for exogenous MNPs to the brain. However, the regional distribution of metals varied across individuals, with no significant difference in metal concentration between AD and controls. Principle component analysis (PCA) identified four components, which are possible indicators of different pollution sources: (1) traffic-related and crustal, (2)

fuel oil combustion, (3) biological and tyre/brake wear, and (4) catalytic converters and dental alloys.

To investigate the routes of entry for exogenous (environmental) metals, and the consequences of their presence in the human body, human lung epithelial cells (Calu-3) were used to model part of the lung-brain-axis to observe biological responses to road deposited dust (RD) samples in paper 3 (Chapter 4). RD from three contrasting cities (Lancaster, Birmingham, and Mexico City) was filtered to extract the ultrafine (<220 nm) fraction, and the metal content was characterized by ICP-MS. Calu-3 cells were exposed to UF-RDPs for 24h to compare the biological responses induced by the different samples, and to look at which (metal) components may be responsible for such changes. The UF-RDPs from Lancaster increased cell viability, whilst Mexico City UF-RDPs were the most toxic and induced the highest amount of oxidative stress (ROS production), and Birmingham UF-RDPs were the most pro-inflammatory. The varied biological responses induced by UF-RDPs from different cities demonstrate the toxicity of UF-RDPs, and the need for specific localised regulations that limit exposure to UF-RDPs and account for regional variation in PM composition.

In addition to the lung-brain-axis, the neuroenteric pathway is another suggested pathway for the entry of environmental nanoparticles and this was explored in paper 4 (Appendix D) by SQUID magnetometry of brainstem samples from Mexico City and TEM imaging of Ti-rich nanorods. Ti-rich particles were present in the brainstem but absent in PM or in previously examined frontal and heart tissue, suggesting an alternative route to entry – ingestion and the neuroenteric system. Two regions of the brainstem were quantified for their magnetic content along with the cerebellum, and it was found that the cerebellum was the most magnetic, followed by the tectum/tegmentum and substantia nigra. This magnetic distribution could be indicative of MNP association with particular cellular targets or anatomical structures which are present in different amounts between these regions.

5.3 Distribution of metals in the brain

The presence of demonstrably exogenous metals in the brain strongly suggests the metals are of environmental origin which is further supported by the identification of potential environmental sources of metals via principal component analysis (PCA) (Paper 2, Chapter 3). There is generally a poor consensus about the distribution of metals in the human brain, including AD brains. Here, exogenous metals and MNPs were heterogeneously distributed across AD and cognitively normal age matched controls from the Manchester Brain Bank (MBB) consistent with varying exposure levels and/or varying abilities to clear the exogenous

material from the brain (Paper 1, Chapter 2). Similar variability between individuals was also seen with brainstem samples from Mexico City residents, again suggested as a consequence of variable exposures (Paper 4, Appendix D). In contrast, Gilder *et. al.* (2018) argued that the ferrimagnetic content of human brains is genetically controlled as magnetite was identically distributed across the seven brains they measured. However, the brains were stored for several decades in 10 % formaldehyde, which was replenished several times. Some evidence exists for dissolution of magnetite by formalin; a 43% decrease in iron concentration was observed after ~4 years storage in formalin (Schrag et al., 2010) and, similarly, a 51% decrease in magnetite concentration was seen after one week of storage in formalin (Dobson and Grassi, 1996). However, when measuring trace elements leached into the formalin, only 3% of iron was lost after 200 days from a fixed spleen sample (Chua-anusorn et al., 1997) and no leaching was observed from human brain tissue after 18 months in formalin (Gellein et al., 2003, Gellein et al., 2008) or from human tissue fixed for 1 week (Bush et al., 1995). A recent study comparing frozen and fixed paired brain samples reported no change in magnetite concentration between frozen tissue and tissue fixed for 5 months in formalin, however the authors acknowledge this could be a consequence of a lack of sensitivity (van der Weerd et al., 2020). The length of storage in formalin is likely critical to the impact it has on measurement of iron within tissue, and thus the magnetic signal measured from the fixed German samples may not accurately represent the ferrimagnetic content of the tissue (Gilder et al., 2018). Fresh frozen tissue is the best starting material for magnetic remanence studies (and ICP-MS); the material is structurally preserved without the potential dissolution of ferrous material including magnetite and loss of signal.

Differences in the capacity for MNP clearance and brain metal homeostasis may explain the heterogeneity of metallic content across individuals. Generally higher metal concentrations were found in female brain tissue, which could arise due to morphological differences between male and female brains (Zhang et al., 2020b). However, there is debate as to whether male and female brains differ significantly on an anatomical level (Eliot et al., 2021, Bourisly et al., 2017). Differences in the ability to clear MNPs and exogenous metals, or differences in antioxidant capacities between the sexes could also account for the generally higher metal concentrations seen in females (Gade et al., 2021). If there is a greater retention of toxic metals in females, this could contribute to the elevated risk of developing AD seen in females (Mazure and Swendsen, 2016).

There were no differences in metal and MNP concentrations when comparing both elderly MBB cohorts. The universal incursion of metals and MNPs likely occurs due to the integrity of

the geriatric BBB being compromised. The BBB is vital in isolating the brain and regulating passage of substances in and out of the brain but is compromised with age (Montagne et al., 2015) and neurodegenerative disease (Sweeney et al., 2018) and can be further exacerbated by air pollution exposure (Oppenheim et al., 2013). The use of younger tissue samples prior to loss of BBB integrity would avoid this issue (see 5.5.1). Using younger (average age 34 years) forensic cases from Mexico City, a gradient in magnetic content was observed in the brainstem with the highest content in the cerebellum, followed by the tectum/tegmentum and finally the substantia nigra (Paper 4, Appendix D). The gradation of MNPs could reflect the targeting of NPs to specific brain regions and cellular targets dependent on their physiochemical properties, and/or the structural and anatomical differences between these regions. The younger BBB has a greater integrity than the geriatric BBB, and investigation of younger tissue samples from less polluted regions would give an insight in to baseline exogenous metal levels in the human brain. In addition to iron rich MNPs, Ti-rich nanorods were observed within the brainstem, but were absent from roadside PM samples and had not previously been seen in frontal or heart tissue. This suggests an alternative route to incursion, such as the swallowing of Ti-NPs from e.g., cosmetic, medicines, food, and transport to the brainstem via the neuroenteric system. It is thus critical to look at all sources of exogenous metals, potential routes of entry and toxic consequences in the body (Calderón-Garcidueñas et al., 2021b).

SQUID magnetometry of post-mortem tissue only provides a snapshot of metal/MNP concentrations at the point of autopsy, so it may not be possible to observe any differences in metal/MNP concentrations which are likely dynamic over time. The fate of (metallic) particles following incursion to the brain is poorly understood, but there is evidence for the dissolution and reprecipitation of MNPs in human mesenchymal stem cells (Van de Walle et al., 2020b).

Other epithelial and endothelial cell barriers throughout the body such as the lung epithelium, are also compromised in response to air pollution exposure and various diseases. The proliferative response seen in Calu-3 cells exposed to Lancaster UF-RDPs could reflect an attempt to maintain barrier function following damage induced by particle exposure (Paper 3, Chapter 4). Similar proliferative responses were seen in another human lung epithelial cell line (L132 cells) exposed to $PM_{2.5}$ from Dunkerque, France, which the authors suggest is a key response to maintaining intact airways (Abbas et al., 2010). A549 human lung cells increased in viability in response to diesel exhaust particle (DEP) exposures, also thought to be a way to prevent against a loss of cell number from exposure to toxic particles (Bayram et al., 2006).

Alternatively, an increase in cell number could reflect pathogenic processes; fibrosis or tumorigenesis. Further work is needed to explore this phenomenon (see 5.5.2).

5.4 International/geographic impact of PM

The magnetite concentrations, metal concentrations and responses to UF-RDPs from different cities vary by their geographic origins. The magnetite content of MBB samples was on average ~11x higher than samples from Germany (Gilder et al., 2018), which may partially be attributed to differences in exposure or PM composition, however the difference in magnitude here is likely due to leaching of magnetite from decades of formaldehyde storage.

The concentration of magnetite in the cerebellum from the Manchester Brain Bank (elderly individuals from Northern England, UK) (Paper 1, Chapter 2) was ~9x lower than the magnetite content of the cerebellum from (younger) forensic cases from Mexico City, Mexico (Paper 4, Appendix D). Both sets of samples were measured with the same techniques at the Centre for Environmental Magnetism and Palaeomagnetism, Lancaster University. In a previous study of MBB and Mexico City frontal cortex tissue, the highest magnetite content was found in a 32-year-old case from Mexico City (Maher et al., 2016). The average annual $PM_{2.5}$ concentration in 2020 was 8.58 $\mu g/m^3$ for Manchester (Manchester City Council, 2021) compared to 18.7 $\mu g/m^3$ for Mexico City in 2021 (SEDEMA, 2021). The higher magnetite content of Mexico City forensic cases is likely due to the life-long exposure of Mexico City residents to high levels of PM compared to Manchester; however, the composition of the PM is also a determining factor. It is likely that Mexico City PM contains a greater amount of magnetite per unit mass of PM compared to Northern England, as seen with the SIRM of bulk road dust samples from Lancaster (36×10^{-3} Am^2/kg) compared to Mexico City (51×10^{-3} Am^2/kg) (Paper 3 SI, Appendix C). The geography of Mexico City exacerbates air pollution; Mexico City is situated within a valley with low wind speeds so there is minimal diffusion of pollutants into the atmosphere, and low oxygen content (due to altitude) meaning internal combustion is less efficient than it would be at sea level, increasing levels of combustion by-products released. The valley is surrounded by mountains, including two volcanoes which are a natural source of magnetite (Ermolin et al., 2018). The population density of Mexico City is greater than that of Northern England (e.g., Manchester) with heavy vehicle usage (Calderón-Garcidueñas et al., 2020c). The combination of anthropogenic and geographical influences in Mexico City coupled with high levels of exposure to PM likely results in the higher magnetite content observed in Mexico City brains compared to the elderly Northern England cohort. Higher magnetite concentrations may also indicate a failure to clear excess magnetite with age or disease state or, alternatively, an increased genetic capacity for production of biogenic magnetite particles.

The reported concentrations of metals in human brain tissue are considerably variable across different studies, which is likely influenced by the exposure environment (location). For example, the levels of Cd, Hg and Pb in our MBB samples are between 10-100 x higher than those reported by Szabo *et al.* (2015) in frontal cortex tissue from (North Carolina) USA cases. However, metal concentrations can be reported on a dry mass or wet mass basis, resulting in different absolute values. When converting our dry weight normalised samples to a wet weight (using dry/wet ratios) in line with Szabo *et al.* (2015), the Cd and Pb levels are of a similar magnitude however the Hg levels are ~63 x higher in the MBB samples. The difference in Hg concentrations could be a result of different environments, i.e., different anthropogenic activities and/or dietary influences, in Northern England compared to North Carolina. Methodological approaches to measuring metal content vary across laboratories from the choice of analytical technique to the sampling of tissue so care must be taken when comparing studies. The metal content of brain tissue from young Mexico City residents is several orders of magnitude higher than other studies using similar analytical approaches (ICP-MS, dry-weight basis) and the same brain region of interest (frontal lobe), for example the concentration of Mn (ICP-MS, dry weight) was 1026 µg/g in Mexico City samples and 689 µg/g in Veracruz samples (Calderón-Garcidueñas et al., 2013b) compared to 2 µg/g in MBB samples and 1 µg/g in samples from Portugal (Ramos et al., 2014a). Mexico City UF-RDPs contained the highest levels of metals for 18 of the 24 metals measured, compared to Birmingham and Lancaster UF-RDPs (Paper 3, Chapter 4). The life-long exposure to (metal-rich) PM in excess of WHO limits likely contributes significantly to the high levels of metals observed within the brains of Mexico City residents.

The differences in PM are evident when comparing the effects of UF-RDPs from different cities (Paper 3, Chapter 4). Variable cytotoxic, oxidative stress, and inflammatory responses were observed in Calu-3 cells when using the same mass concentration of UF-RDPs, exposure time and assay conditions. Such differences likely arise from differences in the physicochemical properties of the RD as a consequence of sampling time; the precise location, season, climate, and anthropogenic activities at the time will alter the composition of RD (Gualtieri et al., 2009, Gustafsson et al., 2019, Heinrich et al., 2003, Johansson et al., 2007, Venkatachari et al., 2007). A similar phenomenon was seen when examining RD from 10 megacities in China; RD from northern industrial cities contained higher heavy metal and PAH concentrations, induced greater ROS production and were more cytotoxic than RD from southern cities which typically consume less energy (Sun et al., 2021). Intra-city differences have also been observed for PM_{10}; northern Mexico City is industrial, whilst the South-Eastern region has windborne dust

from a dry lake basin which is reflected in their PM composition and biological effects – higher concentration of anthropogenic elements (e.g. Cu, Ni, Zn, Pb) were seen in Northern PM coupled with a greater cytotoxic effect compared to South-Eastern PM (Osornio-Vargas et al., 2003). Collectively this suggests RD is a hazard to human health, with the UF fraction potentially being more toxic due to the high surface area reactivity of UFPs, and pervasiveness of RD. Approximately 57-84% of road sediment is ultrafine (< 0.1 μm), which can readily be resuspended in to the atmosphere and travel long distances especially where road sweeping is poorly maintained and traffic volumes are high (Chen et al., 2019). There is a lack of biological studies on roadside dust in general, but especially for the ultrafine fraction. The results here (Paper 3, Chapter 4) provide a basis for further exploration of the toxic effects of UF-RDPs (See 5.6.2).

The current World Health Organisation (WHO) recommended maximal limits for PM_{10} and $PM_{2.5}$ are 15 μg/m^3 and 5 μg/m^3 respectively (WHO, 2021a). These are *suggested* global limits; individual countries and localities often have higher limits within legislation or no regulations at all. A global approach to such limits is ineffective due to the heterogenous composition of PM across different locations (de Jesus et al., 2019). Susceptibility to air pollution on a population basis (Dos Santos et al., 2021, Kulick et al., 2020) is also variable and should be considered when creating regulative measures to limit the effects of air pollution. Mass-based regulations do not account for the fact that ultrafine particles, which are thought to be more toxic than their larger counterparts (Oberdörster et al., 1994), constitute a large proportion (90-99%) of PM by particle number, but only make a small contribution to mass (Johansson et al., 2007). It is therefore essential to identify the sources and components of UF-RDPs which contribute most to the observed negative effects and, taking account of their spatial heterogeneities and resultant differential toxicity, to regulate them at appropriate spatial scales and with biologically relevant metrics. Such limitations would also reduce the amount of metal and magnetic material deposited in the human brain and minimize the risk of disturbing brain metal homeostasis.

5.5 Impact and Prospects for future research

AD has great financial, social and emotional burden on societies across the globe. There are a limited number of treatments available that do not work for all individuals and merely provide symptomatic relief. The number of dementia cases is predicted to rise to 152 million by 2050, with an estimated cost of $1 trillion annually (Patterson, 2018), but both figures can be

reduced by focusing on the modifiable risk factors. Air pollution is one the 12 modifiable risk factors the Lancet commission has identified which are collectively responsible for 40% of dementia cases worldwide (Livingston et al., 2020). Exposure to pollution is also costly, it is responsible for between 1.7 and 7% of annual health care spending and estimated annual global cost of $4.6 trillion (Landrigan et al., 2018). Air pollution is responsible for 4.2 million premature deaths a year (WHO, 2021a), which could increase by up to 50% by 2050 (Lelieveld et al., 2015). The financial and healthcare burden of both dementia and pollution weigh most heavily on the poor, with 91% of premature deaths occurring in lower- and middle-income countries (WHO, 2021a) that are home to ~ two thirds of people living with dementia globally (Patterson, 2018). Thus, identification of specific components of pollution which are most toxic, understanding of their relationship to AD and dementia incidence, and localised preventative measures and pollution limits would undoubtedly result in a significant reduction in both the financial, societal and health burden of air pollution and AD on a global scale.

5.5.1 Magnetic and metallic tissue measurements

The limited availability of tissue poses a major challenge to characterising the magnetic and metallic content of the human brain. Despite this challenge, we report the largest number of human brains analysed magnetically to date (Paper 1) but recognise the advantages of larger sample sizes. Future experiments would seek to have both age and sex-matched controls to limit any confounding effect sex may have on metal/magnetic content. Access to a larger number of samples would increase the statistical power of comparisons, as well as make other analyses such as linear regression a possibility. Linear regression could make use of the additional data which is available on the samples, such as the APOE genotype, plaque counts and tangle counts, to generate a model that would predict whether a sample originated from an AD case or age-matched control. A greater number of samples would also improve the linear modelling of the metals data (Paper 2) and would allow for subdivision by region and other characteristic data which is not feasible with the current case number. If a greater sample size is not feasible, the metal analysis could focus on a smaller number of metals such as one of the metal groupings identified via principal component analysis. As well as a larger number of individuals, a greater number of samples from each case would be beneficial to look at the intra-regional variation with a more systematic mapping of tissue samples as seen with Gilder *et al*. (2018).

In paper 1 (Chapter 2) and paper 4 (Appendix D), we report magnetic concentrations in human brain tissue from Northern England, UK, and Mexico City, Mexico. The comparison of additional geographical locations would be beneficial, particularly the comparison of cities of

a similar size, population density and geography (preferably within the same country), but with different levels of air pollution. Data for UFP levels would be ideal, but it is more likely that $PM_{2.5}$ data would be available as UFP measurements are not routinely conducted. This would provide as close as possible control population when comparing the effects of air pollution exposure on metal and magnetic brain tissue content. The metal content of brain tissue from Mexico City residents has been compared to residents of the less-polluted Veracruz (Calderón-Garcidueñas et al., 2013b), but such comparisons have yet to be made outside of Mexico. There is no true 'control' due to differences in populations, environment, genetic susceptibilities, diet, etc, but factors that can be matched such as sex, age, education level, APOE genotype will reduce the variation between the two populations to be compared.

The age of individuals is critical, as the compromised geriatric BBB likely allows for universal incursion of metals and MNPs, so to look at changes to metal levels, tissue must be examined from younger individuals prior to loss of BBB integrity. Utilisation of biobank samples would be instrumental in achieving this and would give an overview of metal and MNP levels in human brains of a particular population at different ages. To date, metal concentrations in young brains has primarily been reported from Mexico City, so it would be of interest to see whether similar concentrations are observed in young brains from other locations with similar PM exposure, and of particular interest to see whether the same AD-like pathology is observed.

Although the brain has been the focus of this work, other organs are exposed to exogenous metals and magnetic particles from the environment, as modelled in paper 3 (Chapter 4). The brain is the most well magnetically characterized organ, followed by the heart. Additional metallic/magnetic investigation of other organs such as the lungs, or specific tissue such as the olfactory epithelium would provide a more complete picture of the fate of exogenous nanoparticles once inside the body.

To confirm the identity of the ferrimagnetic species as magnetite, additional characterisation such as energy dispersive X-ray spectroscopy (EDX) or electron energy loss spectroscopy (EELS) is needed. EELS has previously been used to confirm the identity of iron oxides within brain tissue (Maher et al., 2016). EELS and EDX can also be used to identify other elements (i.e., metals) which are associated with the magnetic particles *in situ*. TEM images would provide size and morphological information which is important when discussing the origin of the particles as biogenic particles are typically euhedral in shape, whilst exogenous particles formed under high temperatures have a spherical structure. Particle size is also indicative of

origin; particles larger than 8 nm (the size of the ferritin core) may have originated from the environment rather than be formed *in situ* within the ferritin core, however larger particles have also been suggested to result from agglomeration (Plascencia-Villa et al., 2016) or may result from re-precipitation of magnetite *in situ* (Van de Walle et al., 2020b).

SIRM measurements were conducted at room temperature, as low temperature measurements are not possible with the magnetometer at Lancaster University. Room temperature (293 K) measurements capture the SIRM of particles ~ >30 nm, whereas measurements at lower temperatures e.g., 77 K would also capture sub-30 nm particles which are too small to be magnetically unstable at room temperature. This could be achieved by modification of the 2G magnetometer to cool samples with piped liquid nitrogen, or by the use of a Magnetic Property Measurement System (MPMS) magnetometer. The sample mass is greatly reduced when using MPMS so may not be sensitive enough to detect ferrimagnetic material in certain samples but has successfully been used to characterise the magnetic content of AD and control brains (van der Weerd et al., 2020).

Further magnetic characterisation of the samples would provide more detail about the type of ferrimagnetic material within the brain. Detailed IRM acquisition curves can reveal information about the magnetic mineralogy of the sample, for example magnetite acquires strong remanence (saturates) at relatively low fields compared to hematite (Frank Oldfield, 1999), and the spread of the IRM acquisition is indicative of particle size. IRM acquisition curves were generated for a few initial samples but were not possible for the majority of the samples as the integrated IRM unit was magnetising the sample holder and causing too much interference with subsequent measurements. Stepwise acquisition of IRM curves is possible with the external magnet used for imparting SIRM but time-consuming. The demagnetization of the samples with increasing alternating magnetic fields would give insight into the domain structure of the particles and magnetostatic interactions between them (Wohlfarth, 1958). Alternating field (AF) demagnetisations were conducted on these samples, however in many cases the noise when adjusting for clingfilm and sample pot meant a full demagnetization curve was not obtainable.

5.5.2 Cytotoxicity experiments

Road dust is a complex heterogenous mixture of metals, organic compounds, and biological elements. The focus here was on metals due to their association with MNPs and the implication of metals in AD aetiology. Investigating the effects of other elements within the RD mixture and/or specific metal elements would usefully identify which components are

responsible for the negative effects on cells, and thus could be targeted e.g., by legislation for reduction. It is possible that here the organic content was largely removed following the filtration and evaporation (Haghani et al., 2020), however, the organic content should be measured e.g., via Gas chromatography to confirm only the metallic composition remains. Although the measured endotoxin content (Paper 3, Chapter 4) was relatively low, to ensure the proinflammatory responses are not triggered by bacteria, the treatment of cells with polymyxin B would remove any microbes present (Cormet-Boyaka et al., 2011), and the activity of any lipopolysaccharides (LPS) present can be inhibited by recombinant endotoxin protein (Osornio-Vargas et al., 2003). Treating cells with specific metal chelators alongside the application of RDPs would help to identify which metals may be responsible for the observed biological responses (Sangani et al., 2010).

Certified standard or reference materials for RD exist but are unable to capture the diverse nature of RD, which is influenced by the natural and anthropogenic activities in the surrounding environment. Here, we magnetically characterised the RD samples, and the concentration of 23 metals and 3 metalloids (Chapter 4). TEM imaging of particles to look at morphology and size distribution was attempted but was not possible due to technical difficulties and the limited sample mass and ageing of the samples. These technical challenges would need to be addressed in future studies as knowledge of the physicochemical properties of the particles is key when comparing different RD compositions. In addition to TEM images, the use of dynamic light scattering (DLS) could provide additional details such as particle surface charge, agglomeration state, and behaviour in test medium (Nemethova et al., 2017). Refinement of the filtration process such as using different filters to size fractionate the samples, characterisation of the ethanol used for filtering, and quantifying the organic content pre and post filtration would improve the filtered product (metallic RDPs). Systematic sampling of cities throughout different seasons, different sites and repeat sampling would provide a more representative profile of RDPs in each city. With data from several cities and/or locations within cities, it would be possible to conduct correlational analysis to identify which components of the UF-RDPs correspond to observed biological effects (Sun et al., 2021).

Exploration of the biochemical pathways responsible for the viability, oxidative and inflammatory responses observed in Calu-3 cells is the next logical step for the RD experiments. The apparent increase in viability (assessed by MTS) in response to treatment with Lancaster UF-RDPs was particularly interesting, as generally PM exposure studies report a decline in viability (Gualtieri et al., 2009, Puisney et al., 2018, Tung et al., 2021, Sun et al., 2021), or no change (Alfaro-Moreno et al., 2009, Cooney and Hickey, 2011). To confirm the

MTS results reflect cell proliferation, a suitable proliferation assay such as counting the cells using a CC8 assay kit could be performed, or more in-depth cell cycle analysis could be conducted using flow cytometry (Ding et al., 2009). The sample mass of extracted particles was relatively small (28-63 mg) so it was not possible to perform additional experiments; future extractions would be carried out with a larger starting volume of bulk material in order to have sufficient material for additional investigations. Confirming whether particles enter cells could be achieved via SEM and TEM (Schrand et al., 2010) but may first require fluorescent labelling of the RDPs which has an obvious disadvantage of changing the physiochemical properties of the particles. Work on the oxidative stress response could be expanded to look at which specific ROS species are produced, using ROS-specific probes, as well as looking at expression levels of antioxidant enzymes such as superoxide dismutase 1 (SOD1) by western blotting. Selective inhibition of Nf-KB, or elements of the MAPK or MEK pathways and monitoring the secretion of cytokines would identify which pathway(s) are responsible for the observed biological effects (Cormet-Boyaka et al., 2011).

Different cell types show different sensitivities to PM (Huang et al., 2015, Kim et al., 2018) and human bronchial epithelial cells (Calu-3) are just one of numerous cell types within the lung-brain axis. Conducting similar cytotoxicity and inflammatory test on other established cell lines such as human neuroblastoma (e.g., SH-SY5Y), human microglia (e.g., HMC3), and human macrophages (e.g., THP-1) would give insight into which cells are the most vulnerable to RD exposure. Creating co-culture systems such as treating neurons with conditioned media from RD-treated lung cells or more complex 3D co-culture organoid systems, would be better representative of the dynamic lung-brain-axis as a system (Miller and Spence, 2017). The use of primary human cells would be an improvement over immortalised cell lines due to their closer resemblance to human cells *in vivo*. Using primary cells can be technically challenging due to the additional optimisation needed with nanoparticles and the limited number of cells available from primary culture, however human mesenchymal stem cells have been used successfully to explore the degradation and fate of engineered magnetic nanoparticles within cells (Van de Walle et al., 2020a, Van de Walle et al., 2019).

5.6 Conclusion

A growing body of evidence identifies exposure to air pollution is an environmental risk factor for the development of AD. Exogenous metals and ferrimagnetic material were variably distributed throughout the human brain, so genetic control of magnetic/metallic distribution

is unlikely. There are likely toxic consequences arising from the presence of these exogenous species within the brain due to their highly oxidative nature and association with neurodegenerative disease.

There were no differences in ferrimagnetic content between AD and aged-matched controls, nor any differences in their metal content likely due to universal incursion of exogenous metals across the compromised geriatric blood brain barrier. Thus, future studies should focus on younger brains with uncompromised BBBs to look for changes in the metal/magnetic profile of the human brain, such as the observed gradient of MNPs within the brainstem of young Mexico City residents (Paper 4, Appendix D). Changes to MNP and metal levels may occur decades prior to the clinical manifestation of AD, as is thought to be the case with several pathological hallmarks of AD.

UFPs are highly penetrative and have been reported in all major organs including the lung. Roadside dust is a rich source of metallic UFPs which is currently not subject to any regulations. Stress and inflammatory responses in the lung can affect the brain via various nervous and chemical mediators collectively known as the lung-brain axis. It is critical to assess the impact of UFPs on different components of the lung-brain-axis to understand how particle incursion may impact on health. Variable cytotoxic, oxidative stress and inflammatory responses were seen in human lung epithelial cells (Calu-3) exposed to ultrafine roadside dust nanoparticles (UF-RDPs) likely due to differences in their physicochemical composition. The composition of road dust (and particulate pollution in general) varies greatly on local levels e.g., due to traffic density, weather, road conditions and industry.

Changes to global air pollution regulations are needed to regulate UFPs, including roadside dust, and this may include specific limits on the most toxic elements. Regional policies are also needed to reflect the unique particulate matter compositions across different localities. This is especially important to protect the poor and vulnerable who are disproportionately affected by air pollution. A combination of public awareness, localised policy, and regulations on UFPs would be invaluable in limiting the impact of environmental metal rich metallic nanoparticles on human health and could prevent ~2% dementia cases worldwide whilst relieving social and health care costs associated with both AD and air pollution.

Chapter 6 References

ABBAS, I., GARÇON, G., SAINT-GEORGES, F., BILLET, S., VERDIN, A., GOSSET, P., MULLIEZ, P. & SHIRALI, P. 2010. Occurrence of molecular abnormalities of cell cycle in L132 cells after in vitro short-term exposure to air pollution PM2.5. *Chemico-Biological Interactions,* 188**,** 558-565.

ABBASPOUR, N., HURRELL, R. & KELISHADI, R. 2014. Review on iron and its importance for human health. *Journal of research in medical sciences : the official journal of Isfahan University of Medical Sciences,* 19**,** 164-174.

ACOSTA-CABRONERO, J., BETTS, M. J., CARDENAS-BLANCO, A., YANG, S. & NESTOR, P. J. 2016. In Vivo MRI Mapping of Brain Iron Deposition across the Adult Lifespan. *J Neurosci,* 36**,** 364-74.

ADACHI, K. & BUSECK, P. R. 2010. Hosted and free-floating metal-bearing atmospheric nanoparticles in Mexico city. *Environmental Science and Technology,* 44**,** 2299-2304.

ADAMASZEK, M., D'AGATA, F., FERRUCCI, R., HABAS, C., KEULEN, S., KIRKBY, K. C., LEGGIO, M., MARIËN, P., MOLINARI, M., MOULTON, E., ORSI, L., VAN OVERWALLE, F., PAPADELIS, C., PRIORI, A., SACCHETTI, B., SCHUTTER, D. J., STYLIADIS, C. & VERHOEVEN, J. 2017. Consensus Paper: Cerebellum and Emotion. *Cerebellum,* 16**,** 552-576.

ADVANI, V. M. & IVANOV, P. 2020. Stress granule subtypes: an emerging link to neurodegeneration. *Cellular and Molecular Life Sciences,* 77**,** 4827-4845.

AFITSKA, K., FUCIKOVA, A., SHVADCHAK, V. V. & YUSHCHENKO, D. A. 2019. α-Synuclein aggregation at low concentrations. *Biochimica et Biophysica Acta - Proteins and Proteomics,* 1867**,** 701-709.

AJMANI, G. S., SUH, H. H., WROBLEWSKI, K. E., KERN, D. W., SCHUMM, L. P., MCCLINTOCK, M. K., YANOSKY, J. D. & PINTO, J. M. 2016. Fine particulate matter exposure and olfactory dysfunction among urban-dwelling older US adults. *Environ Res,* 151**,** 797-803.

AKATSU, H., HORI, A., YAMAMOTO, T., YOSHIDA, M., MIMURO, M., HASHIZUME, Y., TOOYAMA, I. & YEZDIMER, E. 2011. Transition metal abnormalities in progressive dementias. *Biometals : an international journal on the role of metal ions in biology, biochemistry, and medicine,* 25**,** 337-50.

AL-KATTAN, A., WICHSER, A., VONBANK, R., BRUNNER, S., ULRICH, A., ZUIN, S. & NOWACK, B. 2013. Release of TiO2 from paints containing pigment-TiO2 or nano-TiO2 by weathering. *Environ Sci Process Impacts,* 15**,** 2186-93.

ALFARO-MORENO, E., TORRES, V., MIRANDA, J., MARTÍNEZ, L., GARCÍA-CUELLAR, C., NAWROT, T. S., VANAUDENAERDE, B., HOET, P., RAMÍREZ-LÓPEZ, P., ROSAS, I., NEMERY, B. & OSORNIO-VARGAS, A. R. 2009. Induction of IL-6 and inhibition of IL-8 secretion in the human airway cell line Calu-3 by urban particulate matter collected with a modified method of PM sampling. *Environmental Research,* 109**,** 528-535.

ALFSEN, E. M., STØRMER, F. C., NJÅ, A. & WALLØE, L. 2018. A proposed tandem mechanism for memory storage in neurons involving magnetite and prions. *Medical Hypotheses,* 119**,** 98-101.

ALLSOP, D., MAYES, J., MOORE, S., MASAD, A. & TABNER, B. J. 2008. Metal-dependent generation of reactive oxygen species from amyloid proteins implicated in neurodegenerative disease. *Biochem Soc Trans,* 36**,** 1293-8.

ANDERSON, J. M., VAN ITALLIE, C. M. & FANNING, A. S. 2004. Setting up a selective barrier at the apical junction complex. *Current Opinion in Cell Biology,* 16**,** 140-145.

ANDRÁSI, E., FARKAS, É., GAWLIK, D., RÖSICK, U. & BRÄTTER, P. 2000. Brain Iron and Zinc Contents of German Patients with Alzheimer Disease. *Journal of Alzheimer's Disease,* 2**,** 17-26.

ANDRÁSI, E., FARKAS, É., SCHEIBLER, H., RÉFFY, A. & BEZÚR, L. 1995. Al, Zn, Cu, Mn and Fe levels in brain in Alzheimer's disease. *Archives of Gerontology and Geriatrics,* 21**,** 89-97.

ANDREAU, K., LEROUX, M. & BOUHARROUR, A. 2012. Health and cellular impacts of air pollutants: from cytoprotection to cytotoxicity. *Biochemistry research international,* 2012**,** 493894-493894.

ANKAMWAR, B., LAI, T. C., HUANG, J. H., LIU, R. S., HSIAO, M., CHEN, C. H. & HWU, Y. K. 2010. Biocompatibility of Fe(3)O(4) nanoparticles evaluated by in vitro cytotoxicity assays using normal, glia and breast cancer cells. *Nanotechnology,* 21**,** 75102.

ANSELMI, L., TOTI, L., BOVE, C. & TRAVAGLI, R. A. 2017. Vagally mediated effects of brain stem dopamine on gastric tone and phasic contractions of the rat. *American Journal of Physiology - Gastrointestinal and Liver Physiology,* 313**,** G434-G441.

ANSELMI, L. & TRAVAGLI, R. A. 2017. A Nigro−Vagal Pathway Controls Gastric Motility and Is Affected in a Rat Model of Parkinsonism. *Gastroenterology,* 153**,** 1581-1593.

ANSTEY, K. J., PETERS, R., MORTBY, M. E., KIELY, K. M., ERAMUDUGOLLA, R., CHERBUIN, N., HUQUE, M. H. & DIXON, R. A. 2021. Association of sex differences in dementia risk factors with sex differences in memory decline in a population-based cohort spanning 20–76 years. *Scientific Reports,* 11**,** 7710.

ARNSTEN, A. F. T., DATTA, D., DEL TREDICI, K. & BRAAK, H. 2021. Hypothesis: Tau pathology is an initiating factor in sporadic Alzheimer's disease. *Alzheimer's & Dementia,* 17**,** 115-124.

ARSHADI, M. Y., S; MOHAMMED MOUSAVI, S. 2017. Analysis on characteristics of different kinds of e waste. *Sixteenth International Waste Management and Landfill Symposium.* Sardinia, Italy.: S. Margherita di Pula,Cagliari, Italy/© 2017 by CISA Publisher, Italy.

ASHBAUGH, L. L., CARVACHO, O. F., BROWN, M. S., CHOW, J. C., WATSON, J. G. & MAGLIANO, K. C. 2003. Soil sample collection and analysis for the Fugitive Dust Characterization Study. *Atmospheric Environment,* 37**,** 1163-1173.

ASHRAF, A., JEANDRIENS, J., PARKES, H. G. & SO, P.-W. 2020. Iron dyshomeostasis, lipid peroxidation and perturbed expression of cystine/glutamate antiporter in Alzheimer's disease: Evidence of ferroptosis. *Redox biology,* 32**,** 101494-101494.

ASSI, M. A., HEZMEE, M. N. M., HARON, A. W., SABRI, M. Y. M. & RAJION, M. A. 2016. The detrimental effects of lead on human and animal health. *Veterinary world,* 9**,** 660-671.

ÅSTRÖM, D. O., ADOLFSSON, R., SEGERSSON, D., FORSBERG, B. & OUDIN, A. 2021. Local Contrasts in Concentration of Ambient Particulate Air Pollution (PM2.5) and Incidence of Alzheimer's Disease and Dementia: Results from the Betula Cohort in Northern Sweden. *J Alzheimers Dis,* 81**,** 83-85.

ATAEEFARD, M., GHASEMI, E. & EBADI, M. 2014. Effect of Micro- and Nanomagnetite on Printing Toner Properties. *The Scientific World Journal,* 2014**,** 7.

ATTEMS, J. & JELLINGER, K. A. 2006. Olfactory tau pathology in Alzheimer disease and mild cognitive impairment. *Clinical Neuropathology,* 25**,** 265-271.

ATTEMS, J., WALKER, L. & JELLINGER, K. A. 2014. Olfactory bulb involvement in neurodegenerative diseases. *Acta Neuropathologica,* 127**,** 459-475.

ATWOOD, C. S., SCARPA, R. C., HUANG, X., MOIR, R. D., JONES, W. D., FAIRLIE, D. P., TANZI, R. E. & BUSH, A. I. 2000. Characterization of copper interactions with alzheimer amyloid beta peptides: identification of an attomolar-affinity copper binding site on amyloid beta1-42. *J Neurochem,* 75**,** 1219-33.

AVASTHI, A., CARO, C., POZO-TORRES, E., LEAL, M. P. & GARCÍA-MARTÍN, M. L. 2020. Magnetic Nanoparticles as MRI Contrast Agents. *Top Curr Chem (Cham),* 378**,** 40.

BAEZA-SQUIBAN, A., BONVALLOT, V., BOLAND, S. & MARANO, F. 1999. Airborne particles evoke an inflammatory response in human airway epithelium. Activation of transcription factors. *Cell Biol Toxicol,* 15**,** 375-80.

BAI, H. & ZHANG, Q. 2021. Activation of NLRP3 Inflammasome and Onset of Alzheimer's Disease. *Frontiers in Immunology,* 12.

BAJINKA, O., SIMBILYABO, L., TAN, Y., JABANG, J. & SALEEM, S. A. 2021. Lung-brain axis. *Critical Reviews in Microbiology***,** 1-13.

BAKULSKI, K. M., SEO, Y. A., HICKMAN, R. C., BRANDT, D., VADARI, H. S., HU, H. & PARK, S. K. 2020. Heavy Metals Exposure and Alzheimer's Disease and Related Dementias. *J Alzheimers Dis,* 76**,** 1215-1242.

BANACLOCHA, M. A., BÓKKON, I. & BANACLOCHA, H. M. 2010. Long-term memory in brain magnetite. *Med Hypotheses,* 74**,** 254-7.

BARANELLO, R. J., BHARANI, K. L., PADMARAJU, V., CHOPRA, N., LAHIRI, D. K., GREIG, N. H., PAPPOLLA, M. A. & SAMBAMURTI, K. 2015. Amyloid-beta protein clearance and degradation (ABCD) pathways and their role in Alzheimer's disease. *Curr Alzheimer Res,* 12**,** 32-46.

BARNES, C. A., MELTZER, J., HOUSTON, F., ORR, G., MCGANN, K. & WENK, G. L. 2000. Chronic treatment of old rats with donepezil or galantamine: effects on memory, hippocampal plasticity and nicotinic receptors. *Neuroscience,* 99**,** 17-23.

BARRITT, J. D. & VILES, J. H. 2015. Truncated Amyloid-β(11-40/42) from Alzheimer Disease Binds Cu2+ with a Femtomolar Affinity and Influences Fiber Assembly. *J Biol Chem,* 290**,** 27791-802.

BARTZOKIS, G., BECKSON, M., HANCE, D. B., MARX, P., FOSTER, J. A. & MARDER, S. R. 1997. MR evaluation of age-related increase of brain iron in young adult and older normal males. *Magn Reson Imaging,* 15**,** 29-35.

BATISTA-NASCIMENTO, L., PIMENTEL, C., ANDRADE MENEZES, R. & RODRIGUES-POUSADA, C. 2012. Iron and Neurodegeneration: From Cellular Homeostasis to Disease. *Oxidative Medicine and Cellular Longevity,* 2012**,** 128647.

BATISTA, A. F., FORNY-GERMANO, L., CLARKE, J. R., LYRA E SILVA, N. M., BRITO-MOREIRA, J., BOEHNKE, S. E., WINTERBORN, A., COE, B. C., LABLANS, A., VITAL, J. F., MARQUES, S. A., MARTINEZ, A. M., GRALLE, M., HOLSCHER, C., KLEIN, W. L., HOUZEL, J.-C., FERREIRA, S. T., MUNOZ, D. P. & DE FELICE, F. G. 2018. The diabetes drug liraglutide reverses cognitive impairment in mice and attenuates insulin receptor and synaptic pathology in a non-human primate model of Alzheimer's disease. *The Journal of pathology,* 245**,** 85-100.

BAUMGARTNER, J., MORIN, G., MENGUY, N., PEREZ GONZALEZ, T., WIDDRAT, M., COSMIDIS, J. & FAIVRE, D. 2013. Magnetotactic bacteria form magnetite from a phosphate-rich ferric hydroxide via nanometric ferric (oxyhydr)oxide intermediates. *Proceedings of the National Academy of Sciences,* 110**,** 14883.

BAYRAM, H., ITO, K., ISSA, R., ITO, M., SUKKAR, M. & CHUNG, K. F. 2006. Regulation of human lung epithelial cell numbers by diesel exhaust particles. *European Respiratory Journal,* 27**,** 705.

BEACH, T. G., WHITE, C. L., HLADIK, C. L., SABBAGH, M. N., CONNOR, D. J., SHILL, H. A., SUE, L. I., SASSE, J., BACHALAKURI, J., HENRY-WATSON, J., AKIYAMA, H. & ADLER, C. H. 2009. Olfactory bulb α-synucleinopathy has high specificity and sensitivity for Lewy body disorders. *Acta Neuropathologica,* 117**,** 169-174.

BEKRIS, L. M., YU, C.-E., BIRD, T. D. & TSUANG, D. W. 2010. Genetics of Alzheimer Disease. *Journal of geriatric psychiatry and neurology,* 23**,** 213-227.

BERGAMINO, M., KEELING, E. G., MISHRA, V. R., STOKES, A. M. & WALSH, R. R. 2020. Assessing white matter pathology in early-stage parkinson disease using diffusion mri: A systematic review. *Frontiers in Neurology,* 11.

BERLETT, B. S. & STADTMAN, E. R. 1997. Protein Oxidation in Aging, Disease, and Oxidative Stress. *Journal of Biological Chemistry,* 272**,** 20313-20316.

BERNDT, D., MILLWARD, J. M., SCHNORR, J., TAUPITZ, M., STANGL, V., PAUL, F., WAGNER, S., WUERFEL, J. T., SACK, I., LUDWIG, A. & INFANTE-DUARTE, C. 2017. Inflammation-induced brain endothelial activation leads to uptake of electrostatically stabilized iron oxide nanoparticles via sulfated glycosaminoglycans. *Nanomedicine: Nanotechnology, Biology, and Medicine,* 13**,** 1411-1421.

BESNARD-GUÉRIN, C. 2020. Cytoplasmic localization of amyotrophic lateral sclerosis-related TDP-43 proteins modulates stress granule formation. *European Journal of Neuroscience,* 52**,** 3995-4008.

BINHI, V. N. & PRATO, F. S. 2018. Rotations of macromolecules affect nonspecific biological responses to magnetic fields. *Scientific Reports,* 8.

BIRMINGHAM CITY COUNCIL. 2018. *Birmingham Population* [Online]. Available: https://www.birmingham.gov.uk/info/20057/about_birmingham/1294/population_and_census/2 [Accessed 26th August 2021].

BIRMINGHAM CITY COUNCIL. 2019. *2019 Air Quality Annual Status Report (ASR)* [Online]. Available: http://62.65.40.208/birmingham//Reports/2019_Birmingham_City_Council_ASR.pdf [Accessed 26th August 2021].

BLANPIED, T. A., BOECKMAN, F. A., AIZENMAN, E. & JOHNSON, J. W. 1997. Trapping channel block of NMDA-activated responses by amantadine and memantine. *J Neurophysiol,* 77**,** 309-23.

BLENNOW, K., DE LEON, M. J. & ZETTERBERG, H. 2006. Alzheimer's disease. *Lancet,* 368**,** 387-403.

BOEHMLER, D. J., O'DELL, Z. J., CHUNG, C. & RILEY, K. R. 2020. Bovine Serum Albumin Enhances Silver Nanoparticle Dissolution Kinetics in a Size- and Concentration-Dependent Manner. *Langmuir,* 36**,** 1053-1061.

BOLOGNIN, S., MESSORI, L., DRAGO, D., GABBIANI, C., CENDRON, L. & ZATTA, P. 2011. Aluminum, copper, iron and zinc differentially alter amyloid-Aβ(1-42) aggregation and toxicity. *Int J Biochem Cell Biol,* 43**,** 877-85.

BONDA, D. J., LEE, H.-G., BLAIR, J. A., ZHU, X., PERRY, G. & SMITH, M. A. 2011. Role of Metal Dyshomeostasis in Alzheimer Disease. *Metallomics : integrated biometal science,* 3**,** 267-270.

BONGAERTS, E., LECANTE, L. L., BOVÉ, H., ROEFFAERS, M. B. J., AMELOOT, M., FOWLER, P. A. & NAWROT, T. S. 2022. Maternal exposure to ambient black carbon particles and their presence in maternal and fetal circulation and organs: an analysis of two independent population-based observational studies. *The Lancet Planetary Health,* 6**,** e804-e811.

BORELLI, V., TREVISAN, E., VITA, F., BOTTIN, C., MELATO, M., RIZZARDI, C. & ZABUCCHI, G. 2012. Peroxidase-Like Activity of Ferruginous Bodies Isolated by Exploiting their Magnetic Property. *Journal of Toxicology and Environmental Health, Part A,* 75**,** 603-623.

BOTSOU, F., MOUTAFIS, I., DALAINA, S. & KELEPERTZIS, E. 2020. Settled bus dust as a proxy of traffic-related emissions and health implications of exposures to potentially harmful elements. *Atmospheric Pollution Research,* 11**,** 1776-1784.

BOURISLY, A. K., GEJO, G., HAYAT, A. A., ALSARRAF, L., DASHTI, F. M. & DI PAOLA, M. 2017. White Matter Sexual Dimorphism of the Adult Human Brain. *Transl Neurosci,* 8**,** 49-53.

BOVE, C. & TRAVAGLI, R. A. 2019. Neurophysiology of the brain stem in Parkinson's disease. *Journal of Neurophysiology,* 121**,** 1856-1864.

BOYES, W. K. & VAN THRIEL, C. 2020. Neurotoxicology of nanomaterials. *Chemical Research in Toxicology,* 33**,** 1121-1144.

BRAAK, H. & BRAAK, E. 1985. On areas of transition between entorhinal allocortex and temporal isocortex in the human brain. Normal morphology and lamina-specific pathology in Alzheimer's disease. *Acta Neuropathologica,* 68**,** 325-332.

BRAAK, H. & BRAAK, E. 1991. Neuropathological stageing of Alzheimer-related changes. *Acta Neuropathologica,* 82**,** 239-259.

BRAAK, H. & DEL TREDICI, K. 2011. The pathological process underlying Alzheimer's disease in individuals under thirty. *Acta Neuropathologica,* 121**,** 171-181.

BRAAK, H. & DEL TREDICI, K. 2015. The preclinical phase of the pathological process underlying sporadic Alzheimer's disease. *Brain,* 138**,** 2814-2833.

BRAAK, H. & DEL TREDICI, K. 2017. Neuropathological Staging of Brain Pathology in Sporadic Parkinson's disease: Separating the Wheat from the Chaff. *Journal of Parkinson's Disease,* 7**,** S73-S87.

BRAAK, H. & DEL TREDICI, K. 2018. Anterior cingulate cortex TDP-43 pathology in sporadic amyotrophic lateral sclerosis. *Journal of Neuropathology and Experimental Neurology,* 77**,** 74-83.

BRAAK, H., DEL TREDICI, K., RÜB, U., DE VOS, R. A. I., JANSEN STEUR, E. N. H. & BRAAK, E. 2003. Staging of brain pathology related to sporadic Parkinson's disease. *Neurobiology of Aging,* 24**,** 197-211.

BRAAK, H., THAL, D. R., GHEBREMEDHIN, E. & DEL TREDICI, K. 2011. Stages of the pathologic process in alzheimer disease: Age categories from 1 to 100 years. *Journal of Neuropathology and Experimental Neurology,* 70**,** 960-969.

BRAAKHUIS, H. M., PARK, M. V., GOSENS, I., DE JONG, W. H. & CASSEE, F. R. 2014. Physicochemical characteristics of nanomaterials that affect pulmonary inflammation. *Part Fibre Toxicol,* 11**,** 18.

BRANN, D. H., TSUKAHARA, T., WEINREB, C., LIPOVSEK, M., BERGE, K. V. D., GONG, B., CHANCE, R., MACAULAY, I. C., CHOU, H.-J., FLETCHER, R. B., DAS, D., STREET, K., BEZIEUX, H. R. D., CHOI, Y.-G., RISSO, D., DUDOIT, S., PURDOM, E., MILL, J., HACHEM, R. A., MATSUNAMI, H., LOGAN, D. W., GOLDSTEIN, B. J., GRUBB, M. S., NGAI, J. & DATTA, S. R. 2020. Non-neuronal expression of SARS-CoV-2 entry genes in the olfactory system suggests mechanisms underlying COVID-19-associated anosmia. *Science Advances,* 6**,** eabc5801.

BREIJYEH, Z. & KARAMAN, R. 2020. Comprehensive Review on Alzheimer's Disease: Causes and Treatment. *Molecules,* 25.

BREM, F., HIRT, A. M., SIMON, C., WIESER, H.-G. & DOBSON, J. 2005a. Characterization of iron compounds in tumour tissue from temporal lobe epilepsy patients using low temperature magnetic methods. *Biometals,* 18**,** 191-197.

BREM, F., HIRT, A. M., SIMON, C., WIESER, H. G. & DOBSON, J. 2005b. Low temperature magnetic analysis in the identification of iron compounds from human brain tumour tissue. *Journal of Physics: Conference Series,* 17**,** 61-64.

BREM, F., HIRT, A. M., WINKLHOFER, M., FREI, K., YONEKAWA, Y., WIESER, H.-G. & DOBSON, J. 2006. Magnetic iron compounds in the human brain: a comparison of tumour and hippocampal tissue. *Journal of The Royal Society Interface,* 3**,** 833-841.

BRETTSCHNEIDER, J., DEL TREDICI, K., TOLEDO, J. B., ROBINSON, J. L., IRWIN, D. J., GROSSMAN, M., SUH, E., VAN DEERLIN, V. M., WOOD, E. M., BAEK, Y., KWONG, L., LEE, E. B., ELMAN, L., MCCLUSKEY, L., FANG, L., FELDENGUT, S., LUDOLPH, A. C., LEE, V. M. Y., BRAAK, H. & TROJANOWSKI, J. Q. 2013. Stages of pTDP-43 pathology in amyotrophic lateral sclerosis. *Annals of Neurology,* 74**,** 20-38.

BRIGHT, J., HUSSAIN, S., DANG, V., WRIGHT, S., COOPER, B., BYUN, T., RAMOS, C., SINGH, A., PARRY, G., STAGLIANO, N. & GRISWOLD-PRENNER, I. 2015. Human secreted tau increases amyloid-beta production. *Neurobiol Aging,* 36**,** 693-709.

BROSTRØM, A., KLING, K. I., KOPONEN, I. K., HOUGAARD, K. S., KANDLER, K. & MØLHAVE, K. 2019. Improving the foundation for particulate matter risk assessment by individual nanoparticle statistics from electron microscopy analysis. *Scientific Reports,* 9.

BROWN, R. J. C. & MILTON, M. J. T. 2005. Analytical techniques for trace element analysis: an overview. *TrAC Trends in Analytical Chemistry,* 24**,** 266-274.

BULK, M., VAN DER WEERD, L., BREIMER, W., LEBEDEV, N., WEBB, A., GOEMAN, J. J., WARD, R. J., HUBER, M., OOSTERKAMP, T. H. & BOSSONI, L. 2018. Quantitative comparison of different iron forms in the temporal cortex of Alzheimer patients and control subjects. *Scientific reports,* 8**,** 6898-6898.

BURNETT, R., CHEN, H., SZYSZKOWICZ, M., FANN, N., HUBBELL, B., POPE, C. A., APTE, J. S., BRAUER, M., COHEN, A., WEICHENTHAL, S., COGGINS, J., DI, Q., BRUNEKREEF, B., FROSTAD, J., LIM, S. S., KAN, H., WALKER, K. D., THURSTON, G. D., HAYES, R. B., LIM, C. C., TURNER, M. C., JERRETT, M., KREWSKI, D., GAPSTUR, S. M., DIVER, W. R., OSTRO, B., GOLDBERG, D., CROUSE, D. L., MARTIN, R. V., PETERS, P., PINAULT, L., TJEPKEMA, M., VAN DONKELAAR, A., VILLENEUVE, P. J., MILLER, A. B., YIN, P., ZHOU, M., WANG, L., JANSSEN, N. A. H., MARRA, M., ATKINSON, R. W., TSANG, H., QUOC THACH, T., CANNON, J. B., ALLEN, R. T., HART, J. E., LADEN, F., CESARONI, G., FORASTIERE, F., WEINMAYR, G., JAENSCH, A., NAGEL, G., CONCIN, H. & SPADARO, J. V. 2018. Global estimates of mortality associated with long-term exposure to outdoor fine particulate matter. *Proceedings of the National Academy of Sciences,* 115**,** 9592-9597.

BUSH, A. I. 2013. The metal theory of Alzheimer's disease. *J Alzheimers Dis,* 33 Suppl 1**,** S277-81.

BUSH, A. I., PETTINGELL, W. H., MULTHAUP, G., D PARADIS, M., VONSATTEL, J. P., GUSELLA, J. F., BEYREUTHER, K., MASTERS, C. L. & TANZI, R. E. 1994. Rapid induction of Alzheimer A beta amyloid formation by zinc. *Science,* 265**,** 1464-7.

BUSH, V. J., MOYER, T. P., BATTS, K. P. & PARISI, J. E. 1995. Essential and toxic element concentrations in fresh and formalin-fixed human autopsy tissues. *Clin Chem,* 41**,** 284-94.

CACCIOTTOLO, M., WANG, X., DRISCOLL, I., WOODWARD, N., SAFFARI, A., REYES, J., SERRE, M. L., VIZUETE, W., SIOUTAS, C., MORGAN, T. E., GATZ, M., CHUI, H. C., SHUMAKER, S. A., RESNICK, S. M., ESPELAND, M. A., FINCH, C. E. & CHEN, J. C. 2017. Particulate air pollutants, APOE alleles and their contributions to cognitive impairment in older women and to amyloidogenesis in experimental models. *Translational Psychiatry,* 7**,** e1022-e1022.

CALDERÓN-GARCIDUEAS, L., KAVANAUGH, M., BLOCK, M., D'ANGIULLI, A., DELGADO-CHÁVEZ, R., TORRES-JARDÓN, R., GONZÁLEZ-MACIEL, A., REYNOSO-ROBLES, R., OSNAYA, N., VILLARREAL-CALDERON, R., GUO, R., HUA, Z., ZHU, H., PERRY, G. & DIAZ, P. 2012. Neuroinflammation, hyperphosphorylated tau, diffuse amyloid plaques, and down-regulation of the cellular prion protein in air pollution exposed children and young adults. *Journal of Alzheimer's Disease,* 28**,** 93-107.

CALDERÓN-GARCIDUEÑAS, L., AVILA-RAMIREZ, J., CALDERON-GARCIDUEÑAS, A., GONZALEZ-HEREDIA, T., ACUNA-AYALA, H., CHAO, C. K., THOMPSON, C., RUIZ-RAMOS, R., CORTES-GONZALEZ, V., MARTINEZ-MARTINEZ, L., GARCIA-PEREZ, M. A., REIS, J., MUKHERJEE, P. S., TORRES-JARDON, R. & LACHMANN, I. 2016a. Cerebrospinal Fluid Biomarkers in Highly Exposed PM2.5 Urbanites: The Risk of Alzheimer's and Parkinson's Diseases in Young Mexico City Residents. *J Alzheimers Dis,* 54**,** 597-613.

CALDERÓN-GARCIDUEÑAS, L., AZZARELLI, B., ACUNA, H., GARCIA, R., GAMBLING, T. M., OSNAYA, N., MONROY, S., DEL ROSARIO TIZAPANTZI, M., CARSON, J. L., VILLARREAL-CALDERON, A. & REWCASTLE, B. 2002. Air Pollution and Brain Damage. *Toxicologic Pathology,* 30**,** 373-389.

CALDERÓN-GARCIDUEÑAS, L., D'ANGIULLI, A., KULESZA, R. J., TORRES-JARDÓN, R., OSNAYA, N., ROMERO, L., KEEFE, S., HERRITT, L., BROOKS, D. M., AVILA-RAMIREZ, J., DELGADO-CHÁVEZ, R., MEDINA-CORTINA, H. & GONZÁLEZ-GONZÁLEZ, L. O. 2011. Air pollution is associated with brainstem auditory nuclei pathology and delayed brainstem auditory evoked potentials. *International Journal of Developmental Neuroscience,* 29**,** 365-375.

CALDERÓN-GARCIDUEÑAS, L. & DE LA MONTE, S. M. 2017. Apolipoprotein E4, Gender, Body Mass Index, Inflammation, Insulin Resistance, and Air Pollution Interactions: Recipe for Alzheimer's Disease Development in Mexico City Young Females. *Journal of Alzheimers Disease,* 58**,** 613-630.

CALDERÓN-GARCIDUEÑAS, L., FRANCO-LIRA, M., HENRÍQUEZ-ROLDÁN, C., OSNAYA, N., GONZÁLEZ-MACIEL, A., REYNOSO-ROBLES, R., VILLARREAL-CALDERON, R., HERRITT, L., BROOKS, D., KEEFE, S., PALACIOS-MORENO, J., VILLARREAL-CALDERON, R., TORRES-JARDÓN, R., MEDINA-CORTINA, H., DELGADO-CHÁVEZ, R., AIELLO-MORA, M., MARONPOT, R. R. & DOTY, R. L. 2010. Urban air pollution: influences on olfactory function and pathology in exposed children and young adults. *Experimental and toxicologic pathology : official journal of the Gesellschaft fur Toxikologische Pathologie,* 62**,** 91-102.

CALDERÓN-GARCIDUEÑAS, L., FRANCO-LIRA, M., MORA-TISCAREÑO, A., MEDINA-CORTINA, H., TORRES-JARDÓN, R. & KAVANAUGH, M. 2013a. Early alzheimer's and parkinson's disease pathology in urban children: Friend versus foe responses - It is time to face the evidence. *BioMed Research International,* 2013.

CALDERÓN-GARCIDUEÑAS, L., FRANCO-LIRA, M., TORRES-JARDÓN, R., HENRIQUEZ-ROLDÁN, C., BARRAGÁN-MEJÍA, G., VALENCIA-SALAZAR, G., GONZALÉZ-MACIEL, A., REYNOSO-ROBLES, R., VILLARREAL-CALDERÓN, R. & REED, W. 2007. Pediatric Respiratory and Systemic Effects of Chronic Air Pollution Exposure: Nose, Lung, Heart, and Brain Pathology. *Toxicologic Pathology,* 35**,** 154-162.

CALDERÓN-GARCIDUEÑAS, L., GONZÁLEZ-GONZÁLEZ, L. O., KULESZA, R. J., FECH, T. M., PÉREZ-GUILLÉ, G., LUNA, M. A. J. B., SORIANO-ROSALES, R. E., SOLORIO, E., MIRAMONTES-HIGUERA, J. D. J., GÓMEZ-MAQUEO CHEW, A., BERNAL-MORÚA, A. F., MUKHERJEE, P. S., TORRES-JARDÓN, R., MILLS, P. C., WILSON, W. J., PÉREZ-GUILLÉ, B. & D'ANGIULLI, A. 2017a. Exposures to fine particulate matter (PM2.5) and ozone above USA standards are associated with auditory brainstem dysmorphology and abnormal auditory brainstem evoked potentials in healthy young dogs. *Environmental Research,* 158**,** 324-332.

CALDERÓN-GARCIDUEÑAS, L., GONZALEZ-MACIEL, A., KULESZA, R. J., GONZALEZ-GONZALEZ, L. O., REYNOSO-ROBLES, R., MUKHERJEE, P. S. & TORRES-JARDON, R. 2019a. Air Pollution, Combustion and Friction Derived Nanoparticles, and Alzheimer's Disease in Urban Children and Young Adults. *Journal of Alzheimers Disease,* 70**,** 341-358.

CALDERÓN-GARCIDUEÑAS, L., GONZÁLEZ-MACIEL, A., MUKHERJEE, P. S., REYNOSO-ROBLES, R., PÉREZ-GUILLÉ, B., GAYOSSO-CHÁVEZ, C., TORRES-JARDÓN, R., CROSS, J. V., AHMED, I. A. M., KARLOUKOVSKI, V. V. & MAHER, B. A. 2019b. Combustion- and friction-derived magnetic air pollution nanoparticles in human hearts. *Environmental Research,* 176**,** 108567.

CALDERÓN-GARCIDUEÑAS, L., GÓNZALEZ-MACIEL, A., REYNOSO-ROBLES, R., DELGADO-CHÁVEZ, R., MUKHERJEE, P. S., KULESZA, R. J., TORRES-JARDÓN, R., ÁVILA-RAMÍREZ, J. & VILLARREAL-RÍOS, R. 2018a. Hallmarks of Alzheimer disease are evolving relentlessly in Metropolitan Mexico City infants, children and young adults. APOE4 carriers have higher suicide risk and higher odds of reaching NFT stage V at ≤ 40 years of age. *Environmental Research,* 164**,** 475-487.

CALDERÓN-GARCIDUEÑAS, L., GONZÁLEZ-MACIEL, A., REYNOSO-ROBLES, R., HAMMOND, J., KULESZA, R., LACHMANN, I., TORRES-JARDÓN, R., MUKHERJEE, P. S. & MAHER, B. A. 2020a. Quadruple abnormal protein aggregates in brainstem pathology and exogenous metal-rich magnetic nanoparticles. The substantia nigrae is a very early target in young urbanites and the gastrointestinal tract likely a key brainstem portal. *Environmental Research***,** 110139.

CALDERÓN-GARCIDUEÑAS, L., GONZALEZ-MACIEL, A., REYNOSO-ROBLES, R., KULESZA, R. J., MUKHERJEE, P. S., TORRES-JARDON, R., RONKKO, T. & DOTY, R. L. 2018b. Alzheimer's disease and alpha-synuclein pathology in the olfactory bulbs of infants, children, teens and adults <= 40 years in Metropolitan Mexico City. APOE4 carriers at higher risk of suicide accelerate their olfactory bulb pathology. *Environmental Research,* 166**,** 348-362.

CALDERÓN-GARCIDUEÑAS, L., HERRERA-SOTO, A., JURY, N., MAHER, B. A., GONZÁLEZ-MACIEL, A., REYNOSO-ROBLES, R., RUIZ-RUDOLPH, P., VAN ZUNDERT, B. & VARELA-NALLAR, L. 2020b. Reduced repressive epigenetic marks, increased DNA damage and Alzheimer's disease hallmarks in the brain of humans and mice exposed to particulate urban air pollution. *Environmental Research,* 183**,** 109226.

CALDERÓN-GARCIDUEÑAS, L., KULESZA, R. J., MANSOUR, Y., AIELLO-MORA, M., MUKHERJEE, P. S. & GONZÁLEZ-GONZÁLEZ, L. O. 2019c. Increased Gain in the Auditory Pathway, Alzheimer's Disease Continuum, and Air Pollution: Peripheral and Central Auditory System Dysfunction Evolves Across Pediatric and Adult Urbanites. *Journal of Alzheimer's Disease,* 70**,** 1275-1286.

CALDERÓN-GARCIDUEÑAS, L., MARONPOT, R. R., TORRES-JARDON, R., HENRÍQUEZ-ROLDÁN, C., SCHOONHOVEN, R., ACUÑA-AYALA, H., VILLARREAL-CALDERÓN, A., NAKAMURA, J., FERNANDO, R., REED, W., AZZARELLI, B. & SWENBERG, J. A. 2003. DNA damage in nasal and brain tissues of canines exposed to air pollutants is associated with evidence of chronic brain inflammation and neurodegeneration. *Toxicologic Pathology,* 31**,** 524-538.

CALDERÓN-GARCIDUEÑAS, L., RAJKUMAR, R. P., STOMMEL, E. W., KULESZA, R., MANSOUR, Y., RICO-VILLANUEVA, A., FLORES-VÁZQUEZ, J. O., BRITO-AGUILAR, R., RAMÍREZ-SÁNCHEZ, S., GARCÍA-ALONSO, G., CHÁVEZ-FRANCO, D. A., LUÉVANO-CASTRO, S. C., GARCÍA-ROJAS, E., REVUELTAS-FICACHI, P., VILLARREAL-RÍOS, R. & MUKHERJEE, P. S. 2021a. Brainstem Quadruple Aberrant Hyperphosphorylated Tau, Beta-Amyloid, Alpha-Synuclein and TDP-43 Pathology, Stress and Sleep Behavior Disorders. *International journal of environmental research and public health,* 18.

CALDERÓN-GARCIDUEÑAS, L., REED, W., MARONPOT, R. R., HENRÍQUEZ-ROLDÁN, C., DELGADO-CHAVEZ, R., CALDERÓN-GARCIDUEÑAS, A., DRAGUSTINOVIS, I., FRANCO-LIRA, M., ARAGÓN-FLORES, M., SOLT, A. C., ALTENBURG, M., TORRES-JARDÓN, R. & SWENBERG, J. A. 2004. Brain inflammation and Alzheimer's-like pathology in individuals exposed to severe air pollution. *Toxicologic Pathology,* 32**,** 650-658.

CALDERÓN-GARCIDUEÑAS, L., REYNOSO-ROBLES, R. & GONZÁLEZ-MACIEL, A. 2019d. Combustion and friction-derived nanoparticles and industrial-sourced nanoparticles: The culprit of Alzheimer and Parkinson's diseases. *Environmental Research,* 176.

CALDERÓN-GARCIDUEÑAS, L., REYNOSO-ROBLES, R., PÉREZ-GUILLÉ, B., MUKHERJEE, P. S. & GÓNZALEZ-MACIEL, A. 2017b. Combustion-derived nanoparticles, the neuroenteric system, cervical vagus, hyperphosphorylated alpha synuclein and tau in young Mexico City residents. *Environmental Research,* 159**,** 186-201.

CALDERÓN-GARCIDUEÑAS, L., REYNOSO-ROBLES, R., VARGAS- MARTÍNEZ, J., GÓMEZ-MAQUEO-CHEW, A., PÉREZ-GUILLÉ, B., MUKHERJEE, P. S., TORRES-JARDÓN, R., PERRY, G. & GÓNZALEZ-MACIEL, A. 2016b. Prefrontal white matter pathology in air pollution exposed Mexico City young urbanites and their potential impact on neurovascular unit

dysfunction and the development of Alzheimer's disease. *Environmental Research,* 146**,** 404-417.

CALDERÓN-GARCIDUEÑAS, L., SERRANO-SIERRA, A., TORRES-JARDÓN, R., ZHU, H., YUAN, Y., SMITH, D., DELGADO-CHÁVEZ, R., CROSS, J. V., MEDINA-CORTINA, H., KAVANAUGH, M. & GUILARTE, T. R. 2013b. The impact of environmental metals in young urbanites' brains. *Experimental and Toxicologic Pathology,* 65**,** 503-511.

CALDERÓN-GARCIDUEÑAS, L., SOLT, A. C., HENRIQUEZ-ROLDAN, C., TORRES-JARDON, R., NUSE, B., HERRITT, L., VILLARREAL-CALDERON, R., OSNAYA, N., STONE, I., GARCIA, R., BROOKS, D. M., GONZALEZ-MACIEL, A., REYNOSO-ROBLES, R., DELGADO-CHAVEZ, R. & REED, W. 2008. Long-term air pollution exposure is associated with neuroinflammation, an altered innate immune response, disruption of the blood-brain barrier, ultrafine particulate deposition, and accumulation of amyloid beta-42 and alpha-synuclein in children and young adults. *Toxicol Pathol,* 36**,** 289-310.

CALDERÓN-GARCIDUEÑAS, L., STOMMEL, E. W., RAJKUMAR, R. P., MUKHERJEE, P. S. & AYALA, A. 2021b. Particulate Air Pollution and Risk of Neuropsychiatric Outcomes. What We Breathe, Swallow, and Put on Our Skin Matters. *Int J Environ Res Public Health,* 18.

CALDERÓN-GARCIDUEÑAS, L., TORRES-JARDON, R., KULESZA, R. J., MANSOUR, Y., GONZALEZ-GONZALEZ, L. O., GONZALEZ-MACIEL, A., REYNOSO-ROBLES, R. & MUKHERJEE, P. S. 2020c. Alzheimer disease starts in childhood in polluted Metropolitan Mexico City. A major health crisis in progress. *Environmental Research,* 183**,** 14.

CALDERÓN-GARCIDUEÑAS, L., TORRES-SOLORIO, A. K., KULESZA, R. J., TORRES-JARDÓN, R., GONZÁLEZ-GONZÁLEZ, L. O., GARCÍA-ARREOLA, B., CHÁVEZ-FRANCO, D. A., LUÉVANO-CASTRO, S. C., HERNÁNDEZ-CASTILLO, A., CARLOS-HERNÁNDEZ, E., SOLORIO-LÓPEZ, E., CRESPO-CORTÉS, C. N., GARCÍA-ROJAS, E., MUKHERJEE, P. S. & RESEARCH UNIVERSIDAD DEL VALLE DE MÉXICO, U. V. M. G. 2020d. Gait and balance disturbances are common in young urbanites and associated with cognitive impairment. Air pollution and the historical development of Alzheimer's disease in the young. *Environmental research,* 191**,** 110087-110087.

CALDERÓN-GARCIDUEÑAS, L., VALENCIA-SALAZAR, G., RODRÍGUEZ-ALCARAZ, A., GAMBLING, T. M., GARCÍA, R., OSNAYA, N., VILLARREAL-CALDERÓN, A., DEVLIN, R. B. & CARSON, J. L. 2001. Ultrastructural nasal pathology in children chronically and sequentially exposed to air pollutants. *Am J Respir Cell Mol Biol,* 24**,** 132-8.

CALHOUN-HANEY, R. & MURPHY, C. 2005. Apolipoprotein epsilon4 is associated with more rapid decline in odor identification than in odor threshold or Dementia Rating Scale scores. *Brain Cogn,* 58**,** 178-82.

CARABALLO, J. C., YSHII, C., WESTPHAL, W., MONINGER, T. & COMELLAS, A. P. 2011. Ambient particulate matter affects occludin distribution and increases alveolar transepithelial electrical conductance. *Respirology (Carlton, Vic.),* 16**,** 340-349.

CAREY, I. M., ANDERSON, H. R., ATKINSON, R. W., BEEVERS, S. D., COOK, D. G., STRACHAN, D. P., DAJNAK, D., GULLIVER, J. & KELLY, F. J. 2018. Are noise and air pollution related to the incidence of dementia? A cohort study in London, England. *BMJ Open,* 8**,** e022404.

CASEY, J. S., ARRIZABALAGA, J. H., ABU-LABAN, M., BECCA, J. C., ROSE, B. J., STRICKLAND, K. T., BURSAVICH, J. B., MCCANN, J. S., PACHECO, C. N., JESSEN, L., ATTALURI, A. & HAYES, D. J. 2020. Alternating magnetic field mediated release of fluorophores from magnetic nanoparticles by hysteretic heating. *Journal of Colloid and Interface Science,* 571**,** 348-355.

CASTELLANI, R. J., MOREIRA, P. I., LIU, G., DOBSON, J., PERRY, G., SMITH, M. A. & ZHU, X. 2007. Iron: The redox-active center of oxidative stress in Alzheimer disease. *Neurochemical Research,* 32**,** 1640-1645.

CASTERTON, R. L., HUNT, R. J. & FANTO, M. 2020. Pathomechanism Heterogeneity in the Amyotrophic Lateral Sclerosis and Frontotemporal Dementia Disease Spectrum:

Providing Focus Through the Lens of Autophagy. *Journal of Molecular Biology,* 432**,** 2692-2713.

CATALANI, S., RIZZETTI, M. C., PADOVANI, A. & APOSTOLI, P. 2012. Neurotoxicity of cobalt. *Hum Exp Toxicol,* 31**,** 421-37.

CATER, M. A., MCINNES, K. T., LI, Q. X., VOLITAKIS, I., LA FONTAINE, S., MERCER, J. F. & BUSH, A. I. 2008. Intracellular copper deficiency increases amyloid-beta secretion by diverse mechanisms. *Biochem J,* 412**,** 141-52.

CAUDILLO, L., SALCEDO, D., PERALTA, O., CASTRO, T. & ALVAREZ-OSPINA, H. 2020. Nanoparticle size distributions in Mexico city. *Atmospheric Pollution Research,* 11**,** 78-84.

CEBALLOS, D., ZHOU, M. & HERRICK, R. 2020. Metals and particulates exposure from a mobile e-waste shredding truck: A pilot study. *Annals of Work Exposures and Health,* 64**,** 890-896.

CEFALU, W. T. & HU, F. B. 2004. Role of Chromium in Human Health and in Diabetes. *Diabetes Care,* 27**,** 2741.

CHANDEL, T. I., ZAMAN, M., KHAN, M. V., ALI, M., RABBANI, G., ISHTIKHAR, M. & KHAN, R. H. 2018. A mechanistic insight into protein-ligand interaction, folding, misfolding, aggregation and inhibition of protein aggregates: An overview. *International Journal of Biological Macromolecules,* 106**,** 1115-1129.

CHANG, K. H., CHANG, M. Y., MUO, C. H., WU, T. N., CHEN, C. Y. & KAO, C. H. 2014. Increased risk of dementia in patients exposed to nitrogen dioxide and carbon monoxide: a population-based retrospective cohort study. *PLoS One,* 9**,** e103078.

CHASON, K. D., JASPERS, I., PARKER, J., SELLERS, S., BRIGHTON, L. E., HUNSUCKER, S. A., ARMISTEAD, P. M. & FISCHER, W. A., 2ND 2018. Age-Associated Changes in the Respiratory Epithelial Response to Influenza Infection. *J Gerontol A Biol Sci Med Sci,* 73**,** 1643-1650.

CHEIGNON, C., JONES, M., ATRIÁN-BLASCO, E., KIEFFER, I., FALLER, P., COLLIN, F. & HUREAU, C. 2017. Identification of key structural features of the elusive Cu-Aβ complex that generates ROS in Alzheimer's disease. *Chem Sci,* 8**,** 5107-5118.

CHEIGNON, C., TOMAS, M., BONNEFONT-ROUSSELOT, D., FALLER, P., HUREAU, C. & COLLIN, F. 2018. Oxidative stress and the amyloid beta peptide in Alzheimer's disease. *Redox Biology,* 14**,** 450-464.

CHEMSEDDINE, A. & MORITZ, T. 1999. Nanostructuring titania: Control over nanocrystal structure, size, shape, and organization. *European Journal of Inorganic Chemistry***,** 235-245.

CHEN, H., KWONG, J. C., COPES, R., HYSTAD, P., VAN DONKELAAR, A., TU, K., BROOK, J. R., GOLDBERG, M. S., MARTIN, R. V., MURRAY, B. J., WILTON, A. S., KOPP, A. & BURNETT, R. T. 2017a. Exposure to ambient air pollution and the incidence of dementia: A population-based cohort study. *Environ Int,* 108**,** 271-277.

CHEN, H., KWONG, J. C., COPES, R., TU, K., VILLENEUVE, P. J., VAN DONKELAAR, A., HYSTAD, P., MARTIN, R. V., MURRAY, B. J., JESSIMAN, B., WILTON, A. S., KOPP, A. & BURNETT, R. T. 2017b. Living near major roads and the incidence of dementia, Parkinson's disease, and multiple sclerosis: a population-based cohort study. *The Lancet,* 389**,** 718-726.

CHEN, J.-C., WANG, X., WELLENIUS, G. A., SERRE, M. L., DRISCOLL, I., CASANOVA, R., MCARDLE, J. J., MANSON, J. E., CHUI, H. C. & ESPELAND, M. A. 2015. Ambient air pollution and neurotoxicity on brain structure: Evidence from women's health initiative memory study. *Annals of neurology,* 78**,** 466-476.

CHEN, R., HU, B., LIU, Y., XU, J., YANG, G., XU, D. & CHEN, C. 2016a. Beyond PM2.5: The role of ultrafine particles on adverse health effects of air pollution. *Biochimica et Biophysica Acta (BBA) - General Subjects,* 1860**,** 2844-2855.

CHEN, R., LI, H., CAI, J., WANG, C., LIN, Z., LIU, C., NIU, Y., ZHAO, Z., LI, W. & KAN, H. 2018. Fine Particulate Air Pollution and the Expression of microRNAs and Circulating Cytokines Relevant to Inflammation, Coagulation, and Vasoconstriction. *Environ Health Perspect,* 126**,** 017007.

CHEN, S., ZHANG, X., LIN, J., HUANG, J., ZHAO, D., YUAN, T., HUANG, K., LUO, Y., JIA, Z., ZANG, Z., QIU, Y. A. & XIE, L. 2019. Fugitive Road Dust PM2.5 Emissions and Their Potential Health Impacts. *Environmental Science & Technology,* 53**,** 8455-8465.

CHEN, X. & MAO, S. S. 2007. Titanium dioxide nanomaterials: Synthesis, properties, modifications and applications. *Chemical Reviews,* 107**,** 2891-2959.

CHEN, Y., LANDIN-ROMERO, R., KUMFOR, F., IRISH, M., HODGES, J. R. & PIGUET, O. 2020. Cerebellar structural connectivity and contributions to cognition in frontotemporal dementias. *Cortex,* 129**,** 57-67.

CHEN, Y., SHAH, N., HUGGINS, F. E. & HUFFMAN, G. P. 2006. Microanalysis of ambient particles from Lexington, KY, by electron microscopy. *Atmospheric Environment,* 40**,** 651-663.

CHEN, Y. W., CHANG, C. W., HUNG, H. S., KUNG, M. L., YEH, B. W. & HSIEH, S. 2016b. Magnetite nanoparticle interactions with insulin amyloid fibrils. *Nanotechnology,* 27**,** 415702.

CHESNEL, K., TREVINO, M., CAI, Y., HANCOCK, J. M., SMITH, S. J. & HARRISON, R. G. 2014. Particle size effects on the magnetic behaviour of 5 to 11 nm Fe3O4nanoparticles coated with oleic acid. *Journal of Physics: Conference Series,* 521**,** 012004.

CHIANCONE, E., CECI, P., ILARI, A., RIBACCHI, F. & STEFANINI, S. 2004. Iron and proteins for iron storage and detoxification. *Biometals,* 17**,** 197-202.

CHIN-CHAN, M., NAVARRO-YEPES, J. & QUINTANILLA-VEGA, B. 2015. Environmental pollutants as risk factors for neurodegenerative disorders: Alzheimer and Parkinson diseases. *Frontiers in Cellular Neuroscience,* 9.

CHO, H. K., PARK, C. G., SHIN, H. J., PARK, K. H. & LIM, H. B. 2018. Comparison of the in vitro toxicological activity of various particulate matter. *Toxicol Ind Health,* 34**,** 99-109.

CHOI, S., HONG, D. K., CHOI, B. Y. & SUH, S. W. 2020. Zinc in the Brain: Friend or Foe? *Int J Mol Sci,* 21.

CHOI, Y. & KIM, J.-K. 2018. Investigation of the redox state of magnetite upon Aβ-fibril formation or proton irradiation; implication of iron redox inactivation and β-amyloidolysis. *MRS Communications,* 8**,** 955-960.

CHUA-ANUSORN, W., WEBB, J., J. MACEY, D., POOTRAKUL, P. & ST. PIERRE, T. G. 1997. The effect of histological processing on the form of iron in iron-loaded human tissues. *Biochimica et Biophysica Acta (BBA) - Molecular Basis of Disease,* 1360**,** 255-261.

CHURG, A., BRAUER, M., DEL CARMEN AVILA-CASADO, M., FORTOUL, T. I. & WRIGHT, J. L. 2003. Chronic exposure to high levels of particulate air pollution and small airway remodeling. *Environmental health perspectives,* 111**,** 714-718.

CILLIERS, K. 2021. Trace element alterations in Alzheimer's disease: A review. *Clin Anat,* 34**,** 766-773.

CILLIERS, K. & MULLER, C. J. F. 2021. Multi-element Analysis of Brain Regions from South African Cadavers. *Biol Trace Elem Res,* 199**,** 425-441.

CIMA, F. 2011. Tin: Environmental Pollution and Health Effects. *In:* NRIAGU, J. O. (ed.) *Encyclopedia of Environmental Health.* Burlington: Elsevier.

COBLEY, J. N., FIORELLO, M. L. & BAILEY, D. M. 2018. 13 reasons why the brain is susceptible to oxidative stress. *Redox Biology,* 15**,** 490-503.

COCCINI, T., CALONI, F., RAMIREZ CANDO, L. J. & DE SIMONE, U. 2017. Cytotoxicity and proliferative capacity impairment induced on human brain cell cultures after short- and long-term exposure to magnetite nanoparticles. *J Appl Toxicol*.

COETZEE, J. J., BANSAL, N. & CHIRWA, E. M. N. 2020. Chromium in Environment, Its Toxic Effect from Chromite-Mining and Ferrochrome Industries, and Its Possible Bioremediation. *Exposure and Health,* 12**,** 51-62.

COLE, S. L. & VASSAR, R. 2008. The Role of Amyloid Precursor Protein Processing by BACE1, the β-Secretase, in Alzheimer Disease Pathophysiology. *The Journal of Biological Chemistry,* 283**,** 29621-29625.

COLLINGWOOD, J. & DOBSON, J. 2006. Mapping and characterization of iron compounds in Alzheimer's tissue. *J Alzheimers Dis,* 10**,** 215-22.

COLLINGWOOD, J. F., CHONG, R. K., KASAMA, T., CERVERA-GONTARD, L., DUNIN-BORKOWSKI, R. E., PERRY, G., POSFAI, M., SIEDLAK, S. L., SIMPSON, E. T., SMITH, M. A. & DOBSON, J. 2008. Three-dimensional tomographic imaging and characterization of iron compounds within Alzheimer's plaque core material. *J Alzheimers Dis,* 14**,** 235-45.

COLLINGWOOD, J. F. & TELLING, N. D. 2016. Iron Oxides in the Human Brain. *In:* FAIVRE, D. (ed.) *Iron Oxides.*

COLOGNATO, R., PARK, M. V. D. Z., WICK, P. & DE JONG, W. H. 2012. Chapter 1 - Interactions with the Human Body. *In:* FADEEL, B., PIETROIUSTI, A. & SHVEDOVA, A. A. (eds.) *Adverse Effects of Engineered Nanomaterials.* Boston: Academic Press.

COMÉRA, C., CARTIER, C., GAULTIER, E., CATRICE, O., PANOUILLE, Q., EL HAMDI, S., TIREZ, K., NELISSEN, I., THÉODOROU, V. & HOUDEAU, E. 2020. Jejunal villus absorption and paracellular tight junction permeability are major routes for early intestinal uptake of food-grade TiO2particles: An in vivo and ex vivo study in mice. *Particle and Fibre Toxicology,* 17.

CONNOR, J. R. & MENZIES, S. L. 1996. Relationship of iron to oligondendrocytes and myelination. *Glia,* 17**,** 83-93.

CONTI, S., HARARI, S., CAMINATI, A., ZANOBETTI, A., SCHWARTZ, JOEL D., BERTAZZI, P. A., CESANA, G. & MADOTTO, F. 2018. The association between air pollution and the incidence of idiopathic pulmonary fibrosis in Northern Italy. *European Respiratory Journal,* 51**,** 1700397.

COONEY, D. J. & HICKEY, A. J. 2011. Cellular response to the deposition of diesel exhaust particle aerosols onto human lung cells grown at the air–liquid interface by inertial impaction. *Toxicology in Vitro,* 25**,** 1953-1965.

COOPER, R. G. & HARRISON, A. P. 2009. The exposure to and health effects of antimony. *Indian journal of occupational and environmental medicine,* 13**,** 3-10.

CORDER, E. H., SAUNDERS, A. M., STRITTMATTER, W. J., SCHMECHEL, D. E., GASKELL, P. C., SMALL, G. W., ROSES, A. D., HAINES, J. L. & PERICAK-VANCE, M. A. 1993. Gene dose of apolipoprotein E type 4 allele and the risk of Alzheimer's disease in late onset families. *Science,* 261**,** 921-3.

CORMET-BOYAKA, E., JOLIVETTE, K., BONNEGARDE-BERNARD, A., RENNOLDS, J., HASSAN, F., MEHTA, P., TRIDANDAPANI, S., WEBSTER-MARKETON, J. & BOYAKA, P. N. 2011. An NF-κB–Independent and Erk1/2-Dependent Mechanism Controls CXCL8/IL-8 Responses of Airway Epithelial Cells to Cadmium. *Toxicological Sciences,* 125**,** 418-429.

CORNETT, C. R., EHMANN, W. D., WEKSTEIN, D. R. & MARKESBERY, W. R. 1998a. Trace elements in Alzheimer's disease pituitary glands. *Biol Trace Elem Res,* 62**,** 107-14.

CORNETT, C. R., MARKESBERY, W. R. & EHMANN, W. D. 1998b. Imbalances of trace elements related to oxidative damage in Alzheimer's disease brain. *Neurotoxicology,* 19**,** 339-45.

CORNIOLA, R. S., TASSABEHJI, N. M., HARE, J., SHARMA, G. & LEVENSON, C. W. 2008. Zinc deficiency impairs neuronal precursor cell proliferation and induces apoptosis via p53-mediated mechanisms. *Brain Res,* 1237**,** 52-61.

CORRIGAN, F. M., REYNOLDS, G. P. & WARD, N. I. 1993. Hippocampal tin, aluminum and zinc in Alzheimer's disease. *Biometals,* 6**,** 149-54.

CORY-SLECHTA, D. A., SOBOLEWSKI, M. & OBERDÖRSTER, G. 2020. Air Pollution-Related Brain Metal Dyshomeostasis as a Potential Risk Factor for Neurodevelopmental Disorders and Neurodegenerative Diseases. *Atmosphere,* 11.

COZZI, A., ROVELLI, E., FRIZZALE, G., CAMPANELLA, A., AMENDOLA, M., AROSIO, P. & LEVI, S. 2010. Oxidative stress and cell death in cells expressing L-ferritin variants causing neuroferritinopathy. *Neurobiol Dis,* 37**,** 77-85.

CRANS, D. C., SMEE, J. J., GAIDAMAUSKAS, E. & YANG, L. 2004. The Chemistry and Biochemistry of Vanadium and the Biological Activities Exerted by Vanadium Compounds. *Chemical Reviews,* 104**,** 849-902.

CULLITY, B. D. & GRAHAM, C. D. 2008. *Introduction to Magnetic Materials 2nd Edition*, Wiley Press.

CURCIO, A., VAN DE WALLE, A., SERRANO, A., PREVERAL, S., PECHOUX, C., PIGNOL, D., MENGUY, N., LEFEVRE, C. T., ESPINOSA, A. & WILHELM, C. 2020. Transformation Cycle of Magnetosomes in Human Stem Cells: From Degradation to Biosynthesis of Magnetic Nanoparticles Anew. *ACS Nano,* 14**,** 1406-1417.

CUSTODIO, N., WHEELOCK, A., THUMALA, D. & SLACHEVSKY, A. 2017. Dementia in Latin America: Epidemiological evidence and implications for public policy. *Frontiers in Aging Neuroscience,* 9.

DADRAS, A., RIAZI, G. H., AFRASIABI, A., NAGHSHINEH, A., GHALANDARI, B. & MOKHTARI, F. 2013. In vitro study on the alterations of brain tubulin structure and assembly affected by magnetite nanoparticles. *JBIC Journal of Biological Inorganic Chemistry,* 18**,** 357-369.

DAGHER, Z., GARÇON, G., BILLET, S., VERDIN, A., LEDOUX, F., COURCOT, D., ABOUKAIS, A. & SHIRALI, P. 2007. Role of nuclear factor-kappa B activation in the adverse effects induced by air pollution particulate matter (PM2.5) in human epithelial lung cells (L132) in culture. *J Appl Toxicol,* 27**,** 284-90.

DAN, X., WECHTER, N., GRAY, S., MOHANTY, J. G., CROTEAU, D. L. & BOHR, V. A. 2021. Olfactory dysfunction in aging and neurodegenerative diseases. *Ageing Research Reviews,* 70**,** 101416.

DANIELSSON, J., PIERATTELLI, R., BANCI, L. & GRÄSLUND, A. 2007. High-resolution NMR studies of the zinc-binding site of the Alzheimer's amyloid beta-peptide. *Febs j,* 274**,** 46-59.

DANSCHER, G., JENSEN, K. B., FREDERICKSON, C. J., KEMP, K., ANDREASEN, A., JUHL, S., STOLTENBERG, M. & RAVID, R. 1997. Increased amount of zinc in the hippocampus and amygdala of Alzheimer's diseased brains: a proton-induced X-ray emission spectroscopic analysis of cryostat sections from autopsy material. *J Neurosci Methods,* 76**,** 53-9.

DE CARITAT, P. & REIMANN, C. 2012. Comparing results from two continental geochemical surveys to world soil composition and deriving Predicted Empirical Global Soil (PEGS2) reference values. *Earth and Planetary Science Letters,* 319-320**,** 269-276.

DE JESUS, A. L., RAHMAN, M. M., MAZAHERI, M., THOMPSON, H., KNIBBS, L. D., JEONG, C., EVANS, G., NEI, W., DING, A., QIAO, L., LI, L., PORTIN, H., NIEMI, J. V., TIMONEN, H., LUOMA, K., PETÄJÄ, T., KULMALA, M., KOWALSKI, M., PETERS, A., CYRYS, J., FERRERO, L., MANIGRASSO, M., AVINO, P., BUONANO, G., RECHE, C., QUEROL, X., BEDDOWS, D., HARRISON, R. M., SOWLAT, M. H., SIOUTAS, C. & MORAWSKA, L. 2019. Ultrafine particles and PM2.5 in the air of cities around the world: Are they representative of each other? *Environment International,* 129**,** 118-135.

DE LA MONTE, S. M. & WANDS, J. R. 2008. Alzheimer's disease is type 3 diabetes-evidence reviewed. *Journal of diabetes science and technology,* 2**,** 1101-1113.

DE LORENZO, A. J. D. (ed.) 1970. *The olfactory neuron and the blood-brain barrier,* London: Churchill Livingstone.

DE VIZCAYA-RUIZ, A., GUTIÉRREZ-CASTILLO, M. E., URIBE-RAMIREZ, M., CEBRIÁN, M. E., MUGICA-ALVAREZ, V., SEPÚLVEDA, J., ROSAS, I., SALINAS, E., GARCIA-CUÉLLAR, C., MARTÍNEZ, F., ALFARO-MORENO, E., TORRES-FLORES, V., OSORNIO-VARGAS, A., SIOUTAS, C., FINE, P. M., SINGH, M., GELLER, M. D., KUHN, T., MIGUEL, A. H., EIGUREN-FERNANDEZ, A., SCHIESTL, R. H., RELIENE, R. & FROINES, J. 2006. Characterization and in vitro biological effects of concentrated particulate matter from Mexico City. *Atmospheric Environment,* 40**,** 583-592.

DEFRA, A. Q. E. G. 2019. Non-Exhaust Emissions from Road Traffic. DEFRA.

DEIBEL, M. A., EHMANN, W. D. & MARKESBERY, W. R. 1996. Copper, iron, and zinc imbalances in severely degenerated brain regions in Alzheimer's disease: possible relation to oxidative stress. *J Neurol Sci,* 143**,** 137-42.

DEL TREDICI, K. & BRAAK, H. 2016. Sporadic Parkinson's disease: Development and distribution of α-synuclein pathology. *Neuropathology and Applied Neurobiology,* 42**,** 33-50.

DEL TREDICI, K., RÜB, U., DE VOS, R. A. I., BOHL, J. R. E. & BRAAK, H. 2002. Where does Parkinson disease pathology begin in the brain? *Journal of Neuropathology and Experimental Neurology,* 61**,** 413-426.

DELFINO, R. J., SIOUTAS, C. & MALIK, S. 2005. Potential role of ultrafine particles in associations between airborne particle mass and cardiovascular health. *Environmental Health Perspectives,* 113**,** 934-946.

DEVOS, S. L., CORJUC, B. T., OAKLEY, D. H., NOBUHARA, C. K., BANNON, R. N., CHASE, A., COMMINS, C., GONZALEZ, J. A., DOOLEY, P. M., FROSCH, M. P. & HYMAN, B. T. 2018. Synaptic Tau Seeding Precedes Tau Pathology in Human Alzheimer's Disease Brain. *Frontiers in Neuroscience,* 12.

DEWEY, C. M., CENIK, B., SEPHTON, C. F., JOHNSON, B. A., HERZ, J. & YU, G. 2012. TDP-43 aggregation in neurodegeneration: Are stress granules the key? *Brain Research,* 1462**,** 16-25.

DIMAKAKOU, E., JOHNSTON, H. J., STREFTARIS, G. & CHERRIE, J. W. 2020. Is Environmental and Occupational Particulate Air Pollution Exposure Related to Type-2 Diabetes and Dementia? A Cross-Sectional Analysis of the UK Biobank. *International Journal of Environmental Research and Public Health,* 17**,** 9581.

DING, J., HE, G., GONG, W., WEN, W., SUN, W., NING, B., HUANG, S., WU, K., HUANG, C., WU, M., XIE, W. & WANG, H. 2009. Effects of Nickel on Cyclin Expression, Cell Cycle Progression and Cell Proliferation in Human Pulmonary Cells. *Cancer Epidemiology, Biomarkers & Prevention,* 18**,** 1720-1729.

DISDIER, C., CHALANSONNET, M., GAGNAIRE, F., GATÉ, L., COSNIER, F., DEVOY, J., SABA, W., LUND, A. K., BRUN, E. & MABONDZO, A. 2017. Brain Inflammation, Blood Brain Barrier dysfunction and Neuronal Synaptophysin Decrease after Inhalation Exposure to Titanium Dioxide Nano-aerosol in Aging Rats. *Scientific Reports,* 7.

DIXON, S. J., LEMBERG, K. M., LAMPRECHT, M. R., SKOUTA, R., ZAITSEV, E. M., GLEASON, C. E., PATEL, D. N., BAUER, A. J., CANTLEY, A. M., YANG, W. S., MORRISON, B., 3RD & STOCKWELL, B. R. 2012. Ferroptosis: an iron-dependent form of nonapoptotic cell death. *Cell,* 149**,** 1060-1072.

DOBSON, J. 2001. Nanoscale biogenic iron oxides and neurodegenerative disease. *FEBS Letters,* 496**,** 1-5.

DOBSON, J. 2002. Investigation of age-related variations in biogenic magnetite levels in the human hippocampus. *Experimental Brain Research,* 144**,** 122-126.

DOBSON, J. & GRASSI, P. 1996. Magnetic properties of human hippocampal tissue—Evaluation of artefact and contamination sources. *Brain Research Bulletin,* 39**,** 255-259.

DONALDSON, K., STONE, V., SEATON, A. & MACNEE, W. 2001. Ambient particle inhalation and the cardiovascular system: potential mechanisms. *Environmental health perspectives,* 109 Suppl 4**,** 523-527.

DONG, J., ATWOOD, C. S., ANDERSON, V. E., SIEDLAK, S. L., SMITH, M. A., PERRY, G. & CAREY, P. R. 2003. Metal Binding and Oxidation of Amyloid-β within Isolated Senile Plaque Cores: Raman Microscopic Evidence. *Biochemistry,* 42**,** 2768-2773.

DORLET, P., GAMBARELLI, S., FALLER, P. & HUREAU, C. 2009. Pulse EPR Spectroscopy Reveals the Coordination Sphere of Copper(II) Ions in the 1–16 Amyloid-β Peptide: A Key Role of the First Two N-Terminus Residues. *Angewandte Chemie International Edition,* 48**,** 9273-9276.

DOS SANTOS, N. V., YARIWAKE, V. Y., MARQUES, K. D. V., VERAS, M. M. & FAJERSZTAJN, L. 2021. Air Pollution: A Neglected Risk Factor for Dementia in Latin America and the Caribbean. *Front Neurol,* 12**,** 684524.

DOTSON, V. M., BEYDOUN, M. A. & ZONDERMAN, A. B. 2010. Recurrent depressive symptoms and the incidence of dementia and mild cognitive impairment. *Neurology,* 75**,** 27-34.

DOTY, R. 2015. *Handbook of Olfaction and Gustation: Third Edition*.

DUBIEL, S. M., ZABLOTNA-RYPIEN, B., MACKEY, J. B. & WILLIAMS, J. M. 1999. Magnetic properties of human liver and brain ferritin. *European Biophysics Journal,* 28**,** 263-267.

DUCE, J. A., TSATSANIS, A., CATER, M. A., JAMES, S. A., ROBB, E., WIKHE, K., LEONG, S. L., PEREZ, K., JOHANSSEN, T., GREENOUGH, M. A., CHO, H.-H., GALATIS, D., MOIR, R. D., MASTERS, C. L., MCLEAN, C., TANZI, R. E., CAPPAI, R., BARNHAM, K. J., CICCOTOSTO, G. D., ROGERS, J. T. & BUSH, A. I. 2010. An iron-export ferroxidase activity of β-amyloid protein precursor is inhibited by zinc in Alzheimer's Disease. *Cell,* 142**,** 857-867.

DUNLOP, D. J. & ÖZDEMIR, Ö. 1997. *Rock Magnetism: Fundamentals and Frontiers,* Cambridge, Cambridge University Press.

DUNN, J. R., FULLER, M., ZOEGER, J., DOBSON, J., HELLER, F., HAMMANN, J., CAINE, E. & MOSKOWITZ, B. M. 1995. Magnetic material in the human hippocampus. *Brain Res Bull,* 36**,** 149-53.

DUONG, T. T. T. & LEE, B.-K. 2011. Determining contamination level of heavy metals in road dust from busy traffic areas with different characteristics. *Journal of Environmental Management,* 92**,** 554-562.

DYTŁOW, S. & GÓRKA-KOSTRUBIEC, B. 2021. Concentration of heavy metals in street dust: an implication of using different geochemical background data in estimating the level of heavy metal pollution. *Environmental Geochemistry and Health,* 43**,** 521-535.

DZEPINA, K., AREY, J., MARR, L. C., WORSNOP, D. R., SALCEDO, D., ZHANG, Q., ONASCH, T. B., MOLINA, L. T., MOLINA, M. J. & JIMENEZ, J. L. 2007. Detection of particle-phase polycyclic aromatic hydrocarbons in Mexico City using an aerosol mass spectrometer. *International Journal of Mass Spectrometry,* 263**,** 152-170.

EHSANIFAR, M., TAMEH, A. A., FARZADKIA, M., KALANTARI, R. R., ZAVAREH, M. S., NIKZAAD, H. & JAFARI, A. J. 2019. Exposure to nanoscale diesel exhaust particles: Oxidative stress, neuroinflammation, anxiety and depression on adult male mice. *Ecotoxicology and Environmental Safety,* 168**,** 338-347.

EJAZ, H. W., WANG, W. & LANG, M. 2020. Copper Toxicity Links to Pathogenesis of Alzheimer's Disease and Therapeutics Approaches. *Int J Mol Sci,* 21.

ELIOT, L., AHMED, A., KHAN, H. & PATEL, J. 2021. Dump the "dimorphism": Comprehensive synthesis of human brain studies reveals few male-female differences beyond size. *Neuroscience & Biobehavioral Reviews,* 125**,** 667-697.

ENVIRONMENTAL PROTECTION AGENCY 2010. The Air Quality Standards Regulations 2010. *Environmental Protection (ed.).*

ERDŐ, F., DENES, L. & DE LANGE, E. 2017. Age-associated physiological and pathological changes at the blood-brain barrier: A review. *Journal of cerebral blood flow and metabolism : official journal of the International Society of Cerebral Blood Flow and Metabolism,* 37**,** 4-24.

ERMOLIN, M. S., FEDOTOV, P. S., MALIK, N. A. & KARANDASHEV, V. K. 2018. Nanoparticles of volcanic ash as a carrier for toxic elements on the global scale. *Chemosphere,* 200**,** 16-22.

EVERETT, J., BROOKS, J., COLLINGWOOD, J. F. & TELLING, N. D. 2021a. Nanoscale chemical speciation of β-amyloid/iron aggregates using soft X-ray spectromicroscopy. *Inorganic Chemistry Frontiers,* 8**,** 1439-1448.

EVERETT, J., CESPEDES, E., SHELFORD, L. R., EXLEY, C., COLLINGWOOD, J. F., DOBSON, J., VAN DER LAAN, G., JENKINS, C. A., ARENHOLZ, E. & TELLING, N. D. 2014a. Evidence of redox-active iron formation following aggregation of ferrihydrite and the Alzheimer's disease peptide beta-amyloid. *Inorg Chem,* 53**,** 2803-9.

EVERETT, J., CÉSPEDES, E., SHELFORD, L. R., EXLEY, C., COLLINGWOOD, J. F., DOBSON, J., VAN DER LAAN, G., JENKINS, C. A., ARENHOLZ, E. & TELLING, N. D. 2014b. Ferrous iron formation following the co-aggregation of ferric iron and the Alzheimer's disease peptide β-amyloid (1-42). *J R Soc Interface,* 11**,** 20140165.

EVERETT, J., COLLINGWOOD, J. F., TJENDANA-TJHIN, V., BROOKS, J., LERMYTE, F., PLASCENCIA-VILLA, G., HANDS-PORTMAN, I., DOBSON, J., PERRY, G. & TELLING, N. D. 2018. Nanoscale synchrotron X-ray speciation of iron and calcium compounds in amyloid plaque cores from Alzheimer's disease subjects. *Nanoscale,* 10**,** 11782-11796.

EVERETT, J., LERMYTE, F., BROOKS, J., TJENDANA-TJHIN, V., PLASCENCIA-VILLA, G., HANDS-PORTMAN, I., DONNELLY, J. M., BILLIMORIA, K., PERRY, G., ZHU, X., SADLER, P. J., O'CONNOR, P. B., COLLINGWOOD, J. F. & TELLING, N. D. 2021b. Biogenic metallic elements in the human brain? *Science Advances,* 7**,** eabf6707.

EVERITT, B. J. & ROBBINS, T. W. 1997. CENTRAL CHOLINERGIC SYSTEMS AND COGNITION. *Annual Review of Psychology,* 48**,** 649-684.

EXLEY, C. & CLARKSON, E. 2020. Aluminium in human brain tissue from donors without neurodegenerative disease: A comparison with Alzheimer's disease, multiple sclerosis and autism. *Scientific Reports,* 10.

FAHMY, H. M., ALY, E. M., MOHAMED, F. F., NOOR, N. A. & ELSAYED, A. A. 2020. Neurotoxicity of green- synthesized magnetic iron oxide nanoparticles in different brain areas of wistar rats. *Neurotoxicology,* 77**,** 80-93.

FALLER, P., HUREAU, C. & BERTHOUMIEU, O. 2013. Role of Metal Ions in the Self-assembly of the Alzheimer's Amyloid-β Peptide. *Inorganic Chemistry,* 52**,** 12193-12206.

FALONE, S., SANTINI, S., JR., CORDONE, V., DI EMIDIO, G., TATONE, C., CACCHIO, M. & AMICARELLI, F. 2018. Extremely low-frequency magnetic fields and redox-responsive pathways linked to cancer drug resistance: Insights from co-exposure-based in vitro studies. *Frontiers in Public Health,* 6.

FARRER, L. A., CUPPLES, L. A., HAINES, J. L., HYMAN, B., KUKULL, W. A., MAYEUX, R., MYERS, R. H., PERICAK-VANCE, M. A., RISCH, N. & VAN DUIJN, C. M. 1997. Effects of age, sex, and ethnicity on the association between apolipoprotein E genotype and Alzheimer disease. A meta-analysis. APOE and Alzheimer Disease Meta Analysis Consortium. *Jama,* 278**,** 1349-56.

FAUCHEUX, B. A., MARTIN, M.-E., BEAUMONT, C., HUNOT, S., HAUW, J.-J., AGID, Y. & HIRSCH, E. C. 2002. Lack of up-regulation of ferritin is associated with sustained iron regulatory protein-1 binding activity in the substantia nigra of patients with Parkinson's disease. *Journal of Neurochemistry,* 83**,** 320-330.

FAUX, N. G., RITCHIE, C. W., GUNN, A., REMBACH, A., TSATSANIS, A., BEDO, J., HARRISON, J., LANNFELT, L., BLENNOW, K., ZETTERBERG, H., INGELSSON, M., MASTERS, C. L., TANZI, R. E., CUMMINGS, J. L., HERD, C. M. & BUSH, A. I. 2010. PBT2 Rapidly Improves Cognition in Alzheimer's Disease: Additional Phase II Analyses. *Journal of Alzheimer's Disease,* 20**,** 509-516.

FDA 2020. Aducanumab - Combined FDA and Applicant PCNS Drugs Advisory Committee Briefing Document.

FEIGIN, V. L., ROTH, G. A., NAGHAVI, M., PARMAR, P., KRISHNAMURTHI, R., CHUGH, S., MENSAH, G. A., NORRVING, B., SHIUE, I., NG, M., ESTEP, K., CERCY, K., MURRAY, C. J. L. & FOROUZANFAR, M. H. 2016. Global burden of stroke and risk factors in 188 countries, during 1990-2013: a systematic analysis for the Global Burden of Disease Study 2013. *Lancet Neurol,* 15**,** 913-924.

FILELLA, M. 2017. Tantalum in the environment. *Earth-Science Reviews,* 173**,** 122-140.

FINCH, C. E. & AUSTAD, S. N. 2012. Primate aging in the mammalian scheme: the puzzle of extreme variation in brain aging. *Age (Dordr),* 34**,** 1075-91.

FINCH, C. E. & MORGAN, T. E. 2020. Developmental Exposure to Air Pollution, Cigarettes, and Lead: Implications for Brain Aging. *Annual Review of Developmental Psychology,* 2**,** 585-614.

FISCHER, P., GOTZ, M. E., DANIELCZYK, W., GSELL, W. & RIEDERER, P. 1997. Blood transferrin and ferritin in Alzheimer's disease. *Life Sci,* 60**,** 2273-8.

FISHMAN, J. B., RUBIN, J. B., HANDRAHAN, J. V., CONNOR, J. R. & FINE, R. E. 1987. Receptor-mediated transcytosis of transferrin across the blood-brain barrier. *Journal of Neuroscience Research,* 18**,** 299-304.

FJELL, A. M., MCEVOY, L., HOLLAND, D., DALE, A. M. & WALHOVD, K. B. 2014. What is normal in normal aging? Effects of aging, amyloid and Alzheimer's disease on the cerebral cortex and the hippocampus. *Progress in Neurobiology,* 117**,** 20-40.

FOLSTEIN, M. F., FOLSTEIN, S. E. & MCHUGH, P. R. 1975. "Mini-mental state". A practical method for grading the cognitive state of patients for the clinician. *J Psychiatr Res,* 12**,** 189-98.

FORLENZA, O. V., DINIZ, B. S., TEIXEIRA, A. L., RADANOVIC, M., TALIB, L. L., ROCHA, N. P. & GATTAZ, W. F. 2015. Lower Cerebrospinal Fluid Concentration of Brain-Derived Neurotrophic Factor Predicts Progression from Mild Cognitive Impairment to Alzheimer's Disease. *Neuromolecular Med,* 17**,** 326-32.

FOX, J. H., KAMA, J. A., LIEBERMAN, G., CHOPRA, R., DORSEY, K., CHOPRA, V., VOLITAKIS, I., CHERNY, R. A., BUSH, A. I. & HERSCH, S. 2007. Mechanisms of copper ion mediated Huntington's disease progression. *PLoS One,* 2**,** e334.

FRANK OLDFIELD, J. W., JOHN SMITH 1999. *Environmental magnetism: a practical guide,* London, Quarternary Research Association.

FRIEDMAN, A., AROSIO, P., FINAZZI, D., KOZIOROWSKI, D. & GALAZKA-FRIEDMAN, J. 2011. Ferritin as an important player in neurodegeneration. *Parkinsonism & Related Disorders,* 17**,** 423-430.

GABBASOV, R. R., CHEREPANOV, V. M., CHUEV, M. A., LOMOV, A. A., MISCHENKO, I. N., NIKITIN, M. P., POLIKARPOV, M. A. & PANCHENKO, V. Y. 2016. Mössbauer and X-ray study of biodegradation of 57Fe3O4 magnetic nanoparticles in rat brain. *Hyperfine Interactions,* 237**,** 54.

GADE, M., COMFORT, N. & RE, D. B. 2021. Sex-specific neurotoxic effects of heavy metal pollutants: Epidemiological, experimental evidence and candidate mechanisms. *Environ Res,* 201**,** 111558.

GAŁĄZKA-FRIEDMAN, J., BAUMINGER, E. R., FRIEDMAN, A., BARCIKOWSKA, M., HECHEL, D. & NOWIK, I. 1996. Iron in parkinsonian and control substantia nigra—A mössbauer spectroscopy study. *Movement Disorders,* 11**,** 8-16.

GALLOCCHIO, F., BIANCOTTO, G., MORESSA, A., PASCOLI, F., PRETTO, T., TOFFAN, A., ARCANGELI, G., MONTESI, F., PETERS, R. & RICCI, A. 2020. Bioaccumulation and in vivo formation of titanium dioxide nanoparticles in edible mussels. *Food Chemistry,* 323.

GAO, H., ZHANG, T., ZHANG, Y., CHEN, Y., LIU, B., WU, J., LIU, X., LI, Y., PENG, M., ZHANG, Y., XIE, G., ZHAO, F. & FAN, H. M. 2020. Ellipsoidal magnetite nanoparticles: A new

member of the magnetic-vortex nanoparticles family for efficient magnetic hyperthermia. *Journal of Materials Chemistry B,* 8**,** 515-522.

GARCÍA, F., MARQUÈS, M., BARBERÍA, E., TORRALBA, P., LANDIN, I., LAGUNA, C., DOMINGO, J. L. & NADAL, M. 2020. Biomonitoring of Trace Elements in Subjects Living Near a Hazardous Waste Incinerator: Concentrations in Autopsy Tissues. *Toxics,* 8.

GARCIA, G. J. M., SCHROETER, J. D. & KIMBELL, J. S. 2015. Olfactory deposition of inhaled nanoparticles in humans. *Inhalation toxicology,* 27**,** 394-403.

GARELICK, H., JONES, H., DYBOWSKA, A. & VALSAMI-JONES, E. 2008. Arsenic pollution sources. *Rev Environ Contam Toxicol,* 197**,** 17-60.

GARTZIANDIA, O., EGUSQUIAGUIRRE, S. P., BIANCO, J., PEDRAZ, J. L., IGARTUA, M., HERNANDEZ, R. M., PRÉAT, V. & BELOQUI, A. 2016. Nanoparticle transport across in vitro olfactory cell monolayers. *Int J Pharm,* 499**,** 81-89.

GATZ, M., REYNOLDS, C. A., FRATIGLIONI, L., JOHANSSON, B., MORTIMER, J. A., BERG, S., FISKE, A. & PEDERSEN, N. L. 2006. Role of genes and environments for explaining Alzheimer disease. *Arch Gen Psychiatry,* 63**,** 168-74.

GAŽOVÁ, Z., ANTOŠOVÁ, A., KRIŠTOFIKOVÁ, Z., BARTOŠ, A., ŘÍČNÝ, J., ČECHOVÁ, L., KLASCHKA, J. & ŘÍPOVÁ, D. 2010. Attenuated antiaggregation effects of magnetite nanoparticles in cerebrospinal fluid of people with Alzheimer's disease. *Molecular BioSystems,* 6**,** 2200-2205.

GEISER, M. 2010. Update on macrophage clearance of inhaled micro- and nanoparticles. *J Aerosol Med Pulm Drug Deliv,* 23**,** 207-17.

GEISER, M., ROTHEN-RUTISHAUSER, B., KAPP, N., SCHÜRCH, S., KREYLING, W., SCHULZ, H., SEMMLER, M., IM HOF, V., HEYDER, J. & GEHR, P. 2005. Ultrafine particles cross cellular membranes by nonphagocytic mechanisms in lungs and in cultured cells. *Environmental health perspectives,* 113**,** 1555-1560.

GELLEIN, K., FLATEN, T. P., ERIKSON, K. M., ASCHNER, M. & SYVERSEN, T. 2008. Leaching of trace elements from biological tissue by formalin fixation. *Biol Trace Elem Res,* 121**,** 221-5.

GELLEIN, K., GARRUTO, R. M., SYVERSEN, T., SJØBAKK, T. E. & FLATEN, T. P. 2003. Concentrations of Cd, Co, Cu, Fe, Mn, Rb, V, and Zn in formalin-fixed brain tissue in amyotrophic lateral sclerosis and parkinsonism-dementia complex of guam determined by high-resolution ICP-MS. *Biological Trace Element Research,* 96**,** 39-60.

GENCHI, G., CAROCCI, A., LAURIA, G., SINICROPI, M. S. & CATALANO, A. 2020. Nickel: Human Health and Environmental Toxicology. *International journal of environmental research and public health,* 17**,** 679.

GEORGE, S., REY, N. L., TYSON, T., ESQUIBEL, C., MEYERDIRK, L., SCHULZ, E., PIERCE, S., BURMEISTER, A. R., MADAJ, Z., STEINER, J. A., ESCOBAR GALVIS, M. L., BRUNDIN, L. & BRUNDIN, P. 2019. Microglia affect α-synuclein cell-to-cell transfer in a mouse model of Parkinson's disease. *Molecular Neurodegeneration,* 14.

GERBER, H., WU, F., DIMITROV, M., GARCIA OSUNA, G. M. & FRAERING, P. C. 2017. Zinc and Copper Differentially Modulate Amyloid Precursor Protein Processing by γ-Secretase and Amyloid-β Peptide Production. *Journal of Biological Chemistry*.

GESER, F., FELLNER, L., HAYBAECK, J. & WENNING, G. K. 2020. Development of neurodegeneration in amyotrophic lateral sclerosis: from up or down? *Journal of Neural Transmission,* 127**,** 1097-1105.

GHOLAMI, A., MOUSAVI, S. M., HASHEMI, S. A., GHASEMI, Y., CHIANG, W. H. & PARVIN, N. 2020. Current trends in chemical modifications of magnetic nanoparticles for targeted drug delivery in cancer chemotherapy. *Drug Metabolism Reviews,* 52**,** 205-224.

GIANNAKOPOULOS, P., HERRMANN, F. R., BUSSIÈRE, T., BOURAS, C., KÖVARI, E., PERL, D. P., MORRISON, J. H., GOLD, G. & HOF, P. R. 2003. Tangle and neuron numbers, but not

amyloid load, predict cognitive status in Alzheimer's disease. *Neurology,* 60**,** 1495-1500.

GIANNAKOPOULOS, P., KÖVARI, E., HERRMANN, F. R., HOF, P. R. & BOURAS, C. 2009. Interhemispheric distribution of Alzheimer disease and vascular pathology in brain aging. *Stroke,* 40**,** 983-986.

GILAN, S. S. T., RAYAT, D. Y., MUSTAFA, T. A., AZIZ, F. M., SHAHPASAND, K., AKHTARI, K., SALIHI, A., ABOU-ZIED, O. K. & FALAHATI, M. 2019. α-synuclein interaction with zero-valent iron nanoparticles accelerates structural rearrangement into amyloid-susceptible structure with increased cytotoxic tendency. *International Journal of Nanomedicine,* 14**,** 4637-4648.

GILDER, S. A., WACK, M., KAUB, L., ROUD, S. C., PETERSEN, N., HEINSEN, H., HILLENBRAND, P., MILZ, S. & SCHMITZ, C. 2018. Distribution of magnetic remanence carriers in the human brain. *Scientific Reports,* 8**,** 11363.

GLENNER, G. G., HENRY, J. H. & FUJIHARA, S. 1981. Congophilic angiopathy in the pathogenesis of Alzheimer's degeneration. *Ann Pathol,* 1**,** 120-9.

GMINSKI, R., DECKER, K., HEINZ, C., SEIDEL, A., KÖNCZÖL, M., GOLDENBERG, E., GROBÉTY, B., EBNER, W., GIERÉ, R. & MERSCH-SUNDERMANN, V. 2011. Genotoxic effects of three selected black toner powders and their dimethyl sulfoxide extracts in cultured human epithelial A549 lung cells in vitro. *Environ Mol Mutagen,* 52**,** 296-309.

GOATE, A., CHARTIER-HARLIN, M. C., MULLAN, M., BROWN, J., CRAWFORD, F., FIDANI, L., GIUFFRA, L., HAYNES, A., IRVING, N., JAMES, L. & ET AL. 1991. Segregation of a missense mutation in the amyloid precursor protein gene with familial Alzheimer's disease. *Nature,* 349**,** 704-6.

GOBBA, F. 2006. Olfactory toxicity: long-term effects of occupational exposures. *Int Arch Occup Environ Health,* 79**,** 322-31.

GONET, T. & MAHER, B. A. 2019. Airborne, vehicle-derived Fe-bearing nanoparticles in the urban environment – A review. *Environmental Science & Technology*.

GONET, T., MAHER, B. A. & KUKUTSCHOVÁ, J. 2021a. Source apportionment of magnetite particles in roadside airborne particulate matter. *Science of The Total Environment,* 752**,** 141828.

GONET, T., MAHER, B. A., NYIRŐ-KÓSA, I., PÓSFAI, M., VACULÍK, M. & KUKUTSCHOVÁ, J. 2021b. Size-resolved, quantitative evaluation of the magnetic mineralogy of airborne brake-wear particulate emissions. *Environmental Pollution,* 288**,** 117808.

GONZÁLEZ-MACIEL, A., REYNOSO-ROBLES, R., TORRES-JARDÓN, R., MUKHERJEE, P. S. & CALDERÓN-GARCIDUEÑAS, L. 2017. Combustion-Derived Nanoparticles in Key Brain Target Cells and Organelles in Young Urbanites: Culprit Hidden in Plain Sight in Alzheimer's Disease Development. *Journal of Alzheimer's Disease,* 59**,** 189-208.

GONZÁLEZ-MARISCAL, L., MIRANDA, J., GALLEGO-GUTIÉRREZ, H., CANO-CORTINA, M. & AMAYA, E. 2020. Relationship between apical junction proteins, gene expression and cancer. *Biochimica et Biophysica Acta (BBA) - Biomembranes,* 1862**,** 183278.

GOROBETS, O., GOROBETS, S. & KORALEWSKI, M. 2017. Physiological origin of biogenic magnetic nanoparticles in health and disease: from bacteria to humans. *International Journal of Nanomedicine,* 12**,** 4371-4395.

GORR, M. W., YOUTZ, D. J., EICHENSEER, C. M., SMITH, K. E., NELIN, T. D., CORMET-BOYAKA, E. & WOLD, L. E. 2015. In vitro particulate matter exposure causes direct and lung-mediated indirect effects on cardiomyocyte function. *American Journal of Physiology-Heart and Circulatory Physiology,* 309**,** H53-H62.

GOUGH, M., PARR-STURGESS, C. & PARKIN, E. 2011. Zinc Metalloproteinases and Amyloid Beta-Peptide Metabolism: The Positive Side of Proteolysis in Alzheimer's Disease. *Biochemistry Research International,* 2011**,** 721463.

GOUVEIA, N., KEPHART, J. L., DRONOVA, I., MCCLURE, L., GRANADOS, J. T., BETANCOURT, R. M., O'RYAN, A. C., TEXCALAC-SANGRADOR, J. L., MARTINEZ-FOLGAR, K., RODRIGUEZ, D. & DIEZ-ROUX, A. V. 2021. Ambient fine particulate matter in Latin American cities: Levels, population exposure, and associated urban factors. *Science of The Total Environment,* 772**,** 145035.

GRANDE, G., LJUNGMAN, P. L. S., ENEROTH, K., BELLANDER, T. & RIZZUTO, D. 2020. Association Between Cardiovascular Disease and Long-term Exposure to Air Pollution With the Risk of Dementia. *JAMA Neurology,* 77**,** 801-809.

GREGORI, M., TAYLOR, M., SALVATI, E., RE, F., MANCINI, S., BALDUCCI, C., FORLONI, G., ZAMBELLI, V., SESANA, S., MICHAEL, M., MICHAIL, C., TINKER-MILL, C., KOLOSOV, O., SHERER, M., HARRIS, S., FULLWOOD, N. J., MASSERINI, M. & ALLSOP, D. 2017. Retro-inverso peptide inhibitor nanoparticles as potent inhibitors of aggregation of the Alzheimer's Aβ peptide. *Nanomedicine: Nanotechnology, Biology and Medicine,* 13**,** 723-732.

GRIFFITHS, P. D. & CROSSMAN, A. R. 1993. Distribution of Iron in the Basal Ganglia and Neocortex in Postmortem Tissue in Parkinson's Disease and Alzheimer's Disease. *Dementia and Geriatric Cognitive Disorders,* 4**,** 61-65.

GRINBERG, L., RUEB, U. & HEINSEN, H. 2011. Brainstem: Neglected Locus in Neurodegenerative Diseases. *Frontiers in Neurology,* 2.

GROCHOWSKI, C., BLICHARSKA, E., KRUKOW, P., JONAK, K., MACIEJEWSKI, M., SZCZEPANEK, D., JONAK, K., FLIEGER, J. & MACIEJEWSKI, R. 2019. Analysis of Trace Elements in Human Brain: Its Aim, Methods, and Concentration Levels. *Frontiers in Chemistry,* 7.

GUALTIERI, M., MANTECCA, P., CORVAJA, V., LONGHIN, E., PERRONE, M. G., BOLZACCHINI, E. & CAMATINI, M. 2009. Winter fine particulate matter from Milan induces morphological and functional alterations in human pulmonary epithelial cells (A549). *Toxicol Lett,* 188**,** 52-62.

GUARINO, F., IMPROTA, G., TRIASSI, M., CICATELLI, A. & CASTIGLIONE, S. 2020. Effects of Zinc Pollution and Compost Amendment on the Root Microbiome of a Metal Tolerant Poplar Clone. *Frontiers in Microbiology,* 11.

GUERRERO, F., ALVAREZ-OSPINA, H., RETAMA, A., LÓPEZ-MEDINA, A., CASTRO, T. & SALCEDO, D. 2017. Seasonal changes in the PM1 chemical composition north of Mexico City. *Atmosfera,* 30**,** 243-258.

GULYAEV, A. E., GELPERINA, S. E., SKIDAN, I. N., ANTROPOV, A. S., KIVMAN, G. Y. & KREUTER, J. 1999. Significant Transport of Doxorubicin into the Brain with Polysorbate 80-Coated Nanoparticles. *Pharmaceutical Research,* 16**,** 1564-1569.

GUMPELMAYER, M., NGUYEN, M., MOLNÁR, G., BOUSSEKSOU, A., MEUNIER, B. & ROBERT, A. 2018. Magnetite Fe3O4 Has no Intrinsic Peroxidase Activity, and Is Probably not Involved in Alzheimer's Oxidative Stress. *Angewandte Chemie International Edition,* 57**,** 14758-14763.

GÜNER, G. & LICHTENTHALER, S. F. 2020. The substrate repertoire of γ-secretase/presenilin. *Seminars in Cell & Developmental Biology,* 105**,** 27-42.

GUPTA, G., GLIGA, A., HEDBERG, J., SERRA, A., GRECO, D., ODNEVALL WALLINDER, I. & FADEEL, B. 2020. Cobalt nanoparticles trigger ferroptosis-like cell death (oxytosis) in neuronal cells: Potential implications for neurodegenerative disease. *FASEB Journal,* 34**,** 5262-5281.

GUSTAFSSON, M., BLOMQVIST, G., GUDMUNDSSON, A., DAHL, A., SWIETLICKI, E., BOHGARD, M., LINDBOM, J. & LJUNGMAN, A. 2008. Properties and toxicological effects of particles from the interaction between tyres, road pavement and winter traction material. *Science of The Total Environment,* 393**,** 226-240.

GUSTAFSSON, M., BLOMQVIST, G., JÄRLSKOG, I., LUNDBERG, J., JANHÄLL, S., ELMGREN, M., JOHANSSON, C., NORMAN, M. & SILVERGREN, S. 2019. Road dust load dynamics and

influencing factors for six winter seasons in Stockholm, Sweden. *Atmospheric Environment: X,* 2**,** 100014.
GUTIÉRREZ, L., DE LA CUEVA, L., MOROS, M., MAZARÍO, E., DE BERNARDO, S., DE LA FUENTE, J. M., MORALES, M. P. & SALAS, G. 2019. Aggregation effects on the magnetic properties of iron oxide colloids. *Nanotechnology,* 30.
GUYENET, P. G., STORNETTA, R. L., SOUZA, G. M. P. R., ABBOTT, S. B. G. & BROOKS, V. L. 2020. Neuronal Networks in Hypertension: Recent Advances. *Hypertension***,** 300-311.
GUZMÁN, P., TARÍN-CARRASCO, P., MORALES-SUÁREZ-VARELA, M. & JIMÉNEZ-GUERRERO, P. 2022. Effects of air pollution on dementia over Europe for present and future climate change scenarios. *Environmental Research,* 204**,** 112012.
GWOREK, B., DMUCHOWSKI, W. & BACZEWSKA-DĄBROWSKA, A. H. 2020. Mercury in the terrestrial environment: a review. *Environmental Sciences Europe,* 32**,** 128.
HAACKE, E. M., CHENG, N. Y., HOUSE, M. J., LIU, Q., NEELAVALLI, J., OGG, R. J., KHAN, A., AYAZ, M., KIRSCH, W. & OBENAUS, A. 2005. Imaging iron stores in the brain using magnetic resonance imaging. *Magn Reson Imaging,* 23**,** 1-25.
HAASS, C., LEMERE, C. A., CAPELL, A., CITRON, M., SEUBERT, P., SCHENK, D., LANNFELT, L. & SELKOE, D. J. 1995. The Swedish mutation causes early-onset Alzheimer's disease by β-secretase cleavage within the secretory pathway. *Nature Medicine,* 1**,** 1291-1296.
HABRE, R., GIRGUIS, M., URMAN, R., FRUIN, S., LURMANN, F., SHAFER, M., GORSKI, P., FRANKLIN, M., MCCONNELL, R., AVOL, E. & GILLILAND, F. 2021. Contribution of tailpipe and non-tailpipe traffic sources to quasi-ultrafine, fine and coarse particulate matter in southern California. *Journal of the Air & Waste Management Association,* 71**,** 209-230.
HAGHANI, A., JOHNSON, R., SAFI, N., ZHANG, H., THORWALD, M., MOUSAVI, A., WOODWARD, N. C., SHIRMOHAMMADI, F., COUSSA, V., WISE, J. P., FORMAN, H. J., SIOUTAS, C., ALLAYEE, H., MORGAN, T. E. & FINCH, C. E. 2020. Toxicity of urban air pollution particulate matter in developing and adult mouse brain: Comparison of total and filter-eluted nanoparticles. *Environment International,* 136**,** 105510.
HAINING, R. L. & ACHAT-MENDES, C. 2017. Neuromelanin, one of the most overlooked molecules in modern medicine, is not a spectator. *Neural Regeneration Research,* 12**,** 372-375.
HALLGREN, B. & SOURANDER, P. 1958. The effect of age on the non-haemin iron in the human brain. *J Neurochem,* 3**,** 41-51.
HALLIWELL, B. 2006. Oxidative stress and neurodegeneration: where are we now? *Journal of Neurochemistry,* 97**,** 1634-1658.
HALSALL, C. J., MAHER, B. A., KARLOUKOVSKI, V. V., SHAH, P. & WATKINS, S. J. 2008. A novel approach to investigating indoor/outdoor pollution links: Combined magnetic and PAH measurements. *Atmospheric Environment,* 42**,** 8902-8909.
HAMMOND, J., MAHER, B. A., AHMED, I. A. M. & ALLSOP, D. 2021. Variation in the concentration and regional distribution of magnetic nanoparticles in human brains, with and without Alzheimer's disease, from the UK. *Scientific Reports,* 11**,** 9363.
HAMPEL, H., HARDY, J., BLENNOW, K., CHEN, C., PERRY, G., KIM, S. H., VILLEMAGNE, V. L., AISEN, P., VENDRUSCOLO, M., IWATSUBO, T., MASTERS, C. L., CHO, M., LANNFELT, L., CUMMINGS, J. L. & VERGALLO, A. 2021. The Amyloid-β Pathway in Alzheimer's Disease. *Molecular Psychiatry,* 26**,** 5481-5503.
HAN, C., LU, Y., CHENG, H., WANG, C. & CHAN, P. 2020. The impact of long-term exposure to ambient air pollution and second-hand smoke on the onset of Parkinson disease: a review and meta-analysis. *Public Health,* 179**,** 100-110.
HARE, D. J., ARORA, M., JENKINS, N. L., FINKELSTEIN, D. I., DOBLE, P. A. & BUSH, A. I. 2015a. Is early-life iron exposure critical in neurodegeneration? *Nature Reviews Neurology,* 11**,** 536-544.

HARE, D. J., DOECKE, J. D., FAUX, N. G., REMBACH, A., VOLITAKIS, I., FOWLER, C. J., GRIMM, R., DOBLE, P. A., CHERNY, R. A., MASTERS, C. L., BUSH, A. I. & ROBERTS, B. R. 2015b. Decreased plasma iron in Alzheimer's disease is due to transferrin desaturation. *ACS Chem Neurosci,* 6**,** 398-402.

HARE, D. J., KYSENIUS, K., PAUL, B., KNAUER, B., HUTCHINSON, R. W., O'CONNOR, C., FRYER, F., HENNESSEY, T. P., BUSH, A. I., CROUCH, P. J. & DOBLE, P. A. 2017. Imaging Metals in Brain Tissue by Laser Ablation - Inductively Coupled Plasma - Mass Spectrometry (LA-ICP-MS). *Journal of visualized experiments : JoVE***,** 55042.

HARE, D. J., RAVEN, E. P., ROBERTS, B. R., BOGESKI, M., PORTBURY, S. D., MCLEAN, C. A., MASTERS, C. L., CONNOR, J. R., BUSH, A. I., CROUCH, P. J. & DOBLE, P. A. 2016. Laser ablation-inductively coupled plasma-mass spectrometry imaging of white and gray matter iron distribution in Alzheimer's disease frontal cortex. *NeuroImage,* 137**,** 124-131.

HARKNESS, J. S., DARRAH, T. H., MOORE, M. T., WHYTE, C. J., MATHEWSON, P. D., COOK, T. & VENGOSH, A. 2017. Naturally Occurring versus Anthropogenic Sources of Elevated Molybdenum in Groundwater: Evidence for Geogenic Contamination from Southeast Wisconsin, United States. *Environmental Science & Technology,* 51**,** 12190-12199.

HARMAN, D. 1992. Free radical theory of aging. *Mutation Research/DNAging,* 275**,** 257-266.

HARRISON, R. M., JONES, A. M., GIETL, J., YIN, J. & GREEN, D. C. 2012. Estimation of the Contributions of Brake Dust, Tire Wear, and Resuspension to Nonexhaust Traffic Particles Derived from Atmospheric Measurements. *Environmental Science & Technology,* 46**,** 6523-6529.

HARRISON, R. M., TILLING, R., CALLÉN ROMERO, M. A. S., HARRAD, S. & JARVIS, K. 2003. A study of trace metals and polycyclic aromatic hydrocarbons in the roadside environment. *Atmospheric Environment,* 37**,** 2391-2402.

HARRISON, W. W., NETSKY, M. G. & BROWN, M. D. 1968. Trace elements in human brain: Copper, zinc, iron, and magnesium. *Clinica Chimica Acta,* 21**,** 55-60.

HARTL, F. U. 2017. Protein misfolding diseases. *Annual Review of Biochemistry.*

HARTMANN, J. T. & LIPP, H. P. 2003. Toxicity of platinum compounds. *Expert Opin Pharmacother,* 4**,** 889-901.

HASEBE, N., FUJITA, Y., UENO, M., YOSHIMURA, K., FUJINO, Y. & YAMASHITA, T. 2013. Soluble β-amyloid Precursor Protein Alpha Binds to p75 Neurotrophin Receptor to Promote Neurite Outgrowth. *PLOS ONE,* 8**,** e82321.

HASHIMOTO, M. & IMAZATO, S. 2015. Cytotoxic and genotoxic characterization of aluminum and silicon oxide nanoparticles in macrophages. *Dental Materials,* 31**,** 556-564.

HAUTOT, D., PANKHURST, Q. A., KHAN, N. & DOBSON, J. 2003. Preliminary evaluation of nanoscale biogenic magnetite in Alzheimer's disease brain tissue. *Proc Biol Sci,* 270 Suppl 1**,** S62-4.

HE, R.-W., GERLOFS-NIJLAND, M. E., BOERE, J., FOKKENS, P., LESEMAN, D., JANSSEN, N. A. H. & CASSEE, F. R. 2020. Comparative toxicity of ultrafine particles around a major airport in human bronchial epithelial (Calu-3) cell model at the air–liquid interface. *Toxicology in Vitro,* 68**,** 104950.

HE, R.-W., SHIRMOHAMMADI, F., GERLOFS-NIJLAND, M. E., SIOUTAS, C. & CASSEE, F. R. 2018. Pro-inflammatory responses to PM0.25 from airport and urban traffic emissions. *Science of The Total Environment,* 640-641**,** 997-1003.

HEAL, M. R. & HAMMONDS, M. D. 2014. Insights into the composition and sources of rural, urban and roadside carbonaceous PM_{10}. *Environ Sci Technol,* 48**,** 8995-9003.

HEINRICH, J., PITZ, M., BISCHOF, W., KRUG, N. & BORM, P. J. A. 2003. Endotoxin in fine (PM2.5) and coarse (PM2.5–10) particle mass of ambient aerosols. A temporo-spatial analysis. *Atmospheric Environment,* 37**,** 3659-3667.

HEYERS, D., ZAPKA, M., HOFFMEISTER, M., WILD, J. M. & MOURITSEN, H. 2010. Magnetic field changes activate the trigeminal brainstem complex in a migratory bird. *Proceedings of the National Academy of Sciences,* 107**,** 9394.

HIEMSTRA, P. S., MCCRAY, P. B., JR. & BALS, R. 2015. The innate immune function of airway epithelial cells in inflammatory lung disease. *The European respiratory journal,* 45**,** 1150-1162.

HIRT, A. M., BREM, F., HANZLIK, M. & FAIVRE, D. 2006. Anomalous magnetic properties of brain tissue at low temperature: The 50 K anomaly. *Journal of Geophysical Research: Solid Earth,* 111.

HITSCHLER, L. & LANG, T. 2022. The transmembrane domain of the amyloid precursor protein is required for antiamyloidogenic processing by α-secretase ADAM10. *Journal of Biological Chemistry,* 298**,** 101911.

HLADKY, S. B. & BARRAND, M. A. 2014. Mechanisms of fluid movement into, through and out of the brain: evaluation of the evidence. *Fluids and Barriers of the CNS,* 11**,** 26.

HODGE, M. X., HENRIQUEZ, A. R. & KODAVANTI, U. P. 2021. Adrenergic and Glucocorticoid Receptors in the Pulmonary Health Effects of Air Pollution. *Toxics,* 9.

HOLMQVIST, S., CHUTNA, O., BOUSSET, L., ALDRIN-KIRK, P., LI, W., BJÖRKLUND, T., WANG, Z. Y., ROYBON, L., MELKI, R. & LI, J. Y. 2014. Direct evidence of Parkinson pathology spread from the gastrointestinal tract to the brain in rats. *Acta Neuropathologica,* 128**,** 805-820.

HONG, N., GUAN, Y., YANG, B., ZHONG, J., ZHU, P., OK, Y. S., HOU, D., TSANG, D. C. W., GUAN, Y. & LIU, A. 2020. Quantitative source tracking of heavy metals contained in urban road deposited sediments. *Journal of Hazardous Materials,* 393**,** 122362.

HOPKINS, L. E., PATCHIN, E. S., CHIU, P.-L., BRANDENBERGER, C., SMILEY-JEWELL, S. & PINKERTON, K. E. 2014. Nose-to-brain transport of aerosolised quantum dots following acute exposure. *Nanotoxicology,* 8**,** 885-893.

HU, C. Y., FANG, Y., LI, F. L., DONG, B., HUA, X. G., JIANG, W., ZHANG, H., LYU, Y. & ZHANG, X. J. 2019. Association between ambient air pollution and Parkinson's disease: Systematic review and meta-analysis. *Environmental Research,* 168**,** 448-459.

HU, X., HE, M. & LI, S. 2015. Antimony leaching release from brake pads: Effect of pH, temperature and organic acids. *J Environ Sci (China),* 29**,** 11-7.

HUANG, M., KANG, Y., WANG, W., CHAN, C. Y., WANG, X. & WONG, M. H. 2015. Potential cytotoxicity of water-soluble fraction of dust and particulate matters and relation to metal(loid)s based on three human cell lines. *Chemosphere,* 135**,** 61-66.

IACCARINO, L., LA JOIE, R., LESMAN-SEGEV, O. H., LEE, E., HANNA, L., ALLEN, I. E., HILLNER, B. E., SIEGEL, B. A., WHITMER, R. A., CARRILLO, M. C., GATSONIS, C. & RABINOVICI, G. D. 2021. Association Between Ambient Air Pollution and Amyloid Positron Emission Tomography Positivity in Older Adults With Cognitive Impairment. *JAMA Neurology,* 78**,** 197-207.

IANKOVA, V., KARIN, I., KLOPSTOCK, T. & SCHNEIDER, S. A. 2021. Emerging Disease-Modifying Therapies in Neurodegeneration With Brain Iron Accumulation (NBIA) Disorders. *Frontiers in Neurology,* 12.

IGBOKWE, I. O., IGWENAGU, E. & IGBOKWE, N. A. 2019. Aluminium toxicosis: a review of toxic actions and effects. *Interdisciplinary toxicology,* 12**,** 45-70.

ILIFF, J. J., WANG, M., LIAO, Y., PLOGG, B. A., PENG, W., GUNDERSEN, G. A., BENVENISTE, H., VATES, G. E., DEANE, R., GOLDMAN, S. A., NAGELHUS, E. A. & NEDERGAARD, M. 2012. A paravascular pathway facilitates CSF flow through the brain parenchyma and the clearance of interstitial solutes, including amyloid β. *Sci Transl Med,* 4**,** 147ra111.

IMAM, S. Z., LANTZ-MCPEAK, S. M., CUEVAS, E., ROSAS-HERNANDEZ, H., LIACHENKO, S., ZHANG, Y., SARKAR, S., RAMU, J., ROBINSON, B. L., JONES, Y., GOUGH, B., PAULE, M. G., ALI, S. F. & BINIENDA, Z. K. 2015. Iron Oxide Nanoparticles Induce Dopaminergic

Damage: In vitro Pathways and In Vivo Imaging Reveals Mechanism of Neuronal Damage. *Molecular Neurobiology,* 52**,** 913-926.

INEGI. 2020. *Population and Housing Census 2020* [Online]. Available: https://www.inegi.org.mx/programas/ccpv/2020/#Resultados_generales [Accessed 26th August 2021].

ISING, C., VENEGAS, C., ZHANG, S., SCHEIBLICH, H., SCHMIDT, S. V., VIEIRA-SAECKER, A., SCHWARTZ, S., ALBASSET, S., MCMANUS, R. M., TEJERA, D., GRIEP, A., SANTARELLI, F., BROSSERON, F., OPITZ, S., STUNDEN, J., MERTEN, M., KAYED, R., GOLENBOCK, D. T., BLUM, D., LATZ, E., BUÉE, L. & HENEKA, M. T. 2019. NLRP3 inflammasome activation drives tau pathology. *Nature,* 575**,** 669-673.

IWASAKI, A., FOXMAN, E. F. & MOLONY, R. D. 2017. Early local immune defences in the respiratory tract. *Nat Rev Immunol,* 17**,** 7-20.

JACK, C. R., BENNETT, D. A., BLENNOW, K., CARRILLO, M. C., DUNN, B., HAEBERLEIN, S. B., HOLTZMAN, D. M., JAGUST, W., JESSEN, F., KARLAWISH, J., LIU, E., MOLINUEVO, J. L., MONTINE, T., PHELPS, C., RANKIN, K. P., ROWE, C. C., SCHELTENS, P., SIEMERS, E., SNYDER, H. M., SPERLING, R., ELLIOTT, C., MASLIAH, E., RYAN, L. & SILVERBERG, N. 2018. NIA-AA Research Framework: Toward a biological definition of Alzheimer's disease. *Alzheimer's and Dementia,* 14**,** 535-562.

JACK, C. R., THERNEAU, T. M., WEIGAND, S. D., WISTE, H. J., KNOPMAN, D. S., VEMURI, P., LOWE, V. J., MIELKE, M. M., ROBERTS, R. O., MACHULDA, M. M., GRAFF-RADFORD, J., JONES, D. T., SCHWARZ, C. G., GUNTER, J. L., SENJEM, M. L., ROCCA, W. A. & PETERSEN, R. C. 2019. Prevalence of Biologically vs Clinically Defined Alzheimer Spectrum Entities Using the National Institute on Aging-Alzheimer's Association Research Framework. *JAMA Neurology,* 76**,** 1174-1183.

JAMES, B. D., WILSON, R. S., BOYLE, P. A., TROJANOWSKI, J. Q., BENNETT, D. A. & SCHNEIDER, J. A. 2016. TDP-43 stage, mixed pathologies, and clinical Alzheimer's-type dementia. *Brain,* 139**,** 2983-2993.

JAMES, S. A., CHURCHES, Q. I., DE JONGE, M. D., BIRCHALL, I. E., STRELTSOV, V., MCCOLL, G., ADLARD, P. A. & HARE, D. J. 2017. Iron, Copper, and Zinc Concentration in Aβ Plaques in the APP/PS1 Mouse Model of Alzheimer's Disease Correlates with Metal Levels in the Surrounding Neuropil. *ACS Chemical Neuroscience,* 8**,** 629-637.

JAN, H. H., CHEN, I. T., TSAI, Y. Y. & CHANG, Y. C. 2002. Structural role of zinc ions bound to postsynaptic densities. *J Neurochem,* 83**,** 525-34.

JAROSZ, M., OLBERT, M., WYSZOGRODZKA, G., MŁYNIEC, K. & LIBROWSKI, T. 2017. Antioxidant and anti-inflammatory effects of zinc. Zinc-dependent NF-κB signaling. *Inflammopharmacology,* 25**,** 11-24.

JARRETT, J. T., BERGER, E. P. & LANSBURY, P. T., JR. 1993. The carboxy terminus of the beta amyloid protein is critical for the seeding of amyloid formation: implications for the pathogenesis of Alzheimer's disease. *Biochemistry,* 32**,** 4693-7.

JELLINGER, K., PAULUS, W., GRUNDKE-IQBAL, I., RIEDERER, P. & YOUDIM, M. B. 1990. Brain iron and ferritin in Parkinson's and Alzheimer's diseases. *J Neural Transm Park Dis Dement Sect,* 2**,** 327-40.

JEONG, S. C., CHO, Y., SONG, M. K., LEE, E. & RYU, J. C. 2017. Epidermal growth factor receptor (EGFR)-MAPK-nuclear factor(NF)-κB-IL8: A possible mechanism of particulate matter(PM) 2.5-induced lung toxicity. *Environ Toxicol,* 32**,** 1628-1636.

JESSEN, N. A., MUNK, A. S., LUNDGAARD, I. & NEDERGAARD, M. 2015. The Glymphatic System: A Beginner's Guide. *Neurochem Res,* 40**,** 2583-99.

JI, X., WANG, H., ZHU, M., HE, Y., ZHANG, H., CHEN, X., GAO, W., FU, Y. & FOR THE ALZHEIMER'S DISEASE NEUROIMAGING, I. 2021. Brainstem atrophy in the early stage of Alzheimer's disease: a voxel-based morphometry study. *Brain Imaging and Behavior,* 15**,** 49-59.

JIA, H., WANG, P. & SONG, T. 2017. Magnetic Nanoparticles Altered the Aggregation and Cytotoxicity of Aβ40. *Journal of Nanoscience and Nanotechnology,* 17**,** 1779-1786.

JIN, S. P., LI, Z., CHOI, E. K., LEE, S., KIM, Y. K., SEO, E. Y., CHUNG, J. H. & CHO, S. 2018. Urban particulate matter in air pollution penetrates into the barrier-disrupted skin and produces ROS-dependent cutaneous inflammatory response in vivo. *J Dermatol Sci*.

JOHANSSON, C., NORMAN, M. & GIDHAGEN, L. 2007. Spatial & temporal variations of PM10 and particle number concentrations in urban air. *Environ Monit Assess,* 127**,** 477-87.

JOHNSON, G. V. & STOOTHOFF, W. H. 2004. Tau phosphorylation in neuronal cell function and dysfunction. *J Cell Sci,* 117**,** 5721-9.

JOHNSON, J. W. & KOTERMANSKI, S. E. 2006. Mechanism of action of memantine. *Current Opinion in Pharmacology,* 6**,** 61-67.

JONSSON, T., STEFANSSON, H., STEINBERG, S., JONSDOTTIR, I., JONSSON, P. V., SNAEDAL, J., BJORNSSON, S., HUTTENLOCHER, J., LEVEY, A. I., LAH, J. J., RUJESCU, D., HAMPEL, H., GIEGLING, I., ANDREASSEN, O. A., ENGEDAL, K., ULSTEIN, I., DJUROVIC, S., IBRAHIM-VERBAAS, C., HOFMAN, A., IKRAM, M. A., VAN DUIJN, C. M., THORSTEINSDOTTIR, U., KONG, A. & STEFANSSON, K. 2013. Variant of TREM2 associated with the risk of Alzheimer's disease. *N Engl J Med,* 368**,** 107-16.

JOSEFSSON, M., LARSSON, M., NORDIN, S., ADOLFSSON, R. & OLOFSSON, J. 2017. APOE-ε4 effects on longitudinal decline in olfactory and non-olfactory cognitive abilities in middle-aged and old adults. *Sci Rep,* 7**,** 1286.

JUNG, C. R., LIN, Y. T. & HWANG, B. F. 2015. Ozone, particulate matter, and newly diagnosed Alzheimer's disease: a population-based cohort study in Taiwan. *J Alzheimers Dis,* 44**,** 573-84.

KALADHAR, M. & NARASINGA RAO, B. S. 1982. Effects of iron deficiency on serotonin uptake in vitro by rat brain synaptic vesicles. *J Neurochem,* 38**,** 1576-81.

KANNINEN, K. M., LAMPINEN, R., RANTANEN, L. M., ODENDAAL, L., JALAVA, P., CHEW, S. & WHITE, A. R. 2020. Olfactory cell cultures to investigate health effects of air pollution exposure: implications for neurodegeneration. *Neurochemistry International***,** 104729.

KANTI DAS, T., WATI, M. R. & FATIMA-SHAD, K. 2015. Oxidative Stress Gated by Fenton and Haber Weiss Reactions and Its Association With Alzheimer's Disease. *Arch Neurosci,* 2**,** e60038.

KARANTH, S., NELSON, P. T., KATSUMATA, Y., KRYSCIO, R. J., SCHMITT, F. A., FARDO, D. W., CYKOWSKI, M. D., JICHA, G. A., VAN ELDIK, L. J. & ABNER, E. L. 2020. Prevalence and Clinical Phenotype of Quadruple Misfolded Proteins in Older Adults. *JAMA Neurology,* 77**,** 1299-1307.

KARIMI, A., GHADIRI MOGHADDAM, F. & VALIPOUR, M. 2020. Insights in the biology of extremely low-frequency magnetic fields exposure on human health. *Molecular Biology Reports,* 47**,** 5621-5633.

KAWAS, C., GRAY, S., BROOKMEYER, R., FOZARD, J. & ZONDERMAN, A. 2000. Age-specific incidence rates of Alzheimer's disease. *The Baltimore Longitudinal Study of Aging,* 54**,** 2072-2077.

KERMENIDOU, M., BALCELLS, L., MARTINEZ-BOUBETA, C., CHATZIAVRAMIDIS, A., KONSTANTINIDIS, I., SAMARAS, T., SARIGIANNIS, D. & SIMEONIDIS, K. 2021. Magnetic nanoparticles: An indicator of health risks related to anthropogenic airborne particulate matter. *Environmental Pollution,* 271**,** 116309.

KHAN, A., DOBSON, J. P. & EXLEY, C. 2006. Redox cycling of iron by Aβ42. *Free Radical Biology and Medicine,* 40**,** 557-569.

KHAN, Q. A. & DIPPLE, A. 2000. Diverse chemical carcinogens fail to induce G(1) arrest in MCF-7 cells. *Carcinogenesis,* 21**,** 1611-8.

KHAN, S. & COHEN, D. 2019. Using the magnetoencephalogram to noninvasively measure magnetite in the living human brain. *Human Brain Mapping,* 40**,** 1654-1665.

KIELHORN, J., MELBER, C., KELLER, D. & MANGELSDORF, I. 2002. Palladium – A review of exposure and effects to human health. *International Journal of Hygiene and Environmental Health,* 205**,** 417-432.

KIM, E.-A. & KOH, B. 2020. Utilization of road dust chemical profiles for source identification and human health impact assessment. *Scientific Reports,* 10**,** 14259.

KIM, J., BASAK, J. M. & HOLTZMAN, D. M. 2009. The Role of Apolipoprotein E in Alzheimer's Disease. *Neuron,* 63**,** 287-303.

KIM, J. S., YOON, T. J., YU, K. N., KIM, B. G., PARK, S. J., KIM, H. W., LEE, K. H., PARK, S. B., LEE, J. K. & CHO, M. H. 2006. Toxicity and tissue distribution of magnetic nanoparticles in mice. *Toxicol Sci,* 89**,** 338-47.

KIM, K. T., EO, M. Y., NGUYEN, T. T. H. & KIM, S. M. 2019. General review of titanium toxicity. *International journal of implant dentistry,* 5**,** 10-10.

KIM, N. & LEE, H. J. 2021. Redox-Active Metal Ions and Amyloid-Degrading Enzymes in Alzheimer's Disease. *Int J Mol Sci,* 22.

KIM, O.-J., LEE, S. H., KANG, S.-H. & KIM, S.-Y. 2020. Incident cardiovascular disease and particulate matter air pollution in South Korea using a population-based and nationwide cohort of 0.2 million adults. *Environmental Health,* 19**,** 113.

KIM, W., CHO, Y., SONG, M.-K., LIM, J.-H., KIM, J. Y., GYE, M. C. & RYU, J.-C. 2018. Effect of particulate matter 2.5 on gene expression profile and cell signaling in JEG-3 human placenta cells. *Environmental Toxicology,* 33**,** 1123-1134.

KIM, Y., KO, S. M. & NAM, J. M. 2016. Protein–Nanoparticle Interaction-Induced Changes in Protein Structure and Aggregation. *Chemistry - An Asian Journal,* 11**,** 1869-1877.

KIRCH, J., GUENTHER, M., DOSHI, N., SCHAEFER, U. F., SCHNEIDER, M., MITRAGOTRI, S. & LEHR, C. M. 2012. Mucociliary clearance of micro- and nanoparticles is independent of size, shape and charge--an ex vivo and in silico approach. *J Control Release,* 159**,** 128-34.

KIRSCHVINK, J. L. & GOULD, J. L. 1981. Biogenic magnetite as a basis for magnetic field detection in animals. *BioSystems,* 13**,** 181-201.

KIRSCHVINK, J. L., KOBAYASHI-KIRSCHVINK, A. & WOODFORD, B. J. 1992a. Magnetite biomineralization in the human brain. *Proceedings of the National Academy of Sciences,* 89**,** 7683-7687.

KIRSCHVINK, J. L., KOBAYASHI-KIRSCHVINK, A., DIAZ-RICCI, J. C. & KIRSCHVINK, S. J. 1992b. Magnetite in human tissues: A mechanism for the biological effects of weak ELF magnetic fields. *Bioelectromagnetics,* 13**,** 101-113.

KIVIPELTO, M., HELKALA, E.-L., LAAKSO, M. P., HÄNNINEN, T., HALLIKAINEN, M., ALHAINEN, K., SOININEN, H., TUOMILEHTO, J. & NISSINEN, A. 2001. Midlife vascular risk factors and Alzheimer's disease in later life: longitudinal, population based study. *BMJ : British Medical Journal,* 322**,** 1447-1451.

KNOPMAN, D. S., PARISI, J. E., SALVIATI, A., FLORIACH-ROBERT, M., BOEVE, B. F., IVNIK, R. J., SMITH, G. E., DICKSON, D. W., JOHNSON, K. A., PETERSEN, L. E., MCDONALD, W. C., BRAAK, H. & PETERSEN, R. C. 2003. Neuropathology of cognitively normal elderly. *J Neuropathol Exp Neurol,* 62**,** 1087-95.

KOCBACH, A., TOTLANDSDAL, A. I., LÅG, M., REFSNES, M. & SCHWARZE, P. E. 2008. Differential binding of cytokines to environmentally relevant particles: A possible source for misinterpretation of in vitro results? *Toxicology Letters,* 176**,** 131-137.

KODAVATI, M., WANG, H. & HEGDE, M. L. 2020. Altered Mitochondrial Dynamics in Motor Neuron Disease: An Emerging Perspective. *Cells,* 9.

KOH, B. & KIM, E.-A. 2019. Comparative analysis of urban road dust compositions in relation to their potential human health impacts. *Environmental Pollution,* 255**,** 113156.

KOREN, S., GALVIS-ESCOBAR, S. & ABISAMBRA, J. F. 2020. Tau-mediated dysregulation of RNA: Evidence for a common molecular mechanism of toxicity in frontotemporal dementia and other tauopathies. *Neurobiology of Disease,* 141.

KORTE, N., NORTLEY, R. & ATTWELL, D. 2020. Cerebral blood flow decrease as an early pathological mechanism in Alzheimer's disease. *Acta neuropathologica,* 140**,** 793-810.

KOSE, O., TOMATIS, M., LECLERC, L., BELBLIDIA, N. B., HOCHEPIED, J. F., TURCI, F., POURCHEZ, J. & FOREST, V. 2020. Impact of the Physicochemical Features of TiO2Nanoparticles on Their in Vitro Toxicity. *Chemical Research in Toxicology,* 33**,** 2324-2337.

KREBS, N., LANGKAMMER, C., GOESSLER, W., ROPELE, S., FAZEKAS, F., YEN, K. & SCHEURER, E. 2014. Assessment of trace elements in human brain using inductively coupled plasma mass spectrometry. *J Trace Elem Med Biol,* 28**,** 1-7.

KREYLING, W. G., SEMMLER, M., ERBE, F., MAYER, P., TAKENAKA, S., SCHULZ, H., OBERDÖRSTER, G. & ZIESENIS, A. 2002. Translocation of ultrafine insoluble iridium particles from lung epithelium to extrapulmonary organs is size dependent but very low. *J Toxicol Environ Health A,* 65**,** 1513-30.

KRIIT, H. K., FORSBERG, B., ÅSTRÖM, D. O. & OUDIN, A. 2021. Annual dementia incidence and monetary burden attributable to fine particulate matter (PM(2.5)) exposure in Sweden. *Environ Health,* 20**,** 65.

KUHN, D. M., RUSKIN, B. & LOVENBERG, W. 1980. Tryptophan hydroxylase. The role of oxygen, iron, and sulfhydryl groups as determinants of stability and catalytic activity. *Journal of Biological Chemistry,* 255**,** 4137-43.

KUHN, P. H., WANG, H., DISLICH, B., COLOMBO, A., ZEITSCHEL, U., ELLWART, J. W., KREMMER, E., ROSSNER, S. & LICHTENTHALER, S. F. 2010. ADAM10 is the physiologically relevant, constitutive alpha-secretase of the amyloid precursor protein in primary neurons. *Embo j,* 29**,** 3020-32.

KUKUTSCHOVÁ, J., MORAVEC, P., TOMÁŠEK, V., MATĚJKA, V., SMOLÍK, J., SCHWARZ, J., SEIDLEROVÁ, J., ŠAFÁŘOVÁ, K. & FILIP, P. 2011. On airborne nano/micro-sized wear particles released from low-metallic automotive brakes. *Environmental Pollution,* 159**,** 998-1006.

KULICK, E. R., ELKIND, M. S. V., BOEHME, A. K., JOYCE, N. R., SCHUPF, N., KAUFMAN, J. D., MAYEUX, R., MANLY, J. J. & WELLENIUS, G. A. 2020. Long-term exposure to ambient air pollution, APOE-ε4 status, and cognitive decline in a cohort of older adults in northern Manhattan. *Environment international,* 136**,** 105440-105440.

KUMAGAI, Y., ARIMOTO, T., SHINYASHIKI, M., SHIMOJO, N., NAKAI, Y., YOSHIKAWA, T. & SAGAI, M. 1997. Generation of Reactive Oxygen Species during Interaction of Diesel Exhaust Particle Components with NADPH-Cytochrome p450 Reductase and Involvement of the Bioactivation in the DNA Damage. *Free Radical Biology and Medicine,* 22**,** 479-487.

KUMAR, A., SINGH, A. & EKAVALI 2015. A review on Alzheimer's disease pathophysiology and its management: an update. *Pharmacol Rep,* 67**,** 195-203.

KUMARI, M., RAJAK, S., SINGH, S. P., KUMARI, S. I., KUMAR, P. U., MURTY, U. S. N., MAHBOOB, M., GROVER, P. & RAHMAN, M. F. 2012. Repeated oral dose toxicity of iron oxide nanoparticles: Biochemical and histopathological alterations in different tissues of rats. *Journal of Nanoscience and Nanotechnology,* 12**,** 2149-2159.

KWAN, J. Y., JEONG, S. Y., VAN GELDEREN, P., DENG, H.-X., QUEZADO, M. M., DANIELIAN, L. E., BUTMAN, J. A., CHEN, L., BAYAT, E., RUSSELL, J., SIDDIQUE, T., DUYN, J. H., ROUAULT, T. A. & FLOETER, M. K. 2012. Iron accumulation in deep cortical layers accounts for MRI signal abnormalities in ALS: correlating 7 tesla MRI and pathology. *PloS one,* 7**,** e35241-e35241.

LACROIX, G., KOCH, W., RITTER, D., GUTLEB, A. C., LARSEN, S. T., LORET, T., ZANETTI, F., CONSTANT, S., CHORTAREA, S., ROTHEN-RUTISHAUSER, B., HIEMSTRA, P. S.,

FREJAFON, E., HUBERT, P., GRIBALDO, L., KEARNS, P., AUBLANT, J.-M., DIABATÉ, S., WEISS, C., DE GROOT, A. & KOOTER, I. 2018. Air–Liquid Interface In Vitro Models for Respiratory Toxicology Research: Consensus Workshop and Recommendations. *Applied In Vitro Toxicology,* 4**,** 91-106.

LADINO, L. A., RAGA, G. B. & BAUMGARDNER, D. 2018. On particle-bound polycyclic aromatic hydrocarbons (PPAH) and links to gaseous emissions in Mexico city. *Atmospheric Environment,* 194**,** 31-40.

LANCASTER CITY COUNCIL. 2020. *2019 Air Quality Annual Status Report (ASR) for Lancaster City Council* [Online]. Available: https://www.lancaster.gov.uk/assets/attach/6104/Air%20Quality%20Annual%20Status%20Report%20-%20Lancaster%202020.pdf [Accessed 26th August 2021].

LANDIS, M. S., PATRICK PANCRAS, J., GRANEY, J. R., WHITE, E. M., EDGERTON, E. S., LEGGE, A. & PERCY, K. E. 2017. Source apportionment of ambient fine and coarse particulate matter at the Fort McKay community site, in the Athabasca Oil Sands Region, Alberta, Canada. *Science of The Total Environment,* 584-585**,** 105-117.

LANDRIGAN, P. J., FULLER, R., ACOSTA, N. J. R., ADEYI, O., ARNOLD, R., BASU, N. N., BALDÉ, A. B., BERTOLLINI, R., BOSE-O'REILLY, S., BOUFFORD, J. I., BREYSSE, P. N., CHILES, T., MAHIDOL, C., COLL-SECK, A. M., CROPPER, M. L., FOBIL, J., FUSTER, V., GREENSTONE, M., HAINES, A., HANRAHAN, D., HUNTER, D., KHARE, M., KRUPNICK, A., LANPHEAR, B., LOHANI, B., MARTIN, K., MATHIASEN, K. V., MCTEER, M. A., MURRAY, C. J. L., NDAHIMANANJARA, J. D., PERERA, F., POTOČNIK, J., PREKER, A. S., RAMESH, J., ROCKSTRÖM, J., SALINAS, C., SAMSON, L. D., SANDILYA, K., SLY, P. D., SMITH, K. R., STEINER, A., STEWART, R. B., SUK, W. A., VAN SCHAYCK, O. C. P., YADAMA, G. N., YUMKELLA, K. & ZHONG, M. 2018. The Lancet Commission on pollution and health. *Lancet,* 391**,** 462-512.

LANNFELT, L., BLENNOW, K., ZETTERBERG, H., BATSMAN, S., AMES, D., HARRISON, J., MASTERS, C. L., TARGUM, S., BUSH, A. I., MURDOCH, R., WILSON, J. & RITCHIE, C. W. 2008. Safety, efficacy, and biomarker findings of PBT2 in targeting Abeta as a modifying therapy for Alzheimer's disease: a phase IIa, double-blind, randomised, placebo-controlled trial. *Lancet Neurol,* 7**,** 779-86.

LANSDOWN, A. B. G. 2010. A Pharmacological and Toxicological Profile of Silver as an Antimicrobial Agent in Medical Devices. *Advances in Pharmacological Sciences,* 2010**,** 910686.

LAVOIE, M. J. & SELKOE, D. J. 2003. The Notch ligands, Jagged and Delta, are sequentially processed by alpha-secretase and presenilin/gamma-secretase and release signaling fragments. *J Biol Chem,* 278**,** 34427-37.

LEE, P. C., LIU, L. L., SUN, Y., CHEN, Y. A., LIU, C. C., LI, C. Y., YU, H. L. & RITZ, B. 2016. Traffic-related air pollution increased the risk of Parkinson's disease in Taiwan: A nationwide study. *Environment International,* 96**,** 75-81.

LEE, P. H., PARK, S., LEE, Y. G., CHOI, S. M., AN, M. H. & JANG, A. S. 2021. The Impact of Environmental Pollutants on Barrier Dysfunction in Respiratory Disease. *Allergy Asthma Immunol Res,* 13**,** 850-862.

LEIBIGER, C., DEISEL, J., AUFSCHNAITER, A., AMBROS, S., TERESHCHENKO, M., VERHEIJEN, B. M., BÜTTNER, S. & BRAUN, R. J. 2018. TDP-43 controls lysosomal pathways thereby determining its own clearance and cytotoxicity. *Human Molecular Genetics,* 27**,** 1593-1607.

LEIKAUF, G. D., KIM, S.-H. & JANG, A.-S. 2020. Mechanisms of ultrafine particle-induced respiratory health effects. *Experimental & Molecular Medicine,* 52**,** 329-337.

LELIEVELD, J., EVANS, J. S., FNAIS, M., GIANNADAKI, D. & POZZER, A. 2015. The contribution of outdoor air pollution sources to premature mortality on a global scale. *Nature,* 525**,** 367-371.

LEMUS, R. & VENEZIA, C. F. 2015. An update to the toxicological profile for water-soluble and sparingly soluble tungsten substances. *Critical Reviews in Toxicology,* 45**,** 388-411.

LENNON, M. J., MAKKAR, S. R., CRAWFORD, J. D. & SACHDEV, P. S. 2019. Midlife Hypertension and Alzheimer's Disease: A Systematic Review and Meta-Analysis. *J Alzheimers Dis,* 71**,** 307-316.

LEWIS, J., BENCH, G., MYERS, O., TINNER, B., STAINES, W., BARR, E., DIVINE, K. K., BARRINGTON, W. & KARLSSON, J. 2005. Trigeminal uptake and clearance of inhaled manganese chloride in rats and mice. *Neurotoxicology,* 26**,** 113-23.

LI, B., ZHAO, Z. B., THAPA, S., SUN, S. J., MA, L. X., GENG, J. L., WANG, K. & QI, H. 2020a. Occurrence, distribution and human exposure of phthalic esters in road dust samples across China. *Environ Res,* 191**,** 110222.

LI, H., CHEN, Z., LI, J., LIU, R., ZHAO, F. & LIU, R. 2020b. Indium oxide nanoparticles induce lung intercellular toxicity between bronchial epithelial cells and macrophages. *Journal of Applied Toxicology,* 40**,** 1636-1646.

LIAO, C.-M. & CHIANG, K.-C. 2006. Probabilistic risk assessment for personal exposure to carcinogenic polycyclic aromatic hydrocarbons in Taiwanese temples. *Chemosphere,* 63**,** 1610-1619.

LIAO, Y. H., CHEN, W. L., WANG, C. C. & LAI, C. H. 2020. Associations between Personal Exposure to Metals in Fine Particulate Matter and Autonomic Nervous System Dysfunction among Healthy Adults. *Aerosol and Air Quality Research,* 20**,** 1842-1849.

LIATI, A., PANDURANGI, S. S., BOULOUCHOS, K., SCHREIBER, D. & DASILVA, Y. A. R. 2015. Metal nanoparticles in diesel exhaust derived by in-cylinder melting of detached engine fragments. *Atmospheric Environment,* 101**,** 34-40.

LIMANAQI, F., BIAGIONI, F., GAMBARDELLA, S., FAMILIARI, P., FRATI, A. & FORNAI, F. 2020. Promiscuous roles of autophagy and proteasome in neurodegenerative proteinopathies. *International Journal of Molecular Sciences,* 21.

LINSE, S., CABALEIRO-LAGO, C., XUE, W. F., LYNCH, I., LINDMAN, S., THULIN, E., RADFORD, S. E. & DAWSON, K. A. 2007. Nucleation of protein fibrillation by nanoparticles. *Proceedings of the National Academy of Sciences of the United States of America,* 104**,** 8691-8696.

LIU, C. & YU, J. 2019. Genome-Wide Association Studies for Cerebrospinal Fluid Soluble TREM2 in Alzheimer's Disease. *Frontiers in Aging Neuroscience,* 11.

LIU, N. M., MIYASHITA, L., MAHER, B. A., MCPHAIL, G., JONES, C. J. P., BARRATT, B., THANGARATINAM, S., KARLOUKOVSKI, V., AHMED, I. A., ASLAM, Z. & GRIGG, J. 2021. Evidence for the presence of air pollution nanoparticles in placental tissue cells. *Science of The Total Environment,* 751**,** 142235.

LIU, Y., LI, J., XU, K., GU, J., HUANG, L., ZHANG, L., LIU, N., KONG, J., XING, M., ZHANG, L. & ZHANG, L. 2018. Characterization of superparamagnetic iron oxide nanoparticle-induced apoptosis in PC12 cells and mouse hippocampus and striatum. *Toxicology Letters,* 292**,** 151-161.

LIVINGSTON, G., HUNTLEY, J., SOMMERLAD, A., AMES, D., BALLARD, C., BANERJEE, S., BRAYNE, C., BURNS, A., COHEN-MANSFIELD, J., COOPER, C., COSTAFREDA, S. G., DIAS, A., FOX, N., GITLIN, L. N., HOWARD, R., KALES, H. C., KIVIMÄKI, M., LARSON, E. B., OGUNNIYI, A., ORGETA, V., RITCHIE, K., ROCKWOOD, K., SAMPSON, E. L., SAMUS, Q., SCHNEIDER, L. S., SELBÆK, G., TERI, L. & MUKADAM, N. 2020. Dementia prevention, intervention, and care: 2020 report of the Lancet Commission. *The Lancet,* 396**,** 413-446.

LIVINGSTON, G., SOMMERLAD, A., ORGETA, V., COSTAFREDA, S. G., HUNTLEY, J., AMES, D., BALLARD, C., BANERJEE, S., BURNS, A., COHEN-MANSFIELD, J., COOPER, C., FOX, N., GITLIN, L. N., HOWARD, R., KALES, H. C., LARSON, E. B., RITCHIE, K., ROCKWOOD, K., SAMPSON, E. L., SAMUS, Q., SCHNEIDER, L. S., SELBÆK, G., TERI, L. & MUKADAM, N. 2017. Dementia prevention, intervention, and care. *Lancet,* 390**,** 2673-2734.

LOVELL, M. A., ROBERTSON, J. D., TEESDALE, W. J., CAMPBELL, J. L. & MARKESBERY, W. R. 1998. Copper, iron and zinc in Alzheimer's disease senile plaques. *J Neurol Sci,* 158**,** 47-52.

LOVELL, M. A., XIE, C. & MARKESBERY, W. R. 1999. Protection against amyloid beta peptide toxicity by zinc. *Brain Res,* 823**,** 88-95.

LOXHAM, M., MORGAN-WALSH, R. J., COOPER, M. J., BLUME, C., SWINDLE, E. J., DENNISON, P. W., HOWARTH, P. H., CASSEE, F. R., TEAGLE, D. A. H., PALMER, M. R. & DAVIES, D. E. 2015. The effects on bronchial epithelial mucociliary cultures of coarse, fine, and ultrafine particulate matter from an underground railway station. *Toxicological sciences : an official journal of the Society of Toxicology,* 145**,** 98-107.

LOXHAM, M., WOO, J., SINGHANIA, A., SMITHERS, N. P., YEOMANS, A., PACKHAM, G., CRAINIC, A. M., COOK, R. B., CASSEE, F. R., WOELK, C. H. & DAVIES, D. E. 2020. Upregulation of epithelial metallothioneins by metal-rich ultrafine particulate matter from an underground railway. *Metallomics,* 12**,** 1070-1082.

LU, D., LUO, Q., CHEN, R., ZHUANSUN, Y., JIANG, J., WANG, W., YANG, X., ZHANG, L., LIU, X., LI, F., LIU, Q. & JIANG, G. 2020. Chemical multi-fingerprinting of exogenous ultrafine particles in human serum and pleural effusion. *Nature Communications,* 11**,** 2567.

MADANE, R. G. & MAHAJAN, H. S. 2016. Curcumin-loaded nanostructured lipid carriers (NLCs) for nasal administration: design, characterization, and in vivo study. *Drug Delivery,* 23**,** 1326-1334.

MAGAKI, S., RAGHAVAN, R., MUELLER, C., OBERG, K. C., VINTERS, H. V. & KIRSCH, W. M. 2007. Iron, copper, and iron regulatory protein 2 in Alzheimer's disease and related dementias. *Neuroscience letters,* 418**,** 72-76.

MAHER, B. A. 1988. Magnetic properties of some synthetic sub-micron magnetites. *Geophysical Journal International,* 94**,** 83-96.

MAHER, B. A. 2019. Airborne Magnetite- and Iron-Rich Pollution Nanoparticles: Potential Neurotoxicants and Environmental Risk Factors for Neurodegenerative Disease, Including Alzheimer's Disease. *Journal of Alzheimer's Disease,* 71**,** 361-375.

MAHER, B. A., AHMED, I. A. M., DAVISON, B., KARLOUKOVSKI, V. & CLARKE, R. 2013. Impact of roadside tree lines on indoor concentrations of traffic-derived particulate matter. *Environmental Science and Technology,* 47**,** 13737-13744.

MAHER, B. A., AHMED, I. A. M., KARLOUKOVSKI, V., MACLAREN, D. A., FOULDS, P. G., ALLSOP, D., MANN, D. M. A., TORRES-JARDÓN, R. & CALDERÓN-GARCIDUENAS, L. 2016. Magnetite pollution nanoparticles in the human brain. *Proceedings of the National Academy of Sciences,* 113**,** 10797-10801.

MAHER, B. A., GONZÁLEZ-MACIEL, A., REYNOSO-ROBLES, R., TORRES-JARDÓN, R. & CALDERÓN-GARCIDUEÑAS, L. 2020. Iron-rich air pollution nanoparticles: An unrecognised environmental risk factor for myocardial mitochondrial dysfunction and cardiac oxidative stress. *Environmental research,* 188**,** 109816-109816.

MAHER, B. A., MOORE, C. & MATZKA, J. 2008. Spatial variation in vehicle-derived metal pollution identified by magnetic and elemental analysis of roadside tree leaves. *Atmospheric Environment,* 42**,** 364-373.

MAHER, B. A., O'SULLIVAN, V., FEENEY, J., GONET, T. & ANNE KENNY, R. 2021. Indoor particulate air pollution from open fires and the cognitive function of older people. *Environmental Research,* 192**,** 110298.

MAHLEY, R. W. & RALL, S. C., JR. 2000. Apolipoprotein E: far more than a lipid transport protein. *Annu Rev Genomics Hum Genet,* 1**,** 507-37.

MAHMOUDI, M., QUINLAN-PLUCK, F., MONOPOLI, M. P., SHEIBANI, S., VALI, H., DAWSON, K. A. & LYNCH, I. 2013. Influence of the Physiochemical Properties of Superparamagnetic Iron Oxide Nanoparticles on Amyloid β Protein Fibrillation in Solution. *ACS Chemical Neuroscience,* 4**,** 475-485.

MANCHESTER CITY COUNCIL. 2021. *Greater Manchester Air Quality Annual Status Report (ASR) 2020* [Online]. Available: https://www.manchester.gov.uk/download/downloads/id/28108/greater_manchester_2020_air_quality_annual_status_report.pdf [Accessed 29th May 2022].

MANDRIOTA, G., DI CORATO, R., BENEDETTI, M., DE CASTRO, F., FANIZZI, F. P. & RINALDI, R. 2019. Design and Application of Cisplatin-Loaded Magnetic Nanoparticle Clusters for Smart Chemotherapy. *ACS Appl Mater Interfaces,* 11**,** 1864-1875.

MANKE, A., WANG, L. & ROJANASAKUL, Y. 2013. Mechanisms of Nanoparticle-Induced Oxidative Stress and Toxicity. *BioMed Research International,* 2013**,** 942916.

MANN, S. 1993. Molecular tectonics in biomineralization and biomimetic materials chemistry. *Nature,* 365**,** 499-505.

MANN, S., FRANKEL, R. B. & BLAKEMORE, R. P. 1984. Structure, morphology and crystal growth of bacterial magnetite. *Nature,* 310**,** 405-407.

MANSOUR, Y., BLACKBURN, K., GONZÁLEZ-GONZÁLEZ, L. O., CALDERÓN-GARCIDUEÑAS, L. & KULESZA, R. J. 2019. Auditory Brainstem Dysfunction, Non-Invasive Biomarkers for Early Diagnosis and Monitoring of Alzheimer's Disease in Young Urban Residents Exposed to Air Pollution. *Journal of Alzheimer's Disease,* 67**,** 1147-1155.

MANSUROGLU, Z., BENHELLI-MOKRANI, H., MARCATO, V., SULTAN, A., VIOLET, M., CHAUDERLIER, A., DELATTRE, L., LOYENS, A., TALAHARI, S., BÉGARD, S., NESSLANY, F., COLIN, M., SOUÈS, S., LEFEBVRE, B., BUÉE, L., GALAS, M. C. & BONNEFOY, E. 2016. Loss of Tau protein affects the structure, transcription and repair of neuronal pericentromeric heterochromatin. *Scientific Reports,* 6.

MANTYH, P. W., GHILARDI, J. R., ROGERS, S., DEMASTER, E., ALLEN, C. J., STIMSON, E. R. & MAGGIO, J. E. 1993. Aluminum, Iron, and Zinc Ions Promote Aggregation of Physiological Concentrations of β-Amyloid Peptide. *Journal of Neurochemistry,* 61**,** 1171-1174.

MAR, T. F., LARSON, T. V., STIER, R. A., CLAIBORN, C. & KOENIG, J. Q. 2004. An analysis of the association between respiratory symptoms in subjects with asthma and daily air pollution in Spokane, Washington. *Inhal Toxicol,* 16**,** 809-15.

MARKESBERY, W. R. & LOVELL, M. A. 2006. DNA oxidation in Alzheimer's disease. *Antioxid Redox Signal,* 8**,** 2039-45.

MASHIK, T., SAKASHITA, E., KASASHIMA, K., TOMINAGA, K., KUROIWA, K., NOZAKI, Y., MATSUURA, T., HAMAMOTO, T. & ENDO, H. 2016. Developmentally regulated RNA-binding protein 1 (Drb1)/ RNA-binding motif protein 45 (RBM45), a nuclear-cytoplasmic trafficking protein, forms TAR DNA-binding protein 43 (TDP-43)-mediated cytoplasmic aggregates. *Journal of Biological Chemistry,* 291**,** 14996-15007.

MASLIAH, E., TERRY, R. D., DETERESA, R. M. & HANSEN, L. A. 1989. Immunohistochemical quantification of the synapse-related protein synaptophysin in Alzheimer disease. *Neurosci Lett,* 103**,** 234-9.

MATTHIAS-MASER, S., OBOLKIN, V., KHODZER, T. & JAENICKE, R. 2000. Seasonal variation of primary biological aerosol particles in the remote continental region of Lake Baikal/Siberia. *Atmospheric Environment,* 34**,** 3805-3811.

MAYES, J., TINKER-MILL, C., KOLOSOV, O., ZHANG, H., TABNER, B. J. & ALLSOP, D. 2014. β-amyloid fibrils in Alzheimer disease are not inert when bound to copper ions but can degrade hydrogen peroxide and generate reactive oxygen species. *J Biol Chem,* 289**,** 12052-12062.

MAYEUX, R., OTTMAN, R., MAESTRE, G., NGAI, C., TANG, M.-X., GINSBERG, H., CHUN, M., TYCKO, B. & SHELANSKI, M. 1995. Synergistic Effects of Traumatic Head Injury and Apolipoprotein-epsilon4 in Patients With Alzheimer's Disease. *Neurology,* 45**,** 555-557.

MAYNARD, C. J., BUSH, A. I., MASTERS, C. L., CAPPAI, R. & LI, Q.-X. 2005. Metals and amyloid-β in Alzheimer's disease. *International Journal of Experimental Pathology,* 86**,** 147-159.

MAZUEL, F., ESPINOSA, A., LUCIANI, N., REFFAY, M., LE BORGNE, R., MOTTE, L., DESBOEUFS, K., MICHEL, A., PELLEGRINO, T., LALATONNE, Y. & WILHELM, C. 2016. Massive Intracellular Biodegradation of Iron Oxide Nanoparticles Evidenced Magnetically at Single-Endosome and Tissue Levels. *ACS Nano,* 10**,** 7627-38.

MAZURE, C. M. & SWENDSEN, J. 2016. Sex differences in Alzheimer's disease and other dementias. *The Lancet. Neurology,* 15**,** 451-452.

MAZURYK, O., STOCHEL, G. & BRINDELL, M. 2020. Variations in Reactive Oxygen Species Generation by Urban Airborne Particulate Matter in Lung Epithelial Cells—Impact of Inorganic Fraction. *Frontiers in Chemistry,* 8.

MBEH, D. A., JAVANBAKHT, T., TABET, L., MERHI, Y., MAGHNI, K., SACHER, E. & YAHIA, L. H. 2015. Protein Corona Formation on Magnetite Nanoparticles: Effects of Culture Medium Composition, and Its Consequences on Superparamagnetic Nanoparticle Cytotoxicity. *J Biomed Nanotechnol,* 11**,** 828-40.

MCKEITH, I. G., DICKSON, D. W., LOWE, J., EMRE, M., O'BRIEN, J. T., FELDMAN, H., CUMMINGS, J., DUDA, J. E., LIPPA, C., PERRY, E. K., AARSLAND, D., ARAI, H., BALLARD, C. G., BOEVE, B., BURN, D. J., COSTA, D., DEL SER, T., DUBOIS, B., GALASKO, D., GAUTHIER, S., GOETZ, C. G., GOMEZ-TORTOSA, E., HALLIDAY, G., HANSEN, L. A., HARDY, J., IWATSUBO, T., KALARIA, R. N., KAUFER, D., KENNY, R. A., KORCZYN, A., KOSAKA, K., LEE, V. M. Y., LEES, A., LITVAN, I., LONDOS, E., LOPEZ, O. L., MINOSHIMA, S., MIZUNO, Y., MOLINA, J. A., MUKAETOVA-LADINSKA, E. B., PASQUIER, F., PERRY, R. H., SCHULZ, J. B., TROJANOWSKI, J. Q. & YAMADA, M. 2005. Diagnosis and management of dementia with Lewy bodies: Third report of the DLB consortium. *Neurology,* 65**,** 1863-1872.

MEALER, R. G., JENKINS, B. G., CHEN, C.-Y., DALY, M. J., GE, T., LEHOUX, S., MARQUARDT, T., PALMER, C. D., PARK, J. H., PARSONS, P. J., SACKSTEIN, R., WILLIAMS, S. E., CUMMINGS, R. D., SCOLNICK, E. M. & SMOLLER, J. W. 2020. The schizophrenia risk locus in SLC39A8 alters brain metal transport and plasma glycosylation. *Scientific Reports,* 10**,** 13162.

MELBER, C. & MANGELSDORF, I. 2006. Palladium Toxicity in Animals and in in vitro Test Systems — An Overview. *In:* ZEREINI, F. & ALT, F. (eds.) *Palladium Emissions in the Environment: Analytical Methods, Environmental Assessment and Health Effects.* Berlin, Heidelberg: Springer Berlin Heidelberg.

MEN, C., LIU, R., XU, F., WANG, Q., GUO, L. & SHEN, Z. 2018. Pollution characteristics, risk assessment, and source apportionment of heavy metals in road dust in Beijing, China. *Science of The Total Environment,* 612**,** 138-147.

MENG, X., MA, Y., CHEN, R., ZHOU, Z., CHEN, B. & KAN, H. 2013. Size-fractionated particle number concentrations and daily mortality in a Chinese city. *Environ Health Perspect,* 121**,** 1174-8.

MHATRE, M., FLOYD, R. A. & HENSLEY, K. 2004. Oxidative stress and neuroinflammation in Alzheimer's disease and amyotrophic lateral sclerosis: common links and potential therapeutic targets. *J Alzheimers Dis,* 6**,** 147-57.

MIGUEL, E. D., LLAMAS, J. F., CHACÓN, E., BERG, T., LARSSEN, S., RØYSET, O. & VADSET, M. 1997. Origin and patterns of distribution of trace elements in street dust: Unleaded petrol and urban lead. *Atmospheric Environment,* 31**,** 2733-2740.

MILATOVIC, D., ZAJA-MILATOVIC, S., GUPTA, R. C., YU, Y. & ASCHNER, M. 2009. Oxidative damage and neurodegeneration in manganese-induced neurotoxicity. *Toxicology and Applied Pharmacology,* 240**,** 219-225.

MILLER, A. J. & SPENCE, J. R. 2017. In Vitro Models to Study Human Lung Development, Disease and Homeostasis. *Physiology (Bethesda),* 32**,** 246-260.

MILLER, L. M., WANG, Q., TELIVALA, T. P., SMITH, R. J., LANZIROTTI, A. & MIKLOSSY, J. 2006. Synchrotron-based infrared and X-ray imaging shows focalized accumulation of Cu and Zn co-localized with beta-amyloid deposits in Alzheimer's disease. *J Struct Biol,* 155**,** 30-7.

MILLER, M. R., RAFTIS, J. B., LANGRISH, J. P., MCLEAN, S. G., SAMUTRTAI, P., CONNELL, S. P., WILSON, S., VESEY, A. T., FOKKENS, P. H. B., BOERE, A. J. F., KRYSTEK, P., CAMPBELL, C. J., HADOKE, P. W. F., DONALDSON, K., CASSEE, F. R., NEWBY, D. E., DUFFIN, R. & MILLS, N. L. 2017. Inhaled Nanoparticles Accumulate at Sites of Vascular Disease. *ACS nano,* 11**,** 4542-4552.

MINERS, J. S., BAIG, S., TAYLER, H., KEHOE, P. G. & LOVE, S. 2009. Neprilysin and insulin-degrading enzyme levels are increased in Alzheimer disease in relation to disease severity. *J Neuropathol Exp Neurol,* 68**,** 902-14.

MIOUSSE, I. R., CHALBOT, M. C., PATHAK, R., LU, X., NZABARUSHIMANA, E., KRAGER, K., AYKIN-BURNS, N., HAUER-JENSEN, M., DEMOKRITOU, P., KAVOURAS, I. G. & KOTURBASH, I. 2015. In Vitro Toxicity and Epigenotoxicity of Different Types of Ambient Particulate Matter. *Toxicol Sci,* 148**,** 473-87.

MIR, M., TAHIRBEGI, I. B., VALLE-DELGADO, J. J., FERNANDEZ-BUSQUETS, X. & SAMITIER, J. 2012. In vitro study of magnetite-amyloid beta complex formation. *Nanomedicine,* 8**,** 974-80.

MIRSADEGHI, S., SHANEHSAZZADEH, S., ATYABI, F. & DINARVAND, R. 2016. Effect of PEGylated superparamagnetic iron oxide nanoparticles (SPIONs) under magnetic field on amyloid beta fibrillation process. *Mater Sci Eng C Mater Biol Appl,* 59**,** 390-7.

MOHAMMADI, S. & NIKKHAH, M. 2017. TiO2 nanoparticles as potential promoting agents of fibrillation of α-synuclein, a parkinson's disease-related protein. *Iranian Journal of Biotechnology,* 15**,** 88-94.

MOLINA, L. T. 2021. Introductory lecture: air quality in megacities. *Faraday Discussions,* 226**,** 9-52.

MOLINA, L. T., MADRONICH, S., GAFFNEY, J. S., APEL, E., DE FOY, B., FAST, J., FERRARE, R., HERNDON, S., JIMENEZ, J. L., LAMB, B., OSORNIO-VARGAS, A. R., RUSSELL, P., SCHAUER, J. J., STEVENS, P. S., VOLKAMER, R. & ZAVALA, M. 2010. An overview of the MILAGRO 2006 Campaign: Mexico City emissions and their transport and transformation. *Atmospheric Chemistry and Physics,* 10**,** 8697-8760.

MOLINA, L. T., VELASCO, E., RETAMA, A. & ZAVALA, M. 2019. Experience from integrated air quality management in the Mexico City Metropolitan Area and Singapore. *Atmosphere,* 10.

MON, E. E., PHAY, N., AGUSA, T., BACH, L. T., YEH, H.-M., HUANG, C.-H. & NAKATA, H. 2020. Polycyclic Aromatic Hydrocarbons (PAHs) in Road Dust Collected from Myanmar, Japan, Taiwan, and Vietnam. *Archives of Environmental Contamination and Toxicology,* 78**,** 34-45.

MONTAGNE, A., BARNES, SAMUEL R., SWEENEY, MELANIE D., HALLIDAY, MATTHEW R., SAGARE, ABHAY P., ZHAO, Z., TOGA, ARTHUR W., JACOBS, RUSSELL E., LIU, COLLIN Y., AMEZCUA, L., HARRINGTON, MICHAEL G., CHUI, HELENA C., LAW, M. & ZLOKOVIC, BERISLAV V. 2015. Blood-Brain Barrier Breakdown in the Aging Human Hippocampus. *Neuron,* 85**,** 296-302.

MOORE, S., RABICHOW, B. E. & SATTLER, R. 2020. The Hitchhiker's Guide to Nucleocytoplasmic Trafficking in Neurodegeneration. *Neurochemical Research,* 45**,** 1306-1327.

MORALES, J., AGUILERA, A., BAUTISTA, F., CEJUDO, R., GOGUITCHAICHVILI, A. & HERNÁNDEZ-BERNAL, M. D. S. 2020. Heavy metal content estimation in the Mexico City Street dust: an inter-method comparison and Pb levels assessment during the last decade. *SN Applied Sciences,* 2**,** 1841.

MORENO, T., MARTINS, V., QUEROL, X., JONES, T., BERUBE, K., MINGUILLON, M. C., AMATO, F., CAPDEVILA, M., DE MIGUEL, E., CENTELLES, S. & GIBBONS, W. 2015. A new look at inhalable metalliferous airborne particles on rail subway platforms. *Sci Total Environ,* 505**,** 367-75.

MORGAN, T. E., DAVIS, D. A., IWATA, N., TANNER, J. A., SNYDER, D., NING, Z., KAM, W., HSU, Y.-T., WINKLER, J. W., CHEN, J.-C., PETASIS, N. A., BAUDRY, M., SIOUTAS, C. & FINCH, C. E. 2011. Glutamatergic neurons in rodent models respond to nanoscale particulate urban air pollutants in vivo and in vitro. *Environmental health perspectives,* 119**,** 1003-1009.

MORRIS, C. M., CANDY, J. M., KEITH, A. B., OAKLEY, A. E., TAYLOR, G. A., EDWARDSON, J. A., BLOXHAM, C. A., PULLEN, R. G. L. & GOCHT, A. 1992. Brain iron homeostasis. *Journal of Inorganic Biochemistry,* 47**,** 257-265.

MORTAMAIS, M., GUTIERREZ, L.-A., DE HOOGH, K., CHEN, J., VIENNEAU, D., CARRIÈRE, I., LETELLIER, N., HELMER, C., GABELLE, A., MURA, T., SUNYER, J., BENMARHNIA, T., JACQUEMIN, B. & BERR, C. 2021. Long-term exposure to ambient air pollution and risk of dementia: Results of the prospective Three-City Study. *Environment International,* 148**,** 106376.

MOSKOWITZ, B. M., FRANKEL, R. B. & BAZYLINSKI, D. A. 1993. Rock magnetic criteria for the detection of biogenic magnetite. *Earth and Planetary Science Letters,* 120**,** 283-300.

MUNKER, S., KILO, S., RÖß, C., JEITNER, P., SCHIERL, R., GÖEN, T. & DREXLER, H. 2016. Exposure of the German general population to platinum and rhodium − Urinary levels and determining factors. *International Journal of Hygiene and Environmental Health,* 219**,** 801-810.

MURPHY, C. 2019. Olfactory and other sensory impairments in Alzheimer disease. *Nature Reviews Neurology,* 15**,** 11-24.

MURROS, K., WASILJEFF, J., MACÍAS-SÁNCHEZ, E., FAIVRE, D., SOINNE, L., VALTONEN, J., POHJA, M., SAARI, P., PESONEN, L. J. & SALMINEN, J. M. 2019. Magnetic Nanoparticles in Human Cervical Skin. *Frontiers in Medicine,* 6.

MUTTER, S. T., TURNER, M., DEETH, R. J. & PLATTS, J. A. 2018. Metal Binding to Amyloid-β1–42: A Ligand Field Molecular Dynamics Study. *ACS Chemical Neuroscience,* 9**,** 2795-2806.

MYHRE, O., UTKILEN, H., DUALE, N., BRUNBORG, G. & HOFER, T. 2013. Metal Dyshomeostasis and Inflammation in Alzheimer's and Parkinson's Diseases: Possible Impact of Environmental Exposures. *Oxidative Medicine and Cellular Longevity,* 2013**,** 726954.

MYLONAS, C. & KOURETAS, D. 1999. Lipid peroxidation and tissue damage. *In Vivo,* 13**,** 295-309.

NEEL, L. 1949. Theorie du trainage magnetique des ferromagnetiques en grains fins avec applications aux terres cuites. *Ann. Geophys.,* 5**,** 99-136.

NELSON, P. T., DICKSON, D. W., TROJANOWSKI, J. Q., JACK, C. R., BOYLE, P. A., ARFANAKIS, K., RADEMAKERS, R., ALAFUZOFF, I., ATTEMS, J., BRAYNE, C., COYLE-GILCHRIST, I. T. S., CHUI, H. C., FARDO, D. W., FLANAGAN, M. E., HALLIDAY, G., HOKKANEN, S. R. K., HUNTER, S., JICHA, G. A., KATSUMATA, Y., KAWAS, C. H., KEENE, C. D., KOVACS, G. G., KUKULL, W. A., LEVEY, A. I., MAKKINEJAD, N., MONTINE, T. J., MURAYAMA, S., MURRAY, M. E., NAG, S., RISSMAN, R. A., SEELEY, W. W., SPERLING, R. A., WHITE III, C. L., YU, L. & SCHNEIDER, J. A. 2019. Limbic-predominant age-related TDP-43 encephalopathy (LATE): Consensus working group report. *Brain,* 142**,** 1503-1527.

NEMETHOVA, V., BULIAKOVA, B., MAZANCOVA, P., BABELOVA, A., SELC, M., MORAVCIKOVA, D., KLESCIKOVA, L., URSINYOVA, M., GABELOVA, A. & RAZGA, F. 2017. Intracellular uptake of magnetite nanoparticles: A focus on physico-chemical characterization and interpretation of in vitro data. *Mater Sci Eng C Mater Biol Appl,* 70**,** 161-168.

NESTOR, S. M., RUPSINGH, R., BORRIE, M., SMITH, M., ACCOMAZZI, V., WELLS, J. L., FOGARTY, J. & BARTHA, R. 2008. Ventricular enlargement as a possible measure of Alzheimer's disease progression validated using the Alzheimer's disease neuroimaging initiative database. *Brain,* 131**,** 2443-54.

NEWMAN, L., RODRIGUES, A. F., JASIM, D. A., VACCHI, I. A., MÉNARD-MOYON, C., BIANCO, A., BUSSY, C. & KOSTARELOS, K. 2020. Nose-to-Brain Translocation and Cerebral Biodegradation of Thin Graphene Oxide Nanosheets. *Cell Reports Physical Science,* 1**,** 100176.

NGUYEN, T. T., TA, Q. T. H., NGUYEN, T. K. O., NGUYEN, T. T. D. & GIAU, V. V. 2020. Type 3 Diabetes and Its Role Implications in Alzheimer's Disease. *International journal of molecular sciences,* 21**,** 3165.

NICOLAS, M. & HASSAN, B. A. 2014. Amyloid precursor protein and neural development. *Development,* 141**,** 2543-2548.

NILAWEERA, D., FREAK-POLI, R., RITCHIE, K., CHAUDIEU, I., ANCELIN, M.-L. & RYAN, J. 2020. The long-term consequences of trauma and posttraumatic stress disorder symptoms on later life cognitive function and dementia risk. *Psychiatry Research,* 294**,** 113506.

NIU, H., ÁLVAREZ-ÁLVAREZ, I., GUILLÉN-GRIMA, F. & AGUINAGA-ONTOSO, I. 2017. Prevalence and incidence of Alzheimer's disease in Europe: A meta-analysis. *Neurologia,* 32**,** 523-532.

NIU, X., WANG, Y., HO, S. S. H., CHUANG, H.-C., SUN, J., QU, L., WANG, G. & HO, K. F. 2021. Characterization of organic aerosols in PM1 and their cytotoxicity in an urban roadside area in Hong Kong. *Chemosphere,* 263**,** 128239.

NORDBERG, G. F., BERNARD, A., DIAMOND, G. L., DUFFUS, J. H., ILLING, P., NORDBERG, M., BERGDAHL, I. A., JIN, T. & SKERFVING, S. 2018. Risk assessment of effects of cadmium on human health (IUPAC Technical Report). *Pure and Applied Chemistry,* 90**,** 755-808.

O'BRYANT, S. E., EDWARDS, M., MENON, C. V., GONG, G. & BARBER, R. 2011. Long-term low-level arsenic exposure is associated with poorer neuropsychological functioning: a Project FRONTIER study. *Int J Environ Res Public Health,* 8**,** 861-74.

O'DONOGHUE, J. L., WATSON, G. E., BREWER, R., ZAREBA, G., ETO, K., TAKAHASHI, H., MARUMOTO, M., LOVE, T., HARRINGTON, D. & MYERS, G. J. 2020. Neuropathology associated with exposure to different concentrations and species of mercury: A review of autopsy cases and the literature. *NeuroToxicology,* 78**,** 88-98.

O'NEAL, S. L. & ZHENG, W. 2015. Manganese Toxicity Upon Overexposure: a Decade in Review. *Current environmental health reports,* 2**,** 315-328.

OBERDÖRSTER, G. 1989. Dosimetric principles for extrapolating results of rat inhalation studies to humans, using an inhaled Ni compound as an example. *Health Phys,* 57 Suppl 1**,** 213-20.

OBERDÖRSTER, G., FERIN, J. & LEHNERT, B. E. 1994. Correlation between particle size, in vivo particle persistence, and lung injury. *Environmental Health Perspectives,* 102**,** 173-179.

OBERDORSTER, G., GELEIN, R. M., FERIN, J. & WEISS, B. 1995. Association of particulate air pollution and acute mortality: involvement of ultrafine particles? *Inhal Toxicol,* 7**,** 111-24.

OBERDÖRSTER, G., OBERDÖRSTER, E. & OBERDÖRSTER, J. 2005. Nanotoxicology: an emerging discipline evolving from studies of ultrafine particles. *Environmental health perspectives,* 113**,** 823-839.

OBERDÖRSTER, G., SHARP, Z., ATUDOREI, V., ELDER, A., GELEIN, R., KREYLING, W. & COX, C. 2004. Translocation of inhaled ultrafine particles to the brain. *Inhal Toxicol,* 16**,** 437-45.

OBERDÖRSTER, G., SHARP, Z., ATUDOREI, V., ELDER, A., GELEIN, R., LUNTS, A., KREYLING, W. & COX, C. 2002. EXTRAPULMONARY TRANSLOCATION OF ULTRAFINE CARBON

PARTICLES FOLLOWING WHOLE-BODY INHALATION EXPOSURE OF RATS. *Journal of Toxicology and Environmental Health, Part A,* 65**,** 1531-1543.

OCTAVE, J. N., PIERROT, N., FERAO SANTOS, S., NALIVAEVA, N. N. & TURNER, A. J. 2013. From synaptic spines to nuclear signaling: nuclear and synaptic actions of the amyloid precursor protein. *J Neurochem,* 126**,** 183-90.

OHGAMI, R. S., CAMPAGNA, D. R., GREER, E. L., ANTIOCHOS, B., MCDONALD, A., CHEN, J., SHARP, J. J., FUJIWARA, Y., BARKER, J. E. & FLEMING, M. D. 2005. Identification of a ferrireductase required for efficient transferrin-dependent iron uptake in erythroid cells. *Nat Genet,* 37**,** 1264-9.

ONG, K. J., MACCORMACK, T. J., CLARK, R. J., EDE, J. D., ORTEGA, V. A., FELIX, L. C., DANG, M. K. M., MA, G., FENNIRI, H., VEINOT, J. G. C. & GOSS, G. G. 2014. Widespread Nanoparticle-Assay Interference: Implications for Nanotoxicity Testing. *PLOS ONE,* 9**,** e90650.

ONS. 2019. *UK population pyramid interactive* [Online]. Available: https://www.ons.gov.uk/peoplepopulationandcommunity/populationandmigration/populationestimates/articles/ukpopulationpyramidinteractive/2020-01-08 [Accessed 26th August 2021].

OPPENHEIM, H. A., LUCERO, J., GUYOT, A.-C., HERBERT, L. M., MCDONALD, J. D., MABONDZO, A. & LUND, A. K. 2013. Exposure to vehicle emissions results in altered blood brain barrier permeability and expression of matrix metalloproteinases and tight junction proteins in mice. *Particle and Fibre Toxicology,* 10**,** 62.

OSORNIO-VARGAS, Á. R., BONNER, J. C., ALFARO-MORENO, E., MARTÍNEZ, L., GARCÍA-CUELLAR, C., SERGIO PONCE-DE-LEÓN, R., MIRANDA, J. & ROSAS, I. 2003. Proinflammatory and Cytotoxic Effects of Mexico City Air Pollution Particulate Matter in Vitro Are Dependent on Particle Size and Composition. *Environmental Health Perspectives,* 111**,** 1289-1293.

OUDIN, A., ANDERSSON, J., SUNDSTRÖM, A., NORDIN ADOLFSSON, A., OUDIN ÅSTRÖM, D., ADOLFSSON, R., FORSBERG, B. & NORDIN, M. 2019. Traffic-Related Air Pollution as a Risk Factor for Dementia: No Clear Modifying Effects of APOE ε4 in the Betula Cohort. *Journal of Alzheimer's Disease,* 71**,** 733-740.

OUDIN, A., FORSBERG, B., ADOLFSSON, A. N., LIND, N., MODIG, L., NORDIN, M., NORDIN, S., ADOLFSSON, R. & NILSSON, L. G. 2016. Traffic-Related Air Pollution and Dementia Incidence in Northern Sweden: A Longitudinal Study. *Environ Health Perspect,* 124**,** 306-12.

OUDIN, A., FORSBERG, B., LIND, N., NORDIN, S., OUDIN ÅSTRÖM, D., SUNDSTRÖM, A. & NORDIN, M. 2017. Is Long-term Exposure to Air Pollution Associated with Episodic Memory? A Longitudinal Study from Northern Sweden. *Scientific Reports,* 7**,** 12789.

OZDEMIR, H. 2019. Mitigation impact of roadside trees on fine particle pollution. *Science of The Total Environment,* 659**,** 1176-1185.

ÖZDEMIR, Ö. & DUNLOP, D. J. 2010. Hallmarks of maghemitization in low-temperature remanence cycling of partially oxidized magnetite nanoparticles. *Journal of Geophysical Research: Solid Earth,* 115.

ÖZDEMIR, Ö., DUNLOP, D. J. & MOSKOWITZ, B. M. 1993. The effect of oxidation on the Verwey transition in magnetite. *Geophysical Research Letters,* 20**,** 1671-1674.

OZGÜR, S., SÜMER, H. & KOÇOĞLU, G. 1996. Rickets and soil strontium. *Archives of disease in childhood,* 75**,** 524-526.

PACAKOVA, B., KUBICKOVA, S., SALAS, G., MANTLIKOVA, A. R., MARCIELLO, M., MORALES, M. P., NIZNANSKY, D. & VEJPRAVOVA, J. 2017. The internal structure of magnetic nanoparticles determines the magnetic response. *Nanoscale,* 9**,** 5129-5140.

PAGE, R. M., BAUMANN, K., TOMIOKA, M., PEREZ-REVUELTA, B. I., FUKUMORI, A., JACOBSEN, H., FLOHR, A., LUEBBERS, T., OZMEN, L., STEINER, H. & HAASS, C. 2008. Generation of

Abeta38 and Abeta42 is independently and differentially affected by familial Alzheimer disease-associated presenilin mutations and gamma-secretase modulation. *J Biol Chem,* 283**,** 677-83.

PALL, M. L. 2018. Wi-Fi is an important threat to human health. *Environmental Research,* 164**,** 405-416.

PANAYI, A. E., SPYROU, N. M., IVERSEN, B. S., WHITE, M. A. & PART, P. 2002. Determination of cadmium and zinc in Alzheimer's brain tissue using inductively coupled plasma mass spectrometry. *J Neurol Sci,* 195**,** 1-10.

PANKHURST, Q., HAUTOT, D., KHAN, N. & DOBSON, J. 2008. Increased levels of magnetic iron compounds in Alzheimer's disease. *J Alzheimers Dis,* 13**,** 49-52.

PANT, P., BAKER, S. J., SHUKLA, A., MAIKAWA, C., GODRI POLLITT, K. J. & HARRISON, R. M. 2015. The PM10 fraction of road dust in the UK and India: Characterization, source profiles and oxidative potential. *Science of The Total Environment,* 530-531**,** 445-452.

PARK, M., JOO, H. S., LEE, K., JANG, M., KIM, S. D., KIM, I., BORLAZA, L. J. S., LIM, H., SHIN, H., CHUNG, K. H., CHOI, Y.-H., PARK, S. G., BAE, M.-S., LEE, J., SONG, H. & PARK, K. 2018. Differential toxicities of fine particulate matters from various sources. *Scientific Reports,* 8**,** 17007.

PARKER, D. & PRINCE, A. 2011. Innate Immunity in the Respiratory Epithelium. *American Journal of Respiratory Cell and Molecular Biology,* 45**,** 189-201.

PARVEEN, R., SHAMSI, T. N. & FATIMA, S. 2017. Nanoparticles-protein interaction: Role in protein aggregation and clinical implications. *International Journal of Biological Macromolecules,* 94**,** 386-395.

PASQUINI, L., NANA, A. L., TOLLER, G., BROWN, J. A., DENG, J., STAFFARONI, A., KIM, E. J., HWANG, J. H. L., LI, L., PARK, Y., GAUS, S. E., ALLEN, I., STURM, V. E., SPINA, S., GRINBERG, L. T., RANKIN, K. P., KRAMER, J. H., ROSEN, H. J., MILLER, B. L. & SEELEY, W. W. 2020. Salience network atrophy links neuron type-specific pathobiology to loss of empathy in frontotemporal dementia. *Cerebral Cortex,* 30**,** 5387-5399.

PATTERSON, C. 2018. *World Alzheimer report 2018*, Alzheimer's Disease International.

PAWLAK, J., ŁODYGA-CHRUŚCIŃSKA, E. & CHRUSTOWICZ, J. 2014. Fate of platinum metals in the environment. *Journal of Trace Elements in Medicine and Biology,* 28**,** 247-254.

PENG, Q., ZHANG, S., YANG, Q., ZHANG, T., WEI, X. Q., JIANG, L., ZHANG, C. L., CHEN, Q. M., ZHANG, Z. R. & LIN, Y. F. 2013. Preformed albumin corona, a protective coating for nanoparticles based drug delivery system. *Biomaterials,* 34**,** 8521-30.

PEREIRA, G. M., TEINILÄ, K., CUSTÓDIO, D., GOMES SANTOS, A., XIAN, H., HILLAMO, R., ALVES, C. A., BITTENCOURT DE ANDRADE, J., OLÍMPIO DA ROCHA, G., KUMAR, P., BALASUBRAMANIAN, R., ANDRADE, M. D. F. & DE CASTRO VASCONCELLOS, P. 2017. Particulate pollutants in the Brazilian city of São Paulo: 1-year investigation for the chemical composition and source apportionment. *Atmos. Chem. Phys.,* 17**,** 11943-11969.

PERL, D. & GOOD, P. 1987. UPTAKE OF ALUMINIUM INTO CENTRAL NERVOUS SYSTEM ALONG NASAL-OLFACTORY PATHWAYS. *The Lancet,* 329**,** 1028.

PERL, D. P. 2010. Neuropathology of Alzheimer's disease. *The Mount Sinai journal of medicine, New York,* 77**,** 32-42.

PERL, D. P. & BRODY, A. R. 1980. Alzheimer's disease: X-ray spectrometric evidence of aluminum accumulation in neurofibrillary tangle-bearing neurons. *Science,* 208**,** 297-299.

PETERS, R. J. B., OOMEN, A. G., VAN BEMMEL, G., VAN VLIET, L., UNDAS, A. K., MUNNIKS, S., BLEYS, R. L. A. W., TROMP, P. C., BRAND, W. & VAN DER LEE, M. 2020. Silicon dioxide and titanium dioxide particles found in human tissues. *Nanotoxicology,* 14**,** 420-432.

PETERSEN, R. C. 2004. Mild cognitive impairment as a diagnostic entity. *J Intern Med,* 256**,** 183-94.

PHILLIPS, B. B., BULLOCK, J. M., OSBORNE, J. L. & GASTON, K. J. 2021. Spatial extent of road pollution: A national analysis. *Science of The Total Environment,* 773**,** 145589.

PIERCE, J. E. & PÉRON, J. 2020. The basal ganglia and the cerebellum in human emotion. *Social Cognitive and Affective Neuroscience,* 15**,** 599-613.

PIMPIN, L., RETAT, L., FECHT, D., DE PREUX, L., SASSI, F., GULLIVER, J., BELLONI, A., FERGUSON, B., CORBOULD, E., JACCARD, A. & WEBBER, L. 2018. Estimating the costs of air pollution to the National Health Service and social care: An assessment and forecast up to 2035. *PLOS Medicine,* 15**,** e1002602.

PLANTIN, L. O., LYING-TUNELL, U. & KRISTENSSON, K. 1987. Trace elements in the human central nervous system studied with neutron activation analysis. *Biol Trace Elem Res,* 13**,** 69-75.

PLASCENCIA-VILLA, G., PONCE, A., COLLINGWOOD, J. F., ARELLANO-JIMÉNEZ, M. J., ZHU, X., ROGERS, J. T., BETANCOURT, I., JOSÉ-YACAMÁN, M. & PERRY, G. 2016. High-resolution analytical imaging and electron holography of magnetite particles in amyloid cores of Alzheimer's disease. 6**,** 24873.

PLASSMAN, B. L., HAVLIK, R. J., STEFFENS, D. C., HELMS, M. J., NEWMAN, T. N., DROSDICK, D., PHILLIPS, C., GAU, B. A., WELSH–BOHMER, K. A., BURKE, J. R., GURALNIK, J. M. & BREITNER, J. C. S. 2000. Documented head injury in early adulthood and risk of Alzheimer's disease and other dementias. *Neurology,* 55**,** 1158-1166.

POLIKARPOV, D., CHEREPANOV, V., CHUEV, M., GABBASOV, R., MISCHENKO, I., NIKITIN, M., VERESHAGIN, Y., YURENIA, A. & PANCHENKO, V. 2014. Mössbauer evidence of 57Fe3O4 based ferrofluid biodegradation in the brain. *Hyperfine Interactions,* 226**,** 421-430.

POPESCU, B. F. & NICHOL, H. 2011. Mapping brain metals to evaluate therapies for neurodegenerative disease. *CNS Neurosci Ther,* 17**,** 256-68.

PORS NIELSEN, S. 2004. The biological role of strontium. *Bone,* 35**,** 583-588.

PRASAD, A. S. 2014. Zinc is an Antioxidant and Anti-Inflammatory Agent: Its Role in Human Health. *Frontiers in Nutrition,* 1.

PRICHARD, H. M. & FISHER, P. C. 2012. Identification of Platinum and Palladium Particles Emitted from Vehicles and Dispersed into the Surface Environment. *Environmental Science & Technology,* 46**,** 3149-3154.

PRINCE, M., WIMO, A., GUERCHET, M., ALI, G.-C., WU, Y.-T. & PRINA, M. 2015. *World Alzheimer Report 2015. The Global Impact of Dementia. An Analysis of Prevalence, Incidence, Cost and Trends*.

PUISNEY, C., OIKONOMOU, E. K., NOWAK, S., CHEVILLOT, A., CASALE, S., BAEZA-SQUIBAN, A. & BERRET, J.-F. 2018. Brake wear (nano)particle characterization and toxicity on airway epithelial cells in vitro. *Environmental Science: Nano,* 5**,** 1036-1044.

QUEROL, X., PEY, J., MINGUILLÓN, M. C., PÉREZ, N., ALASTUEY, A., VIANA, M., MORENO, T., BERNABÉ, R. M., BLANCO, S., CÁRDENAS, B., VEGA, E., SOSA, G., ESCALONA, S., RUIZ, H. & ARTÍÑANO, B. 2008. PM speciation and sources in Mexico during the MILAGRO-2006 campaign. *Atmospheric Chemistry and Physics,* 8**,** 111-128.

QUINTANA, C., BELLEFQIH, S., LAVAL, J. Y., GUERQUIN-KERN, J. L., WU, T. D., AVILA, J., FERRER, I., ARRANZ, R. & PATIÑO, C. 2006. Study of the localization of iron, ferritin, and hemosiderin in Alzheimer's disease hippocampus by analytical microscopy at the subcellular level. *Journal of Structural Biology,* 153**,** 42-54.

QUINTANA, C., COWLEY, J. M. & MARHIC, C. 2004. Electron nanodiffraction and high-resolution electron microscopy studies of the structure and composition of physiological and pathological ferritin. *Journal of Structural Biology,* 147**,** 166-178.

QUINTANA, C. & GUTIÉRREZ, L. 2010. Could a dysfunction of ferritin be a determinant factor in the aetiology of some neurodegenerative diseases? *Biochimica et Biophysica Acta (BBA) - General Subjects,* 1800**,** 770-782.

RAHIL-KHAZEN, R., BOLANN, B. J., MYKING, A. & ULVIK, R. J. 2002. Multi-element analysis of trace element levels in human autopsy tissues by using inductively coupled atomic emission spectrometry technique (ICP-AES). *J Trace Elem Med Biol,* 16**,** 15-25.

RAHMAN, M. A., HANNAN, M. A., UDDIN, M. J., RAHMAN, M. S., RASHID, M. M. & KIM, B. 2021. Exposure to Environmental Arsenic and Emerging Risk of Alzheimer's Disease: Perspective Mechanisms, Management Strategy, and Future Directions. *Toxics,* 9.

RAJAN, M. T., JAGANNATHA RAO, K. S., MAMATHA, B. M., RAO, R. V., SHANMUGAVELU, P., MENON, R. B. & PAVITHRAN, M. V. 1997. Quantification of trace elements in normal human brain by inductively coupled plasma atomic emission spectrometry. *J Neurol Sci,* 146**,** 153-66.

RAMESH, V., RAVICHANDRAN, P., COPELAND, C. L., GOPIKRISHNAN, R., BIRADAR, S., GOORNAVAR, V., RAMESH, G. T. & HALL, J. C. 2012. Magnetite induces oxidative stress and apoptosis in lung epithelial cells. *Molecular and Cellular Biochemistry,* 363**,** 225-234.

RAMOS, P., SANTOS, A., PINTO, N. R., MENDES, R., MAGALHÃES, T. & ALMEIDA, A. 2014a. Anatomical Region Differences and Age-Related Changes in Copper, Zinc, and Manganese Levels in the Human Brain. *Biological Trace Element Research,* 161**,** 190-201.

RAMOS, P., SANTOS, A., PINTO, N. R., MENDES, R., MAGALHÃES, T. & ALMEIDA, A. 2014b. Iron levels in the human brain: A post-mortem study of anatomical region differences and age-related changes. *Journal of Trace Elements in Medicine and Biology,* 28**,** 13-17.

RAN, J., ZHANG, Y., HAN, L., SUN, S., ZHAO, S., SHEN, C., ZHANG, X., CHAN, K.-P., LEE, R. S.-Y., QIU, Y. & TIAN, L. 2021. The joint association of physical activity and fine particulate matter exposure with incident dementia in elderly Hong Kong residents. *Environment International,* 156**,** 106645.

RANFT, U., SCHIKOWSKI, T., SUGIRI, D., KRUTMANN, J. & KRÄMER, U. 2009. Long-term exposure to traffic-related particulate matter impairs cognitive function in the elderly. *Environ Res,* 109**,** 1004-11.

RAO, K. J., RAO, R., SHANMUGAVELU, P. & MENON, R. 1999. Trace elements in Alzheimer's disease brain: a new hypothesis. *Alzheimers Rep,* 2**,** 241-46.

RAY, L., ILIFF, J. J. & HEYS, J. J. 2019. Analysis of convective and diffusive transport in the brain interstitium. *Fluids and Barriers of the CNS,* 16**,** 6.

REDDY, U. A., PRABHAKAR, P. V. & MAHBOOB, M. 2017. Biomarkers of oxidative stress for in vivo assessment of toxicological effects of iron oxide nanoparticles. *Saudi Journal of Biological Sciences,* 24**,** 1172-1180.

REGISTRY, A. F. T. S. A. D. 2012. TOXICOLOGICAL PROFILE FOR VANADIUM U.S. DEPARTMENT OF HEALTH.

REHMAN, M., LIU, L., WANG, Q., SALEEM, M. H., BASHIR, S., ULLAH, S. & PENG, D. 2019. Copper environmental toxicology, recent advances, and future outlook: a review. *Environmental Science and Pollution Research,* 26**,** 18003-18016.

RELIGA, D., STROZYK, D., CHERNY, R. A., VOLITAKIS, I., HAROUTUNIAN, V., WINBLAD, B., NASLUND, J. & BUSH, A. I. 2006. Elevated cortical zinc in Alzheimer disease. *Neurology,* 67**,** 69-75.

REMBACH, A., HARE, D. J., LIND, M., FOWLER, C. J., CHERNY, R. A., MCLEAN, C., BUSH, A. I., MASTERS, C. L. & ROBERTS, B. R. 2013. Decreased copper in Alzheimer's disease brain is predominantly in the soluble extractable fraction. *Int J Alzheimers Dis,* 2013**,** 623241.

REY, N. L., WESSON, D. W. & BRUNDIN, P. 2018. The olfactory bulb as the entry site for prion-like propagation in neurodegenerative diseases. *Neurobiology of Disease,* 109**,** 226-248.

RHEW, S. H., KRAVCHENKO, J. & LYERLY, H. K. 2021. Exposure to low-dose ambient fine particulate matter PM2.5 and Alzheimer's disease, non-Alzheimer's dementia, and Parkinson's disease in North Carolina. *PLOS ONE,* 16**,** e0253253.

RICE, K. M., WALKER, E. M., JR., WU, M., GILLETTE, C. & BLOUGH, E. R. 2014. Environmental mercury and its toxic effects. *Journal of preventive medicine and public health = Yebang Uihakhoe chi,* 47**,** 74-83.

RIES, M. & SASTRE, M. 2016. Mechanisms of Aβ Clearance and Degradation by Glial Cells. *Frontiers in Aging Neuroscience,* 8.

RIM, K. T., KOO, K. H. & PARK, J. S. 2013. Toxicological Evaluations of Rare Earths and Their Health Impacts to Workers: A Literature Review. *Safety and Health at Work,* 4**,** 12-26.

RIUS-PÉREZ, S., TORMOS, A. M., PÉREZ, S. & TALÉNS-VISCONTI, R. 2018. Vascular pathology: Cause or effect in Alzheimer disease? *Neurología (English Edition),* 33**,** 112-120.

RIVERS-AUTY, J., TAPIA, V. S., WHITE, C. S., DANIELS, M. J. D., DRINKALL, S., KENNEDY, P. T., SPENCE, H. G., YU, S., GREEN, J. P., HOYLE, C., COOK, J., BRADLEY, A., MATHER, A. E., PETERS, R., TZENG, T.-C., GORDON, M. J., BEATTIE, J. H., BROUGH, D. & LAWRENCE, C. B. 2021. Zinc Status Alters Alzheimer's Disease Progression through NLRP3-Dependent Inflammation. *The Journal of Neuroscience,* 41**,** 3025-3038.

ROGAWSKI, M. A. & WENK, G. L. 2003. The neuropharmacological basis for the use of memantine in the treatment of Alzheimer's disease. *CNS Drug Rev,* 9**,** 275-308.

ROGERS, J., BUSH, A., CHO, H.-H., SMITH, D., THOMSON, A., FRIEDLICH, A., LAHIRI, D. K., LEEDMAN, P., HUANG, X. & CAHILL, C. C. 2008. Iron and the translation of the amyloid precursor protein (APP) and ferritin: riboregulation against neural oxidative damage in Alzheimer's disease. *Biochemical Society transactions,* 36**,** 1282-1287.

ROGERS, J. T., RANDALL, J. D., CAHILL, C. M., EDER, P. S., HUANG, X., GUNSHIN, H., LEITER, L., MCPHEE, J., SARANG, S. S., UTSUKI, T., GREIG, N. H., LAHIRI, D. K., TANZI, R. E., BUSH, A. I., GIORDANO, T. & GULLANS, S. R. 2002. An Iron-responsive Element Type II in the 5'-Untranslated Region of the Alzheimer's Amyloid Precursor Protein Transcript*. *Journal of Biological Chemistry,* 277**,** 45518-45528.

ROMERO, T. 2021. *Total population in Mexico City between 2008 and 2018* [Online]. Available: https://www.statista.com/statistics/1038080/mexico-city-total-population/ [Accessed 26th August 2021].

ROUAULT, T. A. & COOPERMAN, S. 2006. Brain iron metabolism. *Semin Pediatr Neurol,* 13**,** 142-8.

ROUSSEAU, M.-C., STRAIF, K. & SIEMIATYCKI, J. 2005. IARC carcinogen update. *Environmental health perspectives,* 113**,** A580-A581.

ROWANGOULD, G. M. 2013. A census of the US near-roadway population: Public health and environmental justice considerations. *Transportation Research Part D: Transport and Environment,* 25**,** 59-67.

RULON, L. L., ROBERTSON, J. D., LOVELL, M. A., DEIBEL, M. A., EHMANN, W. D. & MARKESBER, W. R. 2000. Serum zinc levels and Alzheimer's disease. *Biol Trace Elem Res,* 75**,** 79-85.

RŸB, U., STRATMANN, K., HEINSEN, H., DEL TURCO, D., SEIDEL, K., DEN DUNNEN, W. & KORF, H. W. 2016. The brainstem tau cytoskeletal pathology of Alzheimer's disease: A brief historical overview and description of its anatomical distribution pattern, evolutional features, pathogenetic and clinical relevance. *Current Alzheimer Research,* 13**,** 1178-1197.

SAFFARI, A., DAHER, N., SHAFER, M. M., SCHAUER, J. J. & SIOUTAS, C. 2014. Global Perspective on the Oxidative Potential of Airborne Particulate Matter: A Synthesis of Research Findings. *Environmental Science & Technology,* 48**,** 7576-7583.

SAHMOUN, A. E., CASE, L. D., JACKSON, S. A. & SCHWARTZ, G. G. 2005. Cadmium and Prostate Cancer: A Critical Epidemiologic Analysis. *Cancer Investigation,* 23**,** 256-263.

SAHU, S. K., BEIG, G. & PARKHI, N. S. 2011. Emissions inventory of anthropogenic PM2.5 and PM10 in Delhi during Commonwealth Games 2010. *Atmospheric Environment,* 45**,** 6180-6190.

SAKONO, M. & ZAKO, T. 2010. Amyloid oligomers: formation and toxicity of Aβ oligomers. *FEBS Journal,* 277**,** 1348-1358.

SALAT, D. H., BUCKNER, R. L., SNYDER, A. Z., GREVE, D. N., DESIKAN, R. S., BUSA, E., MORRIS, J. C., DALE, A. M. & FISCHL, B. 2004. Thinning of the cerebral cortex in aging. *Cereb Cortex,* 14**,** 721-30.

SALAZAR, J., MENA, N. & NUNEZ, M. T. 2006. Iron dyshomeostasis in Parkinson's disease. *J Neural Transm Suppl***,** 205-13.

SALINAS-RODRÍGUEZ, A., FERNÁNDEZ-NIÑO, J. A., MANRIQUE-ESPINOZA, B., MORENO-BANDA, G. L., SOSA-ORTIZ, A. L., QIAN, Z. & LIN, H. 2018. Exposure to ambient PM2.5 concentrations and cognitive function among older Mexican adults. *Environment International,* 117**,** 1-9.

SALO, L., HYVÄRINEN, A., JALAVA, P., TEINILÄ, K., HOODA, R. K., DATTA, A., SAARIKOSKI, S., LINTUSAARI, H., LEPISTÖ, T., MARTIKAINEN, S., ROSTEDT, A., SHARMA, V. P., RAHMAN, M. H., SUBUDHI, S., ASMI, E., NIEMI, J. V., LIHAVAINEN, H., LAL, B., KESKINEN, J., KUULUVAINEN, H., TIMONEN, H. & RÖNKKÖ, T. 2021. The characteristics and size of lung-depositing particles vary significantly between high and low pollution traffic environments. *Atmospheric Environment,* 255**,** 118421.

SAMUDRALWAR, D. L., DIPRETE, C. C., NI, B. F., EHMANN, W. D. & MARKESBERY, W. R. 1995. Elemental imbalances in the olfactory pathway in Alzheimer's disease. *J Neurol Sci,* 130**,** 139-45.

SANDERSON, P., SU, S. S., CHANG, I. T. H., DELGADO SABORIT, J. M., KEPAPTSOGLOU, D. M., WEBER, R. J. M. & HARRISON, R. M. 2016. Characterisation of iron-rich atmospheric submicrometre particles in the roadside environment. *Atmospheric Environment,* 140**,** 167-175.

SANGANI, R. G., SOUKUP, J. M. & GHIO, A. J. 2010. Metals in air pollution particles decrease whole-blood coagulation time. *Inhalation Toxicology,* 22**,** 621-626.

SANT'OVAIA, H., MARQUES, G., SANTOS, A., GOMES, C. & ROCHA, A. 2015. Magnetic susceptibility and isothermal remanent magnetization in human tissues: a study case. *Biometals,* 28**,** 951-8.

SAPTARSHI, S. R., DUSCHL, A. & LOPATA, A. L. 2013. Interaction of nanoparticles with proteins: Relation to bio-reactivity of the nanoparticle. *Journal of Nanobiotechnology,* 11.

SASTRE, M., RITCHIE, C. & HAJJI, N. 2015. Metal Ions in Alzheimer's disease brain. *JSM Alzheimer's Disease and Related Dementia*.

SCAIANO, J., MONAHAN, S. & RENAUD, J. 2008. Dramatic Effect of Magnetite Particles on the Dynamics of Photogenerated Free Radicals. *Photochemistry and Photobiology,* 65**,** 759-762.

SCHEIBER, I. F., MERCER, J. F. B. & DRINGEN, R. 2014. Metabolism and functions of copper in brain. *Progress in Neurobiology,* 116**,** 33-57.

SCHEUNER, D., ECKMAN, C., JENSEN, M., SONG, X., CITRON, M., SUZUKI, N., BIRD, T. D., HARDY, J., HUTTON, M., KUKULL, W., LARSON, E., LEVY-LAHAD, L., VIITANEN, M., PESKIND, E., POORKAJ, P., SCHELLENBERG, G., TANZI, R., WASCO, W., LANNFELT, L., SELKOE, D. & YOUNKIN, S. 1996. Secreted amyloid [beta]-protein similar to that in the senile plaques of Alzheimer's disease is increased in vivo by the presenilin 1 and 2 and APP mutations linked to familial Alzheimer's disease. *Nat Med,* 2**,** 864-870.

SCHIKOWSKI, T., VOSSOUGHI, M., VIERKÖTTER, A., SCHULTE, T., TEICHERT, T., SUGIRI, D., FEHSEL, K., TZIVIAN, L., BAE, I.-S., RANFT, U., HOFFMANN, B., PROBST-HENSCH, N., HERDER, C., KRÄMER, U. & LUCKHAUS, C. 2015. Association of air pollution with

cognitive functions and its modification by APOE gene variants in elderly women. *Environmental Research,* 142**,** 10-16.

SCHOLEFIELD, M., CHURCH, S. J., XU, J., KASSAB, S., GARDINER, N. J., RONCAROLI, F., HOOPER, N. M., UNWIN, R. D. & COOPER, G. J. S. 2020. Evidence that levels of nine essential metals in post-mortem human-Alzheimer's-brain and ex vivo rat-brain tissues are unaffected by differences in post-mortem delay, age, disease staging, and brain bank location. *Metallomics,* 12**,** 952-962.

SCHOLEFIELD, M., CHURCH, S. J., XU, J., PATASSINI, S., RONCAROLI, F., HOOPER, N. M., UNWIN, R. D. & COOPER, G. J. S. 2021. Widespread Decreases in Cerebral Copper Are Common to Parkinson's Disease Dementia and Alzheimer's Disease Dementia. *Frontiers in Aging Neuroscience,* 13.

SCHRAG, M., CROFTON, A., ZABEL, M., JIFFRY, A., KIRSCH, D., DICKSON, A., MAO, X. W., VINTERS, H. V., DOMAILLE, D. W., CHANG, C. J. & KIRSCH, W. 2011a. Effect of cerebral amyloid angiopathy on brain iron, copper, and zinc in Alzheimer's disease. *Journal of Alzheimer's disease : JAD,* 24**,** 137-149.

SCHRAG, M., DICKSON, A., JIFFRY, A., KIRSCH, D., VINTERS, H. V. & KIRSCH, W. 2010. The effect of formalin fixation on the levels of brain transition metals in archived samples. *Biometals,* 23**,** 1123-7.

SCHRAG, M., MUELLER, C., OYOYO, U., SMITH, M. A. & KIRSCH, W. M. 2011b. Iron, zinc and copper in the Alzheimer's disease brain: A quantitative meta-analysis. Some insight on the influence of citation bias on scientific opinion. *Progress in Neurobiology,* 94**,** 296-306.

SCHRAND, A. M., SCHLAGER, J. J., DAI, L. & HUSSAIN, S. M. 2010. Preparation of cells for assessing ultrastructural localization of nanoparticles with transmission electron microscopy. *Nature Protocols,* 5**,** 744-757.

SCHULTHEISS-GRASSI, P. P., WESSIKEN, R. & DOBSON, J. 1999. TEM investigations of biogenic magnetite extracted from the human hippocampus. *Biochimica et Biophysica Acta (BBA) - General Subjects,* 1426**,** 212-216.

SEAGRAVE, J., CAMPEN, M. J., MCDONALD, J. D., MAUDERLY, J. L. & ROHR, A. C. 2008. Oxidative Stress, Inflammation, and Pulmonary Function Assessment in Rats Exposed to Laboratory-Generated Pollutant Mixtures. *Journal of Toxicology and Environmental Health, Part A,* 71**,** 1352-1362.

SEDEMA. 2021. *Mexico City Air Quality Monitoring System public database* [Online]. Available: http://www.aire.cdmx.gob.mx/default.php [Accessed 26th August 2021].

SEO, S.-J., CHANG, W.-S., JEON, J.-G., CHOI, Y., KIM, E. & KIM, J.-K. 2021. Proton Stimulation Targeting Plaque Magnetite Reduces Amyloid-β Plaque and Iron Redox Toxicity and Improves Memory in an Alzheimer's Disease Mouse Model. *Journal of Alzheimer's Disease,* 84**,** 377-392.

SEVIGNY, J., CHIAO, P., BUSSIERE, T., WEINREB, P. H., WILLIAMS, L., MAIER, M., DUNSTAN, R., SALLOWAY, S., CHEN, T., LING, Y., O'GORMAN, J., QIAN, F., ARASTU, M., LI, M. W., CHOLLATE, S., BRENNAN, M. S., QUINTERO-MONZON, O., SCANNEVIN, R. H., ARNOLD, H. M., ENGBER, T., RHODES, K., FERRERO, J., HANG, Y. M., MIKULSKIS, A., GRIMM, J., HOCK, C., NITSCH, R. M. & SANDROCK, A. 2016. The antibody aducanumab reduces A beta plaques in Alzheimer's disease. *Nature,* 537**,** 50-56.

SHAFEI, R., WOOLLACOTT, I. O. C., MUMMERY, C. J., BOCCHETTA, M., GUERREIRO, R., BRAS, J., WARREN, J. D., LASHLEY, T., JAUNMUKTANE, Z. & ROHRER, J. D. 2020. Two pathologically confirmed cases of novel mutations in the MAPT gene causing frontotemporal dementia. *Neurobiology of Aging,* 87**,** 141.e15-141.e20.

SHAFFER, R. M., BLANCO, M. N., LI, G., ADAR, S. D., CARONE, M., SZPIRO, A. A., KAUFMAN, J. D., LARSON, T. V., LARSON, E. B., CRANE, P. K. & SHEPPARD, L. 2021. Fine Particulate

Matter and Dementia Incidence in the Adult Changes in Thought Study. *Environmental Health Perspectives,* 129**,** 087001.

SHAHMORADIAN, S. H., LEWIS, A. J., GENOUD, C., HENCH, J., MOORS, T. E., NAVARRO, P. P., CASTAÑO-DÍEZ, D., SCHWEIGHAUSER, G., GRAFF-MEYER, A., GOLDIE, K. N., SÜTTERLIN, R., HUISMAN, E., INGRASSIA, A., GIER, Y., ROZEMULLER, A. J. M., WANG, J., PAEPE, A. D., ERNY, J., STAEMPFLI, A., HOERNSCHEMEYER, J., GROßERÜSCHKAMP, F., NIEDIEKER, D., EL-MASHTOLY, S. F., QUADRI, M., VAN IJCKEN, W. F. J., BONIFATI, V., GERWERT, K., BOHRMANN, B., FRANK, S., BRITSCHGI, M., STAHLBERG, H., VAN DE BERG, W. D. J. & LAUER, M. E. 2019. Lewy pathology in Parkinson's disease consists of crowded organelles and lipid membranes. *Nature Neuroscience,* 22**,** 1099-1109.

SHANG, N., ZHANG, P., WANG, S., CHEN, J., FAN, R., CHEN, J., HUANG, T., WANG, Y., DUNCAN, J., ZHANG, L., NIU, Q. & ZHANG, Q. 2020. Aluminum-Induced Cognitive Impairment and PI3K/Akt/mTOR Signaling Pathway Involvement in Occupational Aluminum Workers. *Neurotoxicity Research,* 38**,** 344-358.

SHARP, E. S. & GATZ, M. 2011. Relationship between education and dementia: an updated systematic review. *Alzheimer disease and associated disorders,* 25**,** 289-304.

SHEYKHANSARI, S., KOZIELSKI, K., BILL, J., SITTI, M., GEMMATI, D., ZAMBONI, P. & SINGH, A. V. 2018. Redox metals homeostasis in multiple sclerosis and amyotrophic lateral sclerosis: a review. *Cell Death & Disease,* 9**,** 348.

SHI, L., STEENLAND, K., LI, H., LIU, P., ZHANG, Y., LYLES, R. H., REQUIA, W. J., ILANGO, S. D., CHANG, H. H., WINGO, T., WEBER, R. J. & SCHWARTZ, J. 2021. A national cohort study (2000–2018) of long-term air pollution exposure and incident dementia in older adults in the United States. *Nature Communications,* 12**,** 6754.

SHI, L., WU, X., DANESH YAZDI, M., BRAUN, D., ABU AWAD, Y., WEI, Y., LIU, P., DI, Q., WANG, Y., SCHWARTZ, J., DOMINICI, F., KIOUMOURTZOGLOU, M.-A. & ZANOBETTI, A. 2020. Long-term effects of PM2.5 on neurological disorders in the American Medicare population: a longitudinal cohort study. *The Lancet Planetary Health,* 4**,** e557-e565.

SHUKLA, A., TIMBLIN, C., BERUBE, K., GORDON, T., MCKINNEY, W., DRISCOLL, K., VACEK, P. & MOSSMAN, B. T. 2000. Inhaled particulate matter causes expression of nuclear factor (NF)-kappaB-related genes and oxidant-dependent NF-kappaB activation in vitro. *Am J Respir Cell Mol Biol,* 23**,** 182-7.

SKJØRRINGE, T., BURKHART, A., JOHNSEN, K. B. & MOOS, T. 2015. Divalent metal transporter 1 (DMT1) in the brain: implications for a role in iron transport at the blood-brain barrier, and neuronal and glial pathology. *Frontiers in Molecular Neuroscience,* 8.

SMITH, N. M., GACHULINCOVA, I., HO, D., BAILEY, C., BARTLETT, C. A., NORRET, M., MURPHY, J., BUCKLEY, A., RIGBY, P. J., HOUSE, M. J., ST. PIERRE, T., FITZGERALD, M., IYER, K. S. & DUNLOP, S. A. 2016. An Unexpected Transient Breakdown of the Blood Brain Barrier Triggers Passage of Large Intravenously Administered Nanoparticles. *Scientific Reports,* 6**,** 22595.

SNOW, S. J., HENRIQUEZ, A. R., COSTA, D. L. & KODAVANTI, U. P. 2018. Neuroendocrine Regulation of Air Pollution Health Effects: Emerging Insights. *Toxicological Sciences,* 164**,** 9-20.

SOENEN, S. J. H., HIMMELREICH, U., NUYTTEN, N., PISANIC II, T. R., FERRARI, A. & DE CUYPER, M. 2010. Intracellular Nanoparticle Coating Stability Determines Nanoparticle Diagnostics Efficacy and Cell Functionality. *Small,* 6.

SOKOLOVA, V., MEKKY, G., VAN DER MEER, S. B., SEEDS, M. C., ATALA, A. J. & EPPLE, M. 2020. Transport of ultrasmall gold nanoparticles (2 nm) across the blood–brain barrier in a six-cell brain spheroid model. *Scientific Reports,* 10**,** 18033.

SOLAIMANI, P., SAFFARI, A., SIOUTAS, C., BONDY, S. C. & CAMPBELL, A. 2017. Exposure to ambient ultrafine particulate matter alters the expression of genes in primary human neurons. *NeuroToxicology,* 58**,** 50-57.

SONAWANE, S. K., AHMAD, A. & CHINNATHAMBI, S. 2019. Protein-Capped Metal Nanoparticles Inhibit Tau Aggregation in Alzheimer's Disease. *ACS omega,* 4**,** 12833-12840.

SQUIRE, L. R., STARK, C. E. L. & CLARK, R. E. 2004. THE MEDIAL TEMPORAL LOBE. *Annual Review of Neuroscience,* 27**,** 279-306.

SQUITTI, R., VENTRIGLIA, M., SIMONELLI, I., BONVICINI, C., COSTA, A., PERINI, G., BINETTI, G., BENUSSI, L., GHIDONI, R., KOCH, G., BORRONI, B., ALBANESE, A., SENSI, S. L. & RONGIOLETTI, M. 2021. Copper Imbalance in Alzheimer's Disease: Meta-Analysis of Serum, Plasma, and Brain Specimens, and Replication Study Evaluating ATP7B Gene Variants. *Biomolecules,* 11.

SRIVASTAVA, R. A. & JAIN, J. C. 2002. Scavenger receptor class B type I expression and elemental analysis in cerebellum and parietal cortex regions of the Alzheimer's disease brain. *J Neurol Sci,* 196**,** 45-52.

STEDMAN, J. D. & SPYROU, N. M. 1995. Major and trace element concentration differences between the right and left hemispheres of the "normal' human brain. *Nutrition,* 11**,** 542-5.

STEDMAN, J. D. & SPYROU, N. M. 1997. Elemental analysis of the frontal lobe of “normal” brain tissue and that affected by Alzheimer's disease. *Journal of Radioanalytical and Nuclear Chemistry,* 217**,** 163-166.

STEELANT, B., FARRÉ, R., WAWRZYNIAK, P., BELMANS, J., DEKIMPE, E., VANHEEL, H., VAN GERVEN, L., KORTEKAAS KROHN, I., BULLENS, D. M. A., CEUPPENS, J. L., AKDIS, C. A., BOECKXSTAENS, G., SEYS, S. F. & HELLINGS, P. W. 2016. Impaired barrier function in patients with house dust mite-induced allergic rhinitis is accompanied by decreased occludin and zonula occludens-1 expression. *J Allergy Clin Immunol,* 137**,** 1043-1053.e5.

STOHS, S. J. & BAGCHI, D. 1995. Oxidative mechanisms in the toxicity of metal ions. *Free Radic Biol Med,* 18**,** 321-36.

STOJSAVLJEVIĆ, A., VUJOTIĆ, L., ROVČANIN, B., BORKOVIĆ-MITIĆ, S., GAVROVIĆ-JANKULOVIĆ, M. & MANOJLOVIĆ, D. 2020. Assessment of trace metal alterations in the blood, cerebrospinal fluid and tissue samples of patients with malignant brain tumors. *Scientific Reports,* 10**,** 3816.

STRIETER, R. M. 2002. Interleukin-8: a very important chemokine of the human airway epithelium. *Am J Physiol Lung Cell Mol Physiol,* 283**,** L688-9.

SU, J. G., APTE, J. S., LIPSITT, J., GARCIA-GONZALES, D. A., BECKERMAN, B. S., DE NAZELLE, A., TEXCALAC-SANGRADOR, J. L. & JERRETT, M. 2015. Populations potentially exposed to traffic-related air pollution in seven world cities. *Environment International,* 78**,** 82-89.

SUMMERS, K. L., ROSEMAN, G., SCHILLING, K. M., DOLGOVA, N. V., PUSHIE, M. J., SOKARAS, D., KROLL, T., HARRIS, H. H., MILLHAUSER, G. L., PICKERING, I. J. & GEORGE, G. N. 2022. Alzheimer’s Drug PBT2 Interacts with the Amyloid β 1–42 Peptide Differently than Other 8-Hydroxyquinoline Chelating Drugs. *Inorganic Chemistry,* 61**,** 14626-14640.

SUN, H., BROCATO, J. & COSTA, M. 2015. Oral Chromium Exposure and Toxicity. *Current environmental health reports,* 2**,** 295-303.

SUN, J., YU, J., SHEN, Z., NIU, X., WANG, D., WANG, X., XU, H., CHUANG, H.-C., CAO, J. & HO, K.-F. 2021. Oxidative stress–inducing effects of various urban PM2.5 road dust on human lung epithelial cells among 10 Chinese megacities. *Ecotoxicology and Environmental Safety,* 224**,** 112680.

SUN, R., WANG, J., FENG, J. & CAO, B. 2022. Zinc in Cognitive Impairment and Aging. *Biomolecules,* 12.

SUNDAR, S. & CHAKRAVARTY, J. 2010. Antimony toxicity. *International journal of environmental research and public health,* 7**,** 4267-4277.

SUNGUR, Ş., KAYA, P. & KOROGLU, M. 2020. Determination of titanium dioxide nanoparticles used in various foods. *Food Additives and Contaminants: Part B Surveillance,* 13**,** 260-267.

SUNYER, J., ESNAOLA, M., ALVAREZ-PEDREROL, M., FORNS, J., RIVAS, I., LÓPEZ-VICENTE, M., SUADES-GONZÁLEZ, E., FORASTER, M., GARCIA-ESTEBAN, R., BASAGAÑA, X., VIANA, M., CIRACH, M., MORENO, T., ALASTUEY, A., SEBASTIAN-GALLES, N., NIEUWENHUIJSEN, M. & QUEROL, X. 2015. Association between Traffic-Related Air Pollution in Schools and Cognitive Development in Primary School Children: A Prospective Cohort Study. *PLOS Medicine,* 12**,** e1001792.

SVOBODOVÁ, H., HLINKOVÁ, J., JANEGA, P., KOSNÁČ, D., FILOVÁ, B., MIGLIERINI, M., DLHÁŇ, Ľ., EHRLICH, H., VALIGURA, D., BOČA, R., POLÁK, Š., NAGY, Š. & KOPÁNI, M. 2019. Deposits of iron oxides in the human globus pallidus. *Open Physics,* 17**,** 291.

SWEENEY, M. D., SAGARE, A. P. & ZLOKOVIC, B. V. 2018. Blood–brain barrier breakdown in Alzheimer disease and other neurodegenerative disorders. *Nature Reviews Neurology,* 14**,** 133-150.

SZABO, S. T., HARRY, G. J., HAYDEN, K. M., SZABO, D. T. & BIRNBAUM, L. 2015. Comparison of Metal Levels between Postmortem Brain and Ventricular Fluid in Alzheimer's Disease and Nondemented Elderly Controls. *Toxicological Sciences,* 150**,** 292-300.

TAHIRBEGI, I. B., PARDO, W. A., ALVIRA, M., MIR, M. & SAMITIER, J. 2016. Amyloid Abeta 42, a promoter of magnetite nanoparticle formation in Alzheimer's disease. *Nanotechnology,* 27**,** 465102.

TAKAO, M., HIROSE, N., ARAI, Y., MIHARA, B. & MIMURA, M. 2016. Neuropathology of supercentenarians - four autopsy case studies. *Acta Neuropathologica Communications,* 4**,** 97.

TAN, L. C., NANCHARAIAH, Y. V., VAN HULLEBUSCH, E. D. & LENS, P. N. L. 2016. Selenium: environmental significance, pollution, and biological treatment technologies. *Biotechnology Advances,* 34**,** 886-907.

TANTRA, R., TOMPKINS, J. & QUINCEY, P. 2010. Characterisation of the de-agglomeration effects of bovine serum albumin on nanoparticles in aqueous suspension. *Colloids and Surfaces B: Biointerfaces,* 75**,** 275-281.

TAO, Y., WANG, Y., ROGERS, J. T. & WANG, F. 2014. Perturbed iron distribution in Alzheimer's disease serum, cerebrospinal fluid, and selected brain regions: a systematic review and meta-analysis. *J Alzheimers Dis,* 42**,** 679-90.

TELLER, S., TAHIRBEGI, I. B., MIR, M., SAMITIER, J. & SORIANO, J. 2015. Magnetite-Amyloid-β deteriorates activity and functional organization in an in vitro model for Alzheimer's disease. *Scientific Reports,* 5**,** 17261.

TELLING, N. D., EVERETT, J., COLLINGWOOD, J. F., DOBSON, J., VAN DER LAAN, G., GALLAGHER, J. J., WANG, J. & HITCHCOCK, A. P. 2017. Iron Biochemistry is Correlated with Amyloid Plaque Morphology in an Established Mouse Model of Alzheimer's Disease. *Cell Chem Biol,* 24**,** 1205-1215.e3.

THAL, D. R., RÜB, U., ORANTES, M. & BRAAK, H. 2002. Phases of Aβ-deposition in the human brain and its relevance for the development of AD. *Neurology,* 58**,** 1791-1800.

THOMSON, E. M. 2019. Air Pollution, Stress, and Allostatic Load: Linking Systemic and Central Nervous System Impacts. *Journal of Alzheimer's Disease,* 69**,** 597-614.

THORN, J. 2001. The inflammatory response in humans after inhalation of bacterial endotoxin: a review. *Inflamm Res,* 50**,** 254-61.

THORPE, A. & HARRISON, R. M. 2008. Sources and properties of non-exhaust particulate matter from road traffic: A review. *Science of The Total Environment,* 400**,** 270-282.

TIMMEL, C. R., TILL, U., BROCKLEHURST, B., MCLAUCHLAN, K. A. & HORE, P. J. 1998. Effects of weak magnetic fields on free radical recombination reactions. *Molecular Physics,* 95**,** 71-89.

TIRA, R., DE CECCO, E., RIGAMONTI, V., SANTAMBROGIO, C., BARRACCHIA, C. G., MUNARI, F., ROMEO, A., LEGNAME, G., PROSPERI, D., GRANDORI, R. & ASSFALG, M. 2020. Dynamic molecular exchange and conformational transitions of alpha-synuclein at the nano-bio interface. *International Journal of Biological Macromolecules,* 154**,** 206-216.

TIWARY, C. S., KISHORE, S., VASIREDDI, R., MAHAPATRA, D. R., AJAYAN, P. M. & CHATTOPADHYAY, K. 2017. Electronic waste recycling via cryo-milling and nanoparticle beneficiation. *Materials Today,* 20**,** 67-73.

TOMÉ, S. O., VANDENBERGHE, R., OSPITALIERI, S., VAN SCHOOR, E., TOUSSEYN, T., OTTO, M., VON ARNIM, C. A. F. & THAL, D. R. 2020. Distinct molecular patterns of TDP-43 pathology in Alzheimer's disease: Relationship with clinical phenotypes. *Acta Neuropathologica Communications,* 8.

TONNE, C., ELBAZ, A., BEEVERS, S. & SINGH-MANOUX, A. 2014. Traffic-related air pollution in relation to cognitive function in older adults. *Epidemiology,* 25**,** 674-81.

TORRES-JARDÓN, R. & SOSA NÚÑEZ, G. S. 2018. Políticas públicas y su efecto en la calidad del aire de la Zona Metropolitana de la Ciudad de México. *Tranversalidad de la Política del Aire en México***,** 43-74.

TOZZI, L., STAVELAND, B., HOLT-GOSSELIN, B., CHESNUT, M., CHANG, S. E., CHOI, D., SHINER, M., WU, H., LERMA-USABIAGA, G., SPORNS, O., BARCH, D. M., GOTLIB, I. H., HASTIE, T. J., KERR, A. B., POLDRACK, R. A., WANDELL, B. A., WINTERMARK, M. & WILLIAMS, L. M. 2020. The human connectome project for disordered emotional states: Protocol and rationale for a research domain criteria study of brain connectivity in young adult anxiety and depression. *NeuroImage,* 214.

TRIST, B. G., HARE, D. J. & DOUBLE, K. L. 2018. A Proposed Mechanism for Neurodegeneration in Movement Disorders Characterized by Metal Dyshomeostasis and Oxidative Stress. *Cell Chemical Biology,* 25**,** 807-816.

TSAI, D.-H., AMYAI, N., MARQUES-VIDAL, P., WANG, J.-L., RIEDIKER, M., MOOSER, V., PACCAUD, F., WAEBER, G., VOLLENWEIDER, P. & BOCHUD, M. 2012. Effects of particulate matter on inflammatory markers in the general adult population. *Particle and Fibre Toxicology,* 9**,** 24.

TSUBOI, Y., WSZOLEK, Z. K., GRAFF-RADFORD, N. R., COOKSON, N. & DICKSON, D. W. 2003. Tau pathology in the olfactory bulb correlates with Braak stage, Lewy body pathology and apolipoprotein ε4. *Neuropathology and Applied Neurobiology,* 29**,** 503-510.

TUNG, N. T., HO, K.-F., NIU, X., SUN, J., SHEN, Z., WU, F., CAO, J., DUNG, H. B., THUY, T. P. C., HSIAO, T.-C., LIU, W.-T. & CHUANG, H.-C. 2021. Loss of E-cadherin due to road dust PM2.5 activates the EGFR in human pharyngeal epithelial cells. *Environmental Science and Pollution Research*.

VAN DE WALLE, A., FROMAIN, A., SANGNIER, A. P., CURCIO, A., LENGLET, L., MOTTE, L., LALATONNE, Y. & WILHELM, C. 2020a. Real-time in situ magnetic measurement of the intracellular biodegradation of iron oxide nanoparticles in a stem cell-spheroid tissue model. *Nano Research,* 13**,** 467-476.

VAN DE WALLE, A., KOLOSNJAJ-TABI, J., LALATONNE, Y. & WILHELM, C. 2020b. Ever-Evolving Identity of Magnetic Nanoparticles within Human Cells: The Interplay of Endosomal Confinement, Degradation, Storage, and Neocrystallization. *Accounts of Chemical Research,* 53**,** 2212-2224.

VAN DE WALLE, A., PLAN SANGNIER, A., ABOU-HASSAN, A., CURCIO, A., HÉMADI, M., MENGUY, N., LALATONNE, Y., LUCIANI, N. & WILHELM, C. 2019. Biosynthesis of magnetic nanoparticles from nano-degradation products revealed in human stem cells. *Proceedings of the National Academy of Sciences,* 116**,** 4044-4053.

VAN DEN BERG, N. S., HUITEMA, R. B., SPIKMAN, J. M., LUIJCKX, G. J. & DE HAAN, E. H. F. 2020. Impairments in Emotion Recognition and Risk-Taking Behavior After Isolated, Cerebellar Stroke. *Cerebellum,* 19**,** 419-425.

VAN DER WEERD, L., LEFERING, A., WEBB, A., EGLI, R. & BOSSONI, L. 2020. Effects of Alzheimer's disease and formalin fixation on the different mineralised-iron forms in the human brain. *Scientific Reports,* 10**,** 16440.

VAN HOESEN, G. W., HYMAN, B. T. & DAMASIO, A. R. 1991. Entorhinal cortex pathology in Alzheimer's disease. *Hippocampus,* 1**,** 1-8.

VANDEN BERGHE, T., KALAI, M., DENECKER, G., MEEUS, A., SAELENS, X. & VANDENABEELE, P. 2006. Necrosis is associated with IL-6 production but apoptosis is not. *Cell Signal,* 18**,** 328-35.

VANNELLA, K. M. & WYNN, T. A. 2017. Mechanisms of Organ Injury and Repair by Macrophages∗. *Annual Review of Physiology.*

VÁRADI, C. 2020. Clinical features of parkinson's disease: The evolution of critical symptoms. *Biology,* 9.

VARIKASUVU, S. R., PRASAD V, S., KOTHAPALLI, J. & MANNE, M. 2019. Brain Selenium in Alzheimer's Disease (BRAIN SEAD Study): a Systematic Review and Meta-Analysis. *Biological Trace Element Research,* 189**,** 361-369.

VELASCO, E. & RETAMA, A. 2017. Ozone's threat hits back Mexico city. *Sustainable Cities and Society,* 31**,** 260-263.

VENKATACHARI, P., HOPKE, P. K., BRUNE, W. H., REN, X., LESHER, R., MAO, J. & MITCHELL, M. 2007. Characterization of Wintertime Reactive Oxygen Species Concentrations in Flushing, New York. *Aerosol Science and Technology,* 41**,** 97-111.

VENKATRAMAN, A., EDLOW, B. L. & IMMORDINO-YANG, M. H. 2017. The brainstem in emotion: A review. *Frontiers in Neuroanatomy,* 11.

VERANTH, J. M., KASER, E. G., VERANTH, M. M., KOCH, M. & YOST, G. S. 2007. Cytokine responses of human lung cells (BEAS-2B) treated with micron-sized and nanoparticles of metal oxides compared to soil dusts. *Part Fibre Toxicol,* 4**,** 2.

VERANTH, J. M., MOSS, T. A., CHOW, J. C., LABBAN, R., NICHOLS, W. K., WALTON, J. C., WATSON, J. G. & YOST, G. S. 2006. Correlation of in vitro cytokine responses with the chemical composition of soil-derived particulate matter. *Environmental health perspectives,* 114**,** 341-349.

VERMA, M. K., POOJAN, S., SULTANA, S. & KUMAR, S. 2014. Mammalian cell-transforming potential of traffic-linked ultrafine particulate matter PM0.056 in urban roadside atmosphere. *Mutagenesis,* 29**,** 335-340.

VERMA, V., SHAFER, M. M., SCHAUER, J. J. & SIOUTAS, C. 2010. Contribution of transition metals in the reactive oxygen species activity of PM emissions from retrofitted heavy-duty vehicles. *Atmospheric Environment,* 44**,** 5165-5173.

VERWEY, E. J. W. 1939. Electronic Conduction of Magnetite (Fe3O4) and its Transition Point at Low Temperatures. *Nature,* 144**,** 327-328.

VIETTI, G., IBOURAADATEN, S., PALMAI-PALLAG, M., YAKOUB, Y., BAILLY, C., FENOGLIO, I., MARBAIX, E., LISON, D. & VAN DEN BRULE, S. 2013. Towards predicting the lung fibrogenic activity of nanomaterials: experimental validation of an in vitro fibroblast proliferation assay. *Particle and fibre toxicology,* 10**,** 52-52.

VILLALOBOS-PIETRINI, R., AMADOR-MUÑOZ, O., VALLE-HERNÁNDEZ, B. L., GÓMEZ-ARROYO, S., WALISZEWSKI, S. & JAZCILEVICH, A. D. 2011. Organic compound in airborne particles and their genotoxic effects in Mexico city. *Air Quality Monitoring, Assessment and Management, Nicolás A. Mazzeo***,** 345-378.

VIRK, S. A. & ESLICK, G. D. 2015. Brief Report: Meta-analysis of Antacid Use and Alzheimer's Disease: Implications for the Aluminum Hypothesis. *Epidemiology,* 26**,** 769-773.

VYSKOCIL, A. & VIAU, C. 1999. Assessment of molybdenum toxicity in humans. *J Appl Toxicol,* 19**,** 185-92.

WALLENBORN, J. G., MCGEE, J. K., SCHLADWEILER, M. C., LEDBETTER, A. D. & KODAVANTI, U. P. 2007. Systemic Translocation of Particulate Matter–Associated Metals Following a Single Intratracheal Instillation in Rats. *Toxicological Sciences,* 98**,** 231-239.

WALSH, D. M., KLYUBIN, I., FADEEVA, J. V., CULLEN, W. K., ANWYL, R., WOLFE, M. S., ROWAN, M. J. & SELKOE, D. J. 2002. Naturally secreted oligomers of amyloid beta protein potently inhibit hippocampal long-term potentiation in vivo. *Nature,* 416**,** 535-9.

WANG, B., YIN, J.-J., ZHOU, X., KURASH, I., CHAI, Z., ZHAO, Y. & FENG, W. 2013. Physicochemical Origin for Free Radical Generation of Iron Oxide Nanoparticles in Biomicroenvironment: Catalytic Activities Mediated by Surface Chemical States. *The Journal of Physical Chemistry C,* 117**,** 383-392.

WANG, C. X., HILBURN, I. A., WU, D.-A., MIZUHARA, Y., COUSTÉ, C. P., ABRAHAMS, J. N. H., BERNSTEIN, S. E., MATANI, A., SHIMOJO, S. & KIRSCHVINK, J. L. 2019a. Transduction of the Geomagnetic Field as Evidenced from alpha-Band Activity in the Human Brain. *eneuro,* 6**,** ENEURO.0483-18.2019.

WANG, F. H., KIM, D. K., YOSHITAKE, T., JOHANSSON, S. M., BJELKE, B., MUHAMMED, M. & KEHR, J. 2011. Diffusion and clearance of superparamagnetic iron oxide nanoparticles infused into the rat striatum studied by MRI and histochemical techniques. *Nanotechnology,* 22**,** 015103.

WANG, G., ZHANG, G., GAO, X., ZHANG, Y., FAN, W., JIANG, J., AN, Z., LI, J., SONG, J. & WU, W. 2020a. Oxidative stress-mediated epidermal growth factor receptor activation regulates PM(2.5)-induced over-secretion of pro-inflammatory mediators from human bronchial epithelial cells. *Biochim Biophys Acta Gen Subj,* 1864**,** 129672.

WANG, J., LI, S., LI, H., QIAN, X., LI, X., LIU, X., LU, H., WANG, C. & SUN, Y. 2017. Trace metals and magnetic particles in PM2.5: Magnetic identification and its implications. *Scientific Reports,* 7**,** 9865.

WANG, R. & REDDY, P. H. 2017. Role of Glutamate and NMDA Receptors in Alzheimer's Disease. *Journal of Alzheimer's Disease,* 57**,** 1041-1048.

WANG, S., ZHANG, B., SU, L., NIE, W., HAN, D., HAN, G., ZHANG, H., CHONG, C. & TAN, J. 2019b. Subcellular distributions of iron oxide nanoparticles in rat brains affected by different surface modifications. *Journal of Biomedical Materials Research - Part A,* 107**,** 1988-1998.

WANG, T. S., COPPENS, I., SAORIN, A., BRADY, N. R. & HAMACHER-BRADY, A. 2020b. Endolysosomal Targeting of Mitochondria Is Integral to BAX-Mediated Mitochondrial Permeabilization during Apoptosis Signaling. *Developmental Cell,* 53**,** 627-645.e7.

WANG, X., YOUNAN, D., PETKUS, A. J., BEAVERS, D. P., ESPELAND, M. A., CHUI, H. C., RESNICK, S. M., GATZ, M., KAUFMAN, J. D., WELLENIUS, G. A., WHITSEL, E. A., MANSON, J. E. & CHEN, J.-C. 2021. Ambient Air Pollution and Long-Term Trajectories of Episodic Memory Decline among Older Women in the WHIMS-ECHO Cohort. *Environmental Health Perspectives,* 129**,** 097009.

WARD, N. & MASON, J. 1987. Neutron activation analysis techniques for identifying elemental status in Alzheimer's disease. *Journal of Radioanalytical and Nuclear Chemistry,* 113**,** 515-526.

WARD, R. J., ZUCCA, F. A., DUYN, J. H., CRICHTON, R. R. & ZECCA, L. 2014. The role of iron in brain ageing and neurodegenerative disorders. *Lancet Neurol,* 13**,** 1045-60.

WASEL, O. & FREEMAN, J. L. 2018. Comparative Assessment of Tungsten Toxicity in the Absence or Presence of Other Metals. *Toxics,* 6**,** 66.

WEICHENTHAL, S., OLANIYAN, T., CHRISTIDIS, T., LAVIGNE, E., HATZOPOULOU, M., VAN RYSWYK, K., TJEPKEMA, M. & BURNETT, R. 2020. Within-city Spatial Variations in Ambient Ultrafine Particle Concentrations and Incident Brain Tumors in Adults. *Epidemiology,* 31**,** 177-183.

WENK, G. L. 2003. Neuropathologic changes in Alzheimer's disease. *J Clin Psychiatry,* 64 Suppl 9**,** 7-10.

WENNBERG, A. M. V., SAVICA, R. & MIELKE, M. M. 2017. Association between Various Brain Pathologies and Gait Disturbance. *Dementia and Geriatric Cognitive Disorders,* 43**,** 128-143.

WENSTRUP, D., EHMAN, W. D. & MARKESBERY, W. R. 1990. Trace element imbalances in isolated subcellular fractions of Alzheimer's disease brains. *Brain Research,* 533**,** 125-131.

WEUVE, J., BENNETT, E. E., RANKER, L., GIANATTASIO, K. Z., PEDDE, M., ADAR, S. D., YANOSKY, J. D. & POWER, M. 2021. Exposure to Air Pollution in Relation to Risk of Dementia and Related Outcomes: An Updated Systematic Review of the Epidemiological Literature. *Environmental Health Perspectives,* 129**,** 1-24.

WHO. 2018. *Arsenic Fact Sheet* [Online]. Available: https://www.who.int/news-room/fact-sheets/detail/arsenic [Accessed 4th November 2021].

WHO. 2021a. *Ambient (outdoor) air pollution* [Online]. Available: https://www.who.int/news-room/fact-sheets/detail/ambient-(outdoor)-air-quality-and-health [Accessed 28th September 2021].

WHO. 2021b. *Dementia Fact Sheet* [Online]. Available: https://www.who.int/en/news-room/fact-sheets/detail/dementia [Accessed 16th September 2021].

WILKER, E. H., PREIS, S. R., BEISER, A. S., WOLF, P. A., AU, R., KLOOG, I., LI, W., SCHWARTZ, J., KOUTRAKIS, P., DECARLI, C., SESHADRI, S. & MITTLEMAN, M. A. 2015. Long-term exposure to fine particulate matter, residential proximity to major roads and measures of brain structure. *Stroke,* 46**,** 1161-1166.

WILSON, R. S., ARNOLD, S. E., SCHNEIDER, J. A., BOYLE, P. A., BUCHMAN, A. S. & BENNETT, D. A. 2009. Olfactory Impairment in Presymptomatic Alzheimer's Disease. *Annals of the New York Academy of Sciences,* 1170**,** 730-735.

WINTER, W. E., BAZYDLO, L. A. L. & HARRIS, N. S. 2014. The Molecular Biology of Human Iron Metabolism. *Laboratory Medicine,* 45**,** 92-102.

WINTERBOURN, C. C. 1995. Toxicity of iron and hydrogen peroxide: the Fenton reaction. *Toxicol Lett,* 82-83**,** 969-74.

WISEMAN, C. L. S., LEVESQUE, C. & RASMUSSEN, P. E. 2021. Characterizing the sources, concentrations and resuspension potential of metals and metalloids in the thoracic fraction of urban road dust. *Science of The Total Environment,* 786**,** 147467.

WISEMAN, F. K., AL-JANABI, T., HARDY, J., KARMILOFF-SMITH, A., NIZETIC, D., TYBULEWICZ, V. L. J., FISHER, E. M. C. & STRYDOM, A. 2015. A genetic cause of Alzheimer disease: mechanistic insights from Down syndrome. *Nature reviews. Neuroscience,* 16**,** 564-574.

WOHLFARTH, E. P. 1958. Relations between Different Modes of Acquisition of the Remanent Magnetization of Ferromagnetic Particles. *Journal of Applied Physics,* 29**,** 595-596.

WOODWARD, N. C., LEVINE, M. C., HAGHANI, A., SHIRMOHAMMADI, F., SAFFARI, A., SIOUTAS, C., MORGAN, T. E. & FINCH, C. E. 2017. Toll-like receptor 4 in glial inflammatory responses to air pollution in vitro and in vivo. *Journal of Neuroinflammation,* 14**,** 84.

WORLD HEALTH, O. & GLOBAL ENVIRONMENT MONITORING, S. 1992. Urban air pollution in megacities of the world. Oxford : Blackwell Reference.

WU, C. C., JIN, L. W., WANG, I. F., WEI, W. Y., HO, P. C., LIU, Y. C. & TSAI, K. J. 2020. HDAC1 dysregulation induces aberrant cell cycle and DNA damage in progress of TDP-43 proteinopathies. *EMBO Molecular Medicine,* 12.

WU, C. H., TANG, S. C., WANG, P. H., LEE, H. & KO, J. L. 2012. Nickel-induced epithelial-mesenchymal transition by reactive oxygen species generation and E-cadherin promoter hypermethylation. *J Biol Chem,* 287**,** 25292-302.

WU, T. & TANG, M. 2018. The inflammatory response to silver and titanium dioxide nanoparticles in the central nervous system. *Nanomedicine,* 13.

WU, W. H., LEI, P., LIU, Q., HU, J., GUNN, A. P., CHEN, M. S., RUI, Y. F., SU, X. Y., XIE, Z. P., ZHAO, Y. F., BUSH, A. I. & LI, Y. M. 2008. Sequestration of copper from beta-amyloid promotes selective lysis by cyclen-hybrid cleavage agents. *J Biol Chem,* 283**,** 31657-64.

WYSS-CORAY, T., LOIKE, J. D., BRIONNE, T. C., LU, E., ANANKOV, R., YAN, F., SILVERSTEIN, S. C. & HUSEMANN, J. 2003. Adult mouse astrocytes degrade amyloid-β in vitro and in situ. *Nature Medicine,* 9**,** 453-457.

XIAN, M., MA, S., WANG, K., LOU, H., WANG, Y., ZHANG, L., WANG, C. & AKDIS, C. A. 2020. Particulate Matter 2.5 Causes Deficiency in Barrier Integrity in Human Nasal Epithelial Cells. *Allergy Asthma Immunol Res,* 12**,** 56-71.

XU, F., SHI, X., QIU, X., JIANG, X., FANG, Y., WANG, J., HU, D. & ZHU, T. 2020a. Investigation of the chemical components of ambient fine particulate matter (PM2.5) associated with in vitro cellular responses to oxidative stress and inflammation. *Environment International,* 136**,** 105475.

XU, J., CHURCH, S. J., PATASSINI, S., BEGLEY, P., WALDVOGEL, H. J., CURTIS, M. A., FAULL, R. L. M., UNWIN, R. D. & COOPER, G. J. S. 2017. Evidence for widespread, severe brain copper deficiency in Alzheimer's dementia. *Metallomics,* 9**,** 1106-1119.

XU, J., KNUTSON, M. D., CARTER, C. S. & LEEUWENBURGH, C. 2008. Iron accumulation with age, oxidative stress and functional decline. *PloS one,* 3**,** e2865-e2865.

XU, S., SUI, J., FU, Y., WU, W., LIU, T., YANG, S. & LIANG, G. 2020b. Titanium dioxide nanoparticles induced the apoptosis of RAW264.7 macrophages through miR-29b-3p/NFAT5 pathway. *Environmental Science and Pollution Research,* 27**,** 26153-26162.

YAMAGUCHI, T. & YAMAZAKI, H. 2001. Cytotoxicity of Airborne Particulates Sampled Roadside in Rodent and Human Lung Fibroblasts. *Journal of Health Science,* 47**,** 272-277.

YAMANE, Y. & KOIZUMI, T. 1982. Protective effect of molybdenum on the acute toxicity of mercuric chloride. *Toxicology and Applied Pharmacology,* 65**,** 214-221.

YANG, L., LIU, G., LIN, Z., WANG, Y., HE, H., LIU, T. & KAMP, D. W. 2016a. Pro-inflammatory response and oxidative stress induced by specific components in ambient particulate matter in human bronchial epithelial cells. *Environ Toxicol,* 31**,** 923-36.

YANG, Y., VANCE, M., TOU, F., TIWARI, A., LIU, M. & HOCHELLA, M. F. 2016b. Nanoparticles in road dust from impervious urban surfaces: distribution, identification, and environmental implications. *Environmental Science: Nano,* 3**,** 534-544.

YAO, L., TANG, Y., CHEN, B., HONG, W., XU, X., LIU, Y., AGUILAR, Z. P. & XU, H. 2020. Oral exposure of titanium oxide nanoparticles induce ileum physical barrier dysfunction via Th1/Th2 imbalance. *Environmental Toxicology,* 35**,** 982-990.

YARJANLI, Z., GHAEDI, K., ESMAEILI, A., RAHGOZAR, S. & ZARRABI, A. 2017. Iron oxide nanoparticles may damage to the neural tissue through iron accumulation, oxidative stress, and protein aggregation. *BMC Neuroscience,* 18**,** 51.

YATKIN, S. & BAYRAM, A. 2007. Elemental composition and sources of particulate matter in the ambient air of a Metropolitan City. *Atmospheric Research,* 85**,** 126-139.

YOON, S., HAN, S., JEON, K. J. & KWON, S. 2018. Effects of collected road dusts on cell viability, inflammatory response, and oxidative stress in cultured human corneal epithelial cells. *Toxicol Lett,* 284**,** 152-160.

YOSHIMASU, F., YASUI, M., YASE, Y., IWATA, S., GAJDUSEK, D. C., GIBBS JR, C. J. & CHEN, K.-M. 1980. Studies on Amyotrophic Lateral Sclerosis by Neutron Activation Analysis-2. Comparative Study of Analytical Results on Guam PD, Japanese ALS and Alzheimer Disease Cases. *Psychiatry and Clinical Neurosciences,* 34**,** 75-82.

YOUDIM, M. B. & GREEN, A. R. 1978. Iron deficiency and neurotransmitter synthesis and function. *Proc Nutr Soc,* 37**,** 173-9.

YOUNAN, D., PETKUS, A. J., WIDAMAN, K. F., WANG, X., CASANOVA, R., ESPELAND, M. A., GATZ, M., HENDERSON, V. W., MANSON, J. E., RAPP, S. R., SACHS, B. C., SERRE, M. L., GAUSSOIN, S. A., BARNARD, R., SALDANA, S., VIZUETE, W., BEAVERS, D. P., SALINAS, J. A., CHUI, H. C., RESNICK, S. M., SHUMAKER, S. A. & CHEN, J.-C. 2019. Particulate matter and episodic memory decline mediated by early neuroanatomic biomarkers of Alzheimer's disease. *Brain,* 143**,** 289-302.

YU, S.-H., TANG, D.-W., HSIEH, H.-Y., WU, W.-S., LIN, B.-X., CHUANG, E.-Y., SUNG, H.-W. & MI, F.-L. 2013. Nanoparticle-induced tight-junction opening for the transport of an anti-angiogenic sulfated polysaccharide across Caco-2 cell monolayers. *Acta Biomaterialia,* 9**,** 7449-7459.

YUCHI, W., SBIHI, H., DAVIES, H., TAMBURIC, L. & BRAUER, M. 2020. Road proximity, air pollution, noise, green space and neurologic disease incidence: a population-based cohort study. *Environmental Health,* 19**,** 8.

ZANETTI, O., SOLERTE, S. B. & CANTONI, F. 2009. Life expectancy in Alzheimer's disease (AD). *Arch Gerontol Geriatr,* 49 Suppl 1**,** 237-43.

ZARAZÚA, S., BÜRGER, S., DELGADO, J. M., JIMÉNEZ-CAPDEVILLE, M. E. & SCHLIEBS, R. 2011. Arsenic affects expression and processing of amyloid precursor protein (APP) in primary neuronal cells overexpressing the Swedish mutation of human APP. *Int J Dev Neurosci,* 29**,** 389-96.

ZECCA, L., BELLEI, C., COSTI, P., ALBERTINI, A., MONZANI, E., CASELLA, L., GALLORINI, M., BERGAMASCHI, L., MOSCATELLI, A., TURRO, N. J., EISNER, M., CRIPPA, P. R., ITO, S., WAKAMATSU, K., BUSH, W. D., WARD, W. C., SIMON, J. D. & ZUCCA, F. A. 2008. New melanic pigments in the human brain that accumulate in aging and block environmental toxic metals. *Proceedings of the National Academy of Sciences of the United States of America,* 105**,** 17567-17572.

ZECCA, L., YOUDIM, M. B. H., RIEDERER, P., CONNOR, J. R. & CRICHTON, R. R. 2004. Iron, brain ageing and neurodegenerative disorders. *Nature Reviews Neuroscience,* 5**,** 863-873.

ZELENA, D., MENANT, O., ANDERSSON, F. & CHAILLOU, E. 2018. Periaqueductal gray and emotions: The complexity of the problem and the light at the end of the tunnel, the magnetic resonance imaging. *Endocrine Regulations,* 52**,** 222-238.

ZHANG, H., LIU, D., HUANG, H., ZHAO, Y. & ZHOU, H. 2018. Characteristics of Insulin-degrading Enzyme in Alzheimer's Disease: A Meta-Analysis. *Curr Alzheimer Res,* 15**,** 610-617.

ZHANG, J., EVERSON, M. P., WALLINGTON, T. J., FIELD, F. R., ROTH, R. & KIRCHAIN, R. E. 2016. Assessing Economic Modulation of Future Critical Materials Use: The Case of Automotive-Related Platinum Group Metals. *Environmental Science & Technology,* 50**,** 7687-7695.

ZHANG, J., LI, R., ZHANG, X., DING, C. & HUA, P. 2019. Traffic contribution to polycyclic aromatic hydrocarbons in road dust: A source apportionment analysis under different antecedent dry-weather periods. *Science of The Total Environment,* 658**,** 996-1005.

ZHANG, Q., LU, D., WANG, D., YANG, X., ZUO, P., YANG, H., FU, Q., LIU, Q. & JIANG, G. 2020a. Separation and Tracing of Anthropogenic Magnetite Nanoparticles in the Urban Atmosphere. *Environmental Science & Technology,* 54**,** 9274-9284.

ZHANG, X., LIANG, M., QIN, W., WAN, B., YU, C. & MING, D. 2020b. Gender Differences Are Encoded Differently in the Structure and Function of the Human Brain Revealed by Multimodal MRI. *Frontiers in Human Neuroscience,* 14.

ZHANG, Y., LARCHER, K. M. H., MISIC, B. & DAGHER, A. 2017. Anatomical and functional organization of the human substantia Nigra and its connections. *eLife,* 6.

ZHANG, Z., ZHU, D., CUI, B., DING, R., SHI, X. & HE, P. 2020c. Association between particulate matter air pollution and lung cancer. *Thorax,* 75**,** 85.

ZHAO, J., LIU, X., XIA, W., ZHANG, Y. & WANG, C. 2020. Targeting Amyloidogenic Processing of APP in Alzheimer's Disease. *Frontiers in Molecular Neuroscience,* 13.

ZHOU, Y., PENG, Z., SEVEN, E. S. & LEBLANC, R. M. 2018. Crossing the blood-brain barrier with nanoparticles. *Journal of Controlled Release,* 270**,** 290-303.

ZHOU, Z. D. & TAN, E.-K. 2017. Iron regulatory protein (IRP)-iron responsive element (IRE) signaling pathway in human neurodegenerative diseases. *Molecular Neurodegeneration,* 12**,** 75.

ZIERDEN, M. R. & VALENTINE, A. M. 2015. Contemplating a role for titanium in organisms. *Metallomics,* 8**,** 9-16.

ZORODDU, M. A., AASETH, J., CRISPONI, G., MEDICI, S., PEANA, M. & NURCHI, V. M. 2019. The essential metals for humans: a brief overview. *Journal of Inorganic Biochemistry,* 195**,** 120-129.

ZOU, K., GONG, J. S., YANAGISAWA, K. & MICHIKAWA, M. 2002. A novel function of monomeric amyloid beta-protein serving as an antioxidant molecule against metal-induced oxidative damage. *J Neurosci,* 22**,** 4833-41.

ZUCCA, F. A., VANNA, R., CUPAIOLI, F. A., BELLEI, C., DE PALMA, A., DI SILVESTRE, D., MAURI, P., GRASSI, S., PRINETTI, A., CASELLA, L., SULZER, D. & ZECCA, L. 2018. Neuromelanin organelles are specialized autolysosomes that accumulate undegraded proteins and lipids in aging human brain and are likely involved in Parkinson's disease. *npj Parkinson's Disease,* 4.

Appendix A : Chapter 2 (Paper 1) Supplementary material

Variation in the concentration and regional distribution of magnetic nanoparticles in human brains (Alzheimer's disease and controls), from the UK

A.1 Supplementary methods

The measurement of (relatively) weakly magnetic samples of a biological nature presents several experimental challenges. At every stage, we have reduced and quantified any potential contamination (Supplementary Table S1). First, an appropriate, magnetically-clean environment was selected for sample preparation; a biological safety cabinet in a class III laboratory. Cabinet air throughflow was sampled using a Leland Legacy pump (SKC, Dorset UK) at 7.5L/min through a magnetically- 'clean' 1 µm PTFE filter, in order to quantify any magnetic 'background' associated with that environment.

Table A.1 Sampling air quality. CL3 = biological safety cabinet in class III laboratory, CEMP = Centre for Environmental Magnetism and Palaeomagnetism. The SIRM of clean 1 µm PTFE filters was measured, these were then placed inside the pump and air was sampled for between 3 and 7 hours, which equates to 1.35-3.15m^3 air. The SIRM of the exposed filters was then measured. The values above reflect the change in filter SIRM, post-exposure, at each location, normalised for the volume of air pumped, or per minute of exposure, on the two tissue sampling days. The last two rows represent a random sampling of the sample preparation area (hood) or sample measurement area (CEMP, bench).

Name	Location	SIRM (x 10^{-10} Am^2)	SIRM (x 10^{-10} Am^2/m^3)	SIRM (x10^{-10} Am^2/min)
CL3(11/10/18)	Hood	18.43	6.15	0.0460
CL3 (10/05/18)	Hood	9.7	5.44	0.0400
CEMP	Bench	3.36	1.14	0.0086
CL3 (03/10/19)	Hood	1.45	0.57	0.0043

The class III laboratory has double filtered air (high efficiency particulate air, HEPA, filters) inside the biological safety cabinet. Tissue samples were exposed within the hood for ~ 3 minutes or less; this translates to potential magnetic accumulation of a minimum 1.20 E^{-12} Am^2 (i.e., ~ 3-4 times lower than a typical 2G sample holder value) or a maximum 1.38 E^{-11} Am^2 (~ 3-4 higher than a typical holder value).

In order to minimize contamination of the sample and clingfilm, all handling of clingfilm and samples was carried out in the biological safety cabinet. Clingfilm is necessary in order to secure and protect the freeze-dried samples which are fragile and will crumble if repeatedly manipulated. For each tissue sample measurement, the specific piece of clingfilm was pre-

measured and demagnetised (pieces with an SIRM ≥ 2 x 10^{-10} Am^2 were rejected and not used for measurement). Clingfilm was cut using a ceramic knife from the centre of the roll. The SIRM of the clingfilm, ave. ~1 x 10^{-10} Am^2, is subtracted in order to isolate the tissue SIRM. On average, the clingfilm contributes ~23% of the total measured SIRM (i.e., sample + pot + clingfilm). Tissue samples were measured in non-magnetised pots; the NRM of an empty pot (~6 x 10^{-12} Am^2) is weaker than a typical 2G sample holder value.

Cutting surfaces and ceramic knives were cleaned with 70% ethanol prior to use and between samples. To quantify any possible contamination from the ethanol, SIRM measurements were made on unfiltered and 1, 2 or 3x filtered 70% ethanol, as well as unfiltered dH_2O. SIRMs were measured at 77K on a JR6A magnetometer (noise level 5 x 10^{-11} Am^2); the SIRM of each solution, approximately 2g (~2-2.3ml), was unmeasurable.

The outer surfaces of each sample were trimmed to remove any potential metal contaminants from the autopsy process such as fragments from stainless steel instruments or debris from metal bone saws as per (Gilder et al., 2018). Some large samples and those with irregular geometry were further sub-divided into two samples, each sample measured separately and the final SIRM calculated by adding the two values as if it were one whole sample. For a selection of samples, the trimmings were measured as well as the sample. In some cases, trimming made little difference; in other cases, a failure to trim the sample would have made a large contribution to the measured signal, emphasising the need to control for contamination at every stage. Wet/dry ratios (i.e., the mean of the freeze-dried weight divided by the wet weight) ranged from 0.16 for entorhinal cortex samples and 0.19 for all other MBB samples.

Data presented here classes each Manchester case as either ‘AD’ or ‘control’. However, the pathological diagnosis in some cases is not as clear; for example, “probable AD” and “possible AD”. Data were also categorised as control, AD or “intermediate” if the case did not clearly belong to either the control or AD group and analysed using this classification system. There was no significant difference in magnetite concentration between AD and controls when using a 3-group classification (AD, Control, intermediate), a 2-group classification (all individuals designated as either control or AD) or a 2-group classification system omitting the intermediate cases (definite AD and definite controls only).

We note that samples from Manchester originated from the right hemisphere, whilst the previously published Mexico City samples (Calderón-Garcidueñas et al., 2020a) originated from the left hemisphere, limited tissue availability prevented us from using the same

hemisphere from both populations. It is possible that variation exists between the left and right hemispheres in terms of magnetite concentration and pathology. However, MRI studies have shown no interhemispheric differences in iron concentrations (Acosta-Cabronero et al., 2016), and pathological examination of both AD and control hemispheres (as a whole group) showed similar Braak NFT staging and Aβ deposition but increased vascular lesions in the left hemisphere (Giannakopoulos et al., 2009). In contrast, Gilder et al. report higher ferrimagnetic concentrations in the left hemisphere of the cerebral cortex than the right hemisphere in six of their seven individuals (Gilder et al., 2018).

Table A.2 Summary case information Manchester, UK. A selection of 30 brains from elderly individuals were obtained from the Manchester Brain Bank. The pathological diagnosis can be summarised as; 10 Alzheimer's Disease (AD), 7 controls (cont.) (age changes only), 4 probable AD, 3 possible AD, 2 incipient AD, 2 moderate small vessel disease (SVD), 1 mild SVD and 1 mild AD pathology in the temporal lobe. Comments from the pathologist on cerebral amyloid angiopathy (CAA), severe vessel disease (SVD) and TAR DNA-binding protein 43 (TDP-43) proteinopathy of each brain are also summarised.

Case	Sex	Age	Pathological Diagnosis	State	Pathologist comment
09/15	F	89	AD	AD	
09/22	F	90	Possible AD	AD	Mild to moderate SVD
09/37	M	90	Age changes only	Cont.	
10/08	F	87	AD	AD	Moderate CAA, mild SVD
10/13	F	85	AD	AD	Very severe CAA
10/16	M	91	Moderate SVD	Cont.	
10/26	M	84	Moderate SVD	Cont.	
10/40	M	86	AD	AD	Mild SVD
12/09	F	87	Mild AD pathology in temporal lobe	AD	
12/23	M	95	Age changes only	Cont.	
12/33	F	81	Probable AD	AD	Moderate CAA & SVD
12/34	F	80	Probable AD	AD	Mild SVD
13/09	F	85	AD	AD	Moderate to severe SVD
13/10	F	85	AD	AD	Severe CAA
14/01	F	93	Probable AD	AD	
14/04	F	87	Age changes only	Cont.	
14/07	F	95	Probable AD	AD	Moderate SVD
14/11	M	91	Mild SVD	Cont.	
14/20	F	90	Age changes only	Cont.	
14/46	F	94	Age changes only	Cont.	Mild SVD
15/01	M	90	Age changes only	Cont.	
15/19	F	98	Possible AD	AD	
15/29	M	81	AD	AD	Mild SVD
15/31	M	91	Age changes only	Cont.	
15/42	M	89	Incipient AD	Cont.	
15/48	F	81	AD	AD	Secondary TDP-43
16/01	M	90	Possible AD	AD	Mild SVD
16/08	M	88	Incipient AD	AD	Moderate to severe SVD
16/13	M	91	AD	AD	
16/14	F	92	AD	AD	Secondary TDP-43 proteinopathy

Table A.3 Regional distribution of magnetic remanence carriers in Alzheimer's disease and controls.
Freeze dried fresh frozen brain tissue samples from the cerebellum, entorhinal cortex (EC), frontal, occipital and temporal lobes were exposed to a saturating field of 1T, and their saturation isothermal remanence magnetisation (SIRM) measured. Individuals were classified as either control(cont.) or Alzheimer's disease (AD) based on their pathological diagnosis.

Region	Samples (n)	SIRM range ($10^{-6}Am^2\ kg^{-1}$)	Mean SIRM ($10^{-6}Am^2\ kg^{-1}$)	Median SIRM ($10^{-6}Am^2\ kg^{-1}$)	Mean magnetite (μg/g)	Mean (10^9) particles/g tissue
Cerebellum AD	17	0.15-1.63	0.63	0.40	0.05	0.57
Cerebellum Cont.	11	0.09-3.31	1.01	0.74	0.07	0.91
EC AD	17	0.13-0.81	0.38	0.30	0.03	0.34
EC Cont.	9	0.06-1.33	0.45	0.38	0.03	0.40
Frontal AD	19	0.16-13.69	1.86	0.57	0.13	1.67
Frontal Cont.	11	0.20-5.33	1.13	0.64	0.08	1.01
Occipital AD	18	0.08-9.73	1.22	0.51	0.09	1.10
Occipital Cont.	10	0.19-1.87	0.73	0.59	0.05	0.66
Temporal AD	18	0.12-5.96	1.14	0.67	0.08	1.02
Temporal Cont.	11	0.17-3.80	0.89	0.49	0.06	0.80

Table A.4 Metal concentrations in the cerebellum of MBB Alzheimer's disease and controls. ICP-MS was conducted on fresh/frozen brain tissue samples from the cerebellum to determine concentrations (µg/g dry tissue) of aluminium, cerium, iron, lead, and platinum. Individuals were classified as either control or Alzheimer's disease (AD) based on their pathological diagnosis. *Excluded from analysis as an extreme outlier.

Pathology	Case	Region	Aluminium	Cerium	Iron	Lead	Platinum
AD	09/15	Cerebellum	2.54	0.0019	321.95	0.09	0.0040
AD	09/22	Cerebellum	5.00	0.0125	251.83	0.04	0.0031
Control	09/37	Cerebellum	1.54	0.0059	313.48	0.09	2.2009*
AD	10/08	Cerebellum	2.50	0.0031	203.23	4.21	0.0005
AD	10/13	Cerebellum	1.20	0.0013	231.30	0.06	0.0011
Control	10/16	Cerebellum	2.01	0.0043	371.22	0.05	0.0004
Control	10/26	Cerebellum	3.54	0.0014	248.54	1.16	0.0025
AD	10/40	Cerebellum	0.84	0.0009	198.48	0.08	0.0007
AD	12/09	Cerebellum	2.13	0.0042	202.37	0.03	0.0012
Control	12/23	Cerebellum	0.48	0.0022	460.43	0.03	0.0006
AD	12/33	Cerebellum	0.79	0.0046	260.53	0.04	0.0015
AD	12/34	Cerebellum	3.13	0.0057	237.42	0.06	0.0000
AD	13/09	Cerebellum	6.06	0.0047	415.17	0.07	0.0067
AD	13/10	Cerebellum	2.29	0.0073	446.60	0.06	0.0023
AD	14/01	Cerebellum	2.27	0.0009	270.21	0.05	0.0002
Control	14/04	Cerebellum	0.68	0.0013	202.61	0.02	0.0007
AD	14/07	Cerebellum	5.45	0.0110	285.95	0.05	0.0019
Control	14/11	Cerebellum	2.69	0.0057	241.34	0.69	0.0024
Control	14/20	Cerebellum	0.46	0.0024	530.43	0.93	0.0011
Control	14/46	Cerebellum	14.83	0.0211	274.13	1.06	0.0029
Control	15/01	Cerebellum	2.59	0.0014	281.04	0.03	0.0015
AD	15/19	Cerebellum	0.74	0.0017	170.89	0.03	0.0005
AD	15/29	Cerebellum	26.20	0.0025	265.09	0.03	0.0014
Control	15/31	Cerebellum	0.87	0.0009	219.66	0.08	0.0011
Control	15/42	Cerebellum	3.99	0.0054	328.71	0.04	0.0008
AD	15/48	Cerebellum	2.09	0.0024	177.40	0.05	0.0011
AD	16/01	Cerebellum	0.96	0.0024	316.42	0.07	0.0029
AD	16/08	Cerebellum	2.50	0.0060	340.20	0.03	0.0015
AD	16/13	Cerebellum	1.68	0.0017	429.83	2.88	0.0026
AD	16/14	Cerebellum	6.19	0.0133	292.79	0.06	0.0037

Table A.5 Metal concentrations in the frontal lobe of MBB Alzheimer's disease and controls. ICP-MS was conducted on fresh frozen brain tissue samples from the frontal lobe to determine concentrations (µg/g dry tissue) of aluminium, cerium, iron, lead, and platinum. Individuals were classified as either control or Alzheimer's disease (AD) based on their pathological diagnosis.

Pathology	Case	Region	Aluminium	Cerium	Iron	Lead	Platinum
AD	09/15	Frontal	2.53	0.0009	350.36	0.07	0.0014
AD	09/22	Frontal	0.70	0.0015	156.49	0.01	0.0000
Control	09/37	Frontal	0.94	0.0040	184.82	0.08	0.0026
AD	10/08	Frontal	3.71	0.0111	296.24	1.12	0.0022
AD	10/13	Frontal	2.09	0.0014	163.26	0.04	0.0007
Control	10/16	Frontal	10.02	0.0109	255.93	0.09	0.0019
Control	10/26	Frontal	1.06	0.0015	200.60	1.00	0.0014
AD	10/40	Frontal	0.57	0.0007	145.48	0.11	0.0005
AD	12/09	Frontal	6.63	0.0090	267.12	0.04	0.0018
Control	12/23	Frontal	1.59	0.0027	204.31	0.05	0.0014
AD	12/33	Frontal	1.27	0.0012	244.31	0.07	0.0006
AD	12/34	Frontal	18.44	0.0398	325.64	1.30	0.0052
AD	13/09	Frontal	2.90	0.0037	209.90	0.08	0.0009
AD	13/10	Frontal	1.82	0.0022	166.75	1.13	0.0004
AD	14/01	Frontal	1.05	0.0008	215.35	0.05	0.0003
Control	14/04	Frontal	2.18	0.0031	249.52	0.09	0.0024
AD	14/07	Frontal	8.05	0.0136	311.85	0.10	0.0020
Control	14/11	Frontal	12.04	0.0056	363.31	0.09	0.0014
Control	14/20	Frontal	3.41	0.0075	395.07	0.15	0.0019
Control	14/46	Frontal	14.06	0.0162	368.40	0.51	0.0022
Control	15/01	Frontal	1.44	0.0008	199.99	0.03	0.0005
AD	15/19	Frontal	1.28	0.0005	218.92	0.10	0.0004
AD	15/29	Frontal	0.47	0.0006	191.17	0.02	0.0005
Control	15/31	Frontal	2.17	0.0012	214.26	0.72	0.0023
Control	15/42	Frontal	3.48	0.0030	257.34	0.04	0.0013
AD	15/48	Frontal	0.93	0.0011	193.87	0.05	0.0006
AD	16/01	Frontal	1.04	0.0012	276.23	0.11	0.0019
AD	16/08	Frontal	3.61	0.0043	255.26	0.04	0.0000
AD	16/13	Frontal	1.07	0.0025	273.38	0.03	0.0015
AD	16/14	Frontal	6.19	0.0074	242.91	0.08	0.0009

Table A.6 Metal concentrations in the occipital lobe of MBB Alzheimer's disease and controls. ICP-MS was conducted on fresh frozen brain tissue samples from the occipital lobe to determine concentrations (µg/g dry tissue) of aluminium, cerium, iron, lead, and platinum. Individuals were classified as either control or Alzheimer's disease (AD) based on their pathological diagnosis.

Pathology	Case	Region	Aluminium	Cerium	Iron	Lead	Platinum
AD	09/15	Occipital	7.95	0.0026	274.71	0.13	0.0031
AD	09/22	Occipital	2.83	0.0059	317.16	0.02	0.0015
Control	09/37	Occipital	1.96	0.0067	229.05	0.11	0.0011
AD	10/08	Occipital	4.01	0.0128	485.98	2.03	0.0050
AD	10/13	Occipital	1.50	0.0013	199.43	0.03	0.0007
Control	10/16	Occipital	2.02	0.0022	288.43	0.06	0.0021
Control	10/26	Occipital	0.68	0.0010	234.02	0.07	0.0007
AD	10/40	Occipital	0.55	0.0006	183.60	0.04	0.0003
AD	12/09	Occipital	2.05	0.0023	345.71	0.02	0.0010
Control	12/23	Occipital	0.53	0.0020	258.43	0.03	0.0011
AD	12/33	Occipital	0.92	0.0011	239.99	0.05	0.0009
AD	12/34	Occipital	9.60	0.0229	426.80	0.11	0.0095
AD	13/09	Occipital	5.88	0.0091	522.22	0.06	0.0010
AD	13/10	Occipital	2.49	0.0058	342.91	0.25	0.0019
AD	14/01	Occipital	1.58	0.0007	176.10	0.03	0.0002
Control	14/04	Occipital	2.03	0.0040	236.08	0.04	0.0011
AD	14/07	Occipital	4.36	0.0088	311.80	0.05	0.0018
Control	14/11	Occipital	4.45	0.0054	336.82	0.04	0.0026
Control	14/20	Occipital	3.09	0.0063	352.72	0.07	0.0015
Control	14/46	Occipital	8.58	0.0127	313.94	0.12	0.0031
Control	15/01	Occipital	0.81	0.0005	223.32	0.02	0.0003
AD	15/19	Occipital	1.25	0.0013	179.53	0.05	0.0003
AD	15/29	Occipital	1.36	0.0015	256.63	0.03	0.0004
Control	15/31	Occipital	2.17	0.0008	282.42	0.34	0.0013
Control	15/42	Occipital	1.69	0.0027	263.99	0.42	0.0008
AD	15/48	Occipital	0.85	0.0012	243.73	0.04	0.0009
AD	16/01	Occipital	1.52	0.0015	204.38	0.06	0.0003
AD	16/08	Occipital	1.91	0.0054	269.33	0.04	0.0000
AD	16/13	Occipital	0.82	0.0004	360.18	0.04	0.0006
AD	16/14	Occipital	3.09	0.0042	287.09	0.06	0.0010

Table A.7 Metal concentrations in the temporal lobe of MBB Alzheimer's disease and controls. ICP-MS was conducted on fresh frozen brain tissue samples from the temporal lobe to determine concentrations (µg/g dry tissue) of aluminium, cerium, iron, lead, and platinum. Individuals were classified as either control or Alzheimer's disease (AD) based on their pathological diagnosis.

Pathology	Case	Region	Aluminium	Cerium	Iron	Lead	Platinum
AD	09/15	Temporal	1.39	0.0002	237.63	0.05	0.0005
AD	09/22	Temporal	6.22	0.0170	336.78	0.05	0.0032
Control	09/37	Temporal	7.46	0.0082	191.31	0.11	0.0031
AD	10/08	Temporal	2.32	0.0066	272.73	0.59	0.0022
AD	10/13	Temporal	1.20	0.0010	193.67	0.03	0.0007
Control	10/16	Temporal	3.96	0.0056	226.83	0.10	0.0009
Control	10/26	Temporal	1.85	0.0001	200.12	0.25	0.0004
AD	10/40	Temporal	0.83	0.0007	192.89	0.11	0.0005
AD	12/09	Temporal	1.35	0.0031	285.63	0.04	0.0004
Control	12/23	Temporal	1.45	0.0034	193.00	0.05	0.0026
AD	12/33	Temporal	1.93	0.0016	261.65	0.10	0.0007
AD	12/34	Temporal	34.70	0.0641	608.76	0.15	0.0000
AD	13/09	Temporal	5.34	0.0076	313.49	0.05	0.0025
AD	13/10	Temporal	1.99	0.0060	311.67	0.12	0.0017
AD	14/01	Temporal	3.71	0.0011	335.14	0.05	0.0003
Control	14/04	Temporal	2.73	0.0038	269.49	0.15	0.0011
AD	14/07	Temporal	8.46	0.0142	322.48	0.07	0.0021
Control	14/11	Temporal	3.32	0.0026	206.06	0.04	0.0006
Control	14/20	Temporal	6.32	0.0116	253.18	0.31	0.0081
Control	14/46	Temporal	10.51	0.0080	241.66	0.09	0.0045
Control	15/01	Temporal	1.82	0.0020	319.96	1.39	0.0017
AD	15/19	Temporal	0.69	0.0012	172.37	0.03	0.0007
AD	15/29	Temporal	1.30	0.0019	355.32	0.04	0.0010
Control	15/31	Temporal	3.93	0.0008	200.53	0.04	0.0016
Control	15/42	Temporal	2.60	0.0047	171.32	0.03	0.0015
AD	15/48	Temporal	6.81	0.0072	556.94	0.14	0.0019
AD	16/01	Temporal	0.87	0.0011	285.57	0.09	0.0009
AD	16/08	Temporal	9.43	0.0112	279.78	0.09	0.0000
AD	16/13	Temporal	1.29	0.0040	321.47	0.49	0.0017
AD	16/14	Temporal	3.71	0.0096	360.64	0.06	0.0000

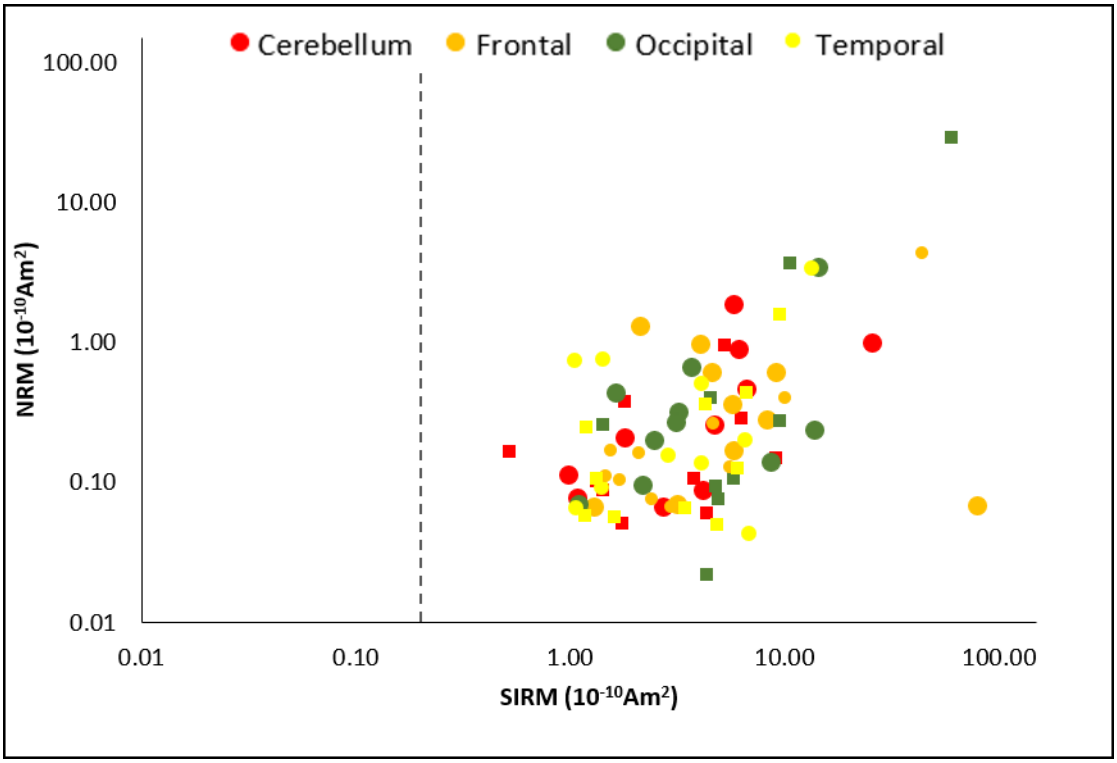

Figure A.1 NRM/SIRM values of human brain tissue samples. The NRM of 83 freeze-dried human brain tissue samples from MBB at 293K ±0.5K. Dashed line indicates the measurement limit (2 x 10^{-11} Am^2) of the 2G SQUID magnetometer (Centre for Environmental Magnetism and Palaeomagnetism, Lancaster University). Circles indicate females, squares indicate males.

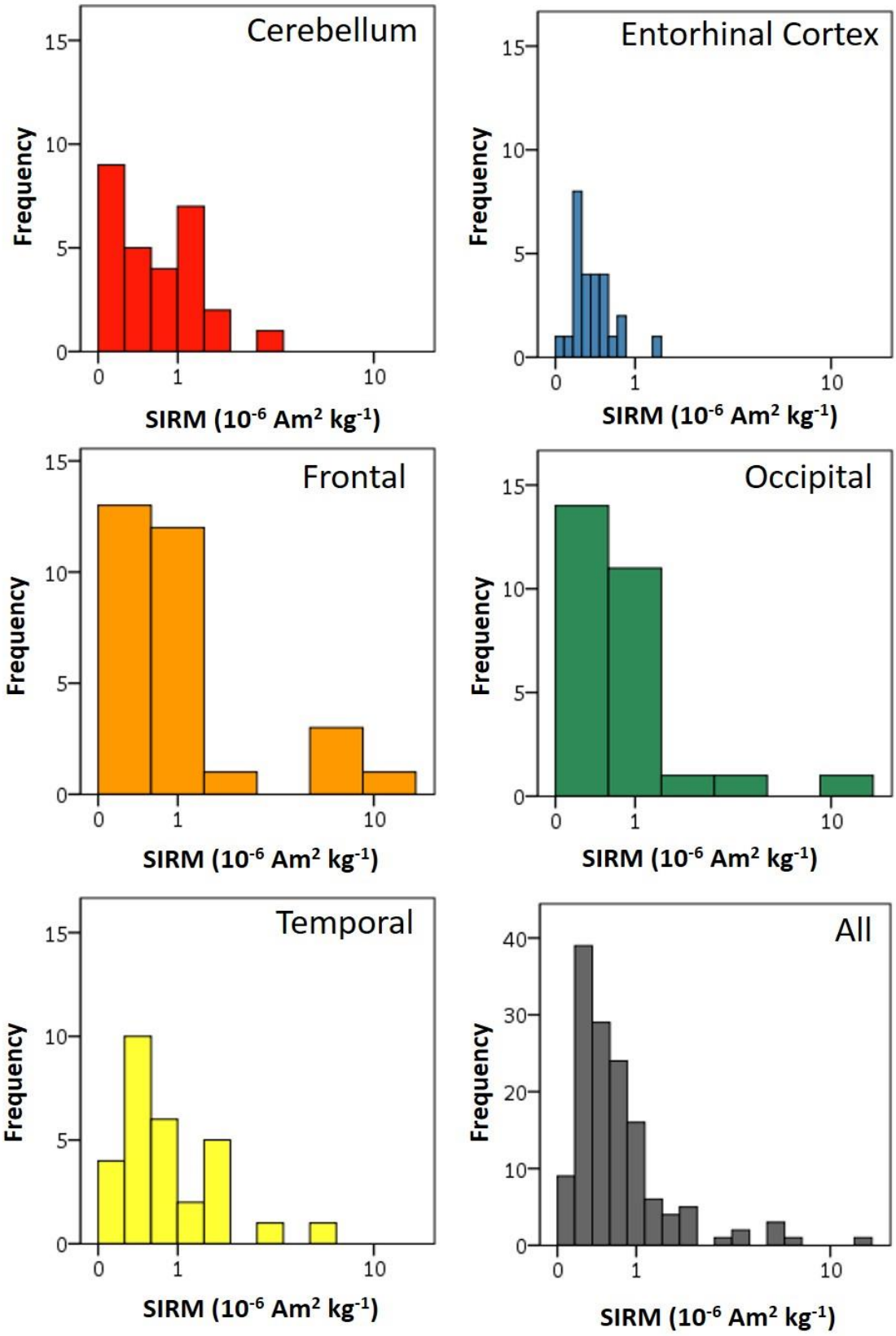

Figure A.2 Mass normalised saturation isothermal remanence magnetisations of human brain regions from Manchester, UK. Histograms depict the mass-normalised (freeze-dried weights) SIRM values of human brain tissue samples (MBB cohort) from the cerebellum, entorhinal cortex, frontal lobe, occipital lobe, temporal lobe and all regions.

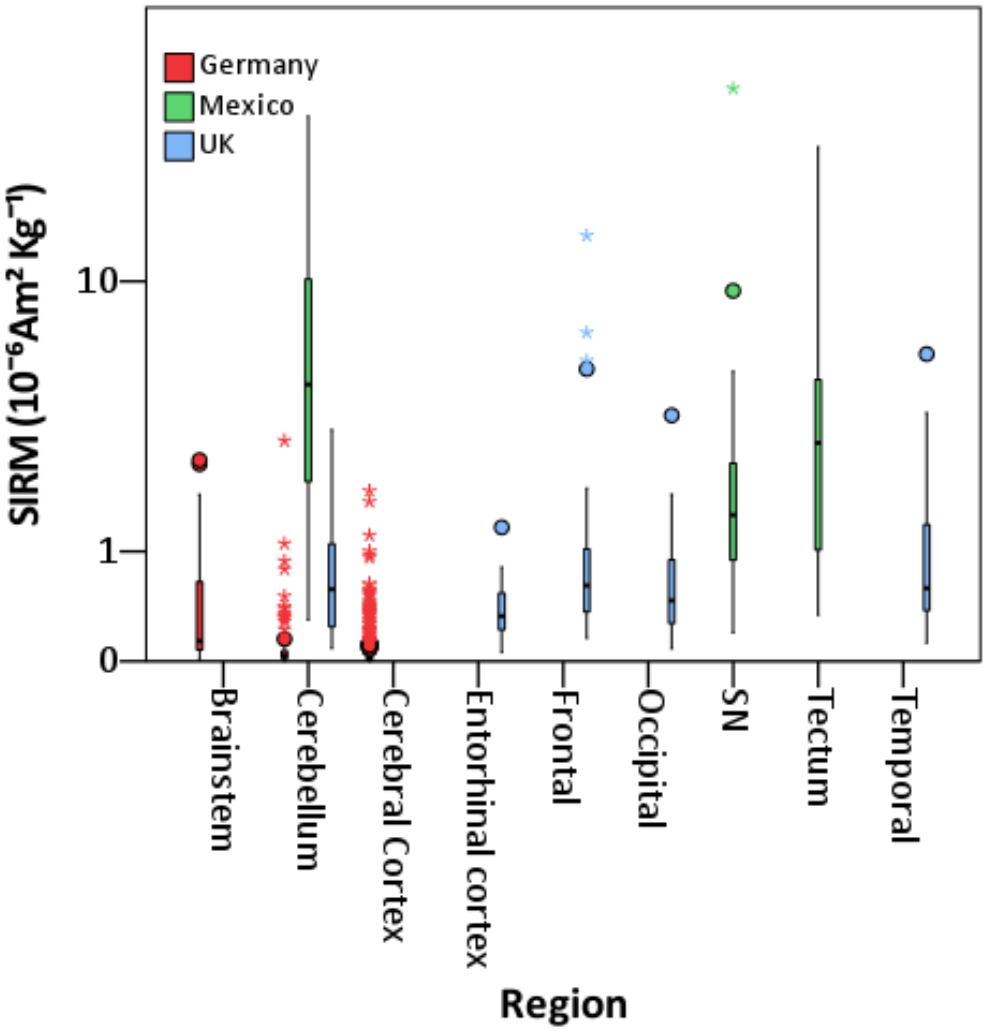

Figure A.3 Box plot of mass normalised SIRM values of human brain regions. Box plots depict the mass-normalised (freeze-dried weights for Mexico and UK, wet/formalin-soaked weights for Germany) saturation isothermal remanence magnetisations (SIRMs) of human brain tissue samples from the brainstem, cerebellum and cerebral cortex from Germany (red)(Gilder et al., 2018), the cerebellum, substantia nigra (SN) and tectum/tegmentum from Mexico City, Mexico (Calderón-Garcidueñas et al., 2020a), and the cerebellum, entorhinal cortex (EC), frontal lobe, occipital lobe and temporal lobe of individuals from MBB, UK (this study, blue). Outliers (○) are more than 1.5x the interquartile range, extremes (*) are more than 3x the interquartile range.

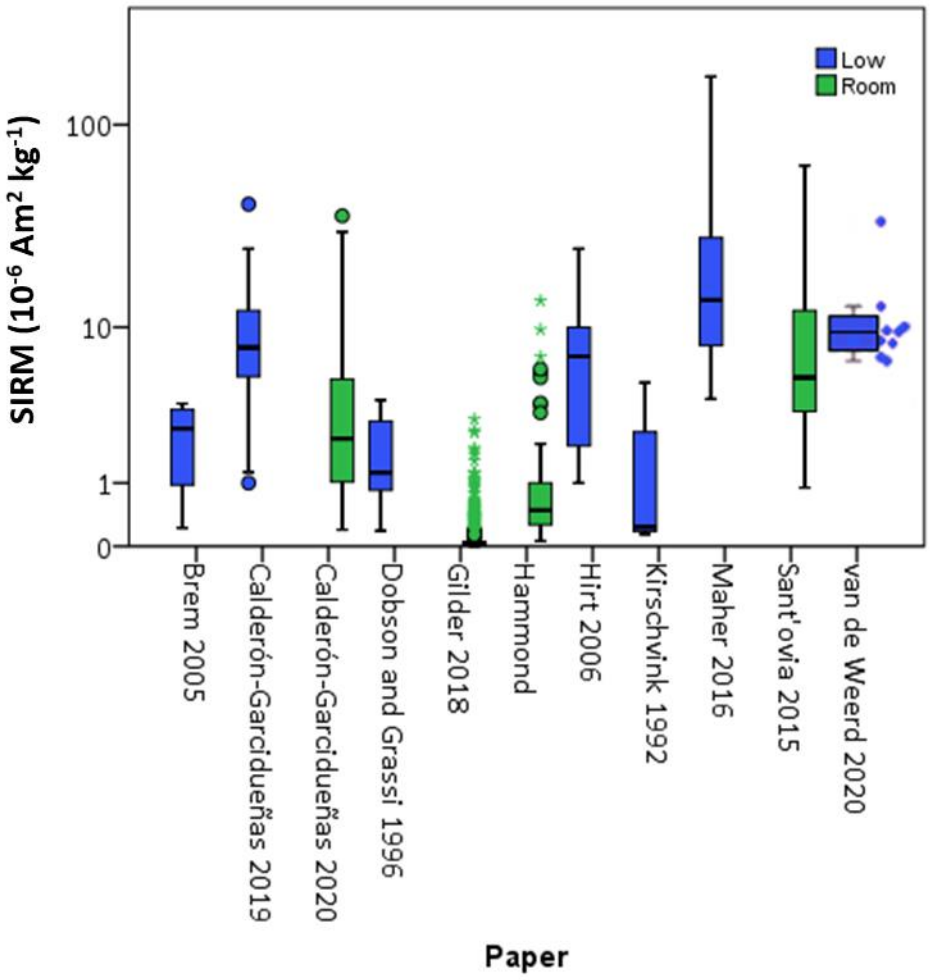

Figure A.4 Box plot of published mass normalised SIRM values of human brain regions. Box plots depict the mass-normalised saturation isothermal remanence magnetisations (SIRMs) of human brain tissue samples measured at 77K (low) or 293K (room) temperature. The 'van de Weerd 2020' data were measured at 100 K, and represents fresh frozen AD tissue (boxplot taken from (van der Weerd et al., 2020)). The 'Calderón-Garcidueñas 2019' boxplot represents human frontal tissue, rather than all measured tissue (primarily heart tissue). Data published in (Brem et al., 2005a, Calderón-Garcidueñas et al., 2019b, Calderón-Garcidueñas et al., 2020a, Dobson and Grassi, 1996, Gilder et al., 2018, Hirt et al., 2006, Kirschvink et al., 1992a, Maher et al., 2016, Sant'Ovaia et al., 2015, van der Weerd et al., 2020).Outliers (○) are more than 1.5x the interquartile range, extremes (*) are more than 3x the interquartile range. Samples obtained from the following locations: (Brem et al., 2005a), Zurich, Switzerland; (Calderón-Garcidueñas et al., 2020a, Calderón-Garcidueñas et al., 2019b), Mexico City and Veracruz, Mexico; (Dobson and Grassi, 1996), Zurich, Switzerland; (Gilder et al., 2018),Heideleberg, Wiesloch, Bayreuth, Germany; Hammond et al. (this study), N. England; (Hirt et al., 2006), Zurich, Switzerland; (Maher et al., 2016), N. England and Mexico City; (Sant'Ovaia et al., 2015), Porto, Portugal; (van der Weerd et al., 2020), Amsterdam, Netherlands.

Appendix B : Chapter 3 (Paper 2) Supplementary material

Trace and ultratrace metal concentrations in human brain tissue from Alzheimer's disease and controls

B.1 Supplementary Methods

B.1.1 Three-way analysis of variance (ANOVA)

A three-way mixed ANOVA was run to understand the effects of disease state, brain region and metal species on metal concentration. Data are mean ± standard deviations unless otherwise stated. The three-way interaction between disease state, brain region and metal species was not statistically significant, $F(36,1312) = 1.096$, $p = 0.386$. There was a statistically significant interaction between metal species and brain region, $F(36,1312)$, $p < 0.001$. All other two-way interactions were not statistically significant ($p > 0.05$). Statistical significance of a simple main effect was accepted at a Sidak-adjusted alpha level of 0.002. There was a statistically significant simple main effect of copper, manganese, and selenium (all $p > 0.001$). All pairwise comparisons were performed for statistically significant simple main effects. Sidak corrections were made with comparisons within each simple main effect considered a family of comparisons. Adjusted p-values are reported. Mean copper, manganese, and selenium levels were higher in the cerebellum compared to the frontal, occipital, and temporal lobes, $p = <0.001$.

B.1.2 Principal component analysis (PCA)

A principal components analysis (PCA) was run on 25 metal concentrations from 120 human brain tissue samples. The suitability of PCA was assessed prior to analysis. Variables without at least one coefficient >0.3 were excluded from analysis (As), as were variables with individual Kaiser-Meyer-Olkin (KMO) measures >0.5 (Pb). The overall KMO measure was 0.85, with a bartlett's test of sphericity of $p<0.001$ indicating the data is likely factorizable. The analysis revealed five components with an eigenvalue of 1 or more, explaining 38.4%, 12.0% 7.9%, 6.1% and 4.6% of the variance respectively. Inspection of the scree plot and rotated matrix indicated retaining four components would be the optimal solution. A varimax orthogonal rotation was employed, which gave an approximate simple structure.

Table B.1 Biological function, environmental sources, and toxicity of metal elements.

Metal	Biological function	Environmental sources	Toxic consequences	Refs.
Al	No known function	Earth's crust (most abundant metal), rock erosion, sea water, medication, dentistry, mining, industrial waste, agriculture, exhaust emissions, tobacco smoke	Pulmonary lesions, potentially neurotoxic/associated with neurological diseases like Alzheimer's disease, may affect fertility	(Igbokwe et al., 2019)
Sb	No known function	Earth's crust, volcanic eruptions, forest fires, sea spray, mining, smelters, coal power plants, fire-retardant treatments, alloys for manufacturing, brake pads, antiprotozoal drugs	Eye, skin, and lung irritation. Long term exposure – antimoniosis, a form of pneumoconiosis. Lung, cardiovascular and GI issues e.g., vomiting, bronchitis, increased blood pressure	(Hu et al., 2015, Sundar and Chakravarty, 2010, Cooper and Harrison, 2009)
As	No known function	Earth's crust (distributed widely in soil, drinking water), tobacco smoke, alloy production, manufacturing, mining, smelting, agricultural	Carcinogenic, highly toxic.	(Garelick et al., 2008, WHO, 2018)
Cd	No known function	Volcanic eruptions, industrial processes, agriculture (fertilizers), batteries, waste incineration, mining, smelting	Kidney, bone, and pulmonary damage. Carcinogenic.	(Nordberg et al., 2018, Sahmoun et al., 2005)
Ce	No known function	Earth's crust, sea water, catalytic converters,	Low to moderate toxicity; methemoglobinemia, itching, skin lesions	(Rim et al., 2013)
Cr	Possible role in lipid and glucose metabolism	Earth's crusts, volcanic eruptions, sea water spray, leather tanning, dyes, steel production	Carcinogenic (hexavalent Cr)	(Sun et al., 2015, Cefalu and Hu, 2004, Coetzee et al., 2020)
Co	Component of vitamin B_{12}	Earth's crust, volcanic ash, forest fire, sea spray, fossil fuel, sewage sludge, engine emissions, production of alloys	Primarily inhalation: possibly carcinogenic, IARC Group 2B, respiratory and cardiovascular issues, memory loss, neuropathy, contact dermatitis	(Catalani et al., 2012)

Cu	Connective tissue, bone, and nerves. Enzymes like superoxide dismutase, dopamine hydroxylase	Volcanoes, sea spray, windblown dust, mining, fossil fuel combustion, factories, fertilizers, brake pads, alloys, paint	Gastrointestinal issues (e.g., vomiting, nausea), anaemia, kidney damage, liver damage	(Rehman et al., 2019)
Fe	Oxygen transport (haemoglobin), energy transport (cytochromes), numerous haem and non-haem proteins	Earth's crust, volcanic eruption, sea water spray, forest fires, fossil fuels, steel production, milling, mining, brake pads	Gastrointestinal stress (e.g., diarrhoea, vomiting), heart, liver, CNS damage	(Winter et al., 2014)
Pb	No known function	Earth's crust, leaded fuel, paints, smelting, water (leaded pipes), cosmetics, traditional medicine, ammunition	Highly toxic; neurotoxic, kidney toxicity, teratogenic, probably carcinogenic	(Assi et al., 2016)
Mn	Cofactor in enzymes e.g., manganese superoxide dismutase, arginase	Earth's crust, rock erosion, fungicides, fuel additive, welding, mining	Manganism – a form of Parkinson's Disease, hepatic cirrhosis, neurotoxicity, altered cardiovascular function	(O'Neal and Zheng, 2015)
Hg	No known function	Volcanic eruption, geothermal sources, forest fires, dentistry, medical devices, fossil fuel emissions, batteries, medical waste incineration,	Highly toxic; endocrine toxicity, diabetes, GI toxicity, liver toxicity, pancreas toxicity, CNS toxicity. Possible carcinogen	(Gworek et al., 2020, Rice et al., 2014)
Mo	Component of enzymes e.g., xanthine reductase	Earth's crust, mining, agriculture, steel alloys, medical devices, adhesive, lubricant	Low toxicity but excess can lead to copper deficiency, anaemia, joint pain	(Harkness et al., 2017, Vyskocil and Viau, 1999)
Ni	No known function	Earth's crust, windblown dust, mining, smelting, tobacco smoke, fossil fuel combustion, sewage, waste incineration	Carcinogenic, contact dermatitis,	(Genchi et al., 2020)

Pd	No known function	Earth's crust, sea water, catalytic converters, exhaust emissions, electrical equipment (e.g., transistors), dentistry, mining, smelting, jewellery	Skin irritation (contact dermatitis), eye irritation, sensitization. Not much data available.	(Melber and Mangelsdorf, 2006, Kielhorn et al., 2002)
Pt	No known function	Catalytic converters, exhaust emissions, mining, dentistry, jewellery, anti-cancer drugs	Increasing toxicity with increasing solubility; neurotoxic, carcinogenic, and mutagenic. Same as Pd (above) Anaemia and kidney damage from prolonged exposure.	(Hartmann and Lipp, 2003, Pawlak et al., 2014)
Se	Important component of antioxidant enzymes e.g., glutathione peroxidase	Earth's crust, rock erosion, soil, volcanic eruption, coal combustion, mining, sewage sludge, fertilizers	Vomiting, abdominal pain, haemolysis, oedema, coma, liver necrosis, selenosis	(Tan et al., 2016)
Ag	No known function	Medical devices, dental fillings, cosmetics, antibacterial agents, textiles, mining, photography industry, high-capacity batteries, jewellery	Argyria. Potentially toxic at high doses but generally low toxicity	(Lansdown, 2010)
Sr	Possibly for prevention of osteoporosis	Earth's crust, sea spray, windblown soil, coal burning, phosphate fertilizers, nuclear power plants, tobacco smoke	Accumulates in bones and has similar chemistry to Ca. May increase chance of developing rickets. Possible carcinogen (Strontium chromate, more likely to be the chromium ion responsible)	(Ozgür et al., 1996, Pors Nielsen, 2004)
Ta	No known function	Earth's crust, medical devices, dentistry, mining, capacitors,	Few studies available. Biocompatibility seen with medical and dental uses.	(Filella, 2017)
Sn	No known function	Earth's crust, sea water, volcanic eruption, forest fires, dentistry, alloy production, agriculture, cosmetics, brake pads, mining	Inorganic tin generally low toxicity but can cause stenosis. Organic tin - neurotoxic	(Cima, 2011)

Ti	No known function	Earth's crusts, dentistry, medical devices, food additives, cosmetics, paint	Generally reported as non-toxic but increasing reports of TiO_2 nanoparticle toxicity in different laboratory models	(Al-Kattan et al., 2013, Chen and Mao, 2007, Kim et al., 2019, Zierden and Valentine, 2015)
W	No known function	Mining, alloy manufacturing, light filaments, cutting tools, military ammunition, Earth's crust	More toxic when alloyed with other metals e.g., Co, Ni. Possible carcinogen	(Wasel and Freeman, 2018, Lemus and Venezia, 2015)
V	Possibly plays a role in glucose metabolism (similar to insulin)	Earth's crust, volcanic eruptions, sea water, fossil fuel combustion, diesel fuel, electric vehicle batteries	Respiratory toxicant, nausea, vomiting, eye irritation, mild GI irritation	(Crans et al., 2004, Registry, 2012)
Zn	Antioxidant, present in over 100 enzymes	Earth's crust, volcanic eruption, sea spray, windblown dust, mining, smelting, steel production, fossil fuel combustion, industrial, tyre wear	Nausea, vomiting, iron and copper deficiency (and associated symptoms)	(Guarino et al., 2020)

Table B.2 Comparison of published metal concentrations in post-mortem human brain tissue from Alzheimer's disease and controls.

Metal(loid)	Comparison of AD and controls
Al	No change - (Schrag et al., 2011a, Stedman and Spyrou, 1997, Religa et al., 2006, Akatsu et al., 2011), ↑ - (Yoshimasu et al., 1980, Andrási et al., 1995, Corrigan et al., 1993, Srivastava and Jain, 2002, Rao et al., 1999)
Sb	No change - (Samudralwar et al., 1995, Ward and Mason, 1987)
As	No change - (Ward and Mason, 1987, Srivastava and Jain, 2002), ↓ - (Szabo et al., 2015)
Cd	No change - (Plantin et al., 1987, Panayi et al., 2002, Stedman and Spyrou, 1997, Srivastava and Jain, 2002, Akatsu et al., 2011), ↑ - (Ward and Mason, 1987), ↓ - (Szabo et al., 2015)
Ce	-
Cr	No change - (Plantin et al., 1987, Ward and Mason, 1987, Wenstrup et al., 1990, Akatsu et al., 2011), ↑ - (Srivastava and Jain, 2002)
Co	No change - (Plantin et al., 1987, Ward and Mason, 1987, Wenstrup et al., 1990, Szabo et al., 2015, Samudralwar et al., 1995)
Cu	No change - (Yoshimasu et al., 1980, Ward and Mason, 1987, Szabo et al., 2015, Corrigan et al., 1993, Religa et al., 2006), ↑ - (Lovell et al., 1998, Rao et al., 1999) , ↓ -(Plantin et al., 1987, Scholefield et al., 2020, Andrási et al., 1995, Deibel et al., 1996, Xu et al., 2017, Schrag et al., 2011a, Magaki et al., 2007, Akatsu et al., 2011)
Fe	No change - (Plantin et al., 1987, Wenstrup et al., 1990, Scholefield et al., 2020, Cornett et al., 1998a, Stedman and Spyrou, 1997, Griffiths and Crossman, 1993, Religa et al., 2006, Akatsu et al., 2011) , ↑ - (Andrási et al., 1995, Andrási et al., 2000, Szabo et al., 2015, Samudralwar et al., 1995, Deibel et al., 1996, Hare et al., 2016, Xu et al., 2017, Schrag et al., 2011a, Lovell et al., 1998, Srivastava and Jain, 2002, Rao et al., 1999) , ↓ - (Ward and Mason, 1987, Andrási et al., 1995, Andrási et al., 2000, Corrigan et al., 1993, Magaki et al., 2007)
Pb	No change - (Szabo et al., 2015)
Mn	No change - (Yoshimasu et al., 1980, Ward and Mason, 1987, Szabo et al., 2015, Akatsu et al., 2011, Andrási et al., 1995, Scholefield et

	al., 2020, Corrigan et al., 1993), ↑ - (Srivastava and Jain, 2002, Xu et al., 2017), ↓ - (Xu et al., 2017)
Hg	No change - (Ward and Mason, 1987, Cornett et al., 1998a, Samudralwar et al., 1995, Szabo et al., 2015), ↑ - (Wenstrup et al., 1990, Cornett et al., 1998b)
Mo	No change - (Corrigan et al., 1993, Srivastava and Jain, 2002)
Ni	No change - (Srivastava and Jain, 2002, Ward and Mason, 1987, Szabo et al., 2015)
Pd	-
Pt	-
Se	No change - (Plantin et al., 1987, Wenstrup et al., 1990, Cornett et al., 1998a, Samudralwar et al., 1995, Srivastava and Jain, 2002), ↓ - (Ward and Mason, 1987, Scholefield et al., 2020, Xu et al., 2017, Stedman and Spyrou, 1997, Corrigan et al., 1993)
Ag	No change - (Ward and Mason, 1987, Wenstrup et al., 1990, Srivastava and Jain, 2002)
Sr	No change - (Corrigan et al., 1993)
Ta	-
Sn	No change - (Corrigan et al., 1993, Ward and Mason, 1987, Szabo et al., 2015)
Ti	No change - (Ward and Mason, 1987, Corrigan et al., 1993)
W	-
V	No change - (Corrigan et al., 1993, Srivastava and Jain, 2002, Szabo et al., 2015) ↓ - (Ward and Mason, 1987)
Zn	No change - (Plantin et al., 1987, Szabo et al., 2015, Scholefield et al., 2020, Cornett et al., 1998a, Rulon et al., 2000, Stedman and Spyrou, 1997, Srivastava and Jain, 2002, Akatsu et al., 2011), ↑ - (Andrási et al., 2000, Samudralwar et al., 1995, Deibel et al., 1996, Xu et al., 2017, Schrag et al., 2011a, Lovell et al., 1998, Rao et al., 1999, Religa et al., 2006, Danscher et al., 1997), ↓ - (Ward and Mason, 1987, Wenstrup et al., 1990, Andrási et al., 2000, Andrási et al., 1995, Xu et al., 2017, Panayi et al., 2002, Corrigan et al., 1993)

Table B.3 Summary case information. A selection of 30 brains from elderly individuals were obtained from the Manchester Brain Bank.

Case	Sex	Age	Braak	Brain (grams)	PMD	Residence	Job
09/15	F	89	V-VI		72	Rowlands Gill	Secondary education teaching professionals
09/22	F	90	III-IV		6	Whitley Bay, Tyne and Wear	receptionist
09/37	M	90	0-I	1325	36	Bolton	No assessment
10/08	F	87	V-VI	1019	60	Heaton Mersey, Stockport	stock control clerk
10/13	F	85	VI	1013	51	Criccieth	Comptometer operator
10/16	M	91	III			Blakelaw, Newcastle-upon-Tyne,	Leisure and travel service occupations n.e.c.
10/26	M	84	0-I	1226	159	Kirkby Stephen	Teacher
10/40	M	86	III	1100 (fixed)	26	Whitley Bay, Tyne and Wear	Counter clerks
12/09	F	87	I-II	1178	87	Shaw, Oldham	General office assistants/clerks
12/23	M	95	I-II	1200 fixed	12	Sunderland	Architects
12/33	F	81	III-IV	1160	113.5	Woolton, Liverpool	Nurse
12/34	F	80	III	1000	81	Gatley, Cheshire	Routine inspectors and testers
13/09	F	85	V-VI	1030	73	Grange-over-Sands	Teacher and college lecturer
13/10	F	85	V-VI	1275	24	Newcastle Upon Tyne	Secondary education teaching professionals
14/01	F	93	III-IV	1133	70.5	Whitley Bay, Tyne and Wear	Special needs education teaching professionals
14/04	F	87	0-I	1152	24	Fenham, Newcastle-upon-Tyne,	Nurse
14/07	F	95	V	1200	39	Dronfield	Infants teacher
14/11	M	91	I-II	1520	43.5	Wilmslow, Cheshire	Personnel and industrial relations officers

14/20	F	90	0-I	1050	39	Gosforth, Newcastle-upon-Tyne	Typist
14/46	F	94	0-I	946	111	Middleton, Manchester	Civil Service administrative officers and assistants
15/01	M	90	I-II		156	Stockport	Directors and chief executives of major organisations
15/19	F	98	III	1029	84	Dukinfield	Publicans and managers of licensed premises
15/29	M	81	V-VI	1318	68	Alderley Edge	Head Teacher
15/31	M	91	I-II	1157	93	Whickham, Newcastle-upon-Tyne	Secondary education teaching professionals
15/42	M	89	III		128	Newcastle-upon-Tyne	Senior officials in national government
15/48	F	81	VI	967	98	Atherton	Drawing office tracer
16/01	M	90	III-IV	1309	26	Washington, Tyne and Wear	Engineering technicians
16/08	M	88	III-IV	1107	114	Sheffield	Bassetts factory worker
16/13	M	91	V		61	Newcastle-upon-Tyne	Graphic designer
16/14	F	92	V-VI	1160	118	Leyland	Water board worker

Table B.4 Dry/wet ratios of human brain tissue. Results of Mann-Whitney U tests, comparing male and female or AD and control are indicated in bold; *, p≤0.05

	Cerebellum	Frontal	Occipital	Temporal	All samples
AD	0.169 ± 0.027	0.199 ± 0.055	0.208 ± 0.028	**0.172 ± 0.028***	0.187 ± 0.039
Control	0.170 ± 0.026	0.179 ± 0.021	0.206 ± 0.025	**0.199 ± 0.039***	0.189 ± 0.031
Female	0.172 ± 0.032	0.202 ± 0.056	0.212 ± 0.027	0.179 ± 0.024	0.191 ± 0.040
Male	0.167 ± 0.168	0.178 ± 0.024	0.201 ± 0.259	0.188 ± 0.045	0.184 ± 0.032
All individuals	0.189 ± 0.026	0.204 ± 0.044	0.218 ± 0.024	0.201 ± 0.035	0.188 ± 0.036

Table B.5 Concentration of metal elements in human brain tissue from Alzheimer's disease and controls. Concentrations are reported as µg/g dry tissue.

		AD	Control
Al	Mean	3.78	3.64
	St. dev.	5.33	3.63
Sb	Mean	0.041	0.039
	St. dev.	0.063	0.044
As	Mean	0.071	0.068
	St. dev.	0.076	0.115
Cd	Mean	0.219	0.230
	St. dev.	0.134	0.120
Ce	Mean	0.006	0.005
	St. dev.	0.009	0.004
Cr	Mean	0.059	0.106
	St. dev.	0.084	0.206
Co	Mean	0.022	0.017
	St. dev.	0.014	0.008
Cu	Mean	30.90	31.49
	St. dev.	14.04	12.22
Fe	Mean	282.29	269.50
	St. dev.	92.73	76.05
Pb	Mean	0.237	0.248
	St. dev.	0.642	0.356
Mn	Mean	2.47	2.31
	St. dev.	1.02	0.77
Hg	Mean	3.61	3.04
	St. dev.	4.14	2.43
Mo	Mean	0.144	0.178
	St. dev.	0.067	0.125
Ni	Mean	0.073	0.079
	St. dev.	0.070	0.096
Pd	Mean	0.528	0.741
	St. dev.	0.858	0.637
Pt	Mean	0.001	0.002
	St. dev.	0.002	0.001
Se	Mean	0.068	0.082
	St. dev.	0.155	0.152

Ag	Mean	0.120	0.123
	St. dev.	0.100	0.126
Sr	Mean	0.254	0.268
	St. dev.	0.208	0.235
Ta	Mean	0.002	0.002
	St. dev.	0.002	0.002
Sn	Mean	0.028	0.030
	St. dev.	0.020	0.020
Ti	Mean	1.18	0.89
	St. dev.	1.80	0.59
W	Mean	0.081	0.063
	St. dev.	0.125	0.051
V	Mean	0.038	0.045
	St. dev.	0.029	0.054
Zn	Mean	118.86	108.49
	St. dev.	32.98	22.83

Table B.6 Regional distribution of metal elements in human brain tissue from females (n=17) and males (n=13). Concentrations are reported as μg/g dry tissue.

		Cerebellum		Frontal		Occipital		Temporal	
		F	M	F	M	F	M	F	M
Al	Mean	3.43	3.84	4.54	3.04	3.65	1.57	5.85	3.08
	St. dev.	3.49	6.80	4.95	3.70	2.76	1.05	7.95	2.64
Sb	Mean	0.036	0.026	0.052	0.030	0.040	0.017	0.075	0.034
	St. dev.	0.037	0.020	0.061	0.028	0.033	0.018	0.112	0.053
As	Mean	0.074	0.062	0.063	0.100	0.068	0.040	0.077	0.076
	St. dev.	0.128	0.049	0.042	0.181	0.058	0.030	0.081	0.087
Cd	Mean	0.314	0.218	0.228	0.179	0.235	0.157	0.245	0.168
	St. dev.	0.195	0.122	0.109	0.103	0.122	0.095	0.100	0.089
Ce	Mean	0.006	0.003	0.007	0.003	0.006	0.002	0.010	0.004
	St. dev.	0.006	0.002	0.010	0.003	0.006	0.002	0.015	0.003
Cr	Mean	0.072	0.049	0.108	0.098	0.074	0.061	0.091	0.044
	St. dev.	0.111	0.041	0.252	0.197	0.106	0.142	0.121	0.026
Co	Mean	0.023	0.020	0.020	0.015	0.022	0.013	0.026	0.016
	St. dev.	0.014	0.010	0.014	0.007	0.012	0.004	0.019	0.011
Cu	Mean	44.85	47.36	23.20	27.88	29.03	26.16	24.50	26.84
	St. dev.	14.29	10.29	7.86	12.50	10.35	8.10	6.48	10.93
Fe	Mean	280.87	308.80	257.41	232.47	309.17	260.82	313.86	241.86
	St. dev.	98.91	78.52	73.48	55.63	99.25	49.38	113.37	61.87
Pb	Mean	0.405	0.403	0.294	0.187	0.185	0.099	0.124	0.218
	St. dev.	1.028	0.816	0.440	0.307	0.478	0.127	0.137	0.374
Mn	Mean	3.57	3.46	1.92	1.92	2.12	1.87	2.33	1.98
	St. dev.	1.02	0.37	0.60	0.53	0.47	0.43	0.97	0.54
Hg	Mean	3.92	2.21	4.24	2.29	3.77	1.62	5.50	2.47
	St. dev.	3.37	0.87	4.24	1.44	2.84	0.80	6.66	1.06
Mo	Mean	0.135	0.097	0.182	0.164	0.158	0.142	0.166	0.201
	St. dev.	0.085	0.028	0.132	0.076	0.069	0.046	0.059	0.163
Ni	Mean	0.100	0.044	0.077	0.080	0.067	0.044	0.090	0.086
	St. dev.	0.135	0.023	0.065	0.077	0.061	0.043	0.079	0.089
Pd	Mean	0.832	0.642	0.531	0.908	0.433	0.422	0.520	0.593
	St. dev.	1.617	0.583	0.445	0.831	0.354	0.520	0.352	0.711
Pt	Mean	0.002	0.001	0.001	0.001	0.002	0.001	0.002	0.001
	St. dev.	0.002	0.001	0.001	0.001	0.002	0.001	0.002	0.001
Se	Mean	0.211	0.173	0.010	0.030	0.051	0.046	0.027	0.033

	St. dev.	0.316	0.159	0.022	0.040	0.094	0.063	0.043	0.049
Ag	Mean	0.161	0.091	0.130	0.085	0.133	0.066	0.169	0.101
	St. dev.	0.182	0.037	0.095	0.059	0.103	0.059	0.150	0.041
Sr	Mean	0.264	0.225	0.276	0.287	0.254	0.161	0.346	0.228
	St. dev.	0.348	0.090	0.138	0.189	0.181	0.068	0.345	0.071
Ta	Mean	0.002	0.002	0.002	0.002	0.002	0.001	0.002	0.002
	St. dev.	0.003	0.002	0.002	0.001	0.002	0.001	0.003	0.002
Sn	Mean	0.029	0.022	0.034	0.028	0.031	0.022	0.034	0.026
	St. dev.	0.020	0.013	0.024	0.026	0.020	0.017	0.023	0.017
Ti	Mean	0.996	0.744	1.911	0.827	0.948	0.574	1.447	0.842
	St. dev.	0.632	0.277	3.479	0.340	0.518	0.218	1.387	0.477
W	Mean	0.076	0.055	0.069	0.049	0.082	0.040	0.143	0.062
	St. dev.	0.071	0.022	0.051	0.030	0.099	0.021	0.231	0.043
V	Mean	0.050	0.028	0.055	0.034	0.042	0.021	0.045	0.039
	St. dev.	0.060	0.018	0.063	0.028	0.033	0.010	0.037	0.019
Zn	Mean	126.12	118.16	111.80	111.20	104.41	90.01	134.87	118.66
	St. dev.	33.74	13.30	30.28	26.15	21.89	16.41	38.34	28.65

Table B.7 Summary of sample group characteristics for females and males.

Variable	**Females (n=17)**	**Males (n=13)**	**P value**
Age (years)	88 ± 5	89 ± 3	0.187
AD (Controls)	14 (3)	5 (8)	**<0.001**
Post-mortem delay (PMD, hours)	67 ± 32	77 ± 50	0.530
Whole brain weight (g)	1087 ± 95	1251± 127	**<0.001**
Dry/wet ratio	0.191 ± 0.04	0.184± 0.03	0.314

Table B.8 Principal component analysis of metal elements in human brain tissue from Alzheimer's disease and controls.

	Component			
	1	2	3	4
Cerium	**.909**	.275	.146	.054
Mercury	**.887**	.355	.122	.134
Titanium	**.800**	.131	-.033	.134
Antimony	**.771**	.278	.043	-.066
Aluminium	**.739**	.399	.162	.055
Cobalt	**.590**	.123	**.438**	.233
Tungsten	**.411**	.344	-.048	.031
Molybdenum	.150	**.787**	.058	.127
Vanadium	**.425**	**.732**	.056	.186
Nickel	.200	**.731**	.033	.041
Silver	**.622**	**.628**	.146	.059
Strontium	.177	**.622**	.150	-.231
Chromium	.248	**.508**	-.015	.194
Tin	**.459**	**.479**	.229	.194
Copper	-.109	.060	**.861**	.053
Manganese	.265	.107	**.833**	.069
Iron	**.448**	.057	**.593**	.125
Selenium	-.145	-.290	**.581**	.060
Zinc	**.455**	.355	**.555**	.240
Cadmium	.098	.206	**.471**	.111
Tantalum	.074	.087	.137	**.911**
Palladium	-.045	.065	.163	**.801**
Platinum	.307	.080	.099	**.757**

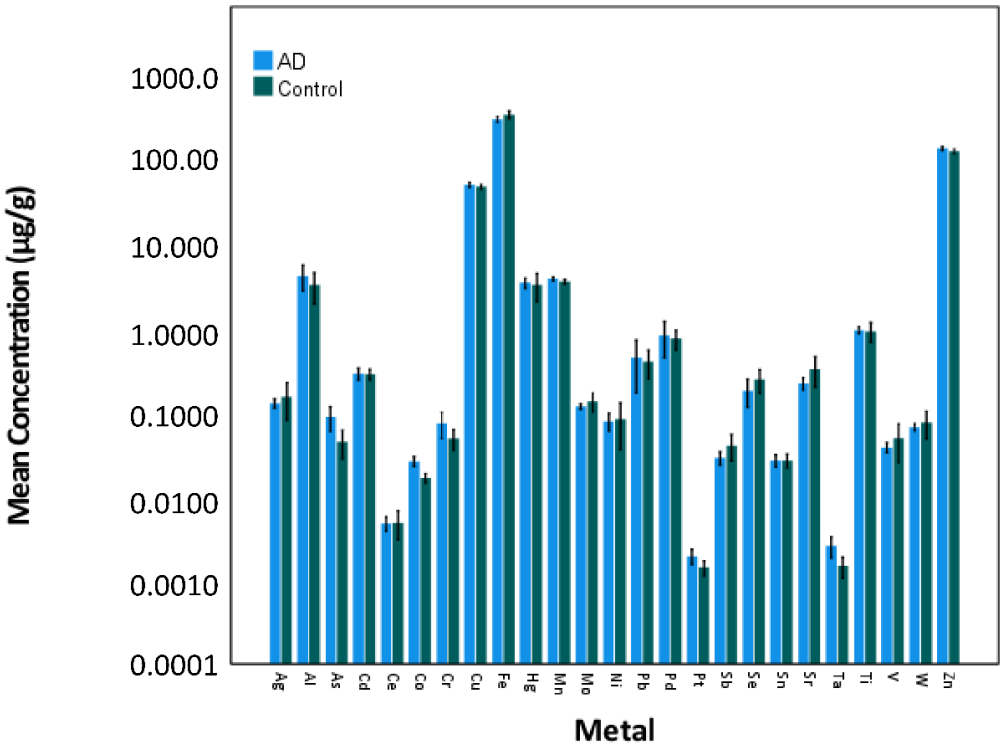

Figure B.1 Regional distribution of metal elements in human cerebellum from Alzheimer's disease (n=19) and controls (n=11). Concentrations are reported as µg/g dry tissue. Error bars show standard error of the mean (SEM).

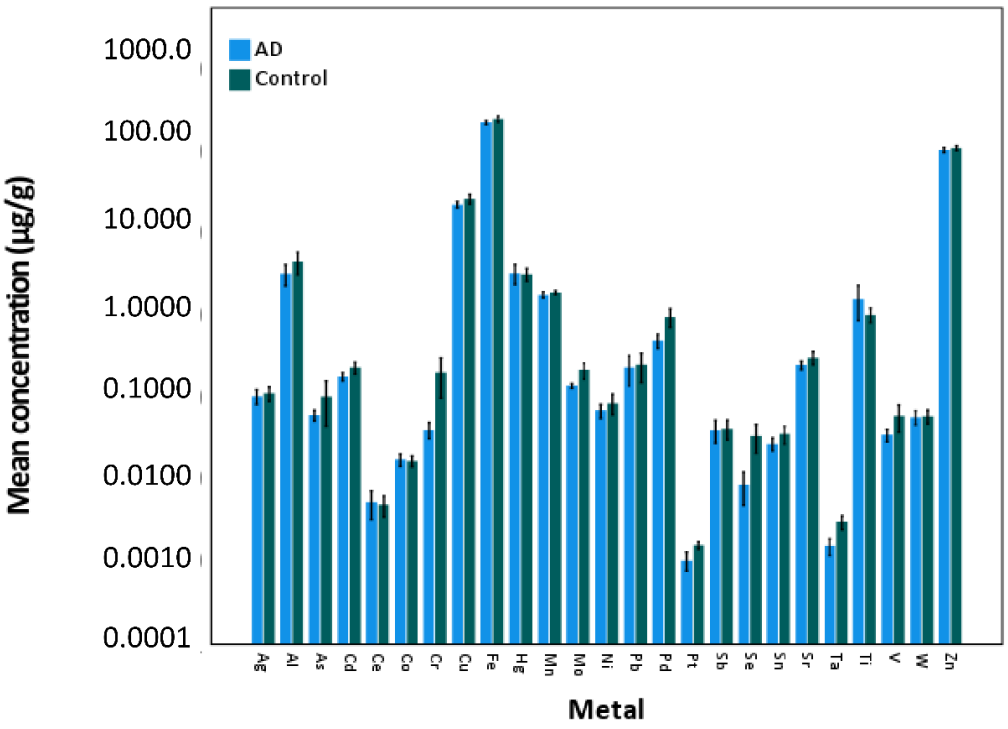

Figure B.2 Regional distribution of metal elements in human frontal lobe from Alzheimer's disease (n=19) and controls (n=11). Concentrations are reported as µg/g dry tissue. Error bars show standard error of the mean (SEM).

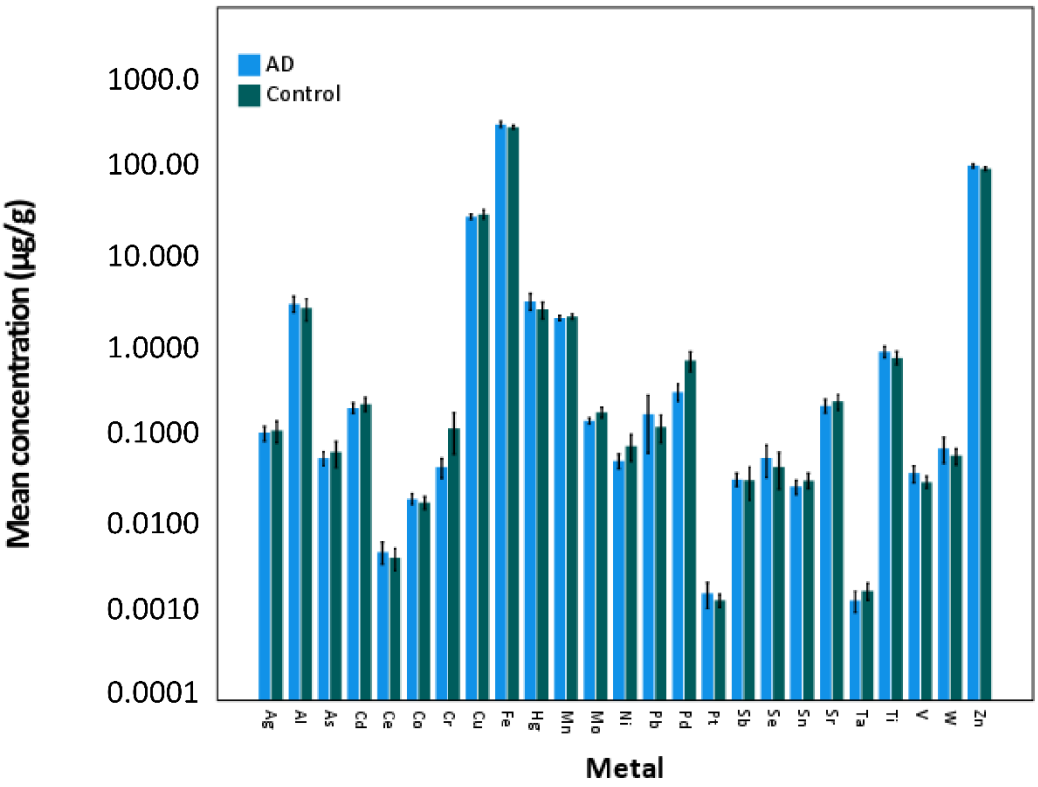

Figure B.3 Regional distribution of metal elements in human occipital lobe from Alzheimer's disease (n=19) and controls (n=11). Concentrations are reported as µg/g dry tissue. Error bars show standard error of the mean (SEM).

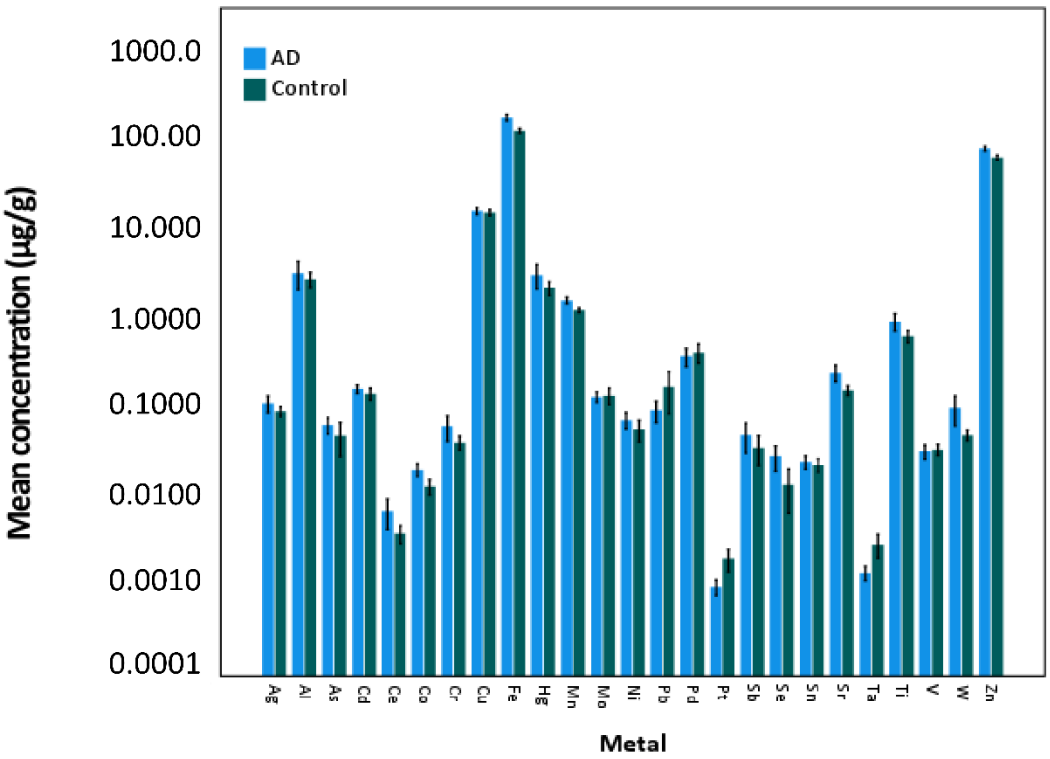

Figure B.4 Regional distribution of metal elements in human temporal lobe from Alzheimer's disease (n=19) and controls (n=11). Concentrations are reported as µg/g dry tissue. Error bars show standard error of the mean (SEM).

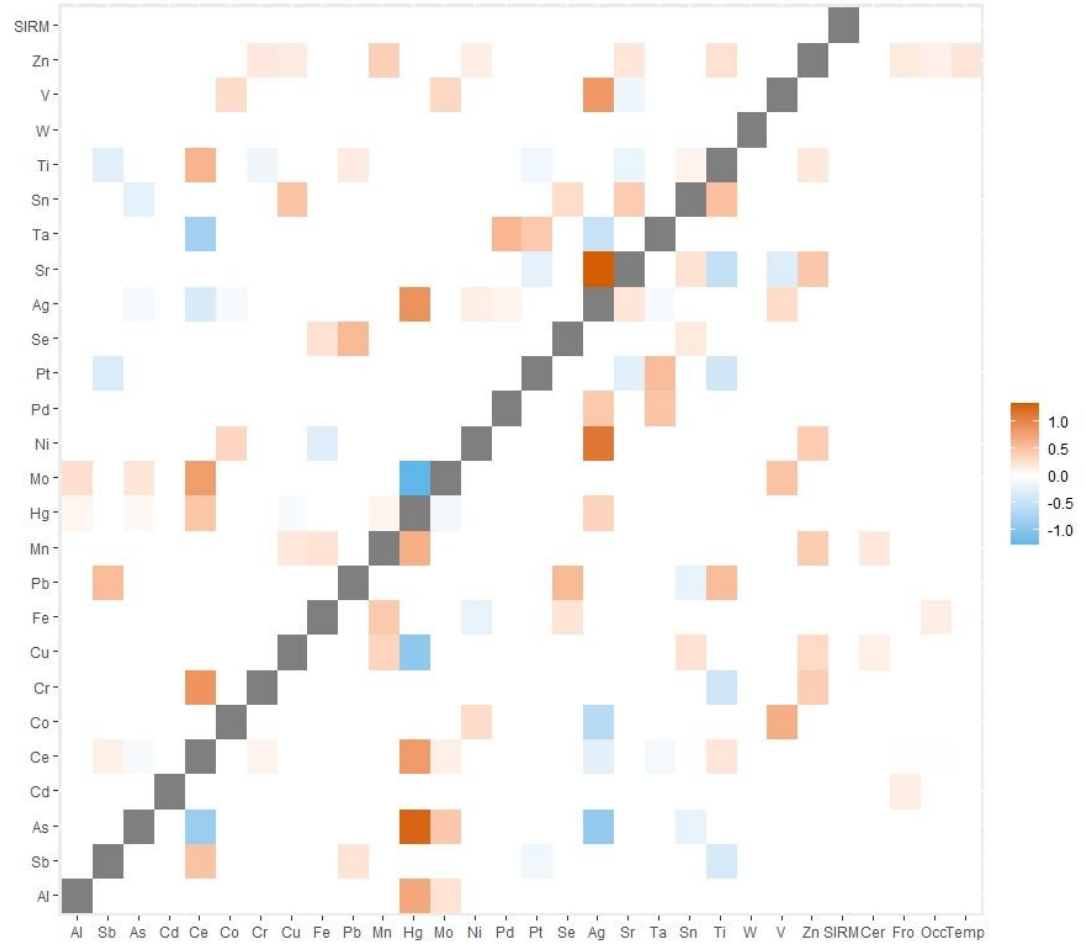

Figure B.5 Relationship between metal elements in human brain tissue. The heatmap depicts a matrix of effect sizes, exploring the impact of metal concentration, region and SIRM on a particular metal. Only significant effects are shown (p>0.05). Orange represents a positive effect (increase), whilst blue represents a negative effect (decrease).

Appendix C : Chapter 4 (Paper 3) Supplementary material

Oxidative stress, cytotoxic and inflammatory effects of urban ultrafine road-deposited dust from the UK and Mexico in human epithelial lung (Calu-3) cells

C.1 Magnetic properties of the total and ultrafine (< 220 nm) road-deposited dust particles

Isothermal remanent magnetisation (IRM) is a commonly used parameter in environmental magnetism. It is dependent on the concentration, mineralogy, and grain size distribution of the magnetically ordered grains within a sample. This parameter is especially sensitive to the presence of strongly magnetic Fe forms, including metallic Fe (α-Fe), magnetite (Fe_3O_4), and its oxidised counterpart, maghemite (γ-Fe_2O_3).

Low-temperature magnetic measurements can be used to identify certain Fe forms in a sample. For instance, if magnetite is present in the sample, the Verwey transition is visible in the zero-field cooling/heating curves (Verwey, 1939, Özdemir et al., 1993). This first order transition is displayed by a sudden decrease in IRM at ~70 – 130 K. The Verwey transition is usually sharp for pure magnetite while partially oxidised (maghemitised) magnetites usually display wider and indistinct Verwey transitions (Özdemir and Dunlop, 2010). Verwey transition is also broadened for magnetites ~20-30 nm in size, close to the border of stable single domain / superparamagnetic grains (Özdemir and Dunlop, 2010).

Supplementary Figure S1 shows the room-temperature (300 K) IRM for bulk, unfiltered road-deposited PM samples from the three locations. The Birmingham sample displays the highest IRM, reaching $71 \cdot 10^{-3}$ Am^2/kg, followed by Mexico City ($51 \cdot 10^{-3}$ Am^2/kg), and Lancaster ($36 \cdot 10^{-3}$ Am^2/kg) (Supplementary Figure S1; Supplementary Table S2). These IRMs correspond to approximately ~0.32 – 0.95 wt.% of magnetite for Birmingham, ~0.24 – 0.79 wt.% of magnetite for Mexico City, and ~0.18 – 0.63 wt.% of magnetite in Lancaster.

The Verwey transition, indicative of the presence of magnetite, is visible on the heating curve at ~75 – 90 K, measured for ultrafine road-deposited dust particles (UF-RDPs) from Mexico City (Supplementary Figure S2). This transition is broad and indistinct, probably reflecting very small grain size (~20 – 30 nm) and/or partial oxidation (maghemitisation) of the magnetite grains (Özdemir and Dunlop, 2010). The presence of superparamagnetic (< ~30 nm) grains is further supported by a relatively low temperature of the Verwey transition and ~43% increase in IRM at low-temperature (10 K), compared to the IRM measured at room temperature; and

~16% increase in IRM at 10 K, compared to IRM at 50 K (Özdemir and Dunlop, 2010, Özdemir et al., 1993).

C.2 Supplementary methods

C.2.1 Ultrafine particle extraction from road-deposited dust

Following evaporation of ethanol, extracted UF-RDPs were weighed in a room with controlled temperature (20°C) and humidity (50%), with a Mettler AT250 balance (accuracy 0.00001 g).

C.2.2 Inductively couple plasma (ICP) mass spectrometry (-MS) and optical emission spectroscopy (-OES)

A subsample of filtered UF-RDPs was taken from each stock and the ethanol fully evaporated. Dried samples were weighed in savillex Teflon vessels and digested overnight (100°C) in digestion mixture (3ml HNO_3, 2ml HCL, 0.5ml HF, all double distilled). After complete digestion and evaporation, samples were acidified in 2-5% ultrapure HNO_3 then analysed for metals and elements of interest using an Agilent Varian Vista Pro (ICP-OES) or Attom Nu (ICP-MS) with the following settings: Analysis mode = Deflector Jump, Dwell time / peak = 1 millisecond, Number of sweeps = 500, Number of cycles = 3, Resolution = 300.

C.2.3 Superconducting quantum interference device (SQUID) magnetometry

The magnetic content of the bulk (unfiltered) RDPs was measured with a 2G RAPID cryogenic magnetometer (at the Centre for Environmental Magnetism & Palaeomagnetism, Lancaster University, UK) by imparting an isothermal remanent magnetisation (IRM) at 1 Tesla (T) (using a Newport Instruments electromagnet) at room temperature.

For UF-RDPs, IRM was imparted at 1T and 300 K, was measured upon cooling to 10 K (at average rate 5 K/min) at the University of Cambridge. Then, IRM was imparted again (at 1 T and 10 K) and measured upon heating to 300 K. To increase signal-to-noise ratio, 10 DC scans were used for IRM at 300 K and 10 K.

C.2.4 Additional cell assay information

All cell culture reagents were purchased from Lonza Ltd (Basel, Switzerland) unless stated otherwise. Fluorescent and absorbance readings were conducted using a Tecan Infinite M200 pro spectrophotometer.

Bovine serum albumin (BSA) has variably been reported to modulate toxicity by enhancing metal dissolution (Boehmler et al., 2020) and/or reduce toxicity by forming a protein corona around dosed metal particles, shielding cells from the inner core (Peng et al., 2013).

Conversely, the presence of a protein corona does not always alter cytotoxicity (Mbeh et al., 2015). BSA was used here as a stabilizing agent. To ensure all test conditions were identical, an appropriate amount of BSA was added to each test condition, including controls, so that the final BSA concentration was consistent across all test conditions (final concentration 0.02% for Lancaster and Mexico City, and 0.04% for Birmingham).

C.2.5 ROS assay

The 4 h timepoint was chosen to reflect the rapid clearance of UFPs from the lungs, from as little as 4 h (Oberdörster et al., 2004). Background controls (n=3) consisting of UF-RDPs or TBHP in UltraMem were measured alongside the cell treatments for intrinsic fluorescence and subtracted from the experimental cell fluorescence readings.

C.2.6 Cytokine ELISAs

UFPs have a high surface area for cytokine adsorption (Kocbach et al., 2008) which can cause interference with ELISA results. Here, known cytokine standards were spiked with UF-RDPs and measured via ELISA. Values were within 5-10% of unspiked samples measured in parallel (data not shown), suggesting any adsorption has limited impact on the assay.

Table C.1 Overview of cytotoxicity studies of road-deposited dust and roadside airborne PM in human and rodent models.

Size	Method of collection	Location	Cell line/model	Exposure	Dose	Assays/outcomes	Ref.
Sieved to <75 µm, then aerosolized to collect $PM_{2.5}$ and PM_{10}. (Settled dust)	Road vacuum sweeper	Gangdong-Gu, Seoul, Korea	Human corneal epithelial cells (2.040 pRSV-T)	Liquid culture	10 - 500 µg/ml	MTT (cell viability) – ↓ LDH (cytotoxicity) – ↑ NO (Oxidative stress) – ↑ (500µg/ml total $PM_{2.5}$ and PM_{10}) IL-8 (cytokine release) -↑ (total $PM_{2.5}$ and PM_{10}) ROS – ↑ (more so for $PM_{2.5}$ than PM_{10})	(Yoon et al., 2018)
Particle number median aerodynamic diameter 2.06 µm (Settled dust)	Sweeping	Little rock, Arkansas, USA	Murine macrophage cells (RAW264.7)	Liquid culture	0, 5, 50 µg/ml	LDH (cytotoxicity) – no effect Hmox1 and cat – ↑ DHE – no change Mitochondrial respiration – ↓ DNA methylation- ↓DMNT expression Major and minor satellite DNA - ↑	(Miousse et al., 2015)
Sieved to <100 µm (Settled dust)	Vacuum cleaner	Daejeon, South Korea	Human adherent lung fibroblasts (WI-38) and human foreskin fibroblasts (BJ)	Liquid culture	0.01 - 2 mg/ml	WST8 (cell viability) – ↓ Association with metals and decrease in viability	(Koh and Kim, 2019)
Sieved to <100 µm (Settled dust)	Vacuum cleaner	South Korea	Human adherent lung fibroblasts (WI-38) and human foreskin fibroblasts (BJ)	Liquid culture	0.01 - 2 mg/ml	CCK8 (cell viability) – ↓ Different responses 28 different samples PAH and metal content correlated to cytotoxicity	(Kim and Koh, 2020)
Sieved to <100 µm. Extracts were filtered with 0.2 µm syringe filter (Settled dust)	Sweeping	Guangzhou, China	Human hepatocellular liver carcinoma (HepG2) and human skin derived keratinocyte (KERTr)	Liquid culture	334 and 667 µg/ml	MTT (cell viability) – ↓	(Huang et al., 2015)

<2.5µm (Settled dust)	Vacuumed with high volume surface sampler	Los Angeles, California, New York, Atlanta, Georgia, USA	Male Sprague Dawley rats	RD was aerosolized with a Wright dust feeder	306 µg/m^3 and 954 µg/m^3	Chemiluminescence (Oxidative stress) – ↑ (heart) TBARS (Oxidative stress) – ↑ (heart) No. of lung macrophages - ↑	(Seagrave et al., 2008)
$PM_{2.5}$ (Settled dust/Airborne PM)	Sweeping to simulate road cleaning then samples collected by pumping air	Harbin, Beijing, Tianjin, Lanzhou, Xi'an, Nanjing, Shanghai, Chengdu, Wuhan, and Guangzhou, China	Human pharynx epithelial cells (FaDu)	Liquid culture	50 µg/ml	SRB (viability) – ↓ LDH (cytotoxicity) – ↑ IL-6 (cytokine release) - ↑ HMBG1 (protein) - ↑ RAGE (protein) - ↑ Occludin (protein) - ↓ E-cadherin (protein) - ↓ EGFR (protein) - ↑ p-EGFR (protein) - ↑	(Tung et al., 2021)
$PM_{2.5}$ (Settled dust/Airborne PM)	Sweeping to simulate road cleaning then samples collected by pumping air	Harbin, Beijing, Tianjin, Lanzhou, Xi'an, Nanjing, Shanghai, Chengdu, Wuhan, and Guangzhou, China	Human alveolar epithelial cells (A549)	Liquid culture	50 µg/ml	ROS – ↑ LDH (cytotoxicity) – ↑ (in industrial cities) Heavy metals correlated to ROS LDH correlated to organic compounds and cations LDH production associated with ROS Vehicle emissions and coal combustion were strongly correlated with cellular ROS	(Sun et al., 2021)
<38 µm initially, then filtered with 1.2 µm filter (Settled dust)	Sweeping	Gwangju unamdong, South Korea	Human alveolar epithelial cells (A549) Chinese hamster ovary strain K1 (CHO-K1) cell line	Liquid culture	0 - 150 µg/ml	Neutral red (cell viability) – no change DCFDA (ROS) – no change	(Cho et al., 2018)
<38 µm then aerosolized in $PM_{2.5}$ filter sampling system	No data	Urban Gwangju, South Korea	Human alveolar epithelial cells (A549)	Liquid culture	0 - 150 µg/ml	DCFDA (ROS) – ↑	(Park et al., 2018)

(Settled dust)							
nPM (<200nm) (Airborne PM)	High volume ultrafine particle sampler	Near CA-110 freeway, Los Angeles, California, USA	Hippocampal slices Primary neurons Primary glial cultures	Liquid culture	1 - 20 µg/ml	Cytotoxicity (LDH) – ↑ Neurite outgrowth – ↓ (inhibition) PI uptake – ↑ (neurotoxic) IL-1α (cytokine mRNA) – ↑ TNFα (cytokine mRNA)– ↑ IL-1β (cytokine mRNA) – ↑ IL-6(cytokine mRNA) – ↑	(Morgan et al., 2011)
nPM (<200nm) (Airborne PM)	High volume ultrafine particle sampler	Near CA-110 freeway, Los Angeles, California, USA	Primary mixed glia (microglia and astrocytes)	Liquid culture	10 µg/ml	TNFα (cytokine release) – ↑ IL-1β (cytokine release) – ↑ IL-6(cytokine release) – ↑ KC (cytokine release) – ↑ IFN-γ (cytokine release) – ↑ IL-5 (cytokine release) – ↑ IL-4(cytokine release) – ↓	(Woodward et al., 2017)
<0.22 µm (Airborne PM)	High volume air sampler	5m from busy road in Kobe, Japan	Chinese hamster lung fibroblasts (CHL/IU) and normal human fibroblasts (WI-38)	Liquid culture	Mean 128.9 µg/m^3	Viability (MTS) – ↓ LDH (cytotoxicity) – ↑ Proliferation – ↓ (inhibition)	(Yamaguchi and Yamazaki, 2001)
$PM_{1.0}$, $PM_{0.56}$ and $PM_{0.056}$ (Airborne PM)	MOUDI-110 cascade impactor	Lucknow, Uttar Pradesh, India	Mouse fibroblast cells (10T1/2)	Liquid culture	3 - 150 µg/ml	MTT (cell viability) – ↓ (dose and particle size dependent) DNA damage – ↑ (dose and particle size dependent)	(Verma et al., 2014)
PM_1 (Airborne PM)	PM_1 cyclone sampler	Hong Kong, China	Human alveolar epithelial cells (A549)	Liquid culture	50 µg/ml	DCFDA (ROS) – ↑ LDH (cytotoxicity) – ↑ IL-6 (cytokine release)– ↑	(Niu et al., 2021)

Table C.2 Elemental composition of the analysed UF-RDPs from Lancaster, Birmingham, and Mexico City (b.d.l. = below detection limit).

Element	Method	Lancaster		Birmingham		Mexico City	
		Concentration	St.dev [%]	Concentration	St.dev [%]	Concentration	St.dev [%]
Al (ppm)	ICP-OES	57.9	2.3	55.8	1.8	97.1	3.2
Ba (ppm)	ICP-MS	0.4	0.6	0.5	6.5	1.6	2.5
Ca (ppm)	ICP-OES	770	0.5	743	0.9	3651	0.7
Cd (ppm)	ICP-OES	1.1	13.9	6.1	4.2	b.d.l.	-
Co (ppm)	ICP-MS	0.4	1.3	0.7	50.7	2.8	2.8
Cr (ppm)	ICP-MS	18.7	1.0	15.0	2.6	125.3	0.6
Cu (ppm)	ICP-MS	29.1	1.7	19.7	0.9	67.2	0.3
Fe (ppm)	ICP-OES	55.9	1.4	14.7	3.3	77.1	1.3
K (ppm)	ICP-OES	256.8	0.8	4.6	5.7	789.7	0.6
Mg (ppm)	ICP-OES	92	3.2	95	3.5	736	1.8
Mn (ppm)	ICP-OES	5.3	1.2	2.5	2.4	8.1	1.9
Na (ppm)	ICP-OES	105,489	0.6	1,003	10.5	42,163	1.0
Ni (ppm)	ICP-OES	b.d.l.	-	1.1	14.9	8.3	12.0
P (ppm)	ICP-OES	43.4	6.1	20.8	20.3	127.9	10.2
Pb (ppm)	ICP-MS	8.0	2.2	0.7	39.8	1.2	6.5
Si (ppm)	ICP-MS	0.08	2.5	0.02	15.5	0.06	2.1
Sn (ppm)	ICP-MS	1.6	2.0	1.7	12.6	15.6	1.7
Sr (ppm)	ICP-OES	0.8	1.9	0.1	6.4	2.1	1.1
Ti (ppm)	ICP-OES	5.3	2.3	2.1	2.1	12.1	1.6
V (ppm)	ICP-MS	5.3	0.2	2.0	18.1	11.1	1.9
Zn (ppm)	ICP-MS	374	2.7	277	5.7	1337	1.2
Ce (ppb)	ICP-MS	3.0	26.6	3.2	17.8	3.1	35.0
Er (ppb)	ICP-MS	0.2	109.1	0.3	42.3	0.4	136.6
Hg (ppb)	ICP-MS	8.6	20.1	6.1	24.0	8.1	17.8
Mo (ppb)	ICP-MS	0.01	32.1	0.01	30.8	0.01	49.2
Zr (ppb)	ICP-MS	0.5	51.4	0.4	80.3	0.8	26.3

Table C.3 Endotoxin content of ultrafine road-deposited dust particles.

City	Endotoxin (EU/mg)
Lancaster	9.25
Birmingham	9.80
Mexico City	8.75

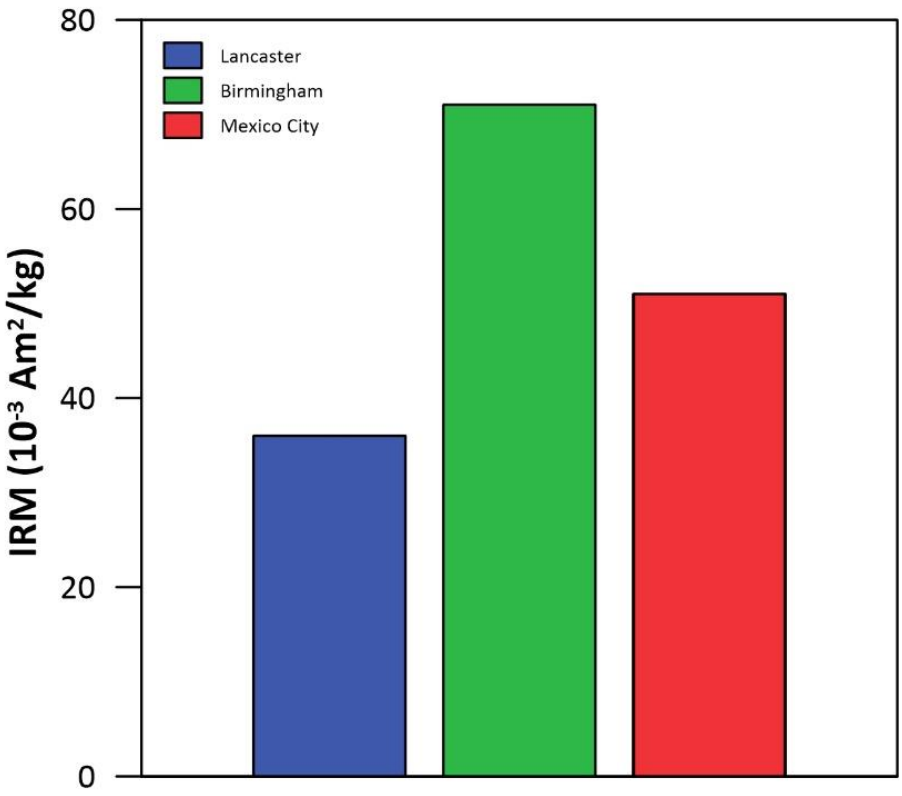

Figure C.1 Isothermal remanence magnetisation (IRM) for the bulk (unfiltered) PM from the three studied sampling sites.

Note. The IRM of bovine serum albumin (BSA) was also measured and was several orders of magnitude lower than the bulk samples (IRM 0.0014 x 10^{-3} Am^2/kg).

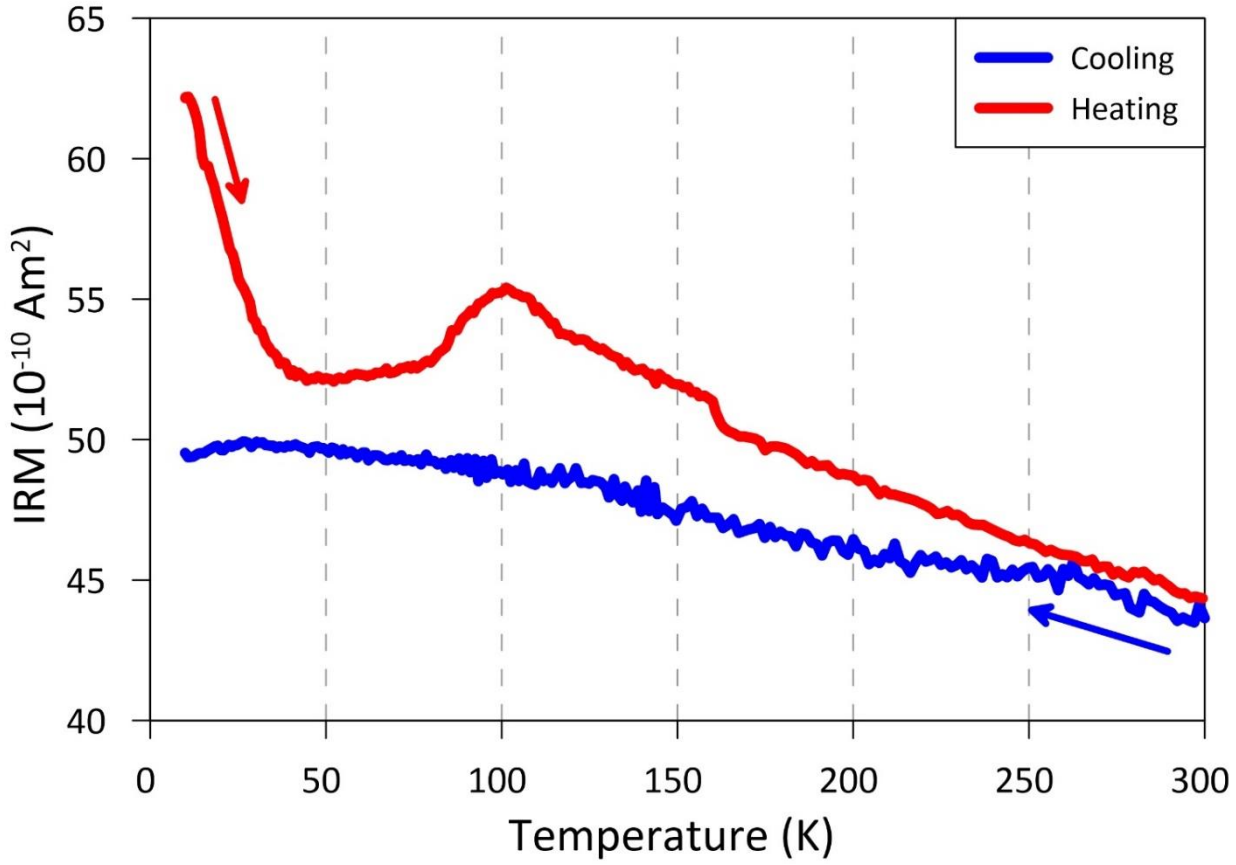

Figure C.2 Zero-field changes in IRM during cooling of the Mexican UF-RDPs, after acquisition of IRM (at 1 T) at 300 K. The Verwey transition at ~75 – 100 K identifies the presence of magnetite. The increase in IRM at low temperatures (~43% increase in IRM at 10 K compared to room temperature IRM; ~16% increase in IRM at 10K compared to IRM at 50 K) indicates the presence of superparamagnetic grains (~20 – 30 nm).

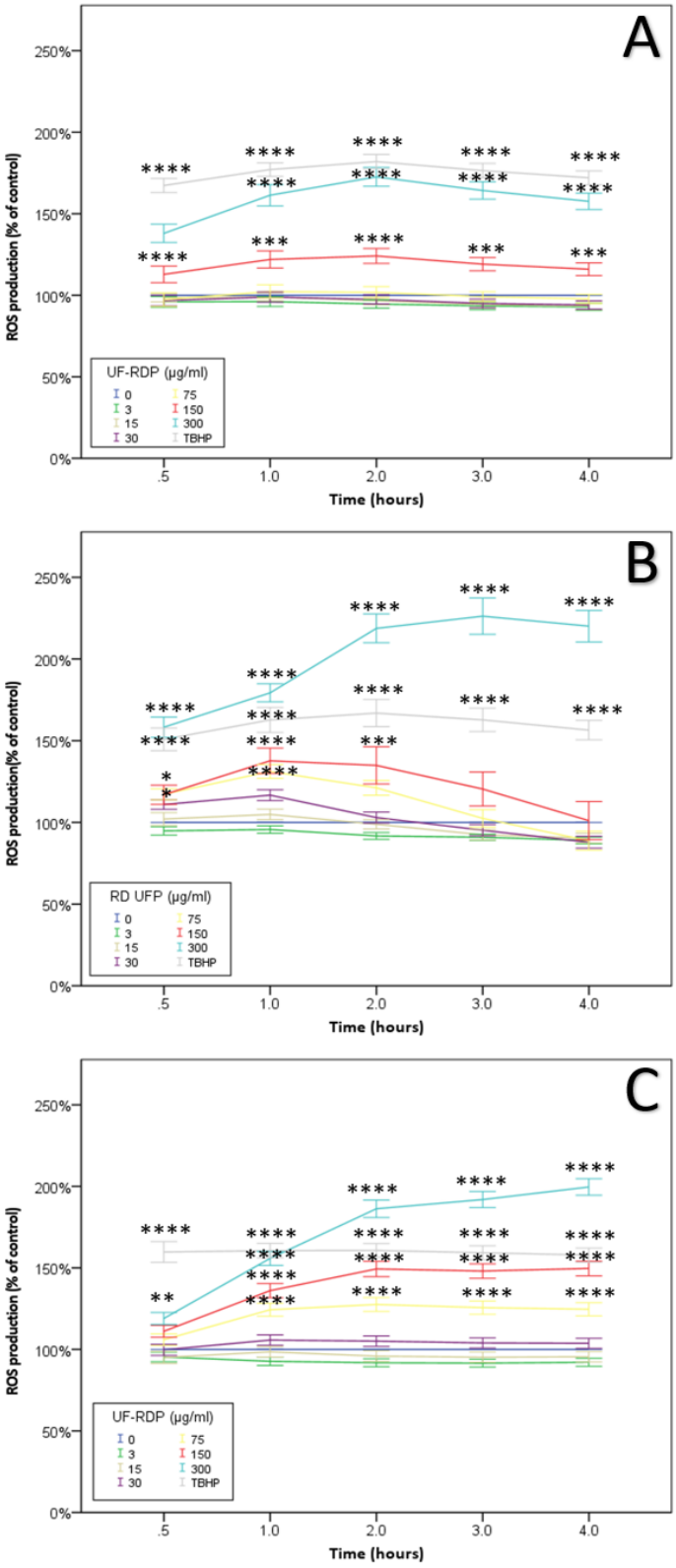

Figure C.3 ROS production over time in Calu-3 cells induced by <220 nm road-deposited dust particles. Calu-3 cells were loaded with the ROS probe CM DCFH-DA and exposed to the sub-micrometre-sized fraction of road-deposited dust particles (at doses from 3-300 µg/ml) from Lancaster, UK (A), Birmingham, UK, (B) and Mexico City, Mexico (C). Generation of fluorescence (indicative of ROS generation) was measured over 4 h exposure. Tert-butyl hydroperoxide (TBHP) was used at 100 µM as a positive control. Statistical analysis was conducted via one-way ANOVA with Dunnett's post-hoc, comparing treated cells to the untreated control (*).

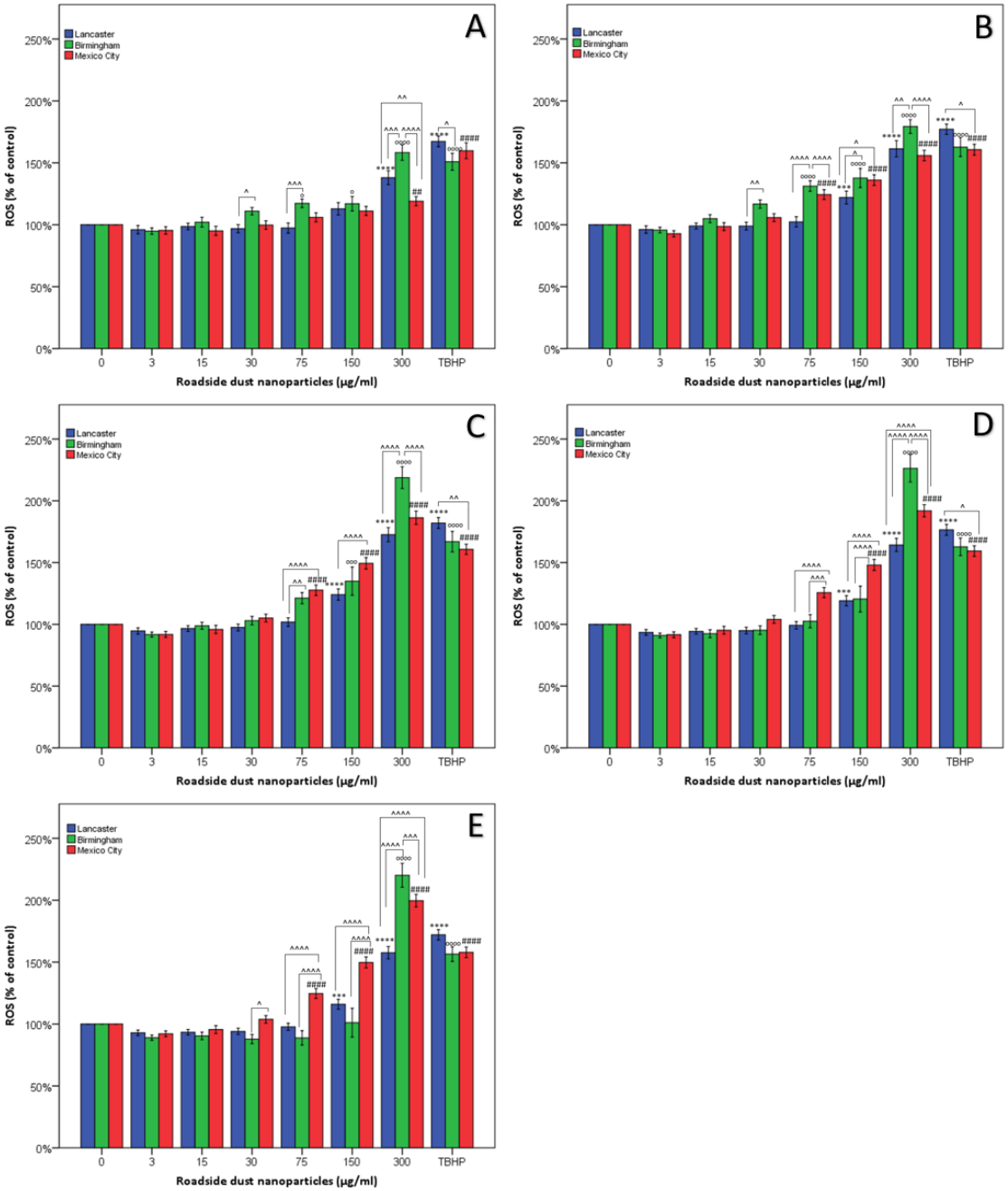

Figure C.4 Oxidative stress in Calu-3 cells induced by < 220 nm road-deposited dust particles. Calu-3 cells were loaded with the ROS probe CM DCFH-DA and exposed to the sub-micrometre-sized fraction of road-deposited dust particles (at doses from 3-300 µg/ml) from Lancaster (UK), Birmingham (UK) and Mexico City (Mexico). Generation of fluorescence (indicative of ROS generation) was measured after 0.5H (A), 1H (B), 2H(C), 3H (D) and 4H (E). Tert-butyl hydroperoxide (TBHP) was used at 100 µM as a positive control. Statistical analysis was conducted via one-way ANOVA with Dunnett's post-hoc, comparing treated cells to the untreated control. (* Lancaster, $_{o}$ Birmingham, # Mexico City) and two-way ANOVA with Bonferroni correction in order to compare the impacts of the UF-RDPs from the three different locations (^).

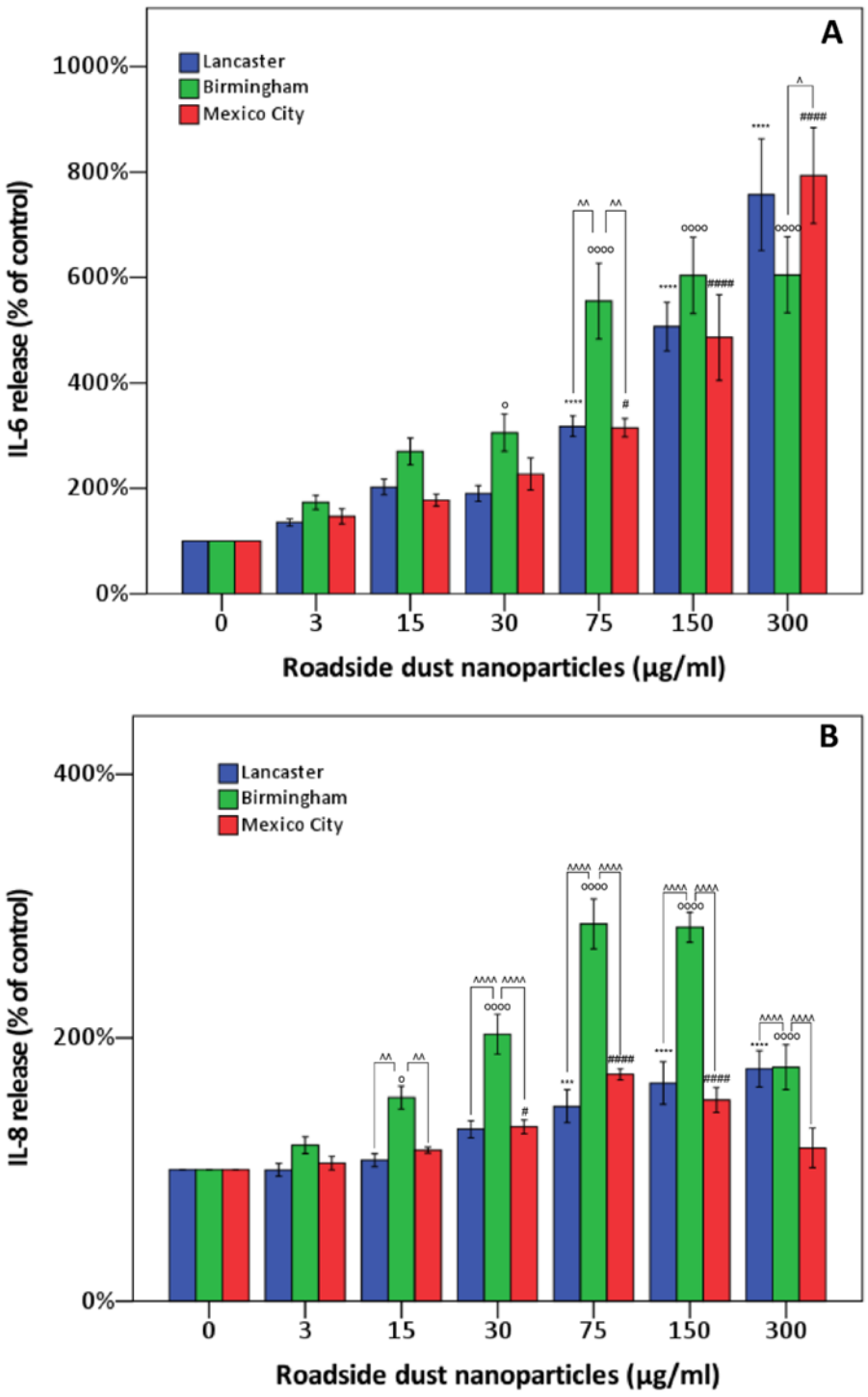

Figure C.5 Release of pro-inflammatory cytokines in Calu-3 cells treated with <220 nm road-deposited dust particles. Calu-3 cells were exposed (at doses from 3 and 300 µg/ml) to the sub-micrometre-sized fraction of road-deposited dust particles from Lancaster (UK), Birmingham (UK) and Mexico City (Mexico) for 24 h and the media collected. The collected media samples were quantified for IL-6 (A) and IL-8 (B) concentrations via ELISA. Statistical analysis was conducted via one-way ANOVA with Dunnett's post-hoc, comparing treated cells to the untreated control. (* Lancaster, $_0$ Birmingham, # Mexico City) and two-way ANOVA with Bonferroni correction in order to compare the impacts of the UF-RDPs from the three different locations (^).

Appendix D : Quadruple abnormal protein aggregates in brainstem pathology and exogenous metal-rich magnetic nanoparticles (and engineered Ti-rich nanorods). The substantia nigrae is a very early target in young urbanites and the gastrointestinal tract a key brainstem portal

D.1 Abstract

Fine particulate air pollution ($PM_{2.5}$) exposures are linked with Alzheimer's and Parkinson's diseases (AD, PD). AD and PD neuropathological hallmarks are documented in children and young adults exposed lifelong to Metropolitan Mexico City air pollution; together with high frontal metal concentrations (especially iron)–rich nanoparticles (NP), matching air pollution combustion- and friction-derived particles. Here, we identify aberrant hyperphosphorylated tau, α synuclein and TDP-43 in the brainstem of 186 Mexico City 27.29 ± 11.8y old residents. Critically, substantia nigrae (SN) pathology seen in mitochondria, endoplasmic reticulum, and neuro-melanin (NM) is co-associated with the abundant presence of exogenous, Fe-, Al- and Ti-rich NPs. The SN exhibits early and progressive neurovascular unit damage and mitochondria and NM are associated with metal-rich NPs including exogenous engineered Ti-rich nanorods, also identified in neuroenteric neurons. Such reactive, cytotoxic, and magnetic NPs may act as catalysts for reactive oxygen species formation, altered cell signalling, and protein misfolding, aggregation and fibril formation. Hence, pervasive, airborne, and environmental, metal-rich, and magnetic nanoparticles may be a common denominator for quadruple misfolded protein neurodegenerative pathologies affecting urbanites from earliest childhood. The substantia nigrae is a very early target and the gastrointestinal tract (and the neuroenteric system) key brainstem portals. The ultimate neural damage and neuropathology (Alzheimer's, Parkinson's and TDP-43 pathology included) could depend on NP characteristics and the differential access and targets achieved via their portals of entry. Thus, where you live, what air pollutants you are exposed to, what you are inhaling and swallowing from the air you breathe, what you eat, how you travel, and your occupational lifelong history are key. Control of NP sources becomes critical.

Published: CALDERÓN-GARCIDUEÑAS, L., GONZÁLEZ-MACIEL, A., REYNOSO-ROBLES, R., **HAMMOND, J**., KULESZA, R., LACHMANN, I., TORRES-JARDÓN, R., MUKHERJEE, P. S. & MAHER, B. A. 2020. Quadruple abnormal protein aggregates in brainstem pathology and exogenous metal-rich magnetic nanoparticles. The substantia nigrae is a very early target in young urbanites and the gastrointestinal tract likely a key brainstem portal. *Environmental Research***,** 110139.

Author contributions

Calderón-Garcidueñas Lilian: Conceptualization, Data curation, Formal analysis, Methodology, Investigation, Writing - original draft preparation, Writing- Reviewing and Editing, Visualization, Supervision, Project administration. Angélica González-Maciel, Rafael Reynoso-Robles, Randy Kulesza, Ingolf Lachmann, Ricardo Torres-Jardón, Partha S. Mukherjee: Formal analysis, Visualization, Investigation, Supervision, Validation, Writing- Reviewing and Editing Barbara Maher: Data curation, Formal analysis, writing-reviewing and editing, Visualization. SIRM, HRSTEM and EDX. HAADF-STEM images. J. Hammond: Formal analysis, visualization, Investigation, and validation.

D.2 Introduction

Exposure to air pollutants has increasingly been associated with the most common neurodegenerative diseases affecting millions of people across the world: Alzheimer's and Parkinson's (Jung et al., 2015, Chen et al., 2017b, Lee et al., 2016, Hu et al., 2019, Han et al., 2020, Calderón-Garcidueñas et al., 2002, Calderón-Garcidueñas et al., 2003, Calderón-Garcidueñas et al., 2004, Calderón-Garcidueñas et al., 2008, Calderón-Garcidueas et al., 2012, Calderón-Garcidueñas et al., 2013b, Calderón-Garcidueñas et al., 2013a, Calderón-Garcidueñas et al., 2017a, Calderón-Garcidueñas et al., 2017b, Calderón-Garcidueñas et al., 2018a, Calderón-Garcidueñas et al., 2019b, Calderón-Garcidueñas et al., 2019d, Calderón-Garcidueñas et al., 2019c, Calderón-Garcidueñas et al., 2020c, Calderón-Garcidueñas et al., 2020b). Neuropathological evidence shows that Alzheimer's disease (AD) is developing and progressing in children, teens, and young adult residents of Metropolitan Mexico City (MMC) (Calderón-Garcidueñas et al., 2018a). In a forensic consecutive autopsy cohort of 203 MMC previously clinically healthy individuals (age 25.36 ± 9.23 y), all, except a 22y female with a TLR4 Asp299Gly polymorphism, exhibited AD hallmarks, as defined by the presence of phosphorylated tau protein (p-τ) and amyloid ß 17–24 (Braak and Del Tredici, 2011, Braak and Del Tredici, 2015, Braak et al., 2003, Braak et al., 2011, Attems and Jellinger, 2006, Attems et al., 2014, Thal et al., 2002, Rüb et al., 2016). Rapid progression to neurofibrillary tangle (NFT) stages III-V was documented in ~25% of 30–40 y olds.

We have previously reported an overlap between the neuropathological hallmarks of AD and PD in young (≤40y) MMC residents, such hallmarks notably appearing in childhood (Calderón-Garcidueñas et al., 2008, Calderón-Garcidueñas et al., 2010, Calderón-Garcidueñas et al., 2011, Calderón-Garcidueñas et al., 2013a, Calderón-Garcidueñas et al., 2016a, Calderón-Garcidueñas et al., 2016b, Calderón-Garcidueñas et al., 2017a, Calderón-Garcidueñas et al., 2017b, Calderón-Garcidueñas et al., 2018b, Calderón-Garcidueñas et al., 2018a, Calderón-Garcidueñas et al., 2019b, Calderón-Garcidueñas et al., 2019d, Calderón-Garcidueñas et al., 2019c, Mansour et al., 2019). Specifically, in a study of 179 MMC residents ≤40y of age, we have identified p-τ and Lewy neurites (LN) in the olfactory bulbs (OBs) of toddlers (Calderón-Garcidueñas et al., 2018b). By the second decade (n:57), 84% of the OBs exhibited p-τ (48/57), 68% exhibited LNs and vascular amyloid (39/57) and 36% (21/57) diffuse amyloid plaques. The overlap of AD and PD hallmarks has been also documented within auditory and vestibular nuclei, together with a marked dysmorphology in the ventral cochlear nucleus and the superior olivary complex (Calderón-Garcidueñas et al., 2011, Calderón-Garcidueñas et al., 2017a). The progressive involvement of the brainstem auditory evoked potentials (BAEPs) reflects the early brainstem participation in the neuroinflammatory and neurodegenerative processes. The compensatory plasticity, and increased auditory gain, are important in identifying strong non-invasive biomarkers of Alzheimer Continuum and early PD (Calderón-Garcidueñas et al., 2019c, Mansour et al., 2019, Jack et al., 2018, Jack et al., 2019).

As we have documented previously, young MMC residents are exposed lifelong to high levels of fine airborne particulate matter ($PM_{2.5}$) and ozone, above the USEPA standards and WHO guidelines; they have high frontal concentrations of metal (especially iron)–rich nanoparticles (NPs) which match air pollution particles formed by combustion and friction processes, such NPs are also evident within both the heart and the neuroenteric system (Calderón-Garcidueñas et al., 2017b, Calderón-Garcidueñas et al., 2019d, Maher et al., 2016, Maher et al., 2020, González-Maciel et al., 2017). The presence within key organelles of brain and heart cells of metal-rich, redox-active, and strongly magnetic NPs raises important questions regarding their potential role in the development of AD and PD and extra-neural pathology in MMC residents (Calderón-Garcidueñas et al., 2013a, Calderón-Garcidueñas et al., 2017a, Calderón-Garcidueñas et al., 2017b, Calderón-Garcidueñas et al., 2019b, Calderón-Garcidueñas et al., 2019d, Calderón-Garcidueñas et al., 2019c, Maher et al., 2016, Maher et al., 2020, Gonet and Maher, 2019, Maher, 2019). Low air pollution, age and gender matched controls have not shown neurodegenerative or heart pathology (Calderón-Garcidueñas et al., 2016b, Calderón-Garcidueñas et al., 2019b, González-Maciel et al., 2017).

Across the world, a significant proportion of the population (including US residents) lives near highly-trafficked roads, where they are exposed to traffic-related air pollution (TRAP), a major contributor to urban air pollution (Villalobos-Pietrini et al., 2011, Rowangould, 2013, Su et al., 2015, Ladino et al., 2018). MMC experiences high levels of TRAP, in addition to pollution emitted both from industrial and natural (windblown, volcanic, forest fires) and trash and stubble-burning sources. Air pollutants associated with health impacts encompass a diverse range of components, including fine and ultrafine particulate matter ($PM_{2.5}$ and $PM_{0.1}$, respectively), containing diesel soot, transition metals, nitrogen oxides and particle-bound phases, such as polycyclic aromatic hydrocarbons (PAHs)(Villalobos-Pietrini et al., 2011, Su et al., 2015, Ladino et al., 2018). Of these components, ultrafine particles ($PM_{0.1}$, i.e., < 100 nm) are increasingly implicated in a wide range of adverse health impacts (Delfino et al., 2005, Solaimani et al., 2017). Compared with larger particles, ultrafine particles are far more numerous, highly reactive, and able to gain access to all major organs of the body (Weichenthal et al., 2020, Brostrøm et al., 2019, Boyes and Van Thriel, 2020, Ceballos et al., 2020).

Of particular concern, transition metal-rich NPs, such as those formed abundantly as combustion- and friction-derived nanoparticles (CFDNPs), may act as catalysts for formation of reactive oxygen species (ROS) and for protein misfolding, aggregation and fibril formation (Calderón-Garcidueñas et al., 2003, Calderón-Garcidueas et al., 2012, Calderón-Garcidueñas et al., 2013a, Calderón-Garcidueñas et al., 2016a, Calderón-Garcidueñas et al., 2016b, Calderón-Garcidueñas et al., 2017b, Calderón-Garcidueñas et al., 2018a, Calderón-Garcidueñas et al., 2018b, Calderón-Garcidueñas et al., 2019b, Calderón-Garcidueñas et al., 2019d, Gonet and Maher, 2019, Linse et al., 2007, Kumari et al., 2012, Yarjanli et al., 2017, Saptarshi et al., 2013, Parveen et al., 2017, Pacakova et al., 2017, Gutiérrez et al., 2019, Imam et al., 2015, Kim et al., 2016, Hartl, 2017, Chandel et al., 2018).

Here, we investigate AD and PD neuropathological hallmarks and DNA-binding protein TDP-43 pathology in the brainstem in young MMC residents, and their associations with the presence, location, and composition of exogenous, metal-rich NPs in the brainstem and cerebellum. Damage to the brainstem and cerebellum will extensively alter key networks modulating autonomic function, arousal, motor control and emotions (Venkatraman et al., 2017, Zhang et al., 2017, Zelena et al., 2018, Adamaszek et al., 2017).

We have three primary aims: 1. to document, by immunohistochemistry, brainstem (including substantia nigra) pathology in a collection of 186 MMC autopsy samples from individuals

average age 27.29 ± 11.8y, and specifically, the presence of p-τ, alpha-synuclein and DNA-binding protein TDP-43; 2. to quantify, by magnetic remanence measurements, the concentrations of ferromagnetic, iron-rich NPs in the substantia nigrae, tectum/tegmentum/periaqueductal gray (PAG) and cerebellum, in a representative sub cohort (n:15, age 34.33 ± 15.6y, range 12–71y); and 3) to achieve, in a pilot sample, the first in situ identification of the composition as well as the location, size and shape of exogenous NPs in the substantia nigra of a 32y old subject, randomly selected from the cohort. For the latter aim, in order to achieve the required spatial resolution, i.e., to image and analyse NPs within the subcellular environment at near-atomic resolution, we used high resolution scanning and transmission electron microscopy (HRSTEM) and energy dispersive X ray analysis (EDX). Precise early identification of NP composition, as well as size, location, and concentration, are critical, since it will establish which organelles are targeted, the NP potential toxicity and the resultant biological impact upon key AD, PD and TDP- 43 targets and connecting brainstem networks.

Our working hypothesis is that exposure to reactive metal-bearing NPs, abundant and pervasive in the urban atmosphere and environment, comprises a biologically plausible common denominator for fatal PD, AD and TDP-43 proteinopathies, starting in paediatric ages.

D.3 Materials and methods

D.3.1 Study area air quality

MMC residents are exposed frequently and lifelong to high levels of particulate air pollution, arising from traffic- and industry-related emissions, combined with unfavourable meteorology (pollution-trapping inversions). Even by conventional measures (i.e., mass concentrations of fine particulate matter, $PM_{2.5}/m^3$), MMC residents are often exposed to pollution levels above World Health Organization (WHO) guidelines and US Environmental Protection Agency (USEPA) standards. The USEPA annual $PM_{2.5}$ standard of 12 $\mu g/m^3$ and 24-h mean standard of 35 $\mu g/m^3$ have been exceeded across the MMC area for the last 16 years (Fig. D.1). (Molina et al., 2010, Molina et al., 2019, Guerrero et al., 2017, Dzepina et al., 2007, Querol et al., 2008, Velasco and Retama, 2017, Torres-Jardón and Sosa Núñez, 2018). Typically, the highest $PM_{2.5}$ concentrations occur in the NE sector, associated with intense industrial and heavy duty diesel traffic, and decrease towards the SW residential area (Villalobos-Pietrini et al., 2011, Ladino et al., 2018, Molina et al., 2019, Guerrero et al., 2017, Torres-Jardón and Sosa Núñez, 2018). Exposures to ozone (O_3) concentrations are also above the USEPA standards (annual fourth-

highest daily maximum 8-h concentration, averaged over 3 years) all year long (Velasco and Retama, 2017). All other criteria pollutants for MMC, including nitrogen dioxide, sulphur dioxide and lead, displayed elevated levels prior to 2000, but have been at or below the current EPA standards in the last 20 years.

In terms of health impact, however, it seems increasingly likely that ultrafine particles, of nanoscale dimensions (<100 nm, so referred to here as nanoparticles, NPs), may pose a major risk (Caudillo et al., 2020). NPs are present in urban air in large numbers, are currently neither monitored nor regulated, and, notably, show little correlation with conventional mass concentration measurements, e.g., $PM_{2.5}$. At heavily trafficked roadsides, NP numbers can reach values in excess of 130,000/cm^3 (Dr. Maher personal communication, data measured in 2019, Manchester, U.K.). Although the majority (~90%) of airborne NPs consist of semi-volatile, carbon-bearing phases, the primary, solid, vehicle-derived NPs are often enriched in highly reactive transition metals, especially Fe, Cu, Mn, Ti and Cr and other metals including Ni, V, Pb and Zn (Verma et al., 2010, Maher et al., 2013, Sanderson et al., 2016). Metal-bearing NPs are abundant in Mexico City air. More than 60% of such NPs, collected and analysed (n=572) by transmission electron microscopy, contain Fe, Pb or Zn (Adachi and Buseck, 2010). Taking account of the abundance of NPs produced by vehicle brake wear (Gonet and Maher, 2019), we describe such particles as combustion- and friction-derived nanoparticles (CFDNPs).

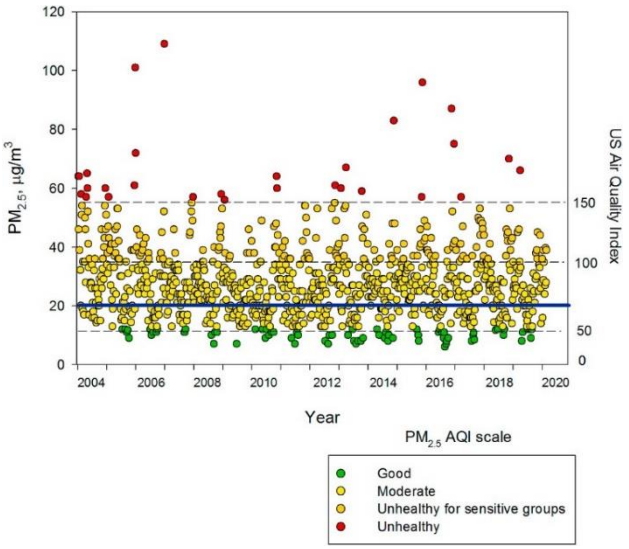

Figure D.1 Trend of maxima PM 2.5 24-h average concentrations registered in all monitoring stations of the MMC from 2004 to April 2020 and their comparison against the WHO daily mean average (blue solid line) and the US Air Quality Index AQI. Data correspond to measurements from the manual PM network of the SEDEMA under a 6-day sampling schedule. Source: http://www.aire.cdmx.gob.mx/default.php#

D.3.2 Study design and samples

One hundred and eighty-six forensic MMC autopsies, age 27.29 ± 11.8y old (range 11 months – 40 years) were selected for this study, from sudden causes of death that did not involve the brain; all have previously been staged for AD and for olfactory bulb α synuclein, ß amyloid and pτ pathology (Calderón-Garcidueñas et al., 2018b, Calderón-Garcidueñas et al., 2018a). Autopsies were performed 3.7 ± 1.7 h after death. Cases were consecutive and included unrelated subjects with no pathological findings at the general autopsy other than the acute cause of death. Examination of autopsy materials was approved by the Forensic Institute in Mexico City and autopsies were performed in a five-year period between 2004 and 2008. Brains were examined macroscopically, sections were selected for light and electron microscopy, and frozen tissues stored at minus 80°C until processed. Age, gender, and Apolipoprotein E (APOE) status in Supplemental Table D.2.

Brainstems were sectioned from the midbrain at the level of the superior colliculi to the lower medulla, with an average of 13.6 ± 4.4 paraffin blocks and 48.7 ± 12.0 slides per individual paraffin block examined. Paraffin embedded tissue was sectioned at a thickness of 7 µm and stained with haematoxylin and eosin (HE). Immunohistochemistry (IHC) was performed on serial sections as previously described (Calderón-Garcidueñas et al., 2018a). Antibodies included: PHF-tau8 phosphorylated at Ser199-202-Thr205 (Innogenetics, Belgium, AT-8 1:1000), α-synuclein phosphorylated at Ser-129, LB509 (In Vitrogen, Carlsbad, CA 1:1000) and TDP43 mab2G10 (Roboscreen GmbH, Leipzig, Germany 1:1000). Examination for AD, alpha-synucleinopathies and TDP-43 hallmarks in each brainstem included substantia nigrae (Braak and Del Tredici, 2011, Braak and Del Tredici, 2015, Braak et al., 2003, Attems and Jellinger, 2006, Attems et al., 2014, Thal et al., 2002, Rüb et al., 2016, Braak and Del Tredici, 2017, Braak and Del Tredici, 2018, Del Tredici and Braak, 2016, Del Tredici et al., 2002, Beach et al., 2009, Tsuboi et al., 2003, McKeith et al., 2005, Brettschneider et al., 2013, Shahmoradian et al., 2019).

D.3.3 Transmission electron microscopy (TEM), high resolution scanning TEM (HRSTEM) and energy dispersive X-ray analysis (EDX)

Separate sets of tissue blocks were prepared for initial, conventional bright-field TEM (osmium stained) and for HRSTEM and EDX (no osmium staining); tissue sections were 100 nm thickness. The focus of the conventional TEM (JEOL-1011, Osaka, Japan, operated at 80 kV), of substantia nigrae, tectum, tegmentum, periaqueductal gray (PAG), and cerebellum, was observation of the integrity of the neurovascular unit and defining the location of the

electrodense NPs present within target organelles and cell types and the subcellular pathology. In order to achieve detection and elemental analysis of intracellular NPs, high angle annular dark field (HAADF) scanning transmission EM (STEM) was used (heavier elements displaying brighter contrast), in combination with multi-detector EDX. TEM grids (holey carbon films on nickel support grids) were randomly selected (2 from 10 grids), carbon-coated to prevent surface charging effects, and scanned using a FEI Titan3 Themis 300 STEM, operated at 300 kV. In identifying the elemental compositions of NPs by EDX (FEI Super-X 4-detector system), a probe current of 60 pA was used to acquire the elemental maps, in order to limit any beam-induced damage.

D.3.4 Magnetic remanence

For room temperature measurements of saturation remanent magnetisation (SIRM), fresh/frozen tissue blocks were prepared by trimming of all external surfaces with a ceramic knife, to remove any possibility of external metallic contamination. All sub-sampling was done in a class II biological safety cabinet inside a class III biological laboratory. Surfaces and tools were treated with 70% ethanol. Inside the cabinet, air throughflow was sampled using a Leland Legacy pump (SKC, Dorset UK) at 7.5 L/min through a magnetically- 'clean' 1 µm PTFE filter, in order to quantify any airborne magnetic 'background' during the few minutes of in cabinet tissue exposure during trimming/sampling. Once trimmed, each sample was subjected to freeze-drying (48 h, Christ Alpha 2–4 LD plus) and placed in pre-measured sterilised polystyrene sample pots (10 cc) for superconducting quantum interference device (SQUID) magnetometry (RAPID 2G DC magnetometer, 2G Enterprises, California USA; mean background noise level ~1 × 10^{-12} Am). All measurements were carried out at room temperature (293 K ± 0.5 K) at the Centre for Environmental Magnetism and Palaeomagnetism, Lancaster University. First, the natural remanent magnetisation (NRM) of each sample was measured. Then, SIRMs were generated in a direct current (dc) magnetic field of 1 T (T), using a Newport 4" Electromagnet Type A. All SIRM values were mass-normalized for freeze-dried brain weight (kg). The NRM or SIRM of all measurement materials (styrene pot, cling film) was measured for every individual sample, and subtracted, in order to isolate the SIRM of the tissue sample. Concentrations of magnetite in the brainstem samples were estimated from their SIRM values, using an experimentally-derived value of 13.8 Am^2 kg^{-1} for a pure magnetite powder, consisting of interacting, mixed, single domain and superparamagnetic (ave. diameter ~31 nm) magnetite particles (Maher, 1988).

D.4 Results

D.4.1 Brainstem neuropathology

The AD staging (pτ, Aβ), substantia nigrae (SN) pτ and αSyn scoring, and the DNA-binding protein (TDP-43) results, are shown in Suppl Table D.2. The earliest immunohistochemical findings in the brainstem of MMC children were pτ threads and neurites (NTs) in lower medulla, followed by Lewy neurites (LNs), as described previously (Calderón-Garcidueñas et al., 2018b, Calderón-Garcidueñas et al., 2018a). Aβ data was taken from the two previous publications (Calderón-Garcidueñas et al., 2018b, Calderón-Garcidueñas et al., 2018a). When comparing the Alzheimer's staging from previous works and substantia nigrae pτ in the different age groups i.e., 0-20y, 21–40 and ≥ 41y olds, it is clear the presence of pτ in SN is an early and common finding. The presence of α synuclein in the SN was similar in the 0-20y and the 21-40y cohort (~20%) and increased in the older≥40y cohort (n:7). On the other hand, TDP-43 abnormalities showed minimal variation within the 0-40y range. Immunocytochemical profiles of the 43-kDa transactive DNA-binding protein were characterized by loss of nuclear TDP-43 expression with powdery (dash-like) cytoplasmic particles (Braak and Del Tredici, 2018, McKeith et al., 2005, Brettschneider et al., 2013) associated with morphological changes of progressive degranulation of dopaminergic SNpc pars compacta neurons.

D.4.2 Representative substantia nigrae and brainstem hyperphosphorylated tau (pτ), β amyloid, alpha synuclein, and DNA-binding protein TDP-43 immunohistochemistry

We documented α-Syn in 23% (n:42), 55% had pτ (n:100) and 18.68% (n:34) had TDP-43 (Suppl Table D.2). Positive pτ neurites and nuclei in brainstem and SN were identified in toddlers (Fig. D.2A). TDP-43 pathology in a 11m old baby was identified in substantia nigrae pars compacta (SNpc) neurons and was characterized by isolated neurons with complete loss of nuclear TDP-43 expression (Fig. D.2 B, C). The same baby had diffuse Aβ plaques in frontal cortex (Fig. D.2D). Teens showed nuclear pτ in brainstem nuclei (i.e., oculomotor nucleus and accessory parasympathetic nucleus) and pτ neurites and nuclear positivity in SNpc (Fig. D.2E, F, G). Extensive arteriolar Aβ accumulation (amyloid angiopathy) was present in supratentorial cortical frontal and temporal lobes, along diffuse Aβ plaques (Fig. D.2 H, I). Alpha-synuclein positive neurites were previously seen in toddlers and young children in the lower brainstem, i.e., medulla (Calderón-Garcidueñas et al., 2008, Calderón-Garcidueñas et al., 2010, Calderón-Garcidueñas et al., 2011, Calderón-Garcidueñas et al., 2013a, Calderón-Garcidueñas et al., 2018b) while, here, SN involvement and other nuclei (i.e., locus coeruleus, dorsal vagal nucleus), was extensively documented in teens (Fig. D.2J). TDP-43 pathology in the brainstem was characterized by dash-like immunopositive particles in the vicinity of the cell nucleus (Fig. D.2

K) with complete loss of nuclear TDP-43 expression. This type of pathology was mostly seen in lower brainstem levels, including medulla and pons and in relation to reticular formation intermediate and large cell neurons in the median column. Teens also showed the presence of glial cytoplasmic inclusions with a coiled body like morphology (Insert in Fig. D.2K). Subjects in the third and fourth decades of life showed advanced lesions, i.e., 32 y old male (subject #20 in Table D.1) with diffuse and mature Aβ plaques in frontal cortex (Fig. D.2L) with reactive GFAP astrocytes surrounding the plaques. Extensive pτ neurites and neurofibrillary tangles are seen in the SNpc of a 36y old male (Fig. D.2M).

Alpha-synuclein positive granules were seen in SNpc in a 26y old female (#15 in Table D.1) (Figure D.2N and insert).While cytoplasmic α-Syn was a frequent finding, Lewy bodies were rare and associated with extensively degranulated neurons (Figure D.2O).By the third decade, SNpc TDP-43 nuclear clearing with progressive neuron degranulation was in place (Fig. 2P). TDP-43 pathology was observed in substantia nigrae, non-motor neurons including reticular nuclei, and pontine neurons with nuclear clearing and dash-like particles, but no neuronal somatic skein-inclusions. Pictures of abnormal SNpc neurons using haematoxylin and eosin (H&E) are seen in Fig. 2 Q-W to illustrate a common finding from childhood: neurons with typical hyaline cytoplasmic inclusions in 14y olds (T) surrounded by macrophages and extra neuronal deposits of NM, as the MMC resident gets older, the changes are striking (Fig. 2X,Y,Z).

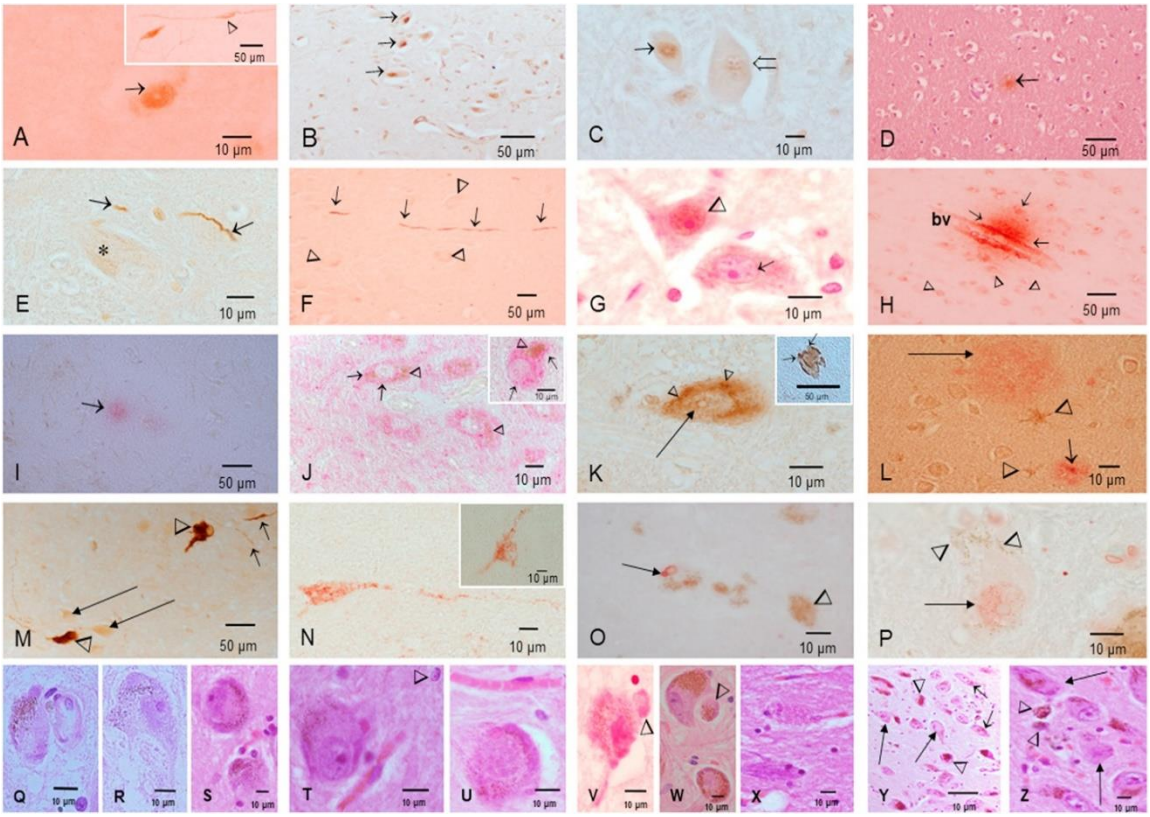

Figure D.2 Immunohistochemistry representative substantia nigrae pars compacta (SNpc) and brainstem sections from subjects in 1st through 6th decades of life. A. SNpc neuron with positive pτ nuclei and a few granular deposits of pτ in perinuclear location in the neuron in Insert. Immunohistochemistry/IHC xAT8, 3,3' - diaminobenzidine DAB/IHC, brown product. Scale bar 10um and 50 µm in the insert. B and C correspond to SNpc neurons in an 11month old baby stained with TDP- 43.In B the neurons marked by arrows show strong nuclear staining (Scale bar 50 µm), while in C we have a neuron with strong nuclear TDP-43 immunoreactivity (short arrow) contrasting with one with loss of nuclear TDP expression (arrow head)Scale bar 10 µm. IHC TDP-43, DAB, brown product. D. Same 11m old baby with a diffuse amyloid plaque in frontal cortex. IHC Aβ, red product. E and F IHC pτ and DAB.E. 17y old male SNpc pτ +neurites marked by arrows while a neuron is marked by *. F corresponds to SNpc in a 11y old female, a long pτ + neurite is marked by short arrows and adjacent neurons are identified by arrow heads. G. 17y old male, same as in E showing two III motor cranial neurons, the one on the upper left one shows a pτ + nucleus (arrowhead), while the right one (short arrow), is negative. IHC pτ and DAB (Scale bar 10 µm).H same as F,11y old female frontal cortex with a blood vessel(bv) with extensive wall amyloid deposition extending into the adjacent neuropil(arrows). Frontal neurons with intracytoplasmic Aβ are marked with arrow heads. IHC Aβ and red product (Scale bar 50 µm). I.17y old frontal cortex with a diffuse Aβ plaque IHCAβ and red product (Scale bar 50 µm). J.13y old female SNpc positive neurons to αSyn, the short arrows point to the + αS granules, the arrow head to the neuromelanin. Insert shows one strongly + αSyn lower brainstem pigmented neuron in the same child. The arrow head point to the neuromelanin and the short arrows to the + αSyn. IHC x αS and red product (Scale bar 10 µm).K.14y old male with a +TDP-43 neuron in pontine reticular formation ,the immunoreactive + particles are mostly in the vicinity of the nucleus (arrow heads), there is nuclear clearing (long arrow). The insert shows the presence of glial cytoplasmic + inclusions with coiled body-like morphology (arrows). IHC TDP-43 DAB (Scale bar 50um). L.32y old frontal cortex with both diffuse (long arrow) and mature (short arrow) Aβ plaques and GFAP reactive astrocytes close-by. IHC Aβ and GFAP Red product/DAB for GFAP (Scale bar 10 µm).M 36 y old male with SNpc with numerous neurons with neurofibrillary tangles (arrow heads), long + neurites (short arrows) and free tangle neurons (long arrows). IHC pτ and DAB (Scale bar 50 µm). N 26y old female SNpc with + granular cytoplasmic αSyn IHC αSyn and red product (Scale bar 10 µm). O. 50y male SNpc with a Lewy-body like structure in a heavily degranulated neuron(arrow), an adjacent neuron (arrow head) shows unremarkable neuromelanin. ICH x αS and red product (Scale bar 10 µm). P. 27y old male SNpc shows a heavily degranulated neuron (arrow heads) with a TDP-43 nuclear clearing (arrow). IHC TDP-43 red product (Scale bar 10 µm).H&E staining Q-Z. Q and R show 2 SNpc neurons in an 11y boy with significant cell damage and macrophages ingesting neuromelanin(Q).S, T and U are SNpc neurons from a 14y old boy with a small number of neuromelanin granules in the midst of a disintegrating cytoplasm and in proximity with macrophages and capillaries. In T the neuron show a typical hyaline cytoplasmic inclusion and in the upper right quadrant a macrophage nuclei show clumping of the chromatin (arrowhead) (legend continues overleaf)

V. 14y old female with a pigmented locus coeruleus neuron showing cytoplasm disintegration and an attached macrophage(arrowhead).W. 15y old male with SNpc neurons with abundant NM and an attached macrophage ingesting NM(arrowhead).X. 22y old female, 2 SNpc neurons, the one on the lower quadrant shows an ill-defined cytoplasm and two nuclei likely from microglial cells, while the upper shows a ghost neuron with a fibrillary ill-defined structure and a few NM granules. Y. 36y old male with a low power view of the SNpc to look at the numerous neurons with no NM (long arrows) at all contrasting with some with NM granules (short arrows). Macrophages among the degranulated neurons are marked with arrowheads. Z Same 36y male with close-up of the area with macrophages (arrowheads) and the severely damaged neurons (long arrows).

D.4.3 Substantia nigrae electron microscopy

TEM findings for the SN were remarkable in relation to early neurovascular unit pathology. Extensive breakdown of the neuropil was present around blood vessels with clusters of lipids, lipofuscin, and vacuolated neuropil around vessel walls (Fig. D.3A and B). Perivascular neuropil breakdown and damaged axons were constant findings (Fig. D.3B and C). Rounded electrodense NPs were common in red blood cells (RBC) in close contact with endothelial cytoplasm in small vessels and inside endothelial cell nuclei (Fig. D.3D). The measurable size of the NPs in the SN was in the range of 9–60 nm (average 19 ± 6 nm).

SN neurons show progressive accumulation of neuromelanin (NM) starting at age 11 months (Fig. D.4A and B) and by age 12y, NM granules are already accumulating in paranuclear neuronal location (Fig. D.4C and D). Clusters of NPs were commonly associated with heterochromatin (Fig. D.4E and F). Strikingly, NPs were present in NM granules, dilated ER, abnormal mitochondria and in mitochondria in close contact with NM (Fig. D.4G and H(insert), I). Oligodendroglia showed adjacent large axons with myelin breakdown and contracted axons (Fig. D.4J). Fibrillary ill- defined structures were seen in the midst of NM with numerous NPs and twisted tubules (Fig. D.4K). Dilated ER, abnormal mitochondria, and mitochondrial-endoplasmic reticulum (ER) contact sites (MERCs) were common in SN neurons (Figure D.4L). In subjects in the 4th decade and beyond, the abundance of NM was striking (Fig. D.5A, B, C). Membranous, vesicular and lipid Lewy body-like structures were identified inside SN neurons (Fig. D.5D)(Shahmoradian et al., 2019). SN blood vessels showed endothelial cells with abnormal tight junctions (TJs) (Fig. D.5E and F). Vascular β-pleated sheets were observed in blood vessels in close contact with lipofuscin (Fig. D.5H). Perineuronal macrophage-type cells were common around neurons (Fig. D.5 I), with numerous lysosomes, a rare one containing contain a lattice image with several layers of well-ordered fringes with a perpendicular alignment (Fig. D.5J). Fig. D.6 illustrates the SN in the 32y old male included in Figs. D.7 and D.8. Extensive damage to the SN NVU is seen with loss of perivascular astrocytic processes, and myelinated and unmyelinated axons. Macrophage processes surround one small blood vessel in the midst of neuropil breakdown (Fig. D.6A). NM is closely associated with NPs; mitochondria exhibited NPs both inside the matrix and in the double membranes (Fig. D.6B and C) (Fig. D.9).

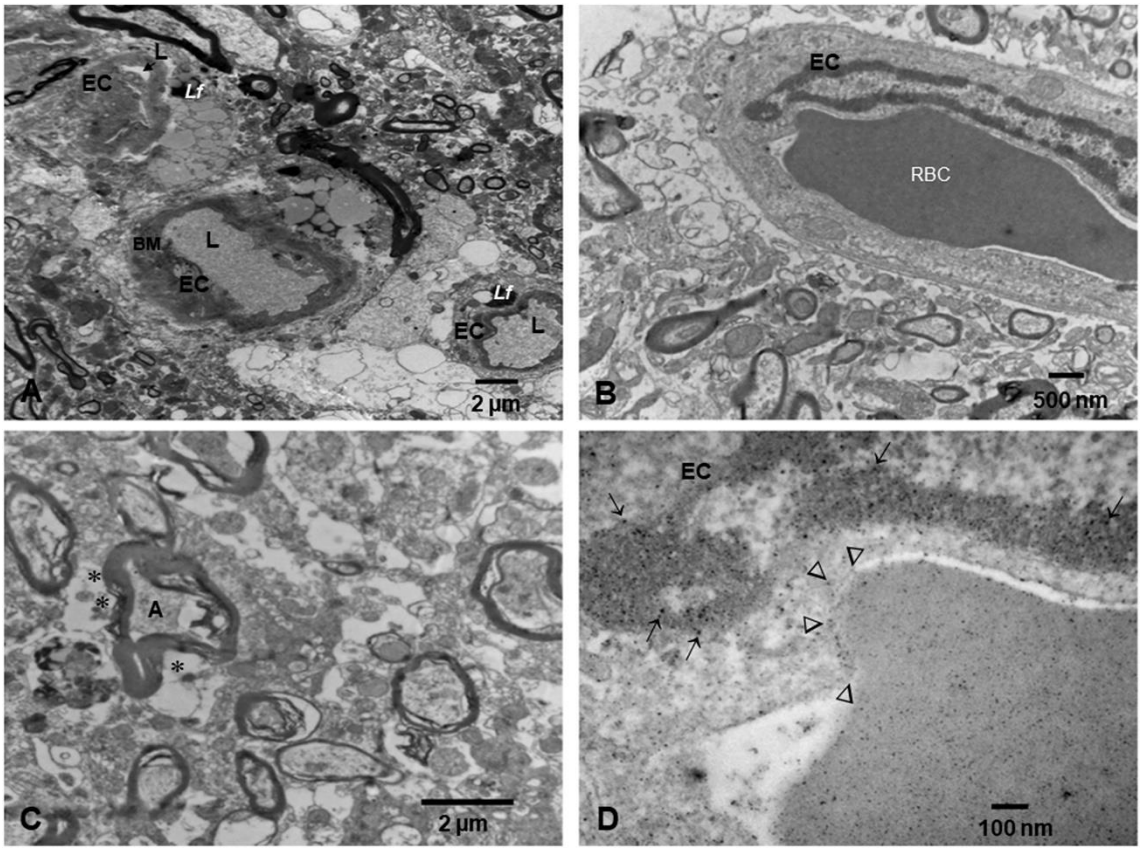

Figure D.3 Neurovascular Unit (NVU) in the substantia nigrae. Small blood vessels, including capillaries and small arterioles exhibited abnormal walls with activated endothelial cells (ECs) and leaking walls. A. Three small blood vessels are seen with leaking walls with clusters of lipids in the neuropil. The neuropil is vacuolated, and fragments of cells are seen around blood vessels. Lipofuscin is seen in smooth muscle cells and pericytes. B. Three y old male SNpc capillary surrounded by a fragmented neuropil (*). Perivascular astrocyte end-feet appear dissociated from the capillary wall. An intact RBC is in the lumen. Extensive areas of vacuolated neuropil with few axons remain. C. SNcp neuropil in a 12y male, note the patchy vacuolated and fragmented neuropil (*). Axons of different sizes and thickness of myelin show focal fragmentation. D. A close-up of a blood vessel in an area close to the one shown in C. Note the close contact between the RBC and the endothelial surface. The arrow heads show the contact area and the presence of nanoparticles (NPs). NPs are also seen in the endothelial cell nucleus (arrows)in close contact with the heterochromatin.

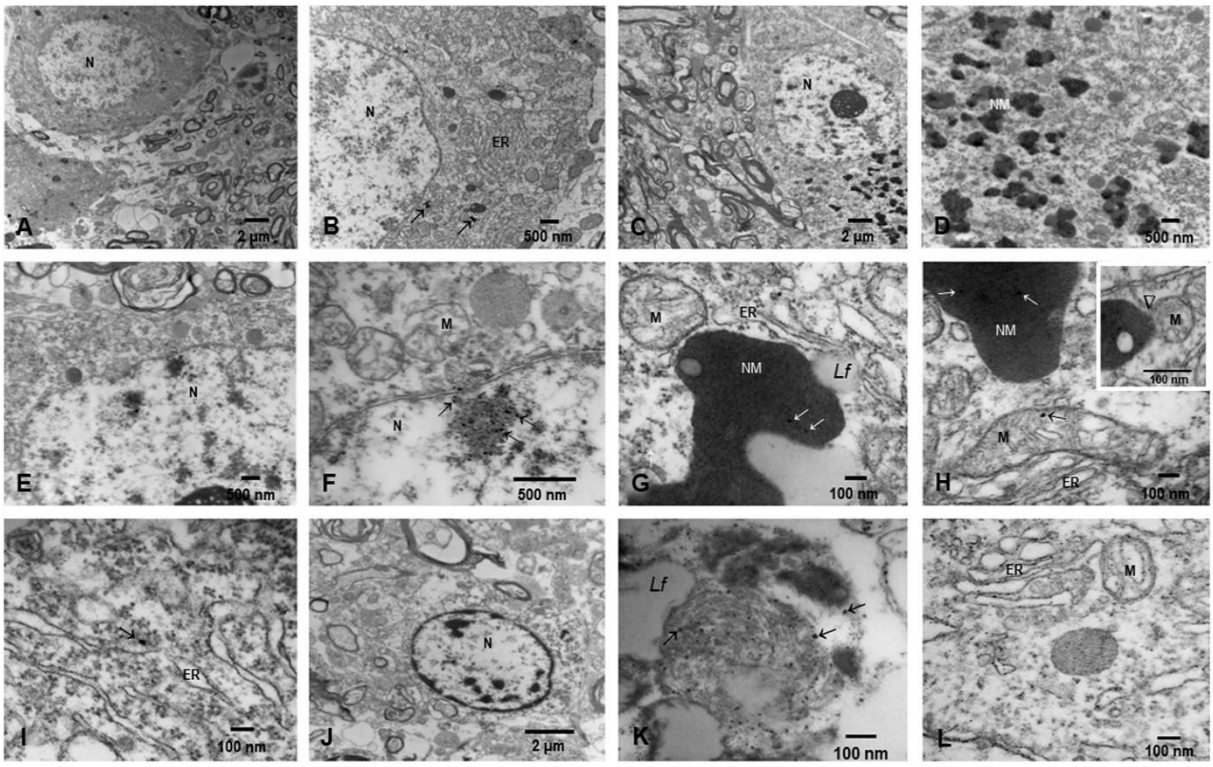

Figure D.4 Substantia nigrae representative electron micrographs from 1st through 3rd decades of life. A. Eleven m old with a SNpc neuron with very few neuromelanin (NM) structures but already significant damage to the neuropil i.e., large vacuolated spaces with debris, fragments of macrophage-like cells (MΘ) and few axons. B. Same neuron as in A to show the few NM (arrows) and an abundant endoplasmic reticulum (ER). C. Twelve y old SNpc neuron with a cluster of NM in a paranuclear location. Note the close contact of axons around this neuron with only a few, small areas of loosening neuropil (*). D.A close-up of the NM cluster to show the uniform size between rough endoplasmic reticulum. E. In the same neuron, a close-up of the nucleus and nucleolus and the loosing of the neuropil adjacent to the neuron cell membrane. F. It is clear the presence of NPs in close contact with heterochromatin (arrows) and the double nuclear membrane with NPs at the intersection. Numerous small mitochondria (M) have fragmented cristae. G. Fifteen y old NM close-up adjacent to dilated ER and abnormal mitochondria (M). Inside the NM we observe NPs (arrows) and lipid structures (lf). H. Same as G to show another NM with NPs (white arrows) and mitochondria with NPs inside (black arrow) and dilated ER. In the Insert a close contact between the NM and a mitochondrion, a relationship expected between a mitochondria and ER, not a NM. I. Abundant and dilated RER with NPs inside (arrow). J. Oligodendroglia with a disrupted cytoplasm and its surrounding abnormal axons vary in size and thickness of the myelin. K. Twenty-six y old SNpc to show a distinct fibrillary structure with NPs (arrows) in the midst and closely attached to a lipid lipofuscin like structure. L. An area with dilated ER and abnormal mitochondria. In the close contact between the dilated ER and the small mitochondria (arrowhead) the resultant MERC is abnormal.

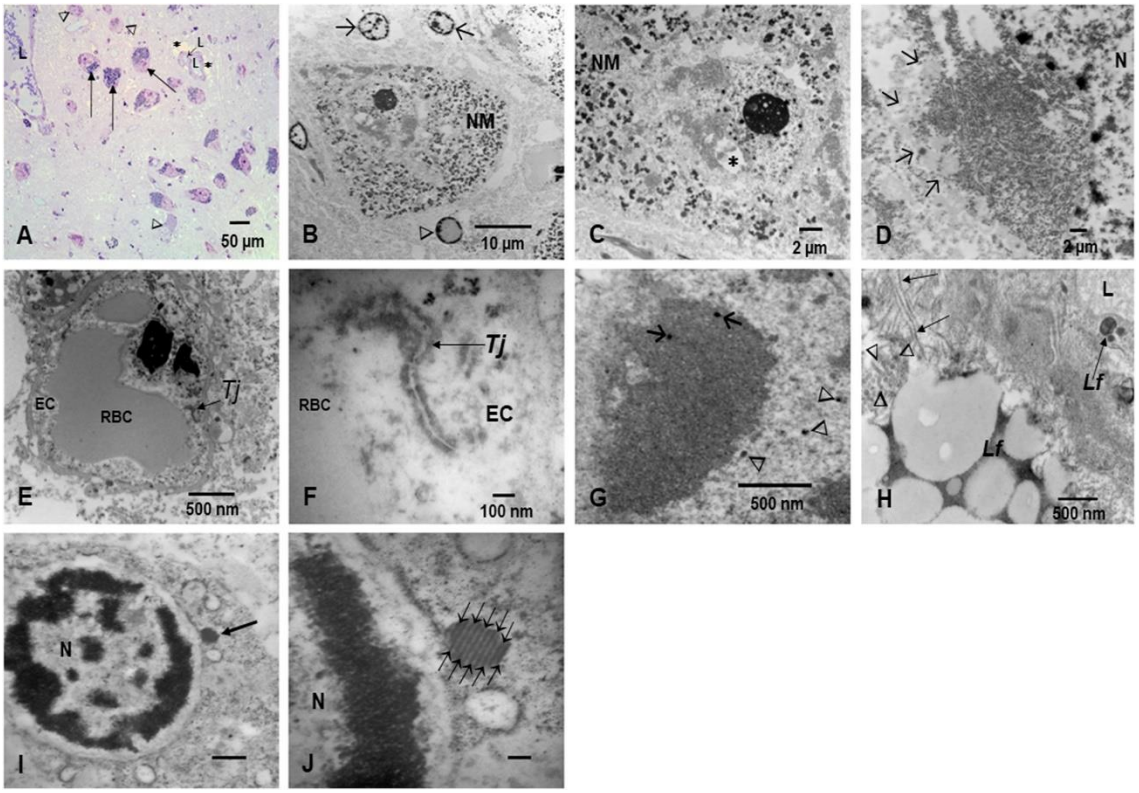

Figure D.5 Substantia nigrae representative electron micrographs from beyond the 5th decade of life. A. Seventy-one y old MMC resident substantia nigrae, 1 µm toluidine blue section showing substantia nigrae pars compacta neurons with abundant cytoplasmic neuromelanin (NM) (long arrows) in sharp contrast with neurons with scanty cytoplasm, few NM, and small nuclear fragments (arrowheads). Blood vessels are marked with an L in their lumen and some small vessels have a vacuolated perivascular neuropil (*). B. Same subject as A, this neuron shows abundant NM and several macrophage-like cells around. The lower macrophage nucleus (arrowhead) shows a pyknotic nucleus, while the upper two (long arrows) exhibit an intact nuclear membrane but their cytoplasm is fragmented. C. At greater magnification, is clear the neuronal cytoplasm is vacuolated and there are clearing of the cytoplasm around a disrupted nucleus. The neuronal inclusion with dysmorphic organelles is adjacent to the empty space (*). D. The intracytoplasmic inclusion characterized by filaments, membrane fragments, dysmorphic organelles, and lipids (Shahmoradian et al., 2019) is marked by several arrows. E. A small blood vessel in the vicinity of the neuron in B-D, with an RBC in the lumen and a tight junction (Tj) (arrow) in the endothelial cell. F. The Tj at higher power shows a common finding in substantia nigrae endothelial cells: the abundant nanoparticles decorating the structure (arrow). G. Cell nuclei with numerous NPs both in the heterochromatin (arrows) and in the nuclear matrix(arrowheads). H. Small blood vessel with a lumen (L) and abundant lipofuscin in close contact with beta β-pleated sheet twisted tubules (arrows). A cluster of twisted tubules in close contact with a lipid portion of lipofuscin (arrowheads). I. Perineuronal macrophages are very common in older subjects and contain numerous lysosomes and rare structures with a lattice image(arrow). J. At higher magnification, the lattice image has 10 layers of well-ordered fringes with a perpendicular alignment(arrows).

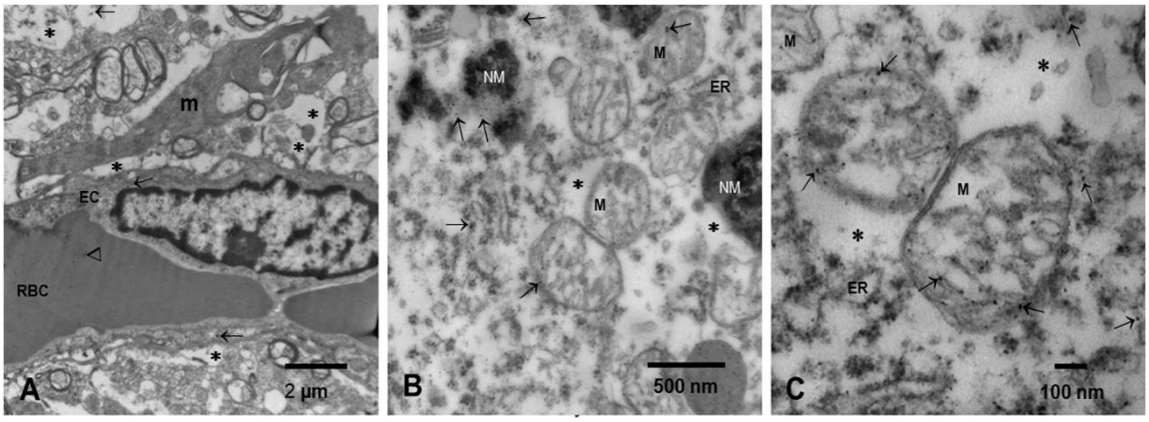

Figure D.6 SNpc electron micrographs of a 32y old male corresponding to Figs. D.7 and D.8. A. The neurovascular unit in this individual is abnormal, with neuropil breakdown (*) and the perivascular astrocyte end-feet dissociating from the capillary wall. In close contact with the blood vessel an elongated fragment of a macrophage-like cell(m) is remarkable. Its cytoplasm is dark and shows numerous vacuoles. Nanoparticles are seen in various locations, within the wall of the capillary (black arrow) and in empty neuropil. B. SNpc neuron with NM granules and ER. Note the numerous NPs in different organelles within the cell (short arrows), including within the NM. The mitochondria show abnormal cristae and the spaces between the ER and other organelles exhibits vaculated, empty areas (*). C. The abnormal mitochondria show numerous NPs, of different sizes within the cristae, matrix, and double membrane. ER structures are dilated and short.

In order to identify the elemental composition of the observed intracellular, electrodense NPs, SN sections from a 32y male were additionally subjected to HRSTEM and EDX. HAADF-STEM images revealed the abundant presence of NPs, often in groups or clusters, in close association with mitochondrial structures and neuromelanin (Figs. D.7–9).

Fig. D.7 shows the presence of NP clusters, of different sizes, shapes, and compositions, in close association with NM in the SN of this 32y old. Some NPs appear as rounded aggregates (NPs marked 1 and 2 in Fig. D.7B), dominantly composed of aluminium (Fig. D.7D) and iron (Fig. D.7E). The cluster of smaller, distinctively elongate NPs (group 3 in Fig. D.7) is dominated by titanium (Fig. D.7F). The EDX spectrum, Fig. D.8C, displays additional marked peaks in silica and nickel, arising from the nickel TEM grid, and chlorine, which occurs all over the analysed area (Fig. D.7G), likely reflecting some aspect of sample preparation. Similar metal compositions are evident for NPs seen in association with, and apparently traversing, the double membrane of an SN mitochondrion (Fig. D.8). In addition to the rounded aggregates of aluminium- and iron- rich particles, discrete and elongate particles of titaniferous composition are evident (Fig. D.8 E, J).

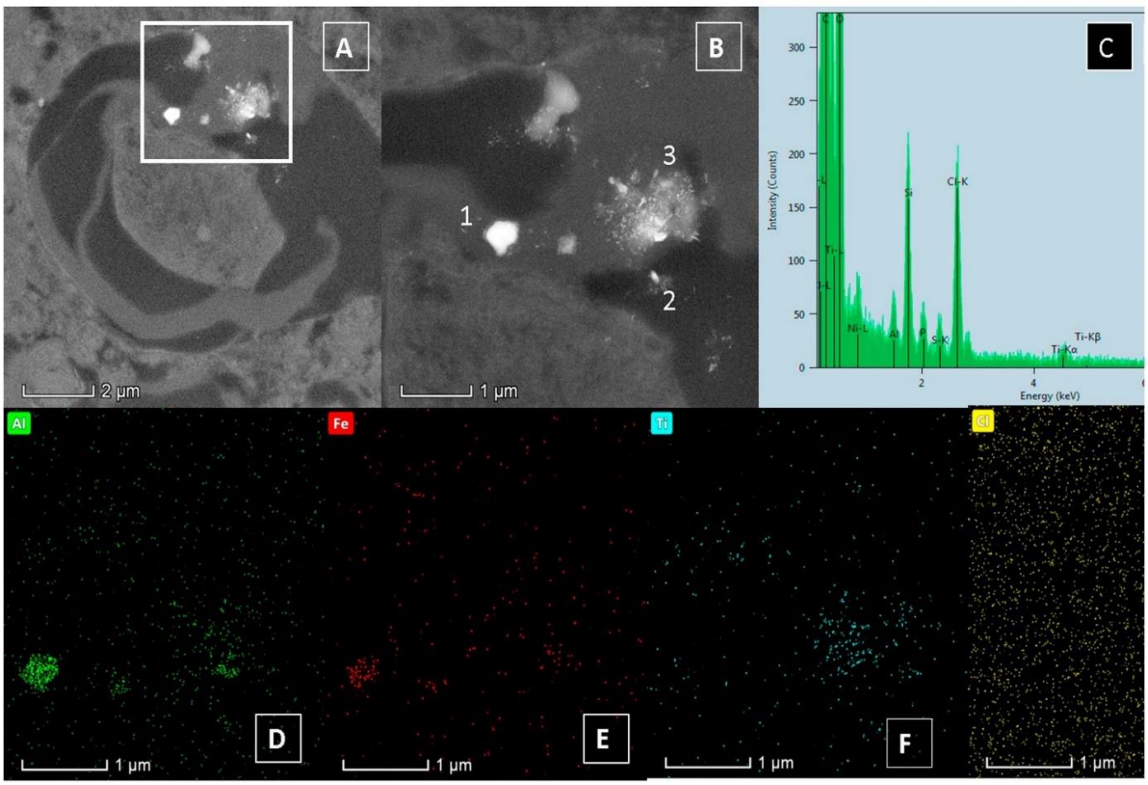

Figure D.7 A, B. High magnification high-angle annular dark field-scanning/transmission electron microscopy (HAADF-STEM) of SN tissue, 32 y old subject (also see Fig. D.8); B: a higher magnification image of the bright, electrodense NPs (marked as 1, 2 and 3) shown in the area in the white box in A. C. EDXA spectrum for the area shown in B. D – F. elemental maps for the area shown in B.

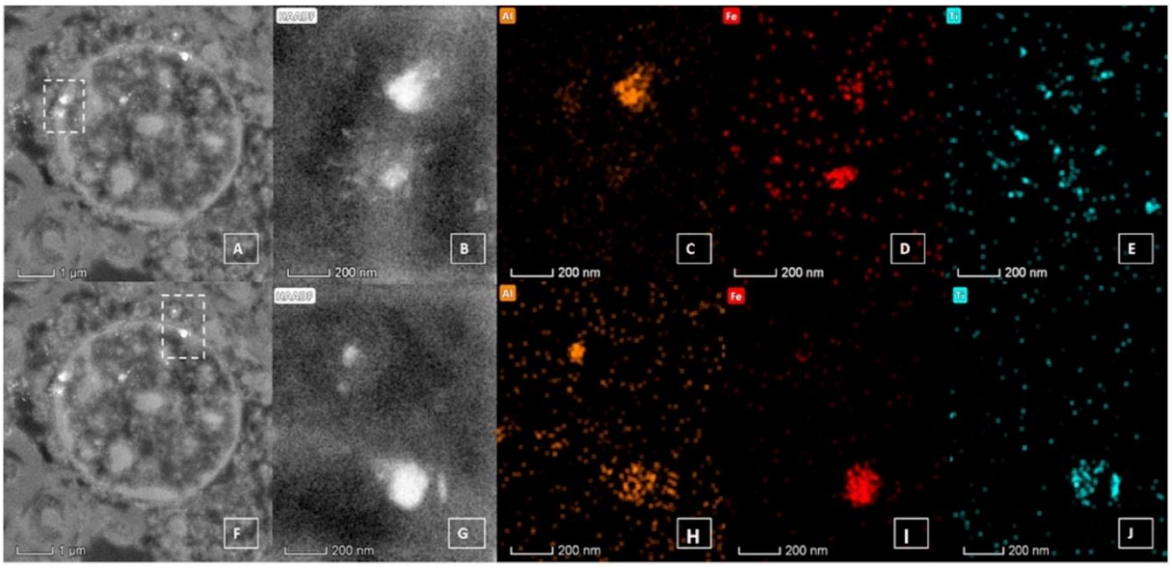

Figure D.8 A and F: HAADF-STEM of NPs around a mitochondrion in SN tissue, 32 y old subject (B and G higher magnification images of the bright, electrodense NPs shown in the white box in A and F, respectively); C–E: elemental maps for the particles in the white box shown in A; H–J: elemental maps for the area shown in F.

These latter titanium-rich, acicular NPs are particularly distinctive; in our prior work on frontal tissue samples, we have not seen particles with this elongate morphology, nor have we observed

them in urban roadside particulate air pollution samples. Conversely, we have observed similarly elongate, Ti-rich particles in neuroenteric tissue samples (Fig. D.9), which, we infer, have been ingested and/or swallowed from airborne sources, and which have traversed the small bowel epithelium to access the neuroenteric pathway.

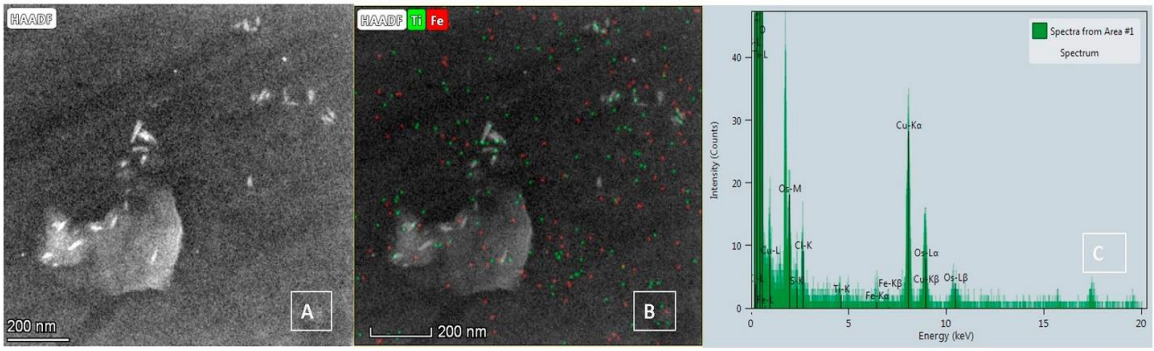

Figure D.9 A and B: HAADF-STEM of Ti-bearing elongated laths, in neuroenteric tissue sample from a 39y old male with both AD and PD hallmarks; C EDX spectrum for the area imaged in A and B (NB Cu peaks reflect the use of a copper TEM support grid).

D.4.4 Magnetic remanence

Fig. D.10 and Table D.1 summarise the SIRM values for each of the SN, tectum, tegmentum, PAG and cerebellum tissue samples measured, versus age. Individual subjects display variable SIRMs, with little apparent correlation with age. However, the three brain regions (Fig. D.10A – C) display significant differences (Fig. D.10 D, p-value = 0.01144) in their magnetic content. Median SIRM values (all × $10^{-6}Am^2kg^{-6}$) vary from 1.52 for SN samples, 2.97 for tectum/tegmentum/PAG, and 4.75 for cerebellum. The estimated ferrimagnetic concentration and numbers of magnetite-like NPs range from 0.01-2.63 (median 0.11) µg/g dry wt. and 0.18-32.52 (median 1.36) × 10^9/g, respectively for the measured SN samples; from 0.02-1.79 (median 0.22) µg/g dry wt. and 0.31-22.20 (median 2.67) × 10^9/g for the tectum/ tegmentum/PAG samples; and from 0.02-2.19(median 0.34) µg/g dry wt. and 0.27-27.11 (median 4.26) × 10^9/g for the cerebellum samples.

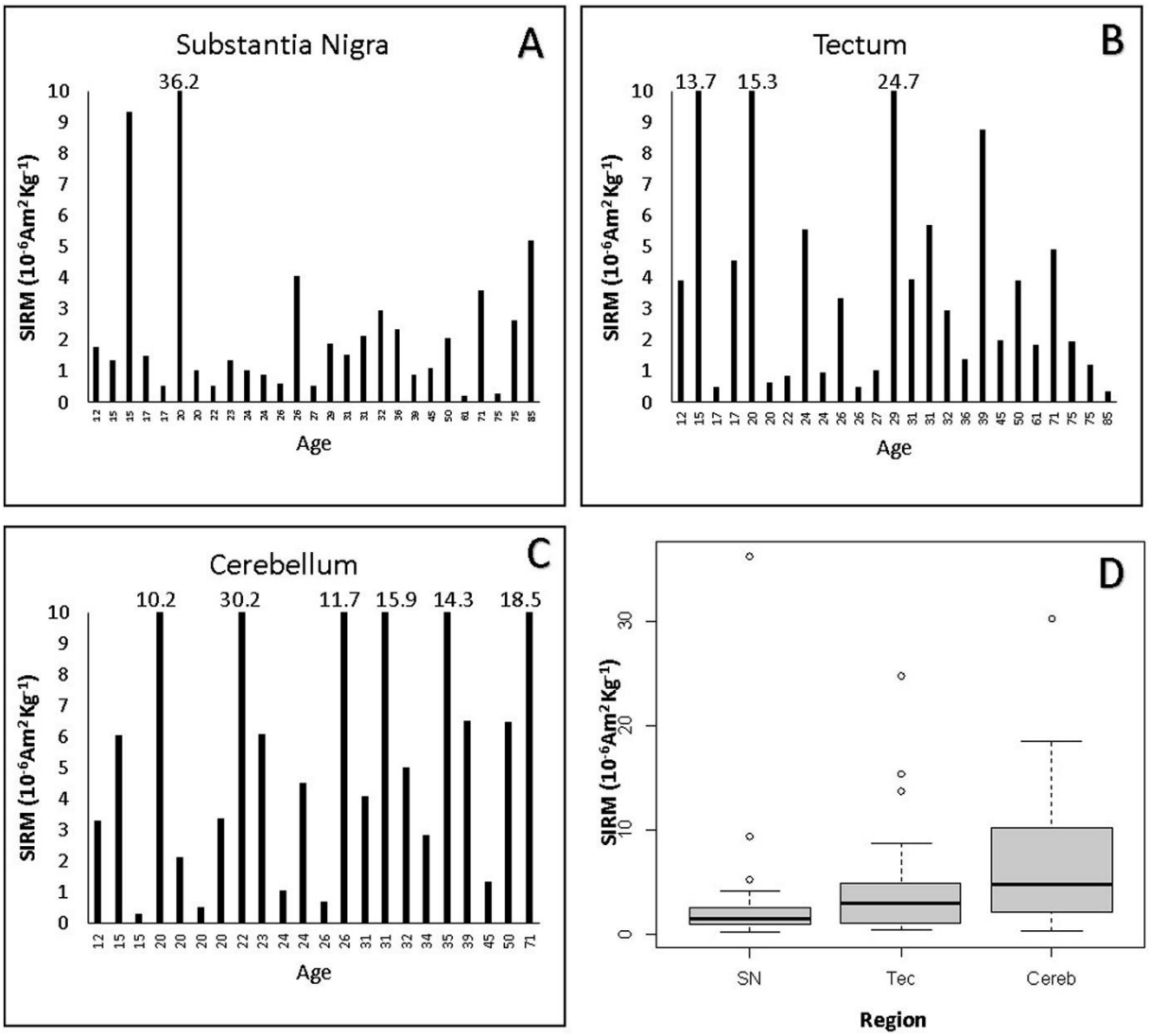

Figure D.10 Room-temperature SIRM values versus age for A. SN samples, B. tectum/tegmentum/PAG, C. cerebellum, and D. box plots, showing significant differences between the magnetic content of the 3 regions (Kruskal-Wallis test, p-value =0.0116).

Table D.1 Room temperature SIRM values for a representative sub-cohort of the MMC subjects, and calculated concentrations and number concentrations of magnetite NPs: SN = substantia nigra; TTP = tectum/tegmentum/PAG; CB = cerebellum.

ID#	Age	SIRM (10^{-6} AmKg^{-1})			Magnetite concentration µg/g			No. magnetite particles 10^9/g		
		SN	TTP	CB	SN	TTP	CB	SN	TTP	CB
1	12	1.8	3.92	3.31	0.13	0.28	0.24	1.61	3.52	2.97
2	15	1.36	13.7	6.05	0.10	0.99	0.44	1.22	12.30	5.43
3	15	9.37		0.3	0.68		0.02	8.41		0.27
4	17	1.52	0.5		0.11	0.04		1.36	0.45	
5	17	0.53	4.57		0.04	0.33		0.48	4.11	
6	20	36.23	15.32	10.16	2.63	1.11	0.74	32.52	13.75	9.12
7	20	1.02	0.63	2.11	0.07	0.05	0.15	0.91	0.57	1.89
8	20			0.5			0.04			0.45
9	20			3.37			0.24			3.02
10	22	0.52	0.87	30.2	0.04	0.06	2.19	0.47	0.78	27.11
11	23	1.37		6.07	0.10		0.44	1.23		5.45
12	24	1.02	5.55	1.03	0.07	0.40	0.08	0.92	4.99	0.93
13	24	0.89	0.95	4.49	0.07	0.07	0.33	0.80	0.85	4.03
14	26	0.6	3.37	0.69	0.04	0.24	0.05	0.54	3.02	0.62
15	26	4.08	0.49	11.72	0.30	0.04	0.85	3.67	0.44	10.52
16	27	0.53	1.02		0.04	0.07		0.47	0.92	
17	29	1.9	24.73		0.14	1.79		1.70	22.20	
18	31	2.15	3.97	4.08		0.29	0.30		3.56	3.66
19	31	1.54	5.72	15.93	0.11	0.41	1.15	1.38	5.13	14.30
20	32	2.95	2.97	5.01	0.21	0.22	0.36	2.65	2.67	4.50
21	34			2.84			0.21			2.55
22	35			14.25			1.03			12.79
23	36	2.35	1.39		0.17	0.10		2.11	1.25	
24	39	0.9	8.78	6.51	0.07	0.64	0.47	0.81	7.88	5.85
25	45	1.1	1.99	1.32	0.08	0.14	0.10	0.99	1.79	1.19
26	50	2.07	3.91	6.47	0.15	0.28	0.47	1.86	3.51	5.81
27	61	0.2	1.86		0.02	0.14		0.18	1.67	
28	71	3.62	4.92	18.46	0.26	0.36	1.34	3.25	4.42	16.57
29	75	0.29	1.96		0.02	0.14		0.26	1.76	
30	75	2.64	1.22		0.19	0.09		2.37	1.09	
31	85	5.23	0.34		0.38	0.03		4.69	0.31	

D.5 Discussion

We are documenting in a collection of 186 brainstems from Mexico City residents age 27.29 ± 11.8y old, the striking overlap of hyper- phosphorylated tau, α synuclein and TDP-43- markers of AD and PD-, and, surprisingly, transactive response DNA-binding protein TDP-43 (a marker for amyotrophic lateral sclerosis (ALS) and frontotemporal lobar degeneration with ubiquitin-positive inclusions (FTLD-TDP) (Dewey et al., 2012, James et al., 2016, Nelson et al., 2019, Kodavati et al., 2020, Besnard-Guérin, 2020, Pasquini et al., 2020, Wu et al., 2020, Mashik et al., 2016) strongly supporting a common denominator impacting the brain early in life. The brainstem and cerebellum are critical not only because they host key networks modulating

autonomic function, arousal, motor control and emotions (Venkatraman et al., 2017, Zhang et al., 2017, Zelena et al., 2018, Adamaszek et al., 2017, Guyenet et al., 2020), but because damage to specific nuclei and network connections shed light on associated early clinical manifestations and critical portals of entry of our culprit: metal-rich exogenous nanoparticles (Calderón-Garcidueñas et al., 2020d). The dominant presence of Fe, Al and Ti in the NPs present in substantia nigrae (SN) mitochondria, points unequivocally to their exogenous sources -including engineered Ti-rich nanorods- and raises serious concerns. TiO_2 NPs are widely manufactured for use in both domestic (e.g. cosmetics, sunscreens) and industrial (e.g. paints, coatings, electroceramics, solar cells) applications (Chemseddine and Moritz, 1999, Chen and Mao, 2007, Kose et al., 2020) and are abundant in E-waste (Ceballos et al., 2020). Al-rich NPs are also abundant in airborne pollution, and, together with Fe and Ti, have been reported in high concentrations in Beijing residents' serum and in pleural effusions (Lu et al., 2020).

The SN presence of distinctive, acicular NPs of titanium-rich composition indicates that NPs have different portals of entry and subsequent transport routes - and, hence, potentially different brain targets. We have not previously observed elongate Ti-rich NPs in frontal or heart samples, nor in roadside airborne PM. Conversely, we have imaged and analysed similar particles in the neuroenteric system (myenteric plexus neurons), suggesting that these engineered NPs have accessed the brainstem via axonal transport, having traversed the gut wall after ingestion (e.g., with food) and/or being inhaled and swallowed. These observations are consistent with the key work of Holmqvist et al. (Holmqvist et al., 2014) showing the transport of αSyn via the vagal nerve to the dorsal motor nucleus of the vagus in a time-dependent manner, and the monosynaptic nigro-vagal connections as discussed by Anselmi et al.(Anselmi et al., 2017, Anselmi and Travagli, 2017).

Notwithstanding the possibility of intracellular dissolution and (slow) clearance of exogenous particles (Maher, 2019), the brainstem metal-rich NPs may reflect the prevalence of those species in the environment to which these young urbanites have been exposed (Arshadi, 2017). Specific metal cytotoxicity is evident from abundant in vitro and animal studies, e.g., TiO2 NPs produce upregulation of miR-29b-3p reinforcing apoptosis, imbalance in the Th1/Th2 cells, small intestine physical(ileum) barrier structural changes in a dose-dependent manner, and epigenetic changes (Sungur et al., 2020, Xu et al., 2020b, Yao et al., 2020, Peters et al., 2020, Coméra et al., 2020, Gallocchio et al., 2020, Yarjanli et al., 2017) . Food sources of TiO_2 NPs are substantial (Sungur et al., 2020), concentrations in food reportedly range from 3 to 2400 mg kg-1 with particle sizes between 30 and 410 nm. Peters et al. described in 15 human autopsies abundant

TiO_2 particles in ileum > jejunum > kidney > spleen > liver in the size range of 50–500 nm, modal size 100–160 nm and ~17% < 100 nm (Peters et al., 2020).

It is remarkable, the distinctive, elongate Ti-rich nanorods observed in the SN and neuroenteric samples here differ from the mostly spherical TiO_2 common in food additives, and may instead reflect handling of, for example, e-waste, or plastics (Chemseddine and Moritz, 1999, Chen and Mao, 2007, Tiwary et al., 2017).

In terms of Fe-rich, ferrimagnetic NPs, the amount of midbrain magnetite measured here varies from subject to subject, an expected finding for individuals with different NPs exposure levels. However, our observation that the amount of magnetite varies significantly between the three different brain regions examined here (cerebellum > tectum/ tegmentum/PAG > SN) is striking. Gilder et al.'s (Gilder et al., 2018) study of 7 formaldehyde-fixed brains displayed ~60 × lower magnetic contents, with little variation between the 7 subjects, but highest magnetite concentrations in olfactory bulb, brainstem and cerebellum. Our findings suggest that different NPs appear to have different portals of entry: Fe- and Al-rich NPs via inhalation and blood systemic circulation and Ti-rich nanorods via neuroenteric axonal transport. Thus, it is possible that the significant differences in magnetite content seen here between the SN, tectum/tegmentum/PAG and cerebellum might reflect not only the nature of the anatomical structures (i.e. cluster of SN neurons versus intraxonal flow in afferent and efferent fibers) but also differential targeting of specific brain regions and cellular targets by NPs with differing exogenous sources, chemical composition, size, shape, and entry portals. Thence, the ultimate neural damage and neuropathological hallmarks incurred would depend both on the NP characteristics and the differential access and targets achieved via their portals of entry.

With regard to the SN, much published evidence demonstrates that both Fe-oxide and Ti-oxide NPs produce cytotoxicity and oxidative stress in specific targets including dopaminergic cells, leading to αSyn aggregation and fibrillation (Imam et al., 2015, Wang et al., 2019b, Bergamino et al., 2020, Liu et al., 2018, Mohammadi and Nikkhah, 2017, Milatovic et al., 2009, Gilan et al., 2019, Tira et al., 2020, Chen et al., 2020, Gupta et al., 2020).

No matter what the entry portal, the chronic delivery of exogenous Fe-rich NPs to the brain is likely to induce oxidative stress and neuroinflammation (Imam et al., 2015, Yarjanli et al., 2017, Reddy et al., 2017, Wu and Tang, 2018). Release of free Fe ions, e.g. within acidic lysosomal environments, can catalyse increased and uncontrolled production of reactive oxygen species (ROS) through the Fenton reaction (Imam et al., 2015, Yarjanli et al., 2017) and neuroinflammation (Wu and Tang, 2018, Disdier et al., 2017, Berndt et al., 2017, Ehsanifar et al.,

2019, Ising et al., 2019). The presence of strongly magnetic NPs in the brainstem and cerebellum, in number concentrations of up to 32× 10^9/g (dry wt.) tissue may carry additional and specific significance; not only providing a source of reactive Fe, but also acting synergistically to promote the toxicity of amyloid-β, as shown by in vitro studies (Teller et al., 2015). Indeed, magnetite NPs have been found directly associated with senile plaques and amyloid-β fibrils in an AD brain (Quintana et al., 2006), and may contribute directly to Alzheimer-like neurodegeneration changes (Allsop et al., 2008, Castellani et al., 2007, Coccini et al., 2017). Depending on their location, concentration, size, degree of aggregation and magnetic interactions between NPs, magnetite NPs might also damage target organelles and cells through hyperthermia and/or magnetic rotation effects. Because magnetite is an excellent absorber of microwave radiation at frequencies of between 0.5 and 10 GHz (cell phones, for example, operate at frequencies of ~1–2 GHz), localised heating effects might be induced (Kirschvink et al., 1992b, Pall, 2018, Karimi et al., 2020, Gholami et al., 2020). That some organisms are able to detect and respond to cues from the Earth's magnetic field, through the presence of biologically formed magnetite NPs, is unequivocal (Kirschvink and Gould, 1981). We suggest that, depending on exposure, the variable ingress of exogenous, pollution-derived magnetite NPs to major organs, including the brain, may account for some findings (Binhi and Prato, 2018, Falone et al., 2018, Casey et al., 2020, Gao et al., 2020) that extremely weak alternating magnetic fields (i.e. with magnetic field amplitudes in the T and nT ranges), can induce statistically significant effects in biological systems. If DNA synthesis, RNA transcription and cell signalling, Ca++ flux, for example, can be thus affected, then the magnetic responses of ~32 × 10^9 /g tissue magnetite pollution may provide a further direct pathway to neurodegeneration.

In the SN, we observe associations between clusters of Fe- (and other metals)-rich NPs and endosomal structures like NM. Magnetic interactions between magnetite NPs can enhance their response to external magnetic fields, even for particles otherwise too small (<~30nm) to align at ambient temperature with applied magnetic fields (Maher, 1988). Even at low concentrations, Fe-rich and TiO2-NPs accelerate αSyn fibrillization, a matter of deep concern for individuals exposed to high concentrations of these airborne NP species, i.e., α-synuclein fibrils can grow at much lower monomer concentrations than that required for *de novo* fibril formation (Afitska et al., 2019). The NPs size is critical: in human neuroblastoma cells, 10 and 30 nm ferric oxide nanoparticles significantly depleted cellular dopamine, increased ROS, damaged the BBB and produced neuronal α-synuclein expression (Imam et al., 2015).

Al-rich NPs in the SN is an interesting finding, Al has, of course, been one of the most studied environmental agents linked with AD, with observational studies indicating that aluminium

levels are significantly elevated in brain, serum, and CSF of AD patients (Virk and Eslick, 2015). Our novel results are consistent, specifically, with Perl and colleagues' work who identified intraneuronal aluminium accumulations (10–50 × adjacent NFT-free neurons and controls) in hippocampal neurons bearing NFTs in AD patients (Perl and Brody, 1980). Using a rabbit model, Perl & Good (Perl and Good, 1987) showed that exposure to intranasal aluminium leads to direct uptake into the brain and distribution along olfactory pathways. In vitro, cytotoxic and genotoxic damage by Al_2O_3 NPs has been associated with Al^{3+} ion release in the acidic environment of vesicles (Hashimoto and Imazato, 2015). Al-induced neurocognitive decline among Al occupational workers is a serious hazard and downregulating PI3K, Akt, and mTOR1 expression and inducing neuronal cell death have been shown experimentally and in Al workers (Shang et al., 2020). Exley and Clarkson suggested that the Al content of brain tissue in Alzheimer's disease, autism spectrum disorder and multiple sclerosis is significantly elevated versus controls in a study of 191 tissue samples (Exley and Clarkson, 2020).

Several SN findings in this work are remarkable, including the mitochondrial and ER abnormalities, and the vesicular structures and dysmorphic organelles; the latter - as described by Shahmoradian et al. (Shahmoradian et al., 2019) surrounded by NM fragments. The observed accumulation of metal-rich NPs in association with the NM raises the issue reported by Haining and Achat-Mendes (Haining and Achat-Mendes, 2017) of NM apparently conferring 'susceptibility to chemical toxicity by providing a large sink of iron-bound, heme-like structures in a pi-conjugated system'. Zecca et al., and Zucca et al.'s excellent (Zecca et al., 2008, Zucca et al., 2018) papers describing the accumulation of neuromelanins in concentrations as high as 1.5–2.6 μg/mg tissue in putamen, cortex, cerebellum and a recent paper describing substantia nigrae membrane and matrix proteins characteristic of lysosomes at a lower number than in typical lysosomes, gave the authors an indication of a reduced enzymatic activity and impaired capacity for lysosomal and autophagosomal fusion. Highly relevant to our findings, Zucca and co-authors (Zucca et al., 2018) suggested that: i. NM-containing organelles likely have impaired capacity for lysosomal and autophagosomal fusion; and ii. the accumulation of proteins of aggregation and degradation pathways supporting the ubiquitin-proteasome system is inadequate. Both suggestions are in accord with a dysfunctional autophagy and ubiquitin proteasome system (UPS) in turn implicated in protein aggregation and toxicity by Limanaqi et al. (Limanaqi et al., 2020). Thus, in the case of young MMC residents, it is highly probable that the variable but extensive accumulation by NM of highly oxidative (and magnetic), metal-rich NPs will accelerate the dopaminergic cell damage at earlier ages, and as documented here, children exhibit extensive damage to SNpc with macrophages phagocytizing neuromelanin loaded neurons.

Activated microglia-mediated engulfment of dopaminergic neurons with abundant NM could increase neuroinflammation on one hand and alter their role in αSyn clearance and degradation on the other (George et al., 2019). NPs engulfed by macrophages affect their phagocytosis and migration capabilities (Li et al., 2020b) and since macrophages (Vannella and Wynn, 2017) are themselves a rich source of inflammatory mediators and matrix metalloproteinases, they can worsen tissue injury by producing ROS, inducing apoptosis, and exacerbating ischemic injury. Our Fig. D.4H insert illustrates a SNpc common phenomenon: the intimate contact between endolysosomes (EL) and mitochondria, an issue Wang et al. (Wang et al., 2020b), discusses in the context of functional mitochondrial outer membrane permeabilization (MOMP) execution during cellular apoptosis signalling. Their exciting paper shows mitochondria are targeted by endolysosomes during MOMP and key to our electron microscopic observation: interactions of ELs with mitochondria control BAX recruitment and pore formation (most certainly an effective pathway to kill SNpc neurons).

Another mechanism to take into account relates to damage to nuclear membranes by NPs: dysregulation of the nucleocytoplasmic transport machinery regulated by the structure and function of nuclear pores and mRNA export mechanisms, could result in protein accumulation (Moore et al., 2020). Leibiger et al. (Leibiger et al., 2018), have proposed that TDP-43 interferes with lysosomal function and its own degradation via lysosomal pathways triggering lethal autophagy. Indeed, common pathways are shared by a number of neurodegenerative diseases, including dysregulation of RNA metabolism and pathological persistence of stress granules (Koren et al., 2020, Advani and Ivanov, 2020).

Our observed magnetic concentrations, in the order SN < tectum/ tegmentum/PAG < cerebellum, likely signal the circuits and systems affected by NP ingress, encompassing the SN and its connectivity-based parcellation with limbic, cognitive, and motor arrangements. determining in part decisional and motor impulsivity, as described by Zhang et al. (Zhang et al., 2017). PAG plays a key role in emotions-related cognitive processes and in neurovegetative regulation (Zelena et al., 2018) while the cerebellum has a pivotal functional role in human affective processing (Adamaszek et al., 2017, Pierce and Péron, 2020, Chen et al., 2020, van den Berg et al., 2020, Tozzi et al., 2020). The elevated concentrations of magnetite in the cerebellum are notable and recall the selective targeting of mercury intoxication (O'Donoghue et al., 2020).

D.5.1 Significance of overlap of four distinct neurodegenerative markers in young pollution-exposed subjects

The overlap of four distinct simultaneous neurodegenerative markers (pτ, Aβ, αSyn and TDP-43) present in 10.98% (20/182) of young MMC urbanites appears crucial; co-existence of markers of two relatively common diseases, sporadic AD and PD, with a less common amyotrophic lateral sclerosis (ALS) disease/frontotemporal degeneration (FTD) suggests a common aetiological denominator. We strongly support mapping out the development of these fatal diseases in forensic autopsies of young people - without either clinical evidence and/or morbidities associated with neurodegeneration – enables characterization of the earlier neurodegenerative pathomechanisms taking decades to become openly clinical. Because NP pollution loadings and compositions will differ between different locations, even within the same city, similar investigations of young fatalities will permit definition in each city and each country of the populations at risk and the identification of potential environmental and/or other factors in common. Hyper- phosphorylated tau was by far the most common misfolded protein in our subjects.

Our TDP-43 immunohistochemistry findings in SN neurons and nonmotor brainstem nuclei are particularly worrisome (34/182 cases, 18.68%), given the young age of affected subjects: 26.8 ± 10.5y. We have documented in the SN an overlap between TDP-43 pathology and αSyn in 20 cases and with p-τ in 30 subjects. Karanth and co-workers (Karanth et al., 2020) in a study of 375 autopsies of demented Alzheimer disease pathology (tau and Aβ) subjects, age 86.9 ± 8.0 with α-synuclein, and TDP-43 data, along with Braak neurofibrillary tangle stages I to VI, found 19.2% with quadruple misfolded proteins. Quadruple misfolded proteins patients had MMSE scores in the severe impairment range and higher odds of APOE4 status. The authors concluded: Quadruple misfolded proteins appear to be a common substrate for cognitive impairment and to be associated with an aggressive course of disease that typically ends with severe dementia (Karanth et al., 2020). They added a statement that is very important for our quadruple misfolding proteins findings in MMC children and young adults: The prevalence of comorbid α-synuclein and TDP-43 with Alzheimer disease pathology (tau and Aβ) may complicate efforts to identify therapies to treat and prevent Alzheimer disease. We fully agreed with them.

Geser et al. (Geser et al., 2020), work posed a key question: Development of Neurodegeneration in Amyotrophic Lateral Sclerosis: From Up or Down? It is evident in our young subjects that the lower brainstem is an early TDP-43 pathology target as it involves the reticular formation in medulla, pons, midbrain, and the SN. Moreover, we also documented glial cells with cytoplasmic positivity. Interestingly, Tomé et al. (Tomé et al., 2020) showed evidence in documented AD

cases that TDP-43 aggregates vary in their composition and relate to the clinical presentation. Here, our findings specifically demonstrate the importance of the nature and number of NPs inhaled and swallowed. Hence, where you live, how you travel, what air pollutants you are exposed to, and your occupational history and exposure to any other environmental sources of NPs are as, if not more, important than all other factors known to be associated with neurodegeneration (CVD, diabetes, nutrition, exercise, etc.).

The study has shortcomings. Our major gap is the lack of funding to extend the high-resolution scanning and transmission electron microscopy (HRSTEM) and energy-dispersive X ray analysis (EDX).

D.5.2 Concluding remarks

1. The neuropathological evidence from this Mexico City study identifies unequivocal development of aberrant misfolding and aggregation of hyperphosphorylated tau, Aβ, α synuclein and TDP-43 in the brainstem of children and young adults.
2. Concentrations of Fe-rich, ferrimagnetic NPs in the brainstem vary from individual to individual, as expected for differing levels of NP exposure. Magnetic concentrations increasing in the order, SN <tectum/tegmentum/PAG < cerebellum, opens up the opportunity of detecting early clinical alterations in motor control learning, motor coordination, gait, and balance (Calderón-Garcidueñas et al., 2020d), cognition and emotion behaviours and neurovegetative regulation.
3. Strikingly, we have identified, in situ, in SNpc neuronal organelles (mitochondria and neuromelanin), NPs containing Fe, Al and Ti in subjects displaying immunoreactive p-τ, αSyn and extensive NVU and mitochondrial damage. The elongate Ti-rich NPs in the SN, identical to Ti NPs in neuroenteric neurons are remarkable findings. Their presence strongly suggests that i. the GI tract is a key portal for Ti NPs, ii. the oral portal of entry is a direct path to the brainstem via vagus nerves and iii. Ti-rich nanorods from e-waste and other sources are reaching the substantia nigrae.
4. The portals of entry, and the specific characteristics (composition, size, etc.) of the NPs may be of key importance in defining which cells and organelles will be affected and by what type of damage. The SN is an early target of metal-rich, and highly magnetic NPs: p-τ is the most common abnormal protein in young individuals.
5. The incursion of magnetite NPs from exogenous sources may not only induce neural ROS- and protein-related dysfunction. Given that magnetite formed biogenically by organisms can respond to small changes in magnetic field gradients and/or intensity (conferring a magnetoreceptive sense), it is possible that magnetite accumulated from

exogenous sources can cause intracellular impacts through particle displacement/rotation, and by localised heating through microwave absorption.

6. Critical here are the co-associations between pathology seen in mitochondria, ER, and NM and the location and abundance of exogenous, Fe-, Al- and T-rich NPs, in close contact with key organelles and neurofilaments, glial fibers, and chromatin. Such reactive, cytotoxic, and magnetic NPs are a specific potential source for all of the following: altered microtubule dynamics; mitochondrial dysfunction; accumulation and aggregation of unfolded proteins; abnormal endosomal systems; altered insulin signalling; altered calcium homeostasis; apoptotic signalling; autophagy; and epigenetic changes.
7. The bleak facts in sporadic PD is that the clinical motor manifestations are late (Bove and Travagli, 2019, Váradi, 2020) with no possibility of reversing the extensive damage to dopaminergic cells, while in AD, the cognitive deficits develop very early and deeply compromise the potential academic, social and economic goals in young subjects. The TDP-43 pathology seen in 18.68% of young MMC urbanites obligate us to revise the dementia numbers in Mexico and Latin America (LA) and the prevalence of frontotemporal dementia (FTD) and frontotemporal lobar degeneration with ubiquitin-positive inclusions(FTLD-TDP) (Custodio et al., 2017, Casterton et al., 2020, Advani and Ivanov, 2020). Custodio et al. (Custodio et al., 2017) discussed LA prevalence of dementia reaching 7.1%, with AD being the most frequent type. FTD cases range from 12 to 18 cases per 1000 people with significant differences among Brazilians > Peruvians > Venezuelans. Mexico and LA are experiencing major demographic changes with increased numbers of people ≥60y and accurate prevalence data for AD and FTD in Mexico are both essential but presently not available.
8. These findings indicate that NP exposure should be included in any assessment of the neurodegenerative risk profile of each individual.
9. Highly oxidative, magnetic, abundant, metal-rich NPs emitted in the urban atmosphere constitute a novel path into AD, PD and TDP-43 pathogenesis. Exposed children and young adults need early neuroprotection and multidisciplinary prevention efforts have to be implemented. Control of combustion and friction nanoparticle sources (traffic, biomass burning, and industry), and of engineered NPs (food products, cosmetics, toothpaste, sun protectors, surface disinfectants, paints, e-waste etc) becomes increasingly important and urgent, in order to diminish the human and economic costs of a global neurodegenerative epidemic.

Declaration of competing interest

The authors declare that they have no known competing financial interests or personal relationships that could have appeared to influence the work reported in this paper.

Acknowledgments

The authors thank Zabeada Aslam and Mark S'Ari of Leeds University's EPSRC Nanoscience and Nanotechnology Facility (LENNF), U.K. for their support and assistance in this work.

Funding

This work was partially supported by E022 Instituto Nacional de Pediatría (AGM). B A Maher receives funding from Jaguar Land Rover.

D.6 Supplementary data

Table D.2 Autopsy and neuropathological data for the 186 cases examined with H&E, PHF-tau8 phosphorylated at Ser199-202-Thr205, α-synuclein phosphorylated at Ser-129, LB509 and TDP-43 mab2G10.

ID#	AGE	GENDER	APOE	AD pτ	AD Aβ	SN pτ	SN αS	TDP-43*
1	1	1	0	1	2	1	0	1
2	1.4	0	0	2	0	0	0	0
3	2	1	0	1	0	1	0	0
4	3	1	0	2	0	1	0	0
5	4	1	0	2	0	0	0	0
6	7	1	0	2	0	0	0	0
7	11	1	0	2	2	1	0	0
8	11	1	0	2	0	0	0	0
9	11	0	0	1	2	1	1	1
10	12	1	0	4	4	1	0	0
11	12	1	0	2	2	0	0	0
12	13	0	1	2	2	0	0	0
13	13	0	0	2	2	1	1	0
14	14	0	0	2	2	0	1	1
15	14	0	0	2	0	0	0	0
16	14	1	0	2	2	0	0	0
17	14	1	0	2	2	1	0	0
18	14	1	0	2	2	1	0	1
19	15	1	1	2	2	1	0	0
20	15	1	0	2	2	0	0	1

21	15	1	0	3	2	1	0	0
22	15	1	0	2	2	0	0	0
23	15	1	0	2	2	1	0	0
24	16	0	0	2	2	0	1	0
25	16	1	0	2	2	0	0	0
26	16	1	0	2	2	1	0	1
27	17	1	0	1	2			
28	17	1	0	3	2	1	0	1
29	17	1	0	2	2	1	0	0
30	17	1	0	2	2	0	0	0
31	17	1	0	2	2	1	0	1
32	17	1	0	2	2	1	0	0
33	17	1	0	2	2	3	1	0
34	17	1	0	2	2	0	0	0
35	17	1	0	2	2	0	0	0
36	17	1	1	2	2	1	1	1
37	17	1	0	2	2	0	0	0
38	18	1	0	2	2			
39	18	1	0	2	2	1	1	0
40	18	1	0	2	2	1	0	0
41	18	1	1	2	2	0	0	0
42	18	1	0	2	2	1	0	1
43	19	1	1	2	2	1	0	0
44	19	1	0	2	2	0	0	0

45	19	1	0	2	2	0	0	0
46	19	1	0	2	2	1	1	1
47	19	0	0	2	2	1	0	0
48	20	1	0	2	2	0	0	0
49	20	1	0	2	2	1	1	0
50	20	1	1	2	2	1	1	0
51	20	1	0	5	2	1	0	0
52	20	1	2	5	2	0	0	0
53	20	1	0	2	2	1	1	0
54	20	0	0	2	2	1	0	0
55	20	1	0	2	2	2	1	1
56	20	1	0	2	2	1	0	0
57	20	1	0	2	2	1	0	0
58	21	1	1	2	2	0	0	0
59	21	1	3	2	0	1	1	0
60	21	1	0	2	2	0	0	0
61	21	1	0	2	2	0	0	0
62	22	1	2	2	2	1	0	0
63	22	0	0	2	2	0	0	0
64	22	0	0	2	2	1	1	1
65	22	1	2	2	2	0	0	0
66	22	0	0	0	0	1	0	0
67	22	1	0	2	2	1	1	0
68	23	1	0	2	2	0	0	0

69	23	1	0	2	2	0	0	0
70	23	1	0	2	2			
71	23	1	0	2	2	1	0	0
72	23	1	0	2	2	1	0	0
73	24	1	0	2	2	0	0	0
74	24	1	0	2	2			
75	24	1	0	2	2	0	0	0
76	24	1	0	2	2	0	0	0
77	24	1	0	2	2	1	1	1
78	24	1	0	5	2	0	0	0
79	24	1	1	2	2	0	0	0
80	24	1	0	2	2	1	0	0
81	24	1	0	2	2	1	0	0
82	24	1	2	5	2	0	0	0
83	24	1	0	2	2	0	0	0
84	25	1	0	2	2	1	1	0
85	25	0	0	2	2	1	0	0
86	25	1	0	1	2	0	0	0
87	25	1	0	2	2	1	0	0
88	25	1	1	5	2	1	0	0
89	25	1	0	2	2	0	1	0
90	26	1	0	2	2	0	0	0
91	26	0	0	2	2	0	0	0
92	26	1	0	2	2	0	0	0

93	26	1	0	2	2	1	1	0
94	26	1	0	2	2	0	1	0
95	26	1	0	2	2	0	0	0
96	27	1	0	2	2	1	0	0
97	27	1	1	2	2	0	0	0
98	27	1	0	2	2	1	1	1
99	27	1	0	2	2	0	0	0
100	27	1	0	2	2	2	1	1
101	27	1	0	2	2	1	0	0
102	27	1	0	2	2	0	0	0
103	27	1	0	2	2	0	0	0
104	27	1	0	2	2	1	1	1
105	28	1	0	2	2	1	0	0
106	28	0	1	5	3	0	0	0
107	29	1	0	2	2	1	0	0
108	29	1	0	2	2	0	0	0
109	29	0	0	2	2	1	1	1
110	30	1	0	2	2	1	0	1
111	30	1	0	2	2	0	0	0
112	30	1	0	2	2	1	0	0
113	30	1	0	2	2	0	0	0
114	31	1	0	2	2	1	1	0
115	31	1	0	2	2	0	0	0
116	31	1	0	2	2	1	0	1

117	31	1	1	5	3	1	0	0
118	31	1	1	5	3	0	0	0
119	31	1	0	2	2	0	0	0
120	32	0	2	5	3	1	0	1
121	32	1	0	2	2	2	0	1
122	32	1	0	2	2	1	1	0
123	32	1	0	5	3	0	0	0
124	32	1	0	2	2	0	0	0
125	32	1	0	4	2	1	1	0
126	32	1	0	4	2	1	0	0
127	33	1	0	2	2	0	0	0
128	33	1	0	2	2	1	0	1
129	34	1	0	2	2	1	1	1
130	34	1	0	2	2	0	0	0
131	34	1	0	4	2	0	0	0
132	34	1	0	3	2	1	0	1
133	34	1	0	3	2	1	0	0
134	34	1	0	5	3	0	0	0
135	34	1	0	2	2	0	0	0
136	34	0	0	2	2	1	1	0
137	35	1	0	2	2	1	0	0
138	35	1	0	3	2	0	0	0
139	35	1	0	2	2	1	0	0
140	35	0	0	2	2	1	1	0

141	35	1	0	5	3	1	0	0
142	35	1	0	3	2	2	1	1
143	35	1	0	5	3	2	0	0
144	36	0	0	2	2	0	0	0
145	36	1	1	5	3	3	1	1
146	36	1	0	3	2	1	1	1
147	36	1	0	3	2	2	0	0
148	36	1	0	2	2	1	0	0
149	36	1	0	4	2	0	0	0
150	36	1	0	4	3	0	0	0
151	37	1	0	5	3	1	0	0
152	37	1	0	3	2	0	0	0
153	37	1	0	3	2	0	0	0
154	37	0	0	5	4	1	1	1
155	37	1	0	3	2	1	1	1
156	37	1	0	2	2	0	0	0
157	38	1	0	2	2	0	0	0
158	38	1	0	4	3	1	0	0
159	38	1	0	4	3	1	0	0
160	38	1	0	3	2	0	0	0
161	38	1	0	3	2	0	0	0
162	38	1	2	5	3	2	1	0
163	39	1	0	3	2	0	0	0
164	39	1	0	4	3	1	0	0

165	39	1	0	4	3	1	0	0
166	39	1	1	4	3	1	0	0
167	39	1	0	3	2	0	0	0
168	39	1	0	3	2	1	1	1
169	39	0	0	4	3	1	0	0
170	39	1	0	3	2	0	0	0
171	39	1	0	3	2	0	0	0
172	39	1	0	4	3	1	0	0
173	39	1	0	3	2	0	0	0
174	39	1	0	4	2	0	0	0
175	39	1	0	5	3	1	1	0
176	40	1	0	4	2	0	0	0
177	40	1	0	4	3	1	1	1
178	40	1	0	5	3	0	0	1
179	40	1	0	5	4	0	0	0
180	45	1	0	4	3	1	0	0
181	50	1	0	5	3	0	1	1
182	54	1	0	3	2	1	0	0
183	61	1	0	3	2	0	0	0
184	71	1	0	4	3	1	1	0
185	75	0	0	4	3	1	1	0
186	85	0	0	4	3	1	0	0

Gender: 0=female, 1=male. APOE 0=3/3, 1=3/4, 2=4/4, 3=2/3

AD staging pτ Stage: 0=absent, 1= pre-tangle stages a-c, 2= pre-tangle stages 1a,1b, 3=NFT stages I, II, 4=NFT stages III-IV, 5=NFT stages V-VI

AD staging Aβ Phase: 0=absent, 1=basal temporal neocortex, 2=all cerebral cortex, 3=subcortical portions forebrain, 4=mesencephalic components, 5=Reticular formation and cerebellum.

Substantia nigrae pτ was evaluated as pre-tangles, positive neurites, and tangles using the

PHF-tau8 phosphorylated at Ser199-202-Thr205 (Innogenetics, Belgium, AT-8 1:1000).

Substantia nigrae α-S was evaluated as neuronal immunoreactive (IR) aggregates in the somato-dendritic compartment, cytoplasmic inclusions, core-halo Lewy bodies and dystrophic neurites (Lewy neurites) using α-synuclein phosphorylated at Ser-129, LB509 (In Vitrogen, Carlsbad, CA 1:1000)

*Brainstem TDP-43 was evaluated by dash-like IR particles in the vicinity of the cell nucleus, with or without complete loss of nuclear TDP-43 expression and somatic skein-inclusions, using mab2G10 (Roboscreen GmbH, Leipzig, Germany 1:1000).